3324.

Mechanics and Materials Center
TEXAS A&M UNIVERSITY
College Station, Texas

NAG3-491

INTEGRATED RESEARCH IN CONSTITUTIVE MODELLING AT ELEVATED TEMPERATURES

FINAL REPORT (145)

by

W.E. Haisler
and
D.H. Allen

Part 1

MM 4998-86-13

June 1986

INTEGRATED RESEARCH IN CONSTITUTIVE MODELLING AT ELEVATED TEMPERATURES

FINAL REPORT

by

W.E. Haisler
and
D.H. Allen

Aerospace Engineering Department
Texas A&M University
College Station, Texas 77843

submitted to

NASA Lewis Research Center
Cleveland, Ohio
Technical Monitor: R.L. Thompson

MM 4998-86-13

June 1986

TABLE OF CONTENTS

omit to p.2

1. INTRODUCTION

1.1 Summary

This report details research performed under NASA Grant NAG3-491, with startup date of November 15, 1983 and completion on December 31, 1985. The research centers on evaluation of thermoviscoplastic constitutive models for metals at elevated temperatures. The primary intent of the research was threefold in nature: 1) to improve existing experimental facilities within the Mechanics and Materials Labs at Texas A&M University in order to perform the complex experiments required under the grant; 2) to compare existing models to experiment for the materials to be discussed herein; and 3) to extend existing models where necessary to better predict complex material response. The research group consists of Drs. W.E. Haisler and D.H. Allen, assisted by five graduate research assistants.

1.2 Acknowledgement

The authors express their thanks for the support provided for this research by the NASA Lewis Research Center. The technical grant monitor is Dr. R.L. Thompson.

2. RESEARCH OUTLINE

2.1 Summary of Completed Research

The important details of the research are outlined in this section. The findings are divided into the following six sections: 1) numerical integration techniques; 2) thermodynamics and internal state variables; 3) experimental lab development; 4) comparison of models at room temperature; 5) comparison of models at elevated temperature; and

6) integrated software development. These topics are summarized in the following seven sections (2.2 through 2.7). Further details are given in the technical reports in the appendix. A summary of important findings is given in Section 2.8.

2.2 Numerical Integration Techniques

The sensitivity of the unified constitutive theories proposed by Bodner, Walker, Krieg, and Miller, to numerical integration techniques and slight changes in material parameters was investigated. Evaluations were based upon numerical simulations of Hastelloy-x at 1800°F, in uniaxial form, by specifying input strain histories and comparing output stress histories. The constitutive models selected for this study were chosen primarily because of the availability of a prescribed methodology for material parameter evaluation. In addition, they appear to be the most qualitatively attractive theories available and thus warrant further evaluation.

The investigation begins by presenting the various models in uniaxial differential equation form, followed by a description of the methods used for material parameter evaluation. The main thrust of the research was to assess the degree of sensitivity of each model to integration techniques and/or variations in the respective material constants. An example is shown in Fig. 1 for Bodner's model.

For the numerical time integration study, four commonly used algorithms were selected. These included Explicit Euler Forward Difference, Implicit Trapezoidal, 4th Order Runge-Kutta, and Trapezoidal Predictor-Correction methods. In addition, four different strain rate input histories were selected to insure that evaluations were not biased

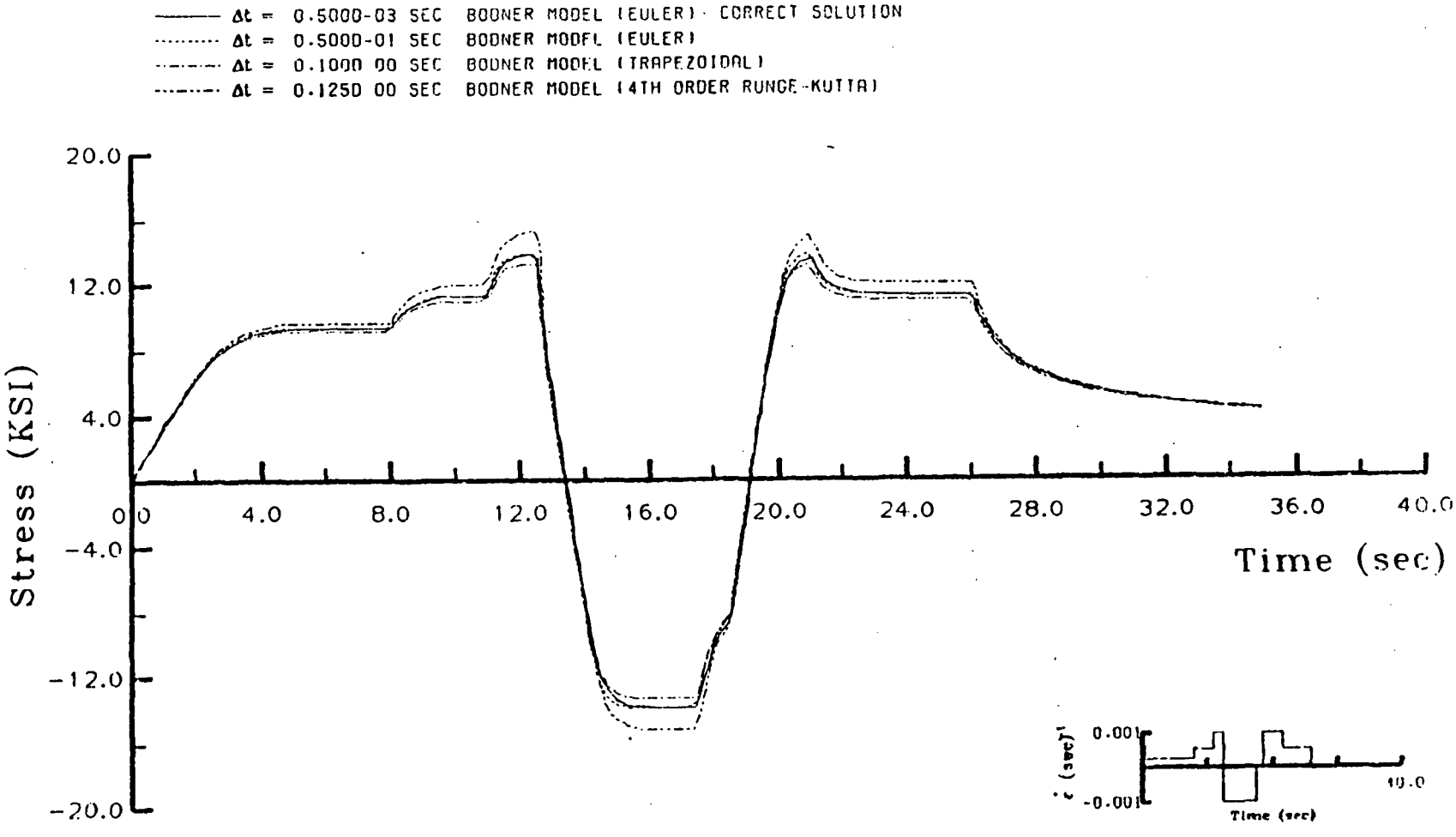

Fig. 1 . Comparison of Integration Methods For Bodner's Model With Equivalent Computation Time Allowed For Each Method (Hastelloy-X at 1800° F).

to one specific simulation. The strain histories considered were not developed to model any specific physical phenomena. However, they are representative of conditions under which a material could be strained either in the laboratory or the field.

The integration investigation was divided into two tasks. The first task included a comparison of the numerical stability of each constitutive theory in order to assess the degree of nonlinearity of the prescribed growth laws. The comparisons were based upon predicted stress-strain behavior for constant strain rate tests simulating monotonic loading. Explicit Euler Forward integration was used to obtain stress histories for various time steps. It was concluded that Miller's model was the most sensitive to step size variation because of the oscillatory response of the stress-strain curve for the larger Δt values. It is postulated that the oscillatory nature of Miller's model can be traced back to the hyperbolic sine function that is used to characterize the inelastic strain rate and other growth laws.

In addition, it was found that the predicted stress response for each model appears to be "self correcting" for large time increments when the constitutive equations are integrated by the Euler method. This "self-correcting" phenomenon appears to be an intrinsic property of the prescribed growth laws and the coupled nature of the equations.

The second task of the integration investigation was to evaluate the constitutive theories in terms of solution stability, accuracy, and computational efficiency when numerically integrated using the various algorithms considered. A test matrix consisting of integration method, time step sizes, and strain input histories was established in order to make qualitative and quantitative comparisons. For each strain history

considered, a baseline or "pseudo correct" solution was obtained analytically, since no experimental data were available.

The computational efficiency of each integration method was obtained through selection of equivalent Δt's. Euler's method was observed to be the most efficient, followed by the Implicit Trapezoidal method, then the 4th order Runge-Kutta method, and finally the Trapezoidal Predictor-Corrector method. In addition, each model was evaluated for its computational efficiency. The results indicate that Walker's model resulted in the fastest execution time, followed by Krieg, Bodner, and Miller, respectively.

In terms of qualitative and quantitative comparisons the following observations were made: 1) In general, for equal time step size and equivalent computation integration times, the 4th order Runge-Kutta method consistently overpredicts the state of stress while the Trapezoidal method generally underestimates the stress history. The Euler and Predictor-corrector methods appear to provide accurate results at any point in the simulation; 2) the amount of stress-overshoot (for the larger step sizes) appears to grow with increasing strain rate; and 3) no "self-correcting" tendency was observed when either the 4th order Runge-Kutta or Trapezoidal method was used.

Another important issue this research addressed was what amount of degradation in predicted response could be expected due to variations in material constants. Two procedures were developed to study this. The first procedure characterized the sensitivity of each constant within a particular constitutive model. Each constant's sensitivity to variation was determined by adjusting it by 5% and comparing predicted results. The second procedure provided an "upper bound" on the effect that

experimental error would have on the determination of the material parameters and ultimately, predicted response. The effect of experimental uncertainty was studied by adjusting numerical test data by ±5% and then using the adjusted data to determine new material constants.

From the results of the sensitivity study, the following observations were made: 1) For the load history considered, constitutive models can have up to a 12% variation in predicted response for as little as a 5% variation in a given material constant; and 2) Miller's model was shown to be the least sensitive to material parameter variation possibly due to its strong microphysical basis. On the other hand, Walker's model was the most sensitive, showing a 30% over-prediction in stress during the relaxation period of the load history considered. Bodner's and Krieg's models were found to be between these two extremes. Further details on this phase of the research can be found in Appendices 6.1 and 6.2.

It should be noted that the conclusions reached from this study are based on the use of uniaxial simulations. It is expected that the conclusions would hold for multiaxial situations. However, further evaluation is needed in this area.

2.3 Thermodynamics and Internal State Variables

As a part of the research effort it was concluded that a casting of the currently available constitutive models into a common framework would help in identifying the relative merits and/or deficiencies of each model. For this purpose it was decided to cast the models into the framework of internal state variable (ISV) theory, in which a set of

state variables which are not observable are utilized to account for thermodynamically dissipative processes such as dislocation movement, grain boundary sliding, deformation twining, phase changes, etc. This framework has been used to determine qualitative differences in the models studied under the current grant. Furthermore, in this process it was found that certain thermodynamic issues could be clarified.

The specific ISV framework uses the approach initially proposed by Coleman and Gurtin [1], in which the observable state variables are supplemented with a set of internal state variables:

$$\alpha_{ij}^{k} = \alpha_{ij}^{k}(x_m, t),\ K = 1,2, \ldots n \quad , \qquad (1)$$

where α_{ij}^{k} are a set of n internal state variables, in this case designated as second order tensor functions of space x_m and time t.

The method of Coleman and Noll [2] may be utilized to obtain thermodynamic constraints on the class above of materials including a broad range of thermoviscoplastic metals. The results are:

$$\sigma_{kl} = \rho \frac{\partial h}{\partial \epsilon_{kl}} \quad , \qquad (2)$$

where σ_{kl} is the stress tensor, ϵ_{kl} is the infinitesimal strain tensor, ρ is the mass density, and h is the specific Helmnoltz free energy, given by

$$h \equiv u - Ts = h(\epsilon_{mn}, T, \alpha_{ij}^{k}) \quad , \qquad (3)$$

where u is the internal energy, T is the temperature, and s is the entropy. The Helmholtz free energy is then expanded in a Taylor series in strain, temperature, and the ISV's and substituted into (2) to obtain the stress-strain relation:

$$\sigma_{ij} = C_{ijkl} (\varepsilon_{kl} - \varepsilon^{T}_{kl} - \alpha^{1}_{kl}) \quad , \qquad (4)$$

where C_{ijkl} is the elastic modulus tensor, and ε^{T}_{kl} is the thermal strain tensor. The above equations serve as a framework of comparison for all of the models considered in this research. These are adjoined with ISV growth laws of the general form:

$$\alpha^{k}_{ij} = \Omega^{k}_{ij} (\varepsilon_{mn}, T, \alpha^{p}_{mn}) \quad , \qquad (5)$$

The ISV's represent locally averaged measures of dislocation arrangement (back stress) dislocation density (drag stress), etc. ISV growth laws (5) represent the principal differences between the models studied in the current research effort. These equations have been itemized in Table 1 for ten different current models. Qualitative differences in the models are also discussed in the table.

The main content of this part of the research has been to review and clarify the continuum and thermodynamics based internal state variable model for application to thermoviscoplastic metals. In this process the following points have been made:

1) the definition of an internal state variable utilized in this model has been clarified;

TABLE 1. COMPARISON OF UNIAXIAL MODELS

Theory	Stress-Strain Relaxation	Internal State Variable Growth Laws	Comments	Material Parameters
Cernocky and Krempl	(T1) $\sigma=E[\varepsilon-\varepsilon^I-\varepsilon^T]$	(T2) $\dot{\varepsilon}^I=\frac{\sigma-G}{Ek}$	1. $G=G(\varepsilon,T)$ is obtained from extrapolation of relaxation data. 2. k is curve-fit to $k=R_0 e^{R_1 e^{-\left[\frac{\lvert\sigma-G\rvert}{R_2}\right]^{R_3}}}$	E, R_0, R_1, R_2, R_3
Krieg, Swearengen, and Rohde	(T3) $\sigma=E[\varepsilon-\varepsilon^I]$	(T4)[1] $\dot{\varepsilon}^I=c_1\left[\frac{\lvert\sigma-\alpha_1\rvert}{\alpha_2}\right]^{c_2}\operatorname{sgn}(\sigma-\alpha_1)$ (T5)[1,2] $\dot{\alpha}_1=c_3\dot{\varepsilon}^I-c_4\alpha_1^2[e^{c_5\alpha_1^2}-1]\operatorname{sgn}(\alpha_1)$ (T6)[2] $\dot{\alpha}_2=c_6\lvert\dot{\varepsilon}^I\rvert-c_7[\alpha_2-\alpha_{2_0}]^n$		$E, c_1, c_2, c_3, c_4, c_5, c_6, c_7, \alpha_{2_0}, n$
Bodner et al.	(T7) $\sigma=E[\varepsilon-\varepsilon^I]$	(T8)[1] $\dot{\varepsilon}^I=\frac{2}{\sqrt{3}}D_0 e^{-\left[\frac{n+1}{2n}\right]\left[\frac{\sigma}{\alpha_2}\right]^{-2n}}\operatorname{sgn}(\sigma)$ (T9) $\dot{\alpha}_2=[Z_1-\alpha_2]\dot{W}_p-AZ_1\left[\frac{\alpha_2-Z_I}{Z_1}\right]^r$	1. $\dot{W}_p=\sigma\dot{\varepsilon}^I$	$E, D_0, n, m, Z_1, Z_I, A, r$
Walker	(T10) $\sigma=E[\varepsilon-\varepsilon^I]$	(T11)[1] $\dot{\varepsilon}^I=\left[\frac{\lvert\sigma-\alpha_1\rvert}{\alpha_2}\right]^n\operatorname{sgn}(\sigma-\alpha_2)$ (T12)[2] $\dot{\alpha}_1=[n_1+n_2]\dot{\varepsilon}^I-[\alpha_1-\alpha_{1_0}-n_1\varepsilon^I][\lvert\dot{\varepsilon}^I\rvert\frac{\partial}{\partial R}([n_3+n_4R][\ln(\frac{n_5R}{1+n_6R}+1)])+n_7\lvert\alpha_1-\alpha_{1_0}\rvert^{m-1}]$ (T13) $\dot{\alpha}_2=n_8\lvert\dot{\varepsilon}^I\rvert-n_9\lvert\dot{\varepsilon}^I\rvert\alpha_2-n_{10}[\alpha_2-\alpha_{2_0}]^q$	1. R is the cumulative inelastic strain: $R=\int_0^t\frac{\partial\varepsilon^I}{\partial\tau}d\tau$. 2. The growth law for α_2, eq.(T13), is not presently used in the model; α_2 is assumed to be a constant.	$E, n, n_1, n_2, n_3, n_4, n_5, n_6, n_7, n_8, n_9, n_{10}, m, q, \alpha_{1_0}, \alpha_{2_0}$
Miller	(T14) $\sigma=E[\varepsilon-\varepsilon^I-\varepsilon^T]$	(T15)[1] $\dot{\varepsilon}^I=B\theta'\left[\sinh(\frac{\lvert\sigma-\alpha_1\rvert}{\alpha_2})1.5\right]^n\operatorname{sgn}(\sigma-\alpha_1)$ (T16)[1,2] $\dot{\alpha}_1=H_1\dot{\varepsilon}^I-H_1B\theta'[\sinh(A_1\lvert\alpha_1\rvert)]^n\operatorname{sgn}(\alpha_1)$ (T17)[2] $\dot{\alpha}_2=H_2\lvert\dot{\varepsilon}^I\rvert[C_2+\lvert\alpha_1\rvert-\frac{A_2}{A_1}\alpha_2^3]-H_2C_2B\theta'[\sinh(A_2\alpha_2^3)]^n$	1. $\theta'=e^{-\frac{Q}{RT}}$ for $T>0.6\,T_m$ $\theta'=e^{-\left[\frac{Q}{0.6RT_m}\right]\left[\ln(\frac{0.6T_m}{T})+1\right]}$ for $T\le 0.6\,T_m$ T_m is the melting temp. k is the gas constant.	$E, B, n, H_1, A_1, H_2, C_2, A_2, Q$

Cescotto and Leckie	(T18) $\sigma=E[\epsilon-\epsilon^I-\epsilon^T]$	(T19)[1] $\dot{\epsilon}^I=f\left(\left\|\frac{\sigma-a_1}{a_2}\right\|\right)\ \mathrm{sgn}(\sigma-a_1)$ (T20)[2] $\dot{a}_1=\frac{3}{2}h_a\dot{\epsilon}^I-r_a a_1$ (T21) $\dot{a}_2=h_\kappa-r_\kappa$	1. f, h_a, r_a, h_κ, and r_κ are experimentally determined functions.	E
Hart	(T22) $\sigma=E[\epsilon-\epsilon^I-\epsilon^T]$	(T23)[1] $\dot{\epsilon}^I=\dot{a}^*\left[\frac{2}{3}\right]^{M/2}\left[\frac{\lvert\sigma-a_1\rvert}{\mu}\right]^M\mathrm{sgn}(\sigma-a_1)$ (T24)[2] $\dot{a}_1=\frac{3}{2}\mu\dot{\epsilon}^I-\frac{\mu\left[\frac{a_2'}{C}\right]^m f_a^{-\frac{Q}{RT}}}{\left[\ln\left(\frac{3a_2'}{2\lvert a_1\rvert}\right)\right]^{1/\lambda}}$ (T25) $\dot{a}_2'=c\left[\frac{2}{3}\right]^{k/2}f_a^{-\frac{Q}{RT}}\left[\frac{\sigma}{a_2'}\right]^k\frac{a_2'}{\left[\ln\left(\frac{a_2'}{\sqrt{\frac{2}{3}}\sigma_1}\right)\right]^{1/\lambda}}$	1. The drag stress is taken to be a constant, μ, hence there is no a_2 as in other models. There is, however, a third internal state variable, termed a_2'. 2. T is the absolute temp. R is the gas constant.	E, $\dot{a}^*$, M, μ, C, m, f, Q, k, λ, c
Robinson	(T26) $\sigma=E[\epsilon-\epsilon^I-\epsilon^T]$	(T27) $\dot{\epsilon}^I=\frac{1}{2\mu}\left[\frac{1}{\sqrt{3}}\left\|\frac{\sigma-a_1}{K}\right\|\right]^{n-1}[\sigma-a_1]$ (T28)[2] $\dot{a}_1=\frac{2\mu H}{\left[\frac{1}{\sqrt{3}}\left\|\frac{a_1}{K}\right\|\right]^\beta}\dot{\epsilon}^I-R\left[\frac{1}{\sqrt{3}}\left\|\frac{a_1}{K}\right\|\right]^{n-\beta-1}a_1$	1. G_0 is the initial value of $\frac{a_1^2}{3K^2}$.	E, μ, K, n, β, H, R, G_0
Valanis	(T29) $\sigma=E[\epsilon-\epsilon^I-\epsilon^T]$	(T30) $\dot{\epsilon}^I=k_1f_1(\sigma,\epsilon)\epsilon+k_2f_2(\sigma,\epsilon)$	1. Represents simplified form of Valanis' model.	E, k_1, k_2, f_1, f_2
Allen and Haisler	(T31) $\sigma=E[\epsilon-\epsilon^I-\epsilon^T]$	(T32) $\dot{\epsilon}^I=\dot{\lambda}[\sigma-a_1]+\dot{g}[\sigma-a_1]$ (T33) $\dot{a}_1=\dot{\mu}[\sigma-a_1]$ (T34) $\dot{a}_2=f(\dot{\epsilon}^{I^2})$	1. Considerable curve-fitting and interpolation of stress-strain and creep data required to obtain material parameters $\dot{\lambda}$, $\dot{g}$, and $\dot{\mu}$.	E, $\dot{\lambda}$, $\dot{g}$, $\dot{\mu}$, f

1 $\mathrm{sgn}(x)\ \begin{cases}1 & x>0\\ 0 & x=0\\ -1 & x<0\end{cases}$

2 $\dot{\epsilon}^I$ can be substituted directly into growth law for a_1 and a_2 to obtain a form consistent with internal state variable growth laws (14).

Note: parentheses ( ) imply "function of", whereas brackets [ ] imply multiplication.

2) internal state variables in metals represent local averages of dislocation arrangement, dislocation density, and intergranular damage,

3) in the context of the ISV definition given here, inelastic strain may also be interpreted as an internal state variable;

4) the path dependent Helmholtz free energy may be expanded in a second order expansion in elastic strain and temperature in order to obtain a stress-strain equation of state;

5) rate dependence enters the constitutive equations implicitly via the inelastic strain, as demonstrated by the nonlinear standard solid analog; and

6) a three-dimensional generalization of the standard solid may be used as a means of comparison of the general form of several currently proposed models.

Further details of this development are contained in Appendix 6.3.

2.4 Experimental Lab Development

This section describes the test equipment used to carry out the tests required for this work. The first sub-section describes the test set-up used for the creep and strain transient tests based on a dead weight creep frame. Topics to be covered include the load frame, data acquisition, and temperature measurement and control. The next sub-section describes the test set-up used for the monotonic strain rate, fully reversed cyclic tests, and transient tests during cyclic loading as well as creep and strain transient tests based on a computer controlled test set-up.

Creep Frame Test Set-up

Load Frame. The load frame utilized was a creep frame produced at Texas A&M University. The initial configuration included a constant load cam and a constant stress cam as described by Garofalo, et al. [3]. The lift for the pan was provided by an ATS (Applied Test Systems) 2081 cyclic load module. Several modifications were made to this set-up. The constant stress cam was removed and a second constant load cam installed. This increased the maximum weight limit from 400 lbs. to 800 lbs. This also increased the stability of the loadpan during load-up and provided a seven to one load magnification. The load pan was increased in size and supports were added to further aid stability during load-up. The cyclic load table was removed and replaced with a Century-Fox model CF-59 5 ton capacity hydraulic jack. This provided more lift capacity and gave more room for machine deflection during load-up. The final configuration of the machine is shown in Fig. 2.

Further improvements included a more advanced load pan which would provide automated removal and replacement of portions of the load. Jones, et al. [4] have described such an apparatus. This modification is needed to improve the results of the strain transient tests. A second improvement was a more advanced method of load-up. For this purpose, a pneumatic jack was included.

Data Acquisition. The load was measured with a Strain sert TLN20-256K Tension Link driven by a Hewlett Packard 8805A Carrier Preamp. The strain was measured with an ATS model 4112 LVDT (Linear Variable Displacement Transducer) and the extensometer was driven by an ATS model 6974 signal conditioner. Two Hewlett Packard 8803A Low Level Preamps

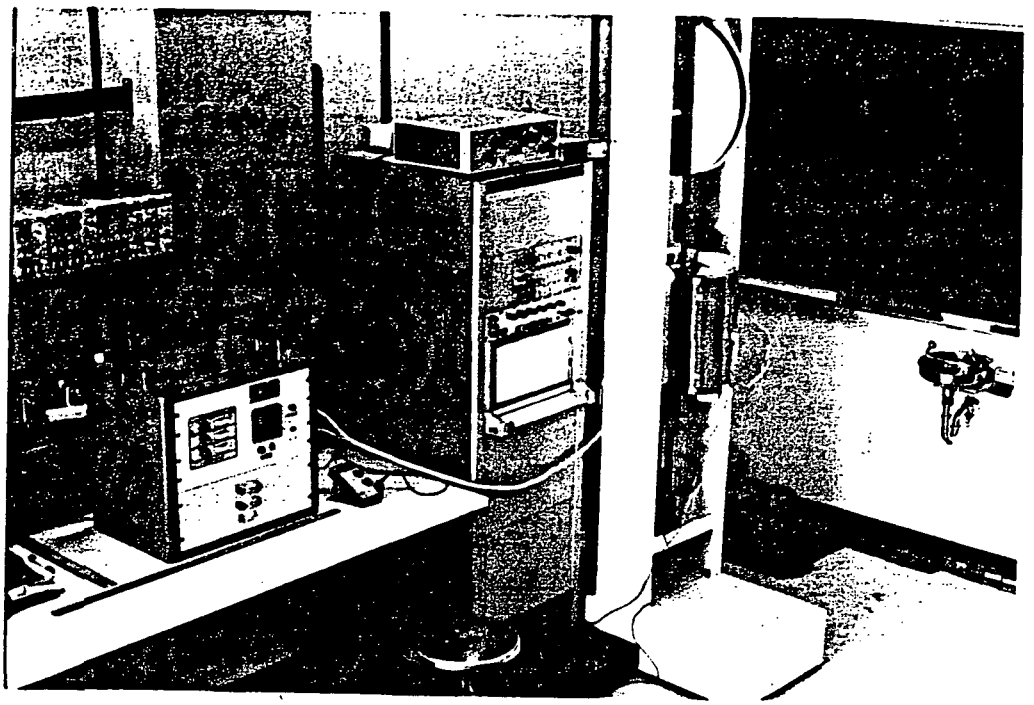

Fig. 2. Creep Frame Final Configuration

Fig. 3. MTS 880 110Kip Testing System

and two low pass filters were necessary to achieve the necessary resolution. Load and strain measurements were recorded on a Hewlett Packard series 7700 strip chart recorder.

This data acquisition system was very prone to drift, noise, and nonlinearity. All strain amplification, filtration, and data acquisition equipment were eventually replaced with a Kiethly model 197 logging digital multimeter. This set-up proved much more stable. However, it lacked the ability to take in a large number of data points. Much improvement is needed in strain data acquisition to produce a system which is stable, can take in large numbers of points, and has sufficient resolution. A common set of transducers and a common data acquisition system should be utilized for both load frames. This would negate errors arising from using two different systems.

Temperature Measurement and Control. An ATS 2961 Clamshell oven and an LFE series 230 temperature controller were used for temperature control. Temperature measurement was handled by two 20 gauge K-type thermocouples. These were placed in contact with the sample in the middle of the gauge section on diametrically opposite sides. One thermocouple was used as input to the temperature controller. The other thermocouple was input to a Fluke 2176A digital thermometer for readout.

Improvements in this system would include the ability to monitor the temperature at several points simultaneously along the gauge section. The temperature should also be input to a data acquisition system. The method of thermocouple attachment should also be upgraded. The optimum method of thermocouple attachment would be individual welding of the leads to the sample surface. This is described in the ASTM Thermocouple Handbook [5]. Such a procedure was attempted with 20

gauge thermocouple wire and a Duracom thermocouple welder. The samples tended to fail prematurely at the thermocouple welds. Therefore, this method of thermocouple attachment was abandoned. Another possible method using smaller 28 gauge thermocouples was used with the strain-controlled set-up and will be discussed in that section. A common temperature measurement and control system for both load frames would be another improvement. This would eliminate relative errors between the two systems.

Computer Controlled Test Set-up

Load Frame. The load frame utilized in this set-up was an MTS (Materials Test System) model 880 electro hydraulic testing machine. MTS 652.01, water-cooled, hydraulic grips allowed fully reversed cyclic tests to be carried out at high temperature. The frame was controlled by a Digital Micro PDP-11. Computer programs were written to run monotonic tension tests, cyclic tests, cyclic tests with hold times, creep tests, and creep stress drop tests. The load frame is shown in Fig. 3.

Data Acquisition. The Micro PDP-11 also handled data acquisition functions. An MTS 661.21A-02 10 kip load cell was the load transducer. An MTS 632.41B-02 axial extensometer was the strain transducer. This device had quartz extension rods which contacted the sample at two 120° punch holes. All data were stored on 5.25 inch floppy diskettes and could be retrieved in hard copy or graphical form.

Temperature Measurement and Control. An MTS 652, three-zone, clamshell furnace and three Research Incorporated 63911 Process Temperature and Power Controllers were used for temperature control. Temperature Measurement was handled by six 28 gauge K-type

thermocouples. These were placed in contact with the sample. Three thermocouples were fed into a Fluke 2176A Digital Thermometer for readout. These were placed with one each at the top, middle, and bottom of the gauge section. The other three thermocouples were fed into the temperature controllers. These were placed in the center of the furnace zone each was to sense. One thermocouple was placed in the center of the gauge section and one on each grip.

The thermocouples were supported at the grips by fiberglass thread. They were fixed to the sample by self-supporting means. The thermocouples at the top and bottom of the gauge section were wound around the sample. The thermocouples used in the center of the gauge section were brought into the oven from different directions and tied to each other. These thermocouples were then wound around the sample. The thermocouples used in the center of the gauge section were brought into the oven from different directions and tied to each other. These thermocouples were then wound around the sample for contact. Welding the thermocouples to the sample would have produced harder contacts with more reliable temperature measurement. However, as mentioned earlier, premature failure occurred at the welds.

Further details about the experimental development are given in Appendix 6.5.

2.5 Comparison of Models at Room Temperature

The purpose of the room temperature testing was to compare three theories based on considerations of microstructural behavior. These theories are those of Krieg, et al., Bodner, et al., and Miller, et al. (references [18], [107], and [115], respectively, in Appendix 6.4).

Each theory is proposed in uniaxial form to simplify experimental and analytical analysis. Since each theory is proposed for a different material, a set of experiments is performed with a candidate material in order to create a common experimental data base with which the mathematical representation of each model can be characterized. These theories are subsequently analyzed qualitatively and quantitatively over a broad range of material behavior to determine their suitability for predicting inelastic deformation.

The experimental data base requirements for each theory are as follows. The theory of Bodner, et al., requires several constant strain rate tensile tests and several creep tests. The theory of Miller, et.al., requires several creep tests, several constant strain rate tensile tests, and some information about the material such as the melting point and the activation energy. The theory of Krieg, et al., requires a constant strain rate tensile test, a creep curve complete with primary and secondary regions, and several stress-drop tests in which the stress is reduced rapidly during steady-state creep in order to examine the resulting transient strain response. In each case the actual number of tests, unless specified, is dependent on the amount of data deemed necessary for accurate evaluation of the material constants. The candidate material chosen is the aluminum alloy 5086 in the form of uniaxial bars, and the material tests are performed at room temperature.

In determining the material constants for each theory from these tests, the procedure proposed by the authors is followed. It is found that some of these procedures may be difficult to implement. In particular, difficulties are encountered in interpreting the stress-drop test, in which the quantity of interest is a zero strain rate or merely

the absence of a resolvable strain rate after unloading. It can be seen that the results of this test are somewhat dependent on the resolution of the experimental equipment. In addition, the values of several constants in the theories are set arbitrarily, possibly leading to inaccuracies in the ensuing predictions. Many procedures require extensive data reduction and graphing, making an interactive data acquisition and computer system an indispensable tool. Finally, correction of the value of any one constant can be a difficult task, as some of the constants of each theory may be interdependent.

Each constitutive theory is presented by highly nonlinear, numerically "stiff" differential equations. Since the objective of this research is not to determine numerically efficient integration techniques for these equations, a stable first order forward integration scheme was used.

Numerical simulations were performed to compare the predictive capability of each theory to experimental results for constant strain rate tensile tests, constant strain rate cyclic tests, and complex strain rate history tests. As an example, Fig. 4 compares theory to experiment for the first cycle of a constant strain rate cyclic test. The experiment is modelled fairly well, but it can be seen that the elastic-inelastic transitions are too sharp, possibly indicating a need for more complex hardening laws. In addition, the Bauschinger effect may not be modelled well by Bodner's theory and Miller's theory due to the lack of a representation for the back stress. The discrepancy in the width and height of the hysteresis loop predicted by Krieg's theory may be due to the ambiguous measurements of the back stress in the stress-drop tests, leading to possible inaccuracies in the material constants. Results and conclusions of comparisons of other tests may be found in detail in Appendix 6.5 of this report.

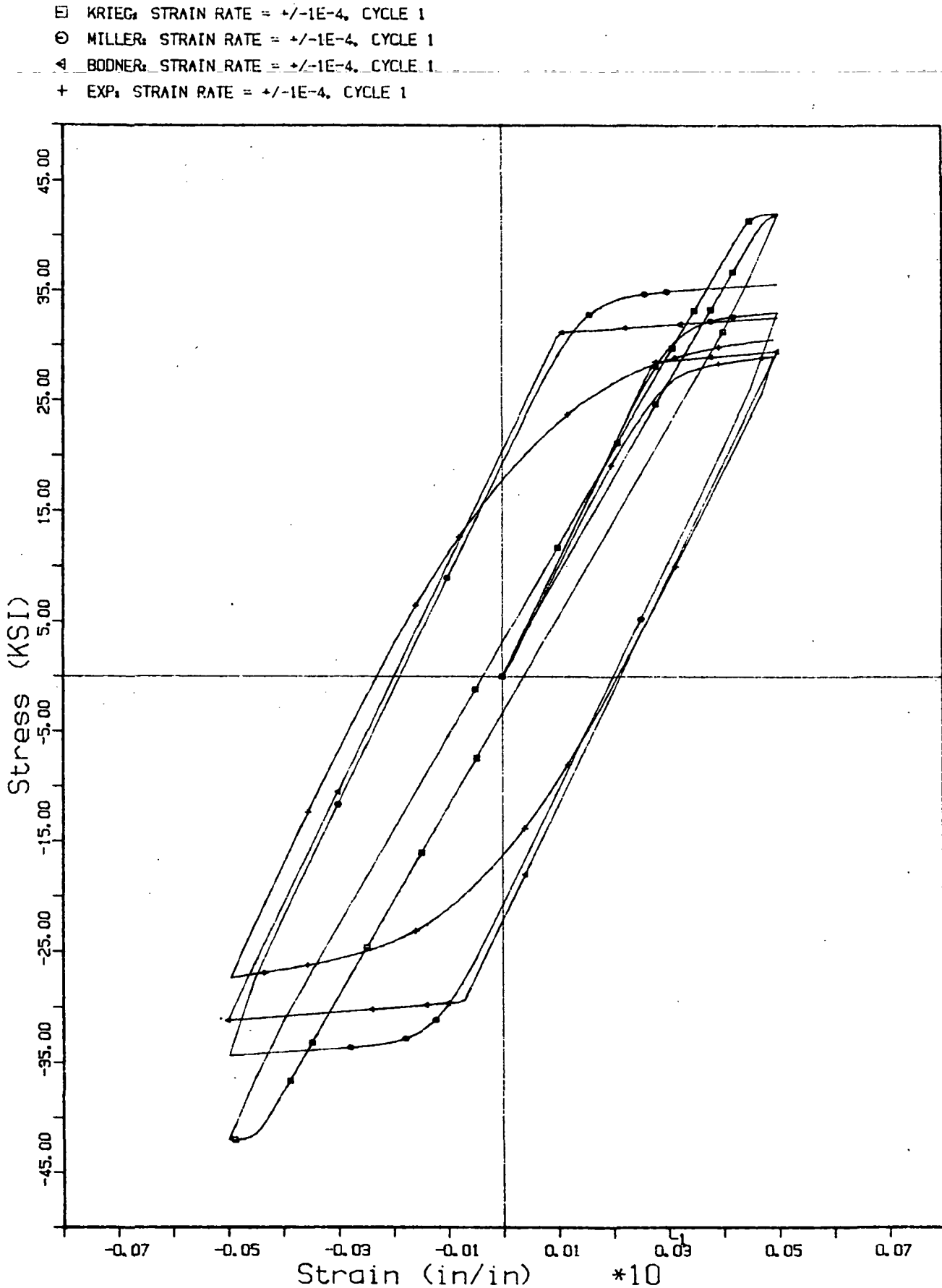

Fig. 4. Comparison of Models to Experiment for IN 718 at 1100°F

2.6 Comparison of Models at Elevated Temperature

The theories used in this work include Bodner's anisotropic model [6]; Krieg, Swearengen, and Rohde's model [7]; Schmidt and Miller's model [8]; and Walker's exponential model [6]. These models have been chosen because they are widely publicized, examples of constant calculation methods have been presented, and the attempt is being made to extend them to non-isothermal modelling.

Bodner's anisotropic model utilizes an inelastic strain rate equation extended from classical plasticity theory. The inelastic strain is assumed to be exponential in stress. A directional parameter has been included as an incrementally isotropic variable. The growth laws are microphenomenologically based and model hardening, dynamic recovery, and static thermal recovery. Bodner's model is given below:

$$\dot{\varepsilon}^D = \frac{2}{3} D_o \exp\left[-\frac{1}{2}\left(\frac{Z}{\sigma}\right)^{2n}\right] \operatorname{sgn}\sigma$$

$$Z = Z^I + Z^A = Z^I + B \operatorname{sgn}\sigma$$

$$\dot{Z}^I = m_1(Z_1 - Z^I)\,\dot{W}_p - A_1 Z_1\left(\frac{Z^I - Z_2}{Z_1}\right)^{r_1}$$

$$\dot{B} = M_2(Z_3 \operatorname{sgn}\sigma - Z^A)\,\dot{W} - A_2 Z_1\left(\frac{|Z^A|}{Z_1}\right)^{r_2} \operatorname{sgn} Z^A \qquad (6)$$

Krieg, Swearengen, and Rhode's model is based on microphenomenological considerations. The inelastic strain rate equation is based on a power law formulation. The growth laws model hardening and static thermal recovery. This model is given below:

$$\dot{\varepsilon}^I = C\left(\frac{\sigma - B}{D}\right)^n \operatorname{sgn}(\sigma - B)$$

$$\dot{B} = A_1\,\dot{\varepsilon}^I - A_2(B - B_o)^2\left(e^{A_3(B-B_o)^2} - 1\right) \operatorname{sgn}(B)$$

$$\dot{D} = A_4|\dot{\varepsilon}^I| - A_5(D-D_o)^n \qquad (7)$$

Schmidt and Miller's model is a microphenomenologically based model which uses a hyperbolic sine inelastic strain rate equation. The growth laws for back stress and drag stress model hardening and static thermal recovery. Parameters have been added to this model which account for strengthening due to solutes. Schmidt and Miller's model is given below:

$$\dot{\varepsilon}^I = B' \sinh\left[\left(\frac{\frac{\sigma}{E} - B}{D + F_{sol}}\right)^{1.5}\right]^n \operatorname{sgn}\left(\frac{\sigma}{E} - B\right)$$

$$\dot{B} = H_1 \dot{\varepsilon}^I - H_1 B' \sinh\left(A_1|B|\right)^n \operatorname{sgn}(B)$$

$$\dot{D} = H_2 |\dot{\varepsilon}^I|\left(C_2 + |B| - \frac{A_2}{A_1} D^3\right) - H_2 C_2 B' \sinh\left(A_2 D^{1.5}\right)^n$$

$$F_{sol} = F_{sol\ max} \exp\left(-\frac{[\log(|\dot{\varepsilon}|) - \log(J)]}{B}\right)^2 \qquad (8)$$

Walker's model has an exponentially based inelastic strain rate equation. The back stress growth law models hardening dynamic recovery, and static thermal recovery. The dynamic recovery term has been modified to handle negative strain rate sensitivity. The drag stress variable allows for cyclic hardening or softening. Walker's model is presented below:

$$\dot{\varepsilon}^I = \frac{\exp(\sigma - B) - 1}{C} \operatorname{sgn}(\sigma - B)$$

$$\dot{B} = n_2 \dot{\varepsilon}^I - B\left[n_3 + n_4 \exp\left(-n_5\left|\log\left(\frac{\dot{R}}{\dot{R}_o}\right)\right|\right)\right] R + n_6$$

$$D = D_1 + D_2 \exp(-n_7 R)$$

$$\dot{R} = |\dot{\varepsilon}^I| \qquad (9)$$

2.6.1 Material Response

The material used in this work is Inconel 718 at 1100° F. All samples have been sent through a common heat treatment prior to being tested. This material system has several distinctive characteristics. The material responds with negative strain rate sensitivity. Discontinuous yielding or the Portevin-Le Chatelier effect is observed. The material cyclically work-softens and has a fatigue life of 5 to 30 cycles when cycled at strain limits over ± 1 percent strain. The yield point of the material is in the region of 95 to 110 ksi.

2.6.2 Experimental Considerations

The material samples were configured to meet ASTM standard E606-77T. The tests were carried out on a computer-controlled, MTS 880, 110 kip, electro-hydraulic testing machine. A Digital Micro PDP-11 computer controlled the tests and acquired the data. An MTS 652 furnace system with three-zone clamshell furnace and hydraulic grips was utilized. An MTS 632-41-02 high-temperature axial extensometer was utilized for displacement measurement. Temperature was monitored with K-type thermocouples and a Fluke 2176A digital thermometer. Welding of the thermocouples to the samples initiated failure and a self-supporting, surface contact method was used for thermocouple attachment.

The test program consisted of the following tests:

(a) 2 monotonic tension tests to 1.5% strain
([1] $3.15 \times 10^{-3} sec^{-1}$ [2] and $7.25 \times 10^{-6} sec^{-1}$)

(b) 5 fully reversed cyclic tests to ± .8% strain
(strain rates between $1 \times 10^{-3} sec^{-1}$ and $7 \times 10^{-6} sec^{-1}$)

(c) 5 constant load creep tests
(applied stresses between 120 ksi & 140 ksi)

(d) Back stress measuring tests during cyclic loading and during secondary creep

(e) a complex history test

2.6.3 Determination of Parameters

Beek [4] has shown that the parameter calculation process presented with each model can produce constants which may produce undesirable model response. A method for determining material parameters which lessened this problem and provided some commonality in the calculations was used. A set of initial assumptions was made based on the expected response of the material. These initial assumptions included the following:

(1) Back stress was responsible for hardening in monotonic tension;

(2) Drag stress was responsible for cyclic softening;

(3) Thermal recovery could be neglected for rapid tests
($\dot{\varepsilon}^T > 1x10^{-4}sec^{-1}$)

(4) Drag stress thermal recovery could be calculated from slow cyclic tests; and

(5) Back stress thermal recovery could be calculated from creep tests.

Hand calculations based on these assumptions provided initial estimates of the material parameters. Computer-aided iterations were then used to tune the response to match specific data points. The parameters which resulted from the iteration process indicated that the following initial assumptions would have been more appropriate:

(1) the inelastic strain rate equation constant could be set to provide the proper scaling and strain rate sensitivity;

(2) back stress hardening produced monotonic hardening;

(3) solution strengthening parameters produced negative strain rate sensitivity;

(4) drag stress hardening could be used to set cyclic work softening characteristics; and

(5) thermal recovery effects were small and masked by solute strengthening.

A comparison of the response of the solute strengthening corrected models to experiment is shown in Fig. 5. These results provide several conclusions concerning various parts of the models. The theories of Walker and Bodner with exponentially based inelastic strain rate equations handle the negative strain rate sensitivity most effectively. The theories of Krieg, et al., Miller, and Bodner produce oversquare stress-strain curves.

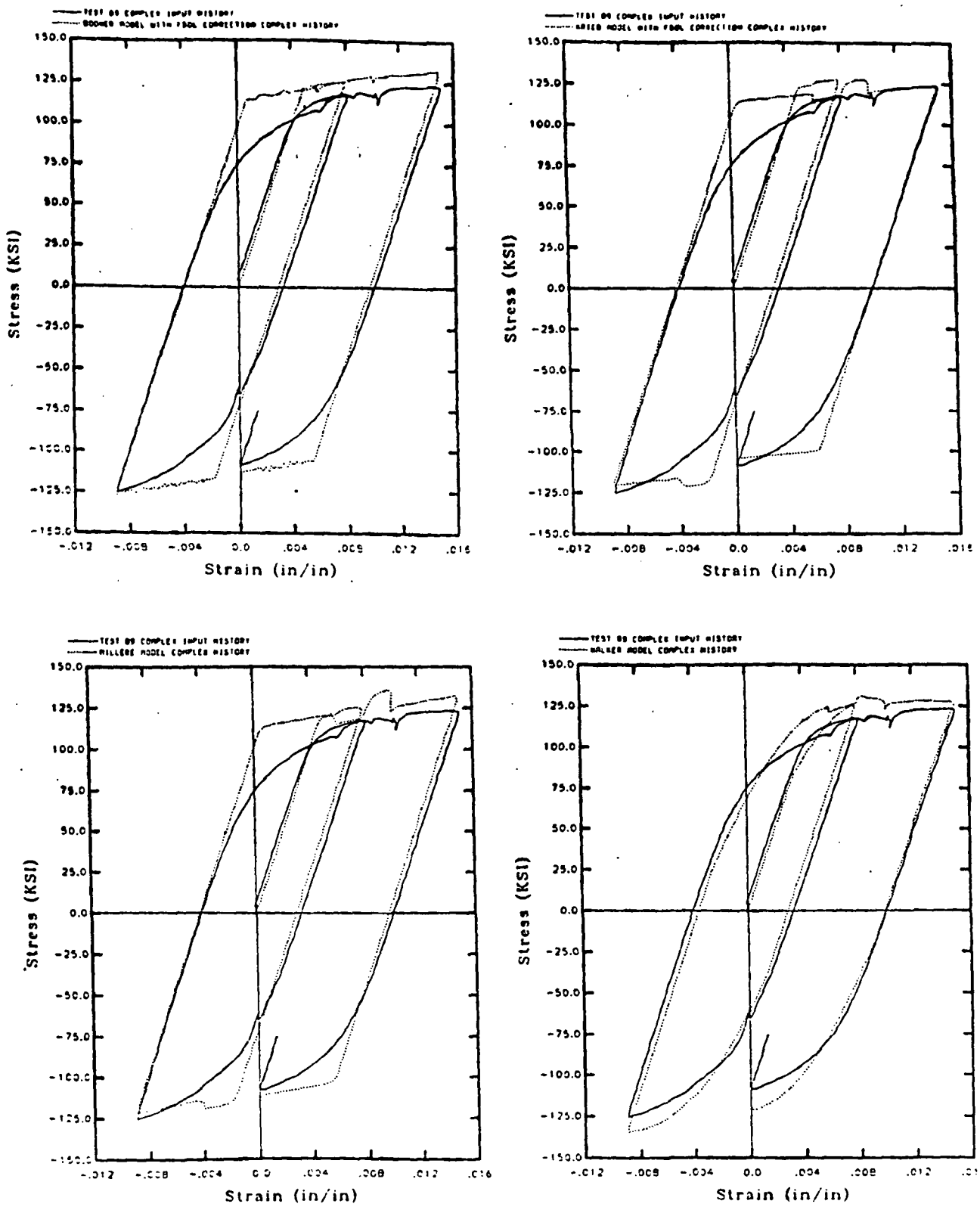

Figure 5. Comparison of Models to a Complex History Test

The addition of dynamic recovery terms to the directional growth law appears to help the strain rate sensitivity problem. Bodner's corrected model shows less response to strain rate jumps. This is due to hardening based on plastic work rate. Walker's correction for solute strengthening comes closest to reproducing the strain rate sensitivity. The correction applied to Bodner's model produces unstable response and a correction similar to Walker's should be considered. The correction factors negated the effects of thermal recovery during hold times for Bodner's and Krieg, et al's. models. The drag stress growth law of Walker provided the closet fit to data over several cycles at the higher strain rates. Lower strain rates showed Bodner's model handling cyclic response most effectively. Walker's model suffers from the lack of drag stress thermal recovery at the lowest strain rate.

These results show that the combination of exponential strain rate equations with dynamic recovery work best for this material system. Isotropic thermal recovery and exponential growth of the isotropic internal state variable are useful for modelling cyclic response.

Further details of this portion of the research are given in Appendix 6.5.

2.7 Integrated Software Development

Because of the vast number of constitutive theories available, only four candidate models were selected for this research. These include the work of Walker[6,9], Krieg, Swearengen, and Rohde[7], Bodner[6], and Schmidt and Miller[10]. These models were chosen primarily because they appear to be the most qualitatively attractive theories available and thus warrant further evaluation. For this paper, only the procedure developed for Walker's model will be presented.

The model proposed by Walker is a viscoplastic theory which uses an exponential type inelastic strain rate relation. The growth law modeling back stress is of the hardening/recovery format and accounts for both dynamic and static thermal recovery. The drag stress term models isotropic hardening, thus taking into account the cyclic hardening or softening characteristics of a material. The uniaxial differential form of Walker's exponential model may be written as:

$$\dot{\varepsilon}^I = \frac{\exp(\frac{\sigma-B}{D}) - 1}{\beta} \operatorname{sgn}(\sigma - B) \tag{10}$$

$$\dot{B} = n_2\dot{\varepsilon}^I - B\{[n_3 + n_4 \exp(-n_5|\log(\frac{\dot{R}}{\dot{R}_0})|]\dot{R} + n_6\} \ , \tag{11}$$

$$D = D_1 - D_2 \exp(-n_7 R) \ , \tag{12}$$

$$\dot{R} = |\dot{\varepsilon}^I| \ , \tag{13}$$

where σ is the applied stress, ε^I is the inelastic strain, B is the back stress, and D is the drag stress. A superposed dot above the variables denotes differentiation with respect to time. In addition, β , n_2, n_3, n_4, n_5, n_6, n_7, D_2 and D_2 are material parameters. Therefore, this model requires nine constants to be evaluated, along with selecting Young's Modulus E and the strain aging parameter $\dot{R}_0$.

The tests required to determine the constants for Walker's model using the following procedure include: 1) A series of constant strain rate steady state hysteresis loops under fully reversed strain controlled conditions; 2) cyclic hold tests performed on the unloading branch of the cyclic tests; and 3) long term monotonic tension tests. The monotonic tension tests may not be necessary if acceptable values of the limiting stress σ_{lim} can be obtained from the first half cycle of the cyclic tests.

The determination of the constants begins by plotting σ_{lim} versus $\ln(\dot{\varepsilon}^I)$. A nonlinear representation signifies that strain aging and/or thermal recovery effects are present and thus need to be modeled. If σ_{lim} is not obtained experimentally, it can be estimated in a manner similar to that proposed by Lindholm, et al.[6].

Under conditions of uniaxial tension loading, when $\dot{\varepsilon}^I$ is assumed to be a constant and equal to the applied strain rate, eq. (10) may be written as:

$$\sigma = D \ln(\beta\dot{\varepsilon}^I) + B \quad . \tag{14}$$

Using the evolution equation defining the back stress (eq. (11)) and on the physical basis that D remains constant during monotonic loading, then $d\sigma/d\varepsilon^I$ (or θ) may be written as:

$$\theta = n_2 - \beta[n_3 + n_4 \exp(-n_5 |\log(\frac{\dot{R}}{\dot{R}_0})|) + n_6/\dot{\varepsilon}^I] \quad . \tag{15}$$

Thus, equations (14) and (15), can be combined yielding

$$\theta = -N\sigma + [n_2 + ND\ln(\beta\dot{\varepsilon}^I)] \quad , \tag{16}$$

where

$$N = n_3 + n_4 \exp(-n_5 |\log(\frac{\dot{R}}{\dot{R}_0})|) + n_6/\dot{\varepsilon}^I \quad . \tag{17}$$

Therefore, equation (16) indicates that a plot of θ versus σ will be linear, having a slope of N and an x-intercept of σ_{lim} .

The constant n_5 is computed by determining where the effect of strain aging is considered negligible and may be written as:

$$n_5 = -[\ln(\tau)/|\log(\frac{\dot{R}}{\dot{R}_0})|] \quad . \tag{18}$$

The constants $\dot{R}_0$ and $\dot{R}_1$ represent the strain rate at which the strain aging correction is a maximum and minimum, respectively, and τ denotes the residual correction at rate $\dot{R}_1$. It should be noted that τ also affects the rate of decay of the strain aging correction and selection of too small of a value will result in a very localized correction.

The next step in this procedure is to compute the dynamic and static thermal recovery constants n_3, n_4, and n_6 using equation (17). Equation (17) can be rewritten a number of times, corresponding to the different monotonic tests as:

$$N_i = n_3 + n_4 f_i + n_6/\dot{\varepsilon}_i^I \quad , \tag{19}$$

where

$$f_i = \exp(-n_5|\log(\frac{\dot{R}}{\dot{R}_0})|) \quad . \tag{20}$$

Thus, the three parameters, n_3, n_4, and n_6, may be obtained simultaneously using a multiple linear regression scheme.

The constant n_2 is computed on the basis that B saturates to B_{lim} at large inelastic strains. Hence, $\dot{B}$=0 and equation (11) reduces to

$$B_{lim} = \frac{n_2}{n_3 + n_4 f + n_6/\dot{\varepsilon}^I} \quad . \tag{21}$$

If it is assumed that the ratio σ_{exp}/B_{exp} will remain the same for the limiting condition at sufficiently large inelastic strains, then

$$\frac{\sigma_{exp}}{B_{exp}} = \frac{\sigma_{lim}}{B_{lim}} \quad . \tag{22}$$

Substituting eq. (21) into (22) and solving for n_2 results in

$$n_2 = \frac{[n_3 + n_4 f + n_6/\dot{\varepsilon}^I]\sigma_{lim} B_{exp}}{\sigma_{exp}} \quad , \tag{23}$$

where σ_{lim} values are obtained from long term monotonic tension tests or θ-plots and σ_{exp} and B_{exp} values come from cyclic hold tests.

The initial value drag stress D_0 and the inelastic strain rate scaler β are determined by rewriting equation (14) using the limiting values of σ and B as:

$$\sigma_{lim} - B_{lim} = D_0 \ln(\dot{\varepsilon}^I) + D_0 \ln(\beta) \quad . \tag{24}$$

Since B_{lim} is given by equation (21), it can be substituted into (24) resulting in

$$\delta_{\sigma B} = D_0 \ln(\dot{\varepsilon}^I) + D_0 \ln(\beta) \quad , \tag{25}$$

where

$$\delta_{\sigma B} = \sigma_{lim} - \frac{n_2}{n_3 + n_4 + n_6/\dot{\varepsilon}^I} \quad . \tag{26}$$

Equation (25) indicates that a plot of $\delta_{\sigma B}$ versus $\ln(\dot{\varepsilon}^I)$ should be linear, having a slope of D_0 and an intercept of D $\ln(\beta)$ from which β can be found directly.

Up to this point, the only tests that were needed, in order to compute the material parameters, have been monotonic tension and cyclic hold tests. To obtain the isotropic hardening and recovery constants D_1, D_2, and n_1, saturated cyclic hysteresis data are required. By estimating the cumulative

inelastic strain from applied stress, E, and strain amplitude and assuming that D saturates to D_1, then n_7 can be approximated as:

$$n_7 = -\ln(\tau)/R_{avg} \quad , \tag{27}$$

where R_{avg} is the average of R for a number of tests and τ is an approximation of zero.

On the physical basis that B saturates much more rapidly than D, equation (14) can be written as:

$$D_{lim} = D_1 = \frac{\sigma_{lim} - B_{lim}}{\ln(\beta\dot{\varepsilon}^I)} \quad , \tag{28}$$

where

$$B_{lim} = n_2/N \quad . \tag{29}$$

The values of σ_{lim} and N in equations (28) and (29) are estimated from the θ-plot after cyclic saturation has occurred. If several tests are used, D_1 would be computed as the arithmetic mean.

The final parameter to determine is D_2. When R=0 equation (12) reduces to

$$D_0 = D_1 - D_2 \quad , \tag{30}$$

from which D_2 may be computed directly, completing the constant calculation procedure.

The computer algorithm used to compute the material parameter proceeds in the following manner:

1) Values of σ_{lim} and N from monotonic tension tests are computed using

equation (16) and a least squares procedure.

2) After selecting R_0, R_1 and τ, n_5 is evaluated using equation (18).

3) The parameters n_3, n_4, n_6 are determined from equations (19) and (20) using a multiple linear regression scheme.

4) The back stress hardening coefficient n_2 is computed directly by equation (23).

5) The constants D_0 and β are evaluated using equations (25) and (26) via a least squares procedure.

6) After computing the cumulative inelastic strain from the experimental data, n_7 is evaluated directly from equation (27).

7) D_1 and D_2 are computed using equation (28) and (30).

A method for obtaining the material parameters for Walker's model has been presented which is a synthesis of both physical and numerical approximations. The associated computer algorithm allows the user to use either a totally automated procedure or engineering intuition at selected points when computing constants. Numerical simulations of Inconel 718 at 1100°F are to be presented.

2.8 Conclusion

Several general conclusions can be made from the current research. These are as follows:

1) Euler's method is the most efficient for integrating the models of those methods considered herein;

2) Walker's model is the most economical to integrate, while Miller's model is least economical and also tends to be unstable;

3) ISV theory can be used as general framework for comparing all of the models in the current literataure;

4) a laboratory has been developed at Texas A&M which is capable of performing all of the complicated elevated temperature experiments necessary to perform the research detailed herein;

5) for aluminum at room temperature, none of the models considered herein appears to be very accurate in predicting uniaxial cyclic response;

6) at 1100°F Walker's model appears to be most accurate for predicting the uniaxial cyclic response of IN718.

2.9 References

1. Coleman, B.D., and Gurtin, M.E., "Thermodynamics with Internal State Variables," Journal of Chemical Physics, Vol. 47, pp. 597-613, 1967.

2. Coleman, B.D., and Noll, W., "The Thermodynamics of Elastic Materials with Heat Conduction and Viscosity," Archive for Rational Mechanics and Analysis, Vol. 13, p. 167, 1963.

3. Garofalo, F., Richmond, O. and Damis, W.F., "Design of Apparatus for Constant-Stress or Constant-Load Creep Tests," Journal of Basic Engineering, 84, 285 (1982).

4. Jones, W.B., Rhode, R.W. and Swearengen, J.C., "Deformation Modelling and the Strain Transient Dip Test," Mechanical Testing for Deformation Model Development, STP 785, ASTM, 102-118 (1982).

5. ASTM Thermocouple Handbook, STP 470A, ASTM, (1974).

6. Lindholm, U.S., Chan, K.S., Bodner, S.R., Weber, R.M., Walker, K.P., and Cassenti, B.N., "Constitutive Modeling for Isotropic Materials," CR-174980, NASA (HOST), (1985).

7. Krieg, R.D., Swearengen, J.C. and Rhode, R.W., "A Physically-based Internal Variable Model for Rate Dependent Plasticity," Proc. ASME/CSSME PVP Conference, 15-27, (1978).

8. Schmidt, C.G., A Unified Phenomenological Model for Solute Hardening, Strain Hardening, and Their Interactions in Type 316 Stainless Steel, Ph.D. Dissertation, Stanford University, Department of Materials Science and Engineering (1979).

9. Walker, K.P. and Wilson, D.A., "Creep Crack Growth Predictions in INCO 718 Using a Continuum Damage Model," 2nd Symposium on Nonlinear Constitutive Relations for High-Temperature Applications, Cleveland, OH, 1984.

10. Schmidt, C.G., A Unified Phenomenological Model for Solute Hardening, Strain Hardening, and Their Interactions in Type 316 Stainless Steel, Ph.D. Dissertation, Stanford University, Dept. of Materials Science and Engineering, 1979.

3. PUBLICATIONS LIST

3.1 Papers Published

1. Haisler, W.E., and Imbrie, P.K., "Numerical Considerations in the Development and Implementation of Constitutive Models," Proceedings Second Symposium on Nonlinear Constitutive Relations for High Temperature Applications, pp. 169-186, June, 1984 (Appendix 6.1).

2. Allen, D.H., and Beek, J.M., "On the Use of Internal State Variables in Thermoviscoplastic Constitutive Equations," Proceedings Second Symposium on Nonlinear Constitutive Relations for High Temperature Applications, pp. 83-102, June, 1984 (Appendix 6.3).3.2. Papers Submitted for Publication

3.2 Papers Accepted for Publication

1. G.H. James, P.K. Imbrie, P.S. Hill, D.H., Allen, and W.E. Haisler, "An Experimental Comparison of Several Current Viscoplastic Constitutive Models at Elevated Temperature," Proceedings Third Symposium on Nonlinear Constitutive Relations for High Temperature Applications, June, 1986 (Appendix 6.5 in part).

2. P.S. Hill, G.H. James, P.K. Imbrie, W.E. Haisler, and D.H. Allen, "An Automated Procedure for Material Parameter Evaluation and Uncertainty Analysis for Viscoplastic Constitutive Models," Proceedings Their Symposium on Nonlinear Constitutive Relations for High Temperature Applications, June, 1986.

3.3 Papers to be Submitted for Publication

1. Beek, J.M., and Allen, D.H., "A Comparison of Current Models for Nonlinear Rate-Dependent Material Behavior of Crystalline Solids," to be submitted to Journal Engineering Materials Technology (Appendix 6.4).

2. Imbrie, P.K., Haisler, W.E., and Allen, D.H., "Evaluation of the Numerical Stability and Sensitivity to Material Parameter Variations for Several Unified Constitutive Models," to be submitted to Journal Engineering Materials Technology (Appendix 6.2).

4. PROFESSIONAL PERSONNEL INFORMATION

4.1 Faculty Research Assignments

1. W.E. Haisler - Numerical code development, computer software/ hardware development, overall program coordination.

2. D.H. Allen - experimental equipment development, experimental testing program, constitutive model development.

4.2 Student Research Assignments

1. J.M. Beek - room temperature testing, model comparisons at room temperature.

2. P.K. Imbrie - numerical code development, computer software/ hardware development.

3. G.H. James - experimental equipment development, elevated tempera-ture testing.

4. P.S. Hill - evaluation of material constants, computer software development.

5. C. Wong - elevated temperature testing.

5. INTERACTIONS

5.1 Papers Presented

The following papers have been presented:

1. W.E. Haisler and P.K. Imbrie, "Numerical Considerations in the Development and Implementation of Constitutive Models," Second Symposium on Nonlinear Constitutive Relations for High Temperature Applications, June, 1984.

2. D.H. Allen and J.M. Beek, "On the Use of Internal State Variables in Thermoviscoplastic Constitutive Equations," Second Symposium on Nonlinear Constitutive Relations for High Temperature Applications, June, 1984.

The following papers are to be presented:

1. G.H. James, P.K. Imbrie, P.S. Hill, D.H. Allen, and W.E. Haisler, "An Experimental Comparison of Several Current Viscoplastic Constitutive Models at Elevated Temperature," Third Symposium on Nonlinear Constitutive Relations for High Temperature Applications, June, 1986.

2. P.S. Hill, G.H. James, P.K. Imbrie, W.E. Haisler, and D.H. Allen, "An Automated Procedure for Material Parameter Evaluation and Uncertainty Analysis for Viscoplastic Constitutive Models," Third Symposium on Nonlinear Constitutive Relations for High Temperature Applications, June, 1986.

5.2 Related Travel and Consultation

1. Drs. Haisler and Allen are consultants with the General Electric Aircraft Engine Business Group on NASA LeRC contract nos. NAS3-23698 and NAS3-24538.

2. Dr. Allen and several of his students have visited Drs. U.S. Lindholm, S. Bodner, and K. Chan on three occasions during the course of the contract at Southwest Research Institute, San Antonio.

APPENDIX

APPENDIX 6.1

NUMERICAL CONSIDERATIONS IN THE DEVELOPMENT AND IMPLEMENTATION OF CONSTITUTIVE MODELS

W.E. Haisler and P.K. Imbrie
Aerospace Engineering Department
Texas A&M University
College Station, Texas 77843

Several unified constitutive models were tested in uniaxial form by specifying input strain histories and comparing output stress histories. The purpose of the tests was to evaluate several time integration methods with regard to accuracy, stability, and computational economy. The sensitivity of the models to slight changes in input constants was also investigated. Results are presented for IN100 at 1350°F and Hastelloy-X at 1800°F.

INTRODUCTION

The characterization of the constitutive behaviour of metals has its roots in the early work of Tresca, Levy, vonMises, Hencky, Prandtl, Reuss, Prager, and Ziegler (Refs. 1-8). These early models are incremental in nature, assume that plasticity and creep can be separated, and they incorporate a yield function, flow rule, and hardening rule to define the plastic strain increment. These original incremental theories have been expanded and modified by many researchers so that they provide adequate, and often very good predictions of rate-independent plastic flow (see for example Refs. 9-10). However, they are sometimes criticized as having no formal micromechanical basis upon which to make the assumption of an uncoupling of the inelastic strain into rate-independent (plastic) and rate-dependent (creep) strain components. Nevertheless, the classical incremental theories are widely used.

During the last ten years, a number of unified constiutive models have been proposed which retain the inelastic strain as a unified quantity without aritifical separation into plasticity and creep components. These include the models developed by Bodner (Refs. 11-13), Stouffer (Refs. 14-15), Krieg (Ref. 16), Miller (Ref. 17), Walker (Refs. 18-19), Valanis (Refs. 20-21), Krempl (Ref. 22), Cernocky (Ref. 23-24), Hart (Ref. 25), Chaboche (Ref. 26), Robinson (Ref. 27), Kocks (Ref. 28), and Cescotto and Leckie (Ref. 29). The applicability of these viscoplastic constitutive theories (mostly to high temperature applications) has been investigated by several researchers. Walker (Ref. 19) compared the predictive capability of several models (Walker, Miller and Krieg) for Hastelloy-X at 1800°F. More recently, Milly and Allen

(Ref. 30) provided a qualitative as well as quantitative comparison of the models developed by Bodner, Krieg, Walker and Krempl for IN100. Both Refs. 19 and 30 conclude that these models generally provide adequate results for elevated isothermal conditions, they provide poor and overly-square results at low temperature, the material constants are often difficult to obtain experimentally, the resulting rate equations are "stiff" and sensitive to numerical integration, and the models do not provide any satisfactory transient temperature capability. Beek, Allen, and Milly (Ref. 31) have shown that all the unified viscoplastic models mentioned above can be cast in a functionally similar form (in terms of internal state variables).

None of the published literature provides a thorough evaluation of current viscoplastic constitutive models with comparison to experimental response for complex input histories. Such an evaluation is difficult at present for many reasons, namely: 1) Material constants for most models are usually available only for a single material and often for a single temperature; 2) The experimental procedures given by model developers for determining material constants from experimental data are often sketchy at best; 3) Material constants for some models are often obtained by trial-and-error and are not based on experiments; and 4) There is a lack of good experimental data against which the models can be evaluated (that is, test data which is significantly different from that used to generate the material constants).

The purpose of the present paper is to report some preliminary evaluations of several of the unified viscoplastic models (Bodner, Krieg, Miller, and Walker). These four models are evaluated with regard to 1) their sensitivity to numerical integration and 2) their sensitivity to slight changes in input material constants.

CONSTITUTIVE MODELS CONSIDERED

The constitutive theories which have been studied to date include Bodner's (Refs. 11-15), Krieg's (Ref. 16), Miller's (Ref. 17), and Walker's (Refs. 18-19). These particular models were selected for this initial study because material constants for Hastelloy-X were available for three of the models. Other models are currently being considered as material constants become available. Each model is listed below in uniaxial form using a consistent notation as presented by Beek, Allen and Milly (Ref. 31). In Ref. 31, it is shown that all of the current viscoplastic models considered may be written in uniaxial form as

$$\sigma = E(\epsilon - \alpha_1 - \epsilon^T) \qquad (1)$$

where σ is stress, E is Young's modulus, ϵ is strain, α_1 is the inelastic strain (internal state variable), and ϵ^T is the thermal strain. Each viscoplastic theory postulates a particular growth law for the internal state variable(s) and the inelastic strain is obtained by time integration of the growth law for α_1, i.e.

$$\alpha_1 = \int_{-\infty}^{t} \dot{\alpha}_1(t')dt' \tag{2}$$

where

$$\dot{\alpha}_1 = \frac{d\alpha_1}{dt} = \dot{\alpha}_i(\varepsilon, T, \alpha_2, \alpha_3, \ldots, \alpha_m) \tag{3}$$

In equations (2) and (3), t is time, T is temperature, α_2 is the back stress (related to the dislocation arrangement and produces kinematic hardening or the Bauschinger effect), and α_3 is the drag stress (which represents the dislocation density and produces isotropic hardening).

Bodner's Theory

The growth law for the inelastic strain in Bodner's model may be written in uniaxial form as

$$\dot{\alpha}_1 = \frac{2}{\sqrt{3}} D_o \exp\left[-\left(\frac{n+1}{2n}\right)\left(\frac{\sigma}{\alpha_3}\right)^{-2n}\right] \operatorname{sgn}(\sigma) \tag{4}$$

where

$$\dot{\alpha}_3 = m(Z_1 - \alpha_3)\dot{W}_p - AZ_1\left(\frac{\alpha_3 - Z_I}{Z_1}\right)^r \tag{5}$$

$$\dot{W}_p = \sigma\,\dot{\alpha}_i \tag{6}$$

The quantities E, D_o, n, m, Z_I, A, Z_1 and r are material constants. As noted before, the variable α_3 is similar to the drag stress used in many models (a measure of isotropic hardening or dislocation density). It is noted that the model contains no parameter representing the back stress and cannot account for the Bauschinger effect in kinematic hardening materials. The material constants are tabulated for IN100 at 1350°F (732°C) in Table 1 (taken from Ref. 14).

Krieg's Theory

The inelastic strain growth law for the model developed by Krieg and coworkers may be written in terms of state variables representing back stress and drag stress:

$$\dot{\alpha}_1 = C_1 \left(\frac{|\sigma - \alpha_2|}{\alpha_3} \right)^{C_2} \operatorname{sgn}(\sigma - \alpha_2) \tag{7}$$

$$\dot{\alpha}_2 = C_3 \dot{\alpha}_1 - C_4 \alpha_2^2 [\exp(C_5 \alpha_2^2) - 1] \operatorname{sgn}(\alpha_2) \tag{8}$$

$$\dot{\alpha}_3 = C_6 |\dot{\alpha}_1| - C_7 (\alpha_3 - \alpha_{3_o})^n \tag{9}$$

The model contains ten constants (C_1, C_2 . . . , C_7, E, α_{3_o}, and n). These have been evaluated by Walker (Ref. 19) for Hastelloy-X at 1800°F (982°C) and are tabulated in Table 2. It should be noted that equations (7), (8) and (9) form a coupled set of ordinary differential equations.

Miller's Theory

The growth laws for Miller's model may be written in uniaxial form as

$$\dot{\alpha}_1 = B\theta' \left[\sinh \left(\frac{|\sigma - \alpha_2|}{\alpha_3} \right)^{1.5} \right]^n \operatorname{sgn}(\sigma - \alpha_2) \tag{10}$$

$$\dot{\alpha}_2 = H_1 \dot{\alpha}_1 - H_1 B\theta' [\sinh (A_1 |\alpha_2|)]^n \operatorname{sgn}(\alpha_2) \tag{11}$$

$$\dot{\alpha}_3 = H_2 |\dot{\alpha}_1| \left(C_2 + |\alpha_2| - \frac{A_2}{A_1} \alpha_3^3 \right) - H_2 C_2 B\theta' \left[\sinh \left(A_2 \alpha_3^3 \right) \right]^n \tag{12}$$

Miller's theory contains nine constants which are tabulated for Hastelloy-X at 1800°F (982°C) in Table 3 (see Ref. 19).

Walker's Theory

Walker's nonlinear viscoplastic theory can be cast in the following uniaxial form

$$\dot{\alpha}_1 = \left(\frac{|\sigma - \alpha_2|}{\alpha_3}\right)^n \operatorname{sgn}(\sigma - \alpha_2) \tag{13}$$

$$\dot{\alpha}_2 = (n_1 + n_2)\dot{\alpha}_1 - (\alpha_2 - \alpha_{2_o} - n_1\alpha_1)\left\{|\dot{\alpha}_1| \frac{\partial}{\partial R}\left[(n_3 + n_4 R)\ln\left(\frac{n_5 R}{1+n_6 R} + 1\right)\right]\right.$$

$$\left. + n_7 |\alpha_2 - \alpha_{2_o}|^{m-1}\right\} \tag{14}$$

$$\dot{\alpha}_3 = n_8 |\dot{\alpha}_1| - n_9 |\dot{\alpha}_1|\alpha_3 - n_{10} (\alpha_3 - \alpha_{3_o})^q \tag{15}$$

where R is the cumulative inelastic strain

$$R = \int_o^t \left|\frac{\partial \alpha_1}{\partial t'}\right| dt' \tag{16}$$

The general model requires sixteen constants (E, n, m, q, n_1, n_2, . . . , n_{10}, α_{2_o} and $\alpha_3(t=0)$. In determining the constants for Hastelloy-X at 1800°F (982°C), Walker made several simplifying assumptions [including α_3 = constant = $\alpha_3(t=0)$] which reduces the number of parameters to those shown in Table 4 (see Ref. 19). Further, the constants reported in Ref. 19 were developed from tests using strain rates in the range 10^{-3} to 10^{-6} sec^{-1} and strain ranges of ±0.6%.

NUMERICAL TIME INTEGRATION STUDY

The integration of the constitutive relationship given by equations (1), (2) and (3) forms an integral and extremely important part in any numerical solution of a nonlinear field problem. It has been observed by many researchers that the coupled system of ordinary differential equations defining the state variables may be locally "stiff" and thus are sensitive to the time step size and numerical algorithm. The accurate integration of these stiff equations can be accomplished by various means: use of small time steps, higher-order or multi-point integration schemes, subincrementation

procedures (Refs. 33-35), "smart" algorithms which attempt to select appropriate time steps in order to achieve accuracy and stability (Refs. 36,37), algorithms tailored for individual constitutive theories (Refs. 32,37), or combinations of these approaches. In general, the computation time required for the accurate solution of materially nonlinear problems is directly related to the numerical integration scheme used.

Regarding the constitutive models reviewed herein, Walker (Ref. 32) uses a stable, iterative implicit scheme which takes advantage of the functional form of the integrand in the development of the reccurence relation. Miller originally used Gear's method (Ref. 36) to integrate the stiff equations in his theory but later concluded in Ref. 37 that an implicit backward difference method was more economical and preferable to either Gear's method or the explicit Euler forward integration method. The type of numerical integration scheme used by Bodner and Krieg is not known.

The selection of an appropriate time integration scheme to be used in a computer code is very important but is often based on the answers to such questions as: "What is available in the present code?", "What will work most of the time?", "What can we use that most users will understand?", "What is the cheapest and easiest to use?", and the like. The usual response given is "it depends on the problem being solved!"

In general, equation (3) may be integrated between time t and t + Δt by writing

$$\int_t^{t+\Delta t} d\alpha_1 = \int_t^{t+\Delta t} \dot{\alpha}_1 \, dt \tag{17}$$

or

$$\Delta\alpha_1 = \alpha_1(t + \Delta t) - \alpha_1(t) = \int_t^{t+\Delta t} \dot{\alpha}_1 \, dt \tag{18}$$

where $\dot{\alpha}_1$ is defined by the particular constitutive theory being used. The present investigation considers four integration schemes: explicit Euler forward integration, implicit trapezoidal method, trapezoidal predictor-corrector (iterative) method, and Runge-Kutta 4th order method. The approximations for each of these methods is given in Table 5.

Each of the integration schemes in Table 5 were used to obtain stress-time and stress-strain responses for the four constitutive models considered herein when subjected to the uniaxial, alternating square-wave strain-rate history shown in Fig. 1. Figure 1 shows the 35 second response obtained

by Krieg's theory for Hastelloy-X at 1800°F using a time step of 0.1 seconds. For this time step, the Euler and trapezoidal predictor-corrector methods provide essentially the same results and are virtually identical to that obtained for all methods using a time step of 0.005 seconds. The 4th order Runge-Kutta method generally overestimates the peak response while the trapezoidal method underestimates the response. Figure 2 presents results for three integration methods such that the total computation time for a 35 second response solution is approximately the same. For equivalent computation times, the Euler method provides the most accurate results although smaller time steps are required. Similar results are observed for Miller's model.

Figures 3 and 4 illustrate that various constitutive models may behave appreciably different using the same integration method (in this case the Euler method). In Fig. 3, Miller's theory (for Hastelloy-X at 1800°F) gives considerable oscillatory response for a time step of 0.005 seconds while Walker's theory shown in Fig. 4 gives a much smoother response for the same time step. Comparing Figs. 3 and 4, it is seen that a smaller time step is required (with Euler integration) in Miller's theory than in Walker's theory.

Figure 5 presents results for IN100 at 1350°F using Bodner's model. Time steps were chosen for each integration scheme to obtain solutions which required approximately equal computation times. These results, when compared to solutions with much smaller time steps, indicate that the Euler method provides the most accurate results. Again, the time step used is smaller than that for the other methods but the computation time is the same (for integrating the constitutive equations).

SENSITIVITY STUDY FOR MATERIAL CONSTANTS

In the previous section, results were presented which showed how the numerical integration method used to integrate the constitutive equations could affect the accuracy and computation times of predicted results for stress-time and stress-strain responses. In this section, we consider another important parameter in the application of any constitutive theory. Namely, "how does the accuracy to which material constants are determined from experimental test data affect the predicted response?"

Figures 6 and 7 present results for Walker's model (Hastelloy-X at 1800°F subjected to an alternating square-wave strain-rate history as shown) wherein specified input material constants have been adjusted by 5%. Figure 6 shows the effect of a -5% change (error) in the stress exponent n (the most sensitive parameter). Figure 7 shows that a +5% error in all test data required to compute material constants results in significant predicted response errors, up to 30% over-prediction in the stress at a time of 35 seconds (during the relaxation period).

Figures 8 and 9 present similar results for Krieg's model (Hastelloy-X at 1800°F) and Bodner's model (IN100 at 1350°F), respectively. Both results indicate that the most sensitive parameter is the stress exponent "n" and

that a 5% error in specifying n may produce significant errors in the predicted response. Miller's model appears to be much less sensitive to errors in input material parameters.

Figure 10 provides a comparison of the Miller, Krieg, and Walker models for the Hastelloy-X test at 1800°F (using constants obtained by Walker for all models). The Euler method was used with a time step of 0.0005 seconds which provides a solution with no significant truncation error. The results obtained here show approximately 10-15% differences in peak stress amplitudes between the three constitutive models. Since no experimental results are available at this time, no conclusions can be drawn as to which model more accurately represents observed test data. However, the results do point out that significant differences (greater than 15%) can be obtained for stress peaks and stress relation values through the use of different constitutive models.

CONCLUSIONS AND FUTURE WORK

The results of this study are not complete since only a portion of the available constitutive models and numerical integration schemes have been considered. However, some tentative conclusions can be reached. First, it appears clear from the present investigation, and the work of others, that simple integration schemes (like the Euler forward defference method) are often preferable to more complex schemes from the standpoint of accuracy, computation time, and ease of implementation. Although not reported herein, our work in progress indicates that Euler's method used with a simple subincrementation strategy provides the most accurate and economical solution for most constitutive models.

The sensitivity study on material constants indicates that most viscoplastic constitutive models are significantly sensitive to one or more material constants derived from laboratory tests. It has been shown that a 5% "error" in laboratory measurements may lead to errors of 25%, or greater, in predicted stress responses. Although most model developers have fine-tuned their models and input material constants for specific material/temperature/strain-rate combinations, it is not clear that end-users will be able to do so when called upon to develop material constants for a new situation. The problem can be negated to some extent by defining more explicit testing procedures for obtaining material constants and by guidelines defining which constants are most sensitive to experimental error.

Our current and future work concerns the application of several integration schemes to the other constitutive theories, investigation of subincremental strategies, and consideration of "smart" integration methods which detect local "stiffness" and adjust time steps but without significant computational expense. The material parameter sensitivity study will be continued by considering other constitutive theories, and more importantly, by comparison with laboratory tests which involve complex thermomechanical loadings including transient temperature inputs.

ACKNOWLEDGEMENT

The authors gratefully acknowledge the financial support for this research by NASA Lewis Research Center under Grant no. NAG3-491.

REFERENCES

1. Tresca, H., "Notes on Yield of Solid Bodies Under Strong Pressures," Comptes Rendus del' Academie des Sciences, Vol. 59, p. 754, 1864.
2. Levy, M., "Memoire sur les equations generales des mouvements interieurs des corps solides ductiles au dela des limites ou l'elasticite pourrait les ramener a leur premier eata.," C.R. Acad. Sci. (Paris), Vol. 70, pp. 1323-1325, 1870.
3. von Mises, R., "Mechanik der Festen Koerper im plastisch deformablen Zustant," Goettinger Nachr., Math.-Phys., Kl, pp. 582-592, 1913.
4. Hencky, H., "Zur Theorie Plastischer Deformationen und die Hierduch im Material Hervorgerufenen Nach-Spannungen," Z. ang. Math. Mech., Vol. 4, pp. 323-334, 1924.
5. Prandtl, L., "Spannungsverteilurg in Plastischen Koerpen," Proceedings of the First International Congress on Applied Mechanics, Delft, Technische Boekhandel en Druckerin, Jr. Waltman, Jr., pp. 43-45, 1925.
6. Reuss, E., "Bereuchkisichtigung der Elastischen Formaenderungen in der Plastizitaetstheorie," Zeitschrift fuer Angewandte Mathematic und Mechanik, Vol. 10, pp. 266-274, 1930.
7. Prager, W., "The Theory of Plasticity: A Survey of Recent Achievements," Proceedings of the Institution of Mechanical Engineers, London, Vol. 169, pp. 41-57, 1955.
8. Ziegler, H., "A Modification of Prager's Hardening Rule," Quarterly of Applied Mathematics, Vol. XVIII, pp. 55-65, 1959.
9. Allen, D.H. and Haisler, W.E., "A Theory for Analysis of Thermoplastic Materials," Computers and Structures, Vol. 13, pp. 125-135, 1981.
10. Haisler, W.E. and Cronenworth, J., "An Uncoupled Viscoplastic Constitutive Model for Metlas at Elevated Temperature," Proceedings of the 24th AIAA Structures, Structural Dynamics and Materials Conference, Lake Tahoe, Nevada, May 2-4, 1983.
11. Bodner, S.R. and Partom, Y., "Constitutive Equations for Elastic-Viscoplastic Strain-Hardening Materials," Journal of Applied Mechanics, Vol. 42, No. 2, pp. 385-389, 1975.
12. Merzer, A. and Bodner, S.R., "Analytical Formulation of a Rate and Temperature Dependent Stress-Strain Relation," Journal of Engineering Materials and Technology, Vol. 101, pp. 254-257, 1979.
13. Bodner, S.R., "Representation of Time Dependent Mechanical Behaviour of Rene 95 by Constitutive Equations," Air Force Materials Laboratory, AFML-TR-4116, 1979.
14. Stouffer, D.C., "A Constitutive Representation for IN100," AFWAL-TR-81-4039, Air Force Materials Laboratory, June 1981.
15. Stouffer, D.C. and Bodner, S.R., "A Relationship Between Theory and Experiment for a State Variable Constitutive Equation," ASTM Special Technical Publication 785, 1982 (also AFWAL-TR-80-4194, 1981).

16. Krieg, R.D., Swearengen, J.C., and Rohde, R.W., "A Physically-Based Internal Variable Model for Rate-Dependent Plasticity," Proceedings ASME/CSME/PVP Conference, pp. 15-27, 1978.
17. Miller, A.K., "An Inelastic Constitutive Model for Monotonic, Cyclic, and Creep Deformation: Part I--Equations Development and Analytical Procedures" and "Part II--Application to Type 304 Stainless Steel," ASME Journal of Engineering Materials and Technology, pp. 97-113, April 1976.
18. Walker, K.P., "Representation of Hastelloy-X Behavior at Elevated Temperature with a Functional Theory of Viscoplasticity," Presented at the ASME Pressure Vessels Conference, San Francisco, 1980, also ASME Journal of Engineering Materials and Technology, 1981.
19. Walker, K.P., "Research and Development Program for Nonlinear Structural Modeling with Advanced Time-Temperature Dependent Constitutive Relationships," PWA-5700-50, United Technologies Research Center, (also NASA CR-165533), 1981.
20. Valanis, K.C., "A Theory of Viscoplasticity Without a Yield Surface - Part I. General Theory," and "Part II. Application to Mechanical Behavior of Metlas," Archives of Mechanics, Vol. 23, pp. 517-533, 1971.
21. Valanis, K.D., "On the Foundations of the Endochronic Theory of Viscoplasticity," Archives of Mechanics, Vol. 27, pp. 857-868.
22. Krempl, E., "On the Interaction of Rate and History Dependence in Structural Materials," Acta Mechanica, Vol. 22, pp. 53-90, 1975.
23. Cernocky, E.P. and Krempl, E., "A Nonlinear Uniaxial Integral Constitutive Equation Incorporating Rate Effects, Creep and Relaxation," International Journal of Nonlinear Mechanics, Vol. 14, pp. 183-205, 1979.
24. Cernocky, E.P. and Krempl, E., "A Theory of Thermoviscoplasticity Based on Infinitesimal Total Strain," International Journal for Solids and Structures, Vol. 16, pp. 723-741, 1980.
25. Hart, E.W., "Constitutive Relations for the Nonelastic Deformation of Metals," ASME Journal of Engineering Materials and Technology, Vol. 98-H, p. 193, 1976.
26. Cailletaud, G. and Chaboche, J.L., "Macroscopic Description of the Microstructural Changes Induced by Varying Temperature: Example of IN100 Cyclic Behaviour," Third International Conference on Mechanical Behaviour of Materials, Vol. 2, pp. 22-32, ICM3, Cambridge, England, August 1979.
27. Robinson, E.N., "A Unified Creep-Plasticity Model for Structural Metals at High Temperatures," ORNL-TM-5969, October 1978.
28. Kocks, U.F., "Laws for Work-Hardening and Low-Temperature Creep," Journal of Engineering Materials and Technology, Vol. 98-H, pp. 76-85, 1976.
29. Cescotto, S. and Leckie, F., "Determination of Unified Constitutive Equations for Metals at High Temperature," Proceedings of the International Conference on Constitutive Laws for Engineering Materials, pp. 105-111, 1983.
30. Milly, T.M. and Allen, D.H., "A Comparative Study of Nonlinear Rate-Dependent Mechanical Constitutive Theories for Crystalline Solids at Elevated Temperature," VPI-E-82-5, Virginia Polytechnic Institute and State University, March 1982.

31. Beek, J.M., Allen, D.H., and Milly, T.M., "A Qualitative Comparison of Current Models for Nonlinear Rate-Dependent Material Behaviour of Crystalline Solids," MM 4246T-83-14, Mechanics and Materials Research Center, Texas A&M University, November 1983.
32. Walker, K.P., "Research and Development Program for Nonlinear Structural Modeling with Advanced Time-Temperature Dependent Constitutive Relations," First Quarterly Technical Narrative, NAS3-22055, January 1980.
33. Bushnell, D., "A Subincremental Strategy for Solving Proglems Involving Large Deflections, Plasticity and Creep," in Constitutive Equations in Viscoplasticity: Computational and Engineering Aspects, AMD Vol. 20 (ASME), p. 171, 1976.
34. Krieg, R.D. and Key, S.W., "Implementation of a Time Independent Plasticity Theory into Structural Computer Programs," in Constitutive Equations in Viscoplasticity: Computational and Engineering Aspects, AMD Vol. 20 (ASME), p. 125, 1976.
35. Zaphir, Z. and Bodner, S.R., "Implementation of Elastic-Viscoplastic Constitutive Equations into NDNSAP with Applications to Fracture Mechanics," presented at the MIT Conference on ADINA, 1979.
36. Gear, C.W., "The Automatic Integration of Ordinary Differential Equations," Communications of ACM, Vol. 14, p. 176, 1971.
37. Miller, A.K. and Shih, C.F., "An Improved Method for Numerical Integration of Constitutive Equations of the Work Hardening-Recovery Type," ASME Journal of Engineering Materials and Technology, Vol. 99-H, p. 275, 1977.

Table 1. Material Constants Used in Bodner's Model for IN100 at 1350°F (732°C)

Bodners notation	Beek and Allen's notation	Numerical Value
E	E	21.3×10^{6} psi
n	n	0.7
Z_1	Z_1	1.105×10^{6} psi
m	m	2.57×10^{3} psi^{-1}
D_o	D_o	10^{4} sec^{-1}
A	A	1.9×10^{-3} sec^{-1}
r	r	2.66
Z_I	Z_I	0.6×10^{6} psi
$\varepsilon^p(t=0)$	$\alpha_1(t=0)$	0.0
Z_o	$\alpha_3(t=0)$	0.915×10^{6} psi

Table 2. Material Constants Used in Krieg's Model for Hastelloy-X at 1800°F (982°C)

Walker's notation for Krieg's constants	Beek and Allen's notation	Numerical Value
	C_1	1.0
n	C_2	4.49
A_1	C_3	1.0×10^{6} psi
A_2	C_4	6.21×10^{-6} psi^{-1} sec^{-1}
A_3	C_5	4.027×10^{-7} psi^{-2}
A_4	C_6	100 psi $sec^{1/n}$
A_5	C_7	4.365 psi^{1-n} $sec^{1/n-2}$
E	E	13.2×10^{6} psi
K_o	α_{3_o}	59,292 psi $sec^{1/n}$
n	n	4.49
c(t=0)	$\alpha_1(t=0)$	0.0
$\Omega(t=0)$	$\alpha_2(t=0)$	0.0
K(t=0)	$\alpha_3(t=0)$	59,292 psi

Table 3. Material Constants Used in Miller's Model for Hastelloy-X at 1800°F (982°C)

Miller's notation	Beek and Allen's notation	Numerical Value
n	n	2.363
$B\theta'$	$B\theta'$	2.616×10^{-5} sec^{-1}
H_1	H_1	1×10^{6} psi
A_1	A_1	1.4053×10^{-3} psi^{-1}
H_2	H_2	100 psi $sec^{1/n}$
C_2	C_2	5,000 psi
A_2	A_2	4.355×10^{-12} psi^{-3}
E	E	13.2×10^{6} psi
$\varepsilon(t=0)$	$\alpha_1(t=0)$	0.0
R(t=0)	$\alpha_2(t=0)$	0.0
D_o	$\alpha_3(t=0)$	8,642 psi

Table 4. Material Constants Used in Walker's Model for Hastelloy-X at 1800°F (982°C)

Walker's notation	Beek and Allen's notation	Numerical Value
$\overset{\circ}{\Omega}$	α_2	-1,200 psi
n_1	n_1	0 psi (not used)
n_2	n_2	1×10^6 psi
n_9	*	312.5
n_7	n_7	2.73×10^{-3} psi^{1-m} sec^{-1}
n	n	4.49
m	m	1.16
E	E	13.2×10^6 psi
c(t=0)	$\alpha_1(t=0)$	0.0
$\Omega(t=0)$	$\alpha_2(t=0)$	0.0
K(t=0)	$\alpha_3(t=0)$	59,292 psi
	n_8, n_9, n_{10}, q	0 (not used)

$$* = \frac{\partial}{\partial R} \left[(n_3 + n_4 R) \ \ell n \left(\frac{n_5 R}{1+n_6 R} + 1 \right) \right]$$

Table 5. Numerical Integration Approximation for $\Delta\alpha_1 = \int_t^{t+\Delta t} \dot{\alpha}_1 \, dt$

Method	Approximation
Euler Forward Difference	$\Delta\alpha_1 = \Delta t \ \dot{\alpha}_1(t)$
Trapezoidal Rule	$\Delta\alpha_1 = \frac{\Delta t}{2}[\dot{\alpha}_1(t) + \dot{\alpha}_1(t+\Delta t)]$
Trapezoidal Predictor-Corrector	Same as trapezoidal except iterate
Runge-Kutta 4th Order	$\Delta\alpha_1 = \frac{1}{6}(K_1 + 2K_2 + 2K_3 + K_4)$
	$K_1 = \Delta t \ \dot{\alpha}_1(t, \alpha_1(t))$
	$K_2 = \Delta t \ \dot{\alpha}_1(t+\Delta t/2, \alpha_1(t)+K_1/2)$
	$K_3 = \Delta t \ \dot{\alpha}_1(t+\Delta t/2, \alpha_1(t)+K_2/2)$
	$K_4 = \Delta t \ \dot{\alpha}_1(t+\Delta t, \alpha_1(t)+K_3)$

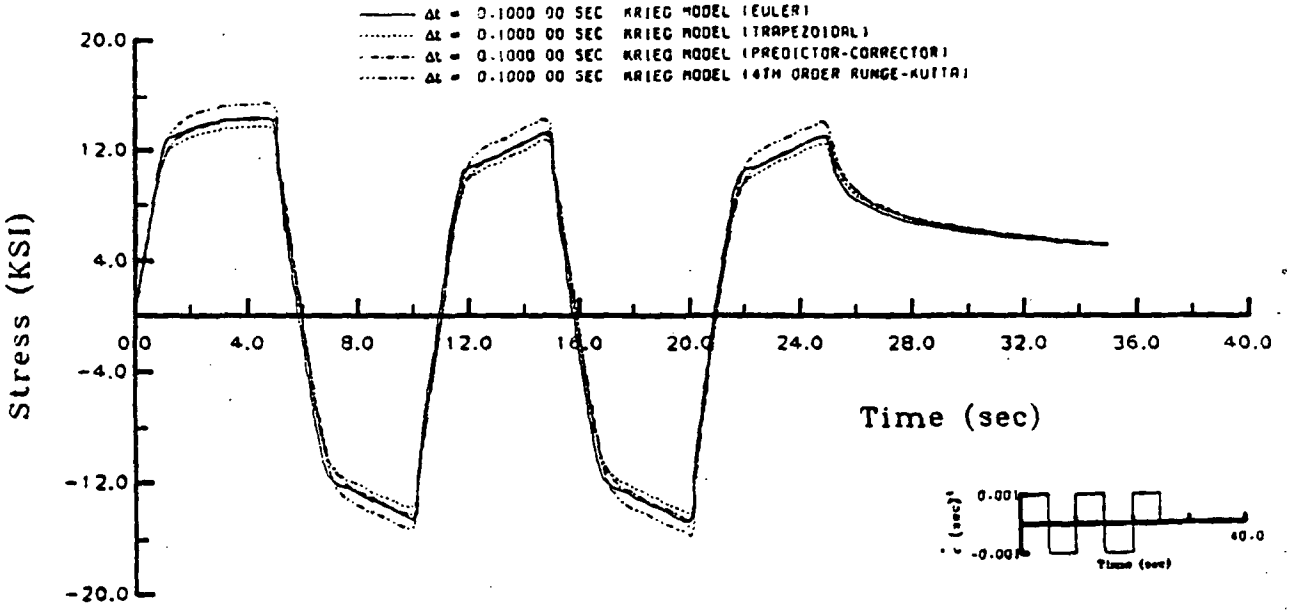

Fig. 1 Comparison of integration methods for Krieg's theory (Hastelloy-X at 1800°F)

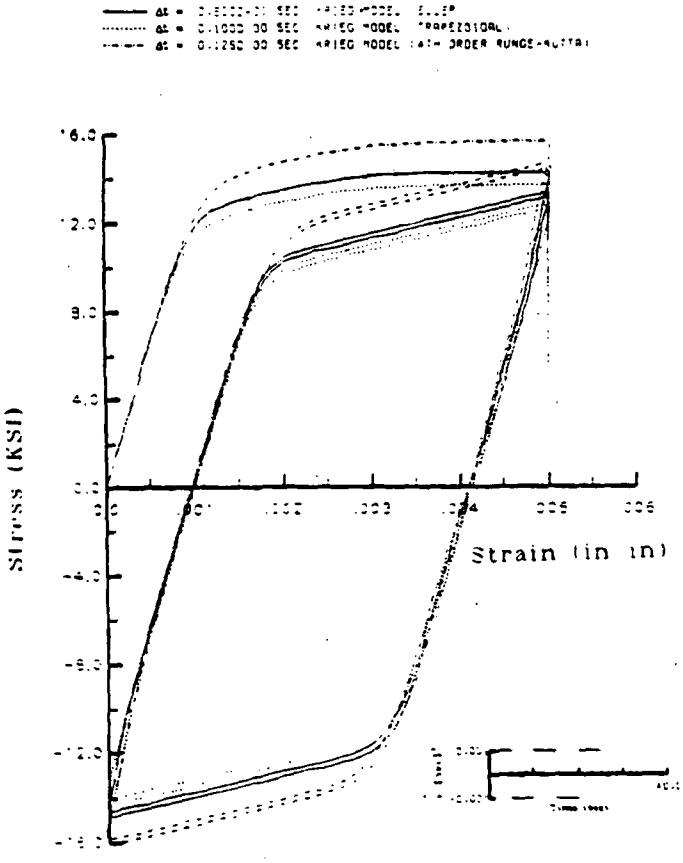

Fig. 2 Comparison of integration methods for Kreig's thoery with equal computation time allowed for each method (Hastelloy-X at 1800°F)

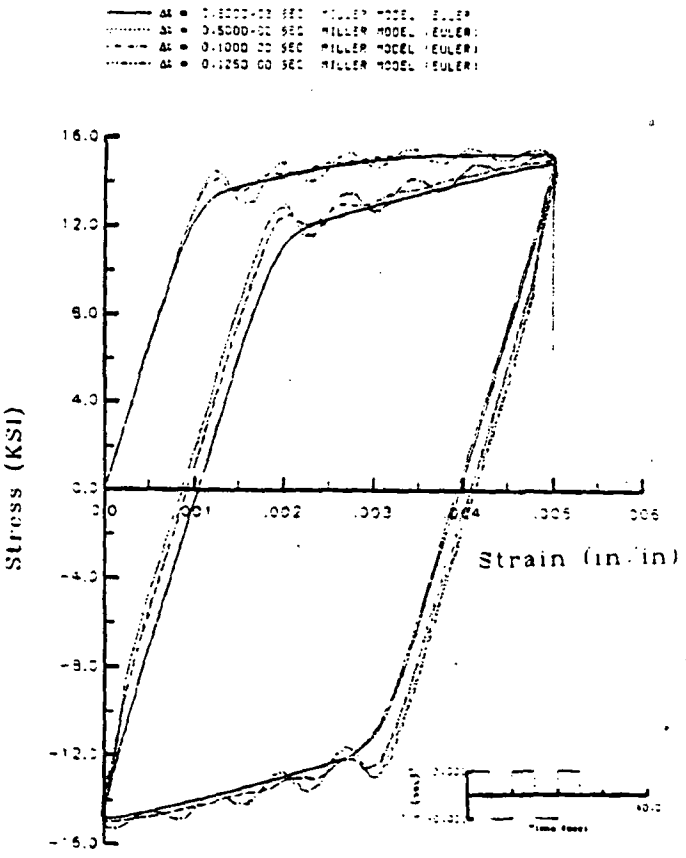

Fig. 3 Stability and accuracy of Euler's method for Miller's theory (Hastelloy-X at 1800°F)

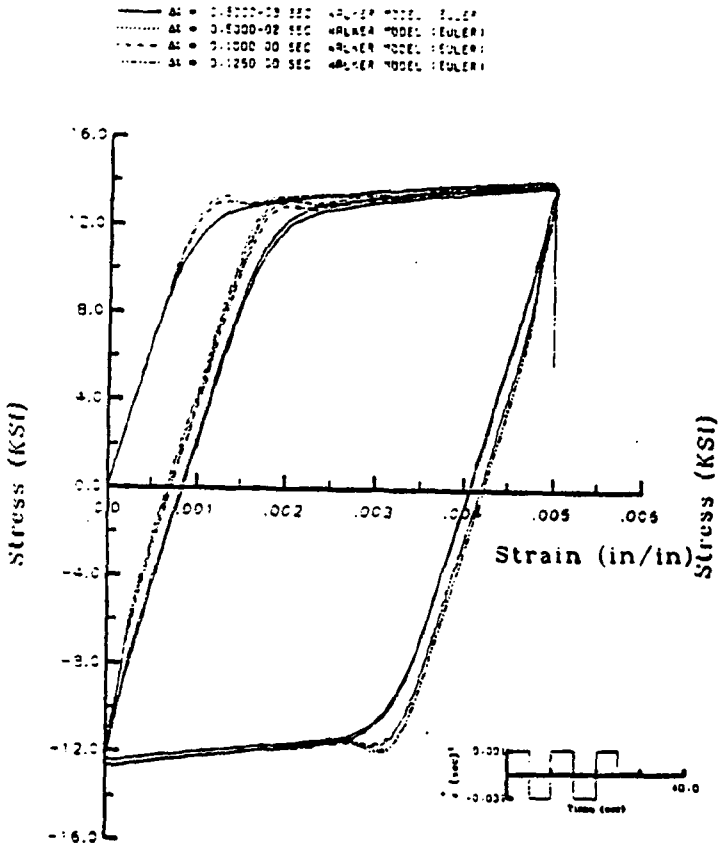

Fig. 4 Stability and accuracy of Euler's method for Walker's theory (Hastelloy-X at 1800°F)

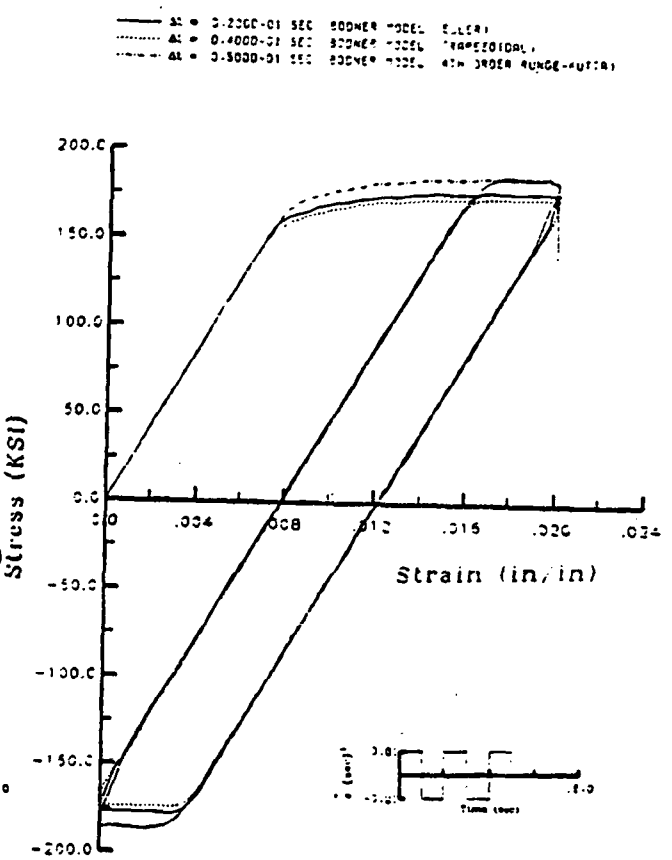

Fig. 5 Comparison of integration methods for Bodner's theory with equal computation time allowed for each method (IN100 at 1350°F)

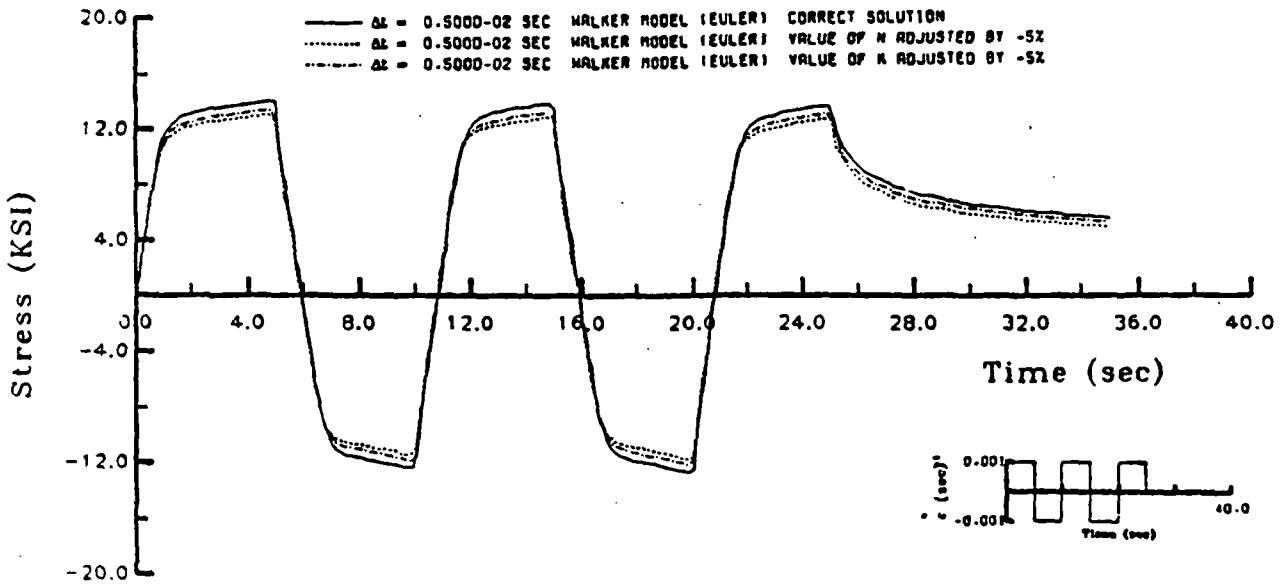

Fig. 6 Sensitivity of Walker's theory to -5% change in input constants (Hastelloy-X at 1800°F)

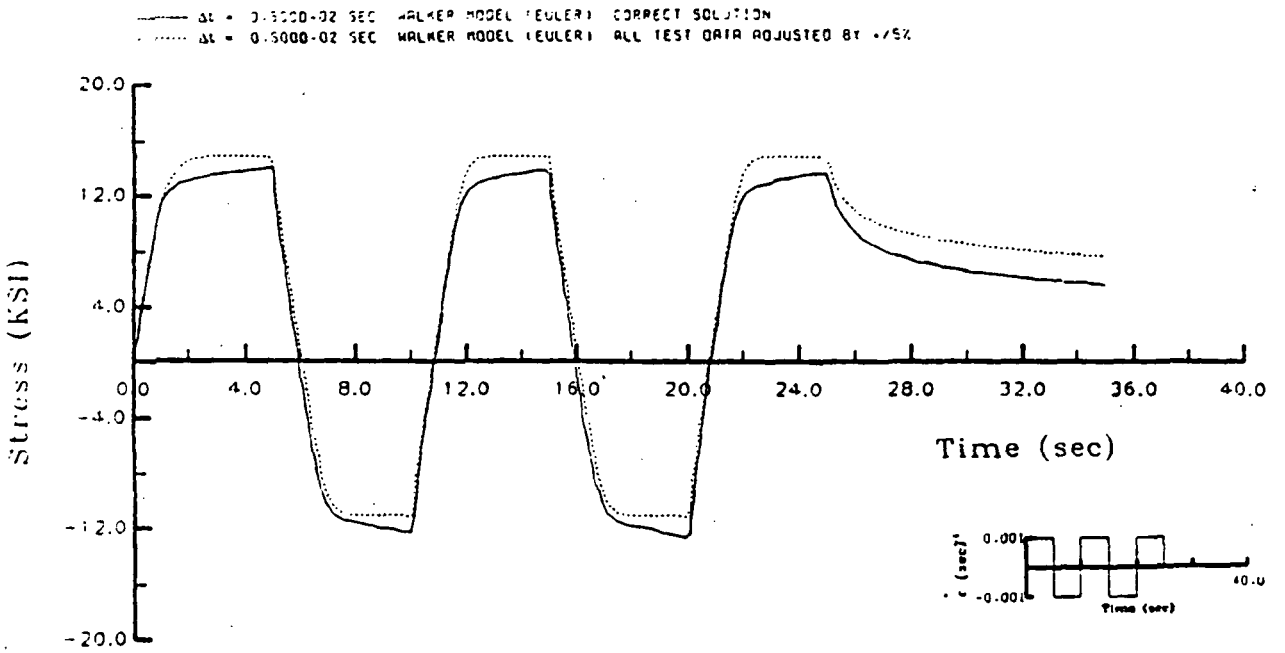

Fig. 7 Sensitivity of Walker's theory to 5% change in experimental test data used to generate constants (Hastelloy-X at 1800°F)

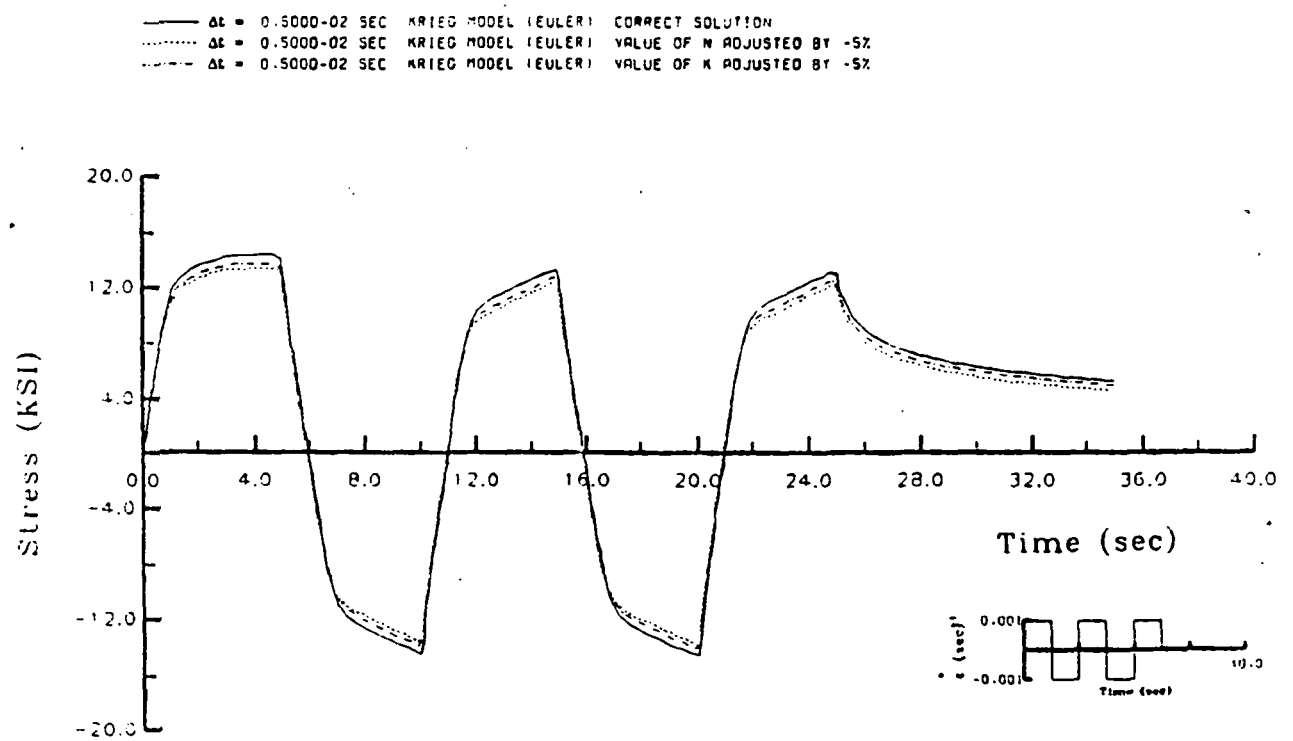

Fig. 8 Sensitivity of Krieg's theory to -5% change in input constants (Hastelloy-X at 1800°F)

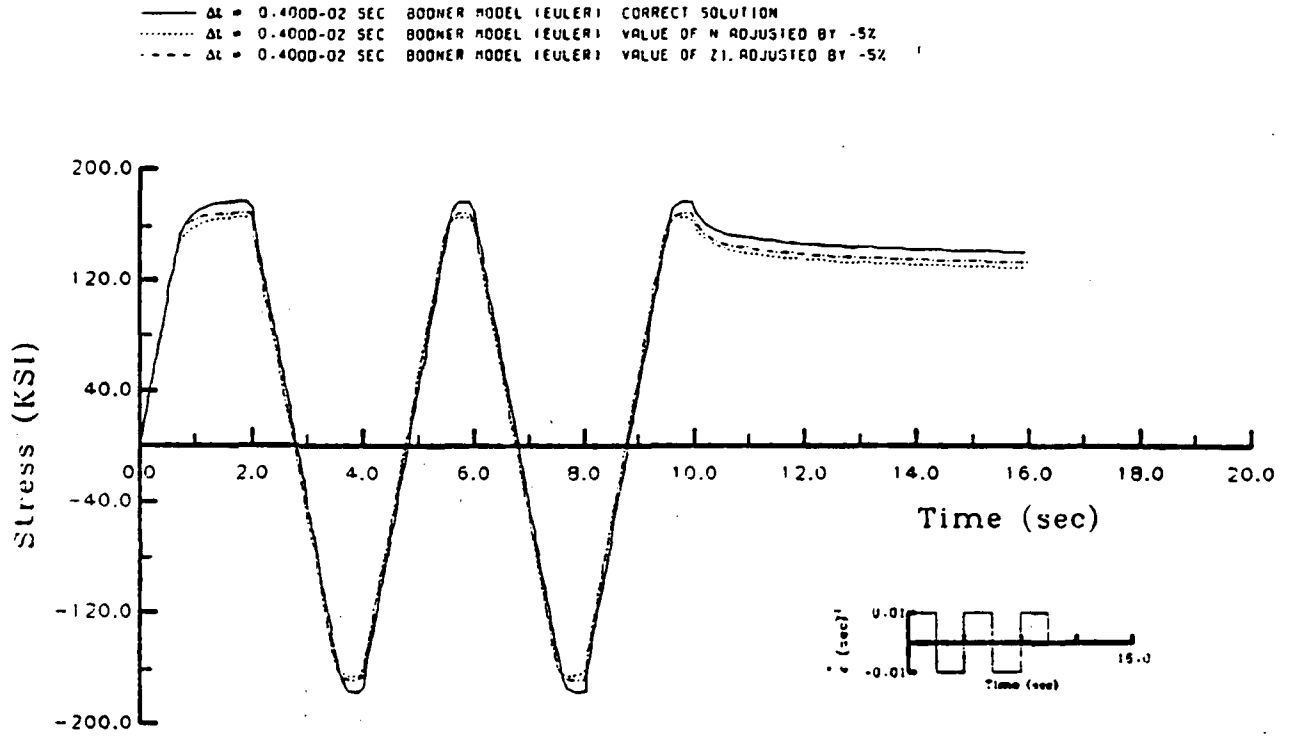

Fig. 9 Sensitivity of Bodner's theory to -5% change in input constants (IN100 at 1350°F)

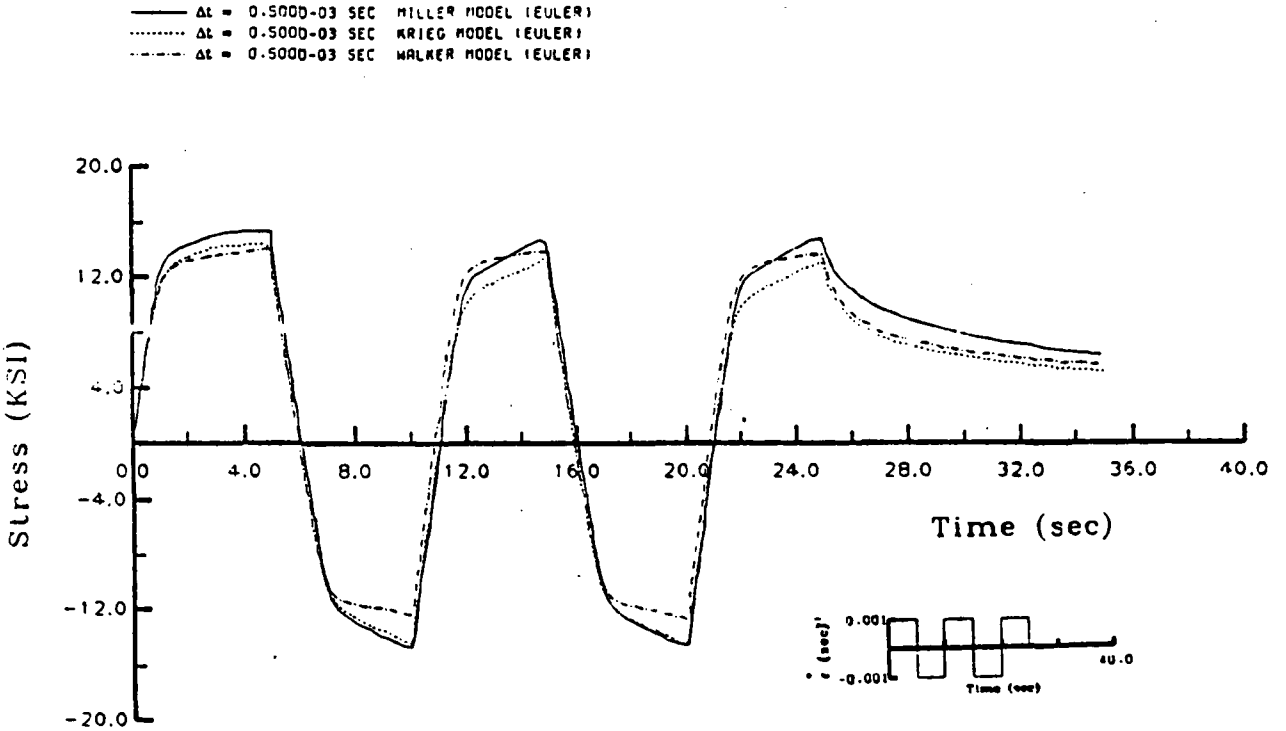

Fig. 10 Comparison of stress-time predictions for Miller, Krieg and Walker theories (Hastelloy-X at 1800°F)

APPENDIX 6.2

EVALUATION OF THE NUMERICAL STABILITY AND SENSITIVITY OF MATERIAL PARAMETER VARIATIONS FOR SEVERAL UNIFIED CONSTITUTIVE MODELS

P.K. Imbrie

W.E. Haisler

D.H. Allen

Aerospace Engineering Department

Texas A&M University

College Station, Texas 77843

NASA Lewis Research Center

Cleveland, OH 44135

Grant No. NAG3-491

MM-4998-85-6

May 1985

ABSTRACT

The sensitivity of the unified constitutive theories, proposed by Bodner, Walker, Krieg, and Miller, to numerical integration techniques and slight changes in material parameters was investigated. Evaluations were based upon numerical simulations of Hastelloy-X at 1800° F in uniaxial form by specifying input strain histories and comparing output stress histories. The integration sensitivity study involved the use of both single and multi-step integration schemes. The various algorithms were compared with regard to accuracy, stability, and computational economy. The material parameter sensitivity was studied by varying the material constants by a specified amount and comparing predicted responses. Numerical comparisons show that, of the numerical integration methods studied, Eulers method is the most accurate, stable, and efficient procedure. The input sensitivity studies indicated that some constitutive models are more sensitive to experimental errors than others and that a 5% error in certain material constrants may lead to 15-30% changes in predicted response.

ACKNOWLEDGEMENTS

The authors gratefully acknowledge the support of this research by NASA Lewis Research Center under Grant no. NAG3-491.

TABLE OF CONTENTS

LIST OF TABLES

LIST OF FIGURES

CHAPTER I
INTRODUCTION

For many years there has been a substantial amount of research performed in the area of modeling the constitutive behavior of inelastic deformation. Recently, new unified formulations have been proposed which are attracting much attention because these theories treat the inelastic strain as a unified quantity, incapable of being separated into time dependent and time independent parts. However, these new models have two potential problems which can effect their predictive capabilities. These include sensitivity to the numerical integration of the differential equations describing the inelastic strain component, as well as a difficult and sometimes ill-defined method of determining the material parameters.

Recently, Beek, Allen and Milly [1] have shown that a number of proposed thermoviscoplastic constitutive models can be cast into a common internal state variable framework. The first state variable is the inelastic strain (ε^I) whose rate of growth is a function of both current conditions (stress σ and temperature T) and one or more internal state variables. These unified formulations form a system of nonlinear ordinary differential equations in the independent variable time (t). Many researchers [2-16] have observed these equations to be well behaved in some portions of the strain response and mathematically

stiff in other regions. Therefore, in order to obtain a stable and accurate prediction of inelastic behavior, one must carefully consider the method of integration. There are a variety of numerical algorithms available, from the simple Euler integration scheme wherein one must judiciously select an appropriate time step size to insure solution stability and accuracy, to the more sophisticated method of Gear [7-9] where the step size is automatically selected after checking for the existence of stiffness.

The growth laws which are used to describe the stress-strain response of a particular material rely on a number of material parameters. The material parameters (or constants) are determined, either implicitly or explicitly, from a series of uniaxial tests which are prescribed by the model developer. Typically some combination of the following tests is required: 1) constant strain rate tensile tests; 2) constant strain rate tensile tests with intermittent hold times; 3) constant strain rate cyclic tests; 4) relaxations tests; 5) creep tests; or 6) stress drop tests. The application of test data in determining material constants varies from model to model. In most cases, because of the lack of standardization, it would appear that the end user will be burdened with a trial-and-error method for determining specific material parameters. This burden might be eased if a quantitative assessment of the model sensitivity to slight changes in material constants was provided. However, there is no such information available in the literature, nor is the problem even addressed.

The purpose of this research will be to evaluate numerical simulations of several unified constitutive models, in uniaxial form, by specifying input strain histories and comparing output stress histories. Integration methods and slight changes to material parameters will be the prime variables. This will allow for a qualitative analysis of solution stability, accuracy, and sensitivity.

In fulfillment of these objectives, this thesis will proceed in the following manner. First, a review of the pertinent literature is presented in addition to a brief overview of the origin of stiffness. Next, the constitutive theories considered herein are discussed and the various methods used to determine their material parameters are outlined. Finally, the numerical integration and parameter sensitivity study is presented, wherein the use of various integration algorithms selected for this study are investigated and the effects of varying material constants, simulating "experimental error", are analyzed. Evaluations are based upon numerical simulations of Hastelloy-X at 1800° F, in uniaxial form, when subjected to several strain input histories.

CHAPTER II

BACKGROUND

Constitutive Modeling

Constitutive modeling of inelastic deformation is not a new concept, it has been in practice since 1864 starting with the early work of Tresca [17]. Levy [18] and von Mises [19] added to the study of plasticity by developing what have come to be known as the Levy-Mises equations. The development of classical plasticity continued with the work of Hencky [20], Prandtl [21], Prager [22], and Ziegler [23] to name just a few. These early models were incremental in nature, assumed that plasticity and creep could be separated, and they incorporated a yield function, flow rule, and hardening rule to define the plastic strain increment.

In addition to classical plasticity based-theories, other fundamental bases were proposed to describe inelastic deformation. These include the microphenomenologically-based theories and thermodynamically-based nonlinear viscoelastic theories. The aforementioned models can be further categorized as unified or uncoupled theories, where the two differ in their treatment of rate-independent and rate-dependent strain components. The uncoupled theories partition the inelastic strain into plastic and creep components; whereas, the unified constitutive models retain the inelastic strain as a unified quantity. However, it should be noted that the partitioning method used in the uncoupled models is questioned because it has no formal micromechanical basis and does not account for creep and plasticity interaction.

Over the past decade a number of unified constitutive theories have been developed. These new theories include the work of Bodner, et al. [24-26], Cernocky and Krempl [27,28], Cescotto [29], Chaboche and Cailletaud [30], Hart [31], Krempl [32], Krieg, et al. [33], Kocks [34], Miller [35], Robinson [36], Stouffer [37,38], Valanis [37,40], and Walker [41,42].

As stated earlier Beek, Allen, and Milly [1] and Krieg [16] have shown that all thermoviscoplastic constitutive models can be cast into a common internal state variable framework. For the uniaxial case, a general form of these unified models may be written as:

$$\sigma = E(\varepsilon - \varepsilon^I - \varepsilon^T) \tag{1}$$

$$\dot{\varepsilon}^I = f(\varepsilon,T,B,D,\ldots,\alpha_m) \tag{2}$$

$$\dot{B} = h_B \dot{\varepsilon}^I - r_B(T,B) \tag{3}$$

$$\dot{D} = h_D \dot{\varepsilon}^I - r_D(T,D) \quad , \tag{4}$$

where σ is the applied stress, E is Young's modulus, ε is the strain, ε^I is the inelastic strain or first state variable (with both plasticity and creep included), ε^T is the thermal strain, B is the back or rest stress corresponding to the dislocation arrangement which produces kinematic hardening or the Bauschinger effect, and D is the drag stress corresponding to the dislocation density which produces isotropic hardening. In addition, f is the inelastic strain rate function, T is the temperature, α_m are additional state variables which are presently undefined, and h_B, h_D, r_B, and r_D are the hardening

and recovery functions for the back or drag stress (designated by the subscript B or D), respectively. A superposed dot above the variables denotes differentiation with respect to time.

The abstract model presented above (equations (1)-(4)) contains all three of the commonly used internal state variables; however, specific theories may omit one or more of the growth laws which characterize either the back stress, drag stress, or other variables. In all cases, the inelastic strain is obtained via time integration of the specified internal state variable growth law for ε^I, i.e.,

$$\varepsilon^I = \int_{-\infty}^{t} \dot{\varepsilon}^I(t')dt' \quad , \tag{5}$$

where $\dot{\varepsilon}^I$ is defined in functional form by (2), t is the current time of interest, and t' is a dummy variable of integration.

Integration Methods

A number of integration strategies have been evaluated [2,3,5,6,10-14] for integrating constitutive equations which have "locally" stiff regimes. These algorithms have been implemented into both large multi-axial finite element programs and small uniaxial constitutive codes. For the purpose of this discussion, only those publications dealing with integration on the constitutive level will be reviewed.

Numerical schemes for the solution of the inelastic response behavior were explored by William [2]. He used a generic constitutive formulation in order to examine the algorithmic properties of various numerical solution methods. These included the explicit forward

Euler method, the forward gradient method, the predictor-corrector method, and the Newton-Raphson method. A qualitative comparison of the four incremental solution methods was presented for pure creep and pure relaxation behavior; however, no specific conclusions were stated with regard to the "best" scheme.

An explicit trapezoidal method for handling deformation in stiff regimes was proposed by Shih, Delorenzi, and Miller [3]. Results using the explicit trapezoidal scheme demonstrated both improved stability and computational efficiency over either explicit forward Euler integration or the trapezoidal method with a Newton-Raphson corrector. It was shown that the predictor-corrector method eventually converged to the same solution predicted by the explicit trapezoidal scheme, while the Euler predicted response was unstable.

Another promising numerical technique, called the α or NONSS (Noniterative, Self-correcting Solution) method, has been developed by Tanaka and Miller and is discussed in Reference [4]. The implicit quantities are removed by a Taylor series expansion of the prescribed growth laws through the use of an integration operator α. The integration operator, α, has the range of (0,1). This alogrithm also incorporates automatic time-step control and an error corrector. Another scheme similar in style to the aforementioned is the Θ-method (described in Reference [5]) which incorporates the explicit forward Euler method (Θ=0), the implicit trapezoidal scheme (Θ=½), or the implicit Euler strategy (Θ=1). Numerical experiments indicated that the forward Euler integration scheme (Θ=0) with an automatic stepping

and error control was computationally more efficient.

For integrating constitutive equations of the work hardening-recovery type, Miller and Shih [6] have developed a method wherein improved accuracy or larger time steps or some combination of both can be obtained. This is accomplished through a Taylor series expansion of the recovery function resulting in a more accurate calculation of the internal variable(s) during each time step. A comparison between this special algorithm and Euler integration from Zircaloy-2 simulations verify the accuracy and stability of this method.

Gear's method [7-9] has also been an effective tool for integrating stiff differential equations. It is a multi-step predictor corrector scheme whose order is automatically chosen. Either an Adams' method or methods suitable for stiff equations can be selected. Three alogrithms are available, STIFF-0, STIFF-1, and STIFF-2. Chang and Chang [5] believe that Gear's package is well suited to solving one-dimensional constitutive relations, but is much too cumbersome for use on the structural level. Based on this work, it may be tentatively concluded that Gear's method is not suitable for implementation into finite element packages.

A very comprehensive study on numerical integration of stiff constitutive models was reported by Kumar, Morjaria, and Mukherjee [10]. Hart's equations for predicting inelastic behavior were used to compare various numerical approximation strategies. Several input histories of stress and strain were considered and the accuracy and computational efficiency of the results were

compared. The study concluded that a simple Euler type one-step method with automatic time-step control worked well; however, it emphasizes that a one-step strategy is not necessarily the best. A combination of the two-step Adams' method (for outside the viscoplastic limit) and Euler's method (for inside the viscoplastic limit), was found to be the most efficient in terms of computational speed and accuracy.

The Origin of Stiffness

The purpose of this section is to familiarize the reader with the concept of stiff equations through a physical and mathematical definition. By understanding this concept, researchers may then devise methods to test for stiffness or more simply concede to its existence and develop appropriate solution algorithms.

A system of differential equations is said to be stiff if the physical processes being modeled contain time constants with different scales. In the case of a uniaxial test specimen, there is grain boundary or dislocation movement in one time scale; whereas the total stress-strain response is measured using a different time constant. The stiffness of equations (2) thru (4) arises from the following phenomenaon. The inelastic strain rate, $\dot{\varepsilon}^I$, may be a strong function of σ, B, and D in (2); that is small changes in σ, B, and D cause large changes in $\dot{\varepsilon}^I$, which then influences σ, B, and D through (1), (3), and (4). Ultimately, the absolute stability of equations (2) thru (4) requires that the step size used during numerical integration be not much greater than the

smallest time constant present in the physical system; however, for computational reasons this is not always possible. Therefore, integration methods must be used that are "stiffly stable".

The mathematical definition as described in [44] is as follows:

"The nonlinear system $Y' = F(X, Y)$ is said to be stiff in an interval I if for $X \in I$ the eigenvalues λ_k of the Jacobian J satisfy the following conditions."

1) $\text{Re } \lambda_k < 0, \quad k = 1,\ldots,m$

2) $\max_{1 \le k \le m} |\text{Re } \lambda_k| \gg \min_{1 \le k \le m} |\text{Re } \lambda_k|$

Where the λ_k, $k=1,\ldots,m$ are the eigenvalues of F. The Ratio

$$\frac{\max_{1 \le k \le m} |\text{Re } \lambda_k|}{\min_{1 \le k \le m} |\text{Re } \lambda_k|} \tag{6}$$

is called the stiffness ratio

Basically this means that if the real eigenvalues are negative or if the spread of real eigenvalues is large, then the equations are stiff. Gear's method [7-9] uses this definition to test for the existence of stiffness. However, this can be very expensive expecially when large systems of equations are being analyzed.

Material Testing

Each constitutive model has a number of material parameters which are determined through a set of complex tests; therefore, the end user must be informed about the effect that small variations, i.e. typical experimental error, have on the particular models' predictive

capabilities. In general, the testing of materials is a difficult process in which the propensity for error is great. This experimental error is known to occur in all stages of testing and will be discussed herein; however, the reasons for its occurrence are beyond the scope of this research.

Experimental error may develop in all phases of testing; however, it occurs most frequently in the following areas. The nonrepeatability of strain measurements for uniaxial strain rate, cyclic or creep tests makes interpretation of results difficult even when new high technology axial and diametral extensometers are used. When testing requires elevated temperatures, error may result while measuring and maintaining the specimen's temperature. Finally, experimental error occurs in its most rudimentary form in the statistical variation of the test sample's measurements. While these are only an example of where experimental error occurs, they are representative of the problems experimentalists must cope with and why absolute values of material constants are difficult if not impossible to obtain.

Objectives

The objective of this research is to study the sensitivity of the unified constitutive theories proposed by 1) Bodner, et al., 2) Krieg, Swearengen and Rohde, 3) Miller, and 4) Walker to numerical integration techniques and slight changes in material parameters. Evaluations are based upon numerical simulations of Hastelloy-X at 1800° F in uniaxial form by specifying input strain histories and comparing output stress histories. The integration sensitivity study involves the use of both single and multi step

integration schemes. The material parameter sensitivity is studied by varying material constants by a specified amount and comparing predicted responses.

CHAPTER III

CONSTITUTIVE THEORIES CONSIDERED

The constitutive models selected for this study include the work of Bodner (et al.) [24-26], Krieg (Swearengen and Rohde) [33], Miller [35], and Walker [41-42]. These models were chosen primarily because of the availability of material parameters for the same material (Hastelloy-X), the exception being Bodner's model (constants for Bodner's model were obtained by simulating the required uniaxial tests using Walker's model). A secondary reason for selecting these models is that they appear to be the most qualitatively attractive theories available [42, 43] and thus warrant further evaluation. In the following sections, each model is presented in one-dimensional form and the methods used to compute the material constants are discussed.

Bodner, et al.'s Theory

The model proposed by Bodner, et al. is a microphenomenologically based theory for characterizing inelastic behavior. This theory was developed to predict the response of a material which work hardens isotropically. The model contains two internal state variables; the inelastic strain and the drag stress. Bodner's model contains no parameter which represents the back stress and thus cannot account for the Bauschinger effect in kinematic hardening materials. The uniaxial-differential form of Bodner's model may be written as

$$\dot{\varepsilon}^I = \frac{2}{\sqrt{3}}\ \varepsilon_o\ e^{\left(-\left(\frac{n+1}{2n}\right)\left(\frac{\sigma}{D}\right)^{-2n}\right)}\ \mathrm{sgn}\ (\sigma) \qquad (7)$$

$$\dot{D} = m(D_1 - D)\dot{W}_p - AD_1 \left(\frac{D-D_2}{D_1} \right)^r \quad , \tag{8}$$

where

$$\dot{W}_p = \sigma \dot{\varepsilon}^I \quad . \tag{9}$$

The material parameters to be determined are E, ε_o, n, m, A, r, D_o, D_1, and D_2, where D_o is the initial value of D. The constant ε_o represents a limiting value of the inelastic strain rate and is usually assumed to be 10^4 sec^{-1} unless the strain rates are very high.

Determination of Material Parameters. The material parameters for Bodner's model are determined through a series of constant strain rate tensile tests and constant stress creep tests. Control parameters for both sets of experiments should encompass values which are compatible with the numerical simulation to be performed.

The first step in the evaluation of the material constants, as described by Stouffer [37] and Milly and Allen [43], is to determine n from the constant strain rate tensile data. By observation, when the stress reaches a saturated value during a constant strain rate test equation (7) is satisfied if and only if D is a constant. Therefore, by neglecting recovery via rapid loading of the test specimen, D can be assumed to be in its fully work hardened state and have a maximum value D_1. Thus (7) may be rewritten, to account for the steady state flow condition, as

$$\ln \left[-\ln \left(\frac{\sqrt{3}}{2} \frac{\dot{\varepsilon}^I}{\varepsilon_o} \right) \right] = -(2n)\ln\sigma + \left[2n \ln D_1 + \ln \left(\frac{n+1}{2n} \right) \right] \quad . \tag{10}$$

If the experimental data base is good, the left hand side of equation

(10) must be a linear function of $\ln\sigma$. Thus, a plot of these two variables (as depicted in Fig. 1(a)) yields a straight line where the slope and intercept are defined by the quantities -2n and $[2n \ln D_1 + \ln((n+1)/2n)]$, respectively, from which n and D_1, may be determined.

To determine the parameters m and D_o, constant strain rate tensile test data is used. If work hardening is assumed negligible, (8) may be rewritten as

$$dD = m(D_1-D)dW_p \quad , \tag{11}$$

which can be integrated to give

$$\ln(D_1-D) = -mW_p + \ln(D_1-D_o) \quad , \tag{12}$$

where W_p is the inelastic work defined by (9) and D_o is the initial value of hardness D. To obtain D for measured values of stress and inelastic strain rate, equation (7) is inverted and may be written as

$$D = \sigma \left[\left(\frac{2n}{n+1}\right) \ln \left(\frac{2\,\varepsilon_o}{\sqrt{3}\,\dot{\varepsilon}^I}\right) \right]^{1/2n} . \tag{13}$$

Therefore, by using values of σ and $\dot{\varepsilon}^I$ from the nonlinear portion of the tensile response data the quantity D may be determined by equation (13). Since equation (12) is a linear representation of $\ln(D_1-D)$ and W_p, a plot of these variables will be a straight line (see Fig. 1(b)) having a slope of m. Thus, knowing m, D_o may be determined through simple substitution and rearrangement of equation (12).

Denoted Experimental Data Points

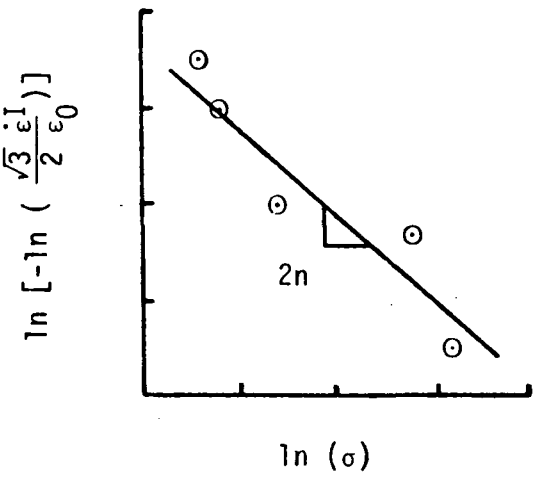

a) Evaluation of Strain Rate Exponent n.

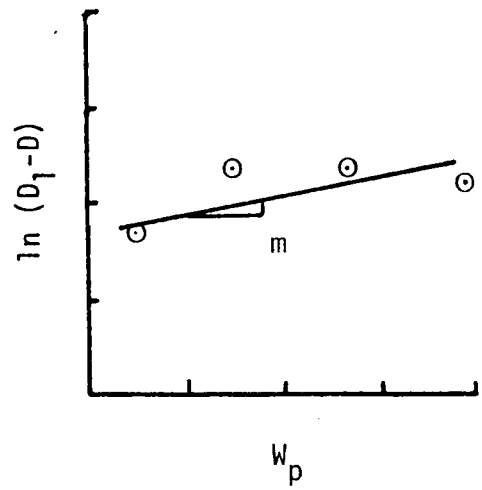

b) Evaluation of Hardening Parameter m.

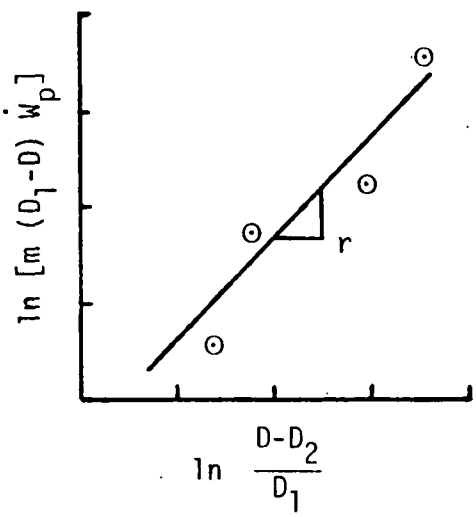

c) Evaluation of Hardening Recovery Parameter r.

Fig. 1. Plots Used to Obtain Material Parameters For Bodner's Model.

The last set of constants, A, r, and D_2 are computed using data obtained from constant stress creep tests. During secondary creep the creep rate is approximately constant; therefore, the value of D must be constant and $\dot{D} = 0$. Thus, the hardening rate equation (8) for secondary creep becomes

$$m(D_1-D)\dot{W}_p = AD_1\left(\frac{D-D_2}{D_1}\right)^r \quad . \tag{14}$$

linearization of (14) results in

$$\ln\left[m(D_1-D)\dot{W}_p\right] = r\ln\left(\frac{D-D_2}{D_1}\right) + \ln(AD_1) \quad , \tag{15}$$

where stable values of D are computed using equation (13) and D_2 is the minimum calculated value of D. By plotting $\ln[m(D_1-D)\dot{W}_p]$ as a function of $\ln(\frac{D-D_2}{D_1})$, similar to Fig. 1(c), the variables A and r may be determined. From equation (15), it may be seen that r represents the slope of the straight line plot and $\ln(AD_1)$ is the intercept. Hence, A may be computed once the value of the $\ln[m(D_1-D)\dot{W}_p]$ intercept is known.

Since no experimental data for Hastelloy-X at 1800° F was available, the material parameters for Bodner's model were computed using Walker's theory (as described in the next section) to predict the deformation response. Numerical simulations included both constant strain rate and constant stress (creep) tests. The material constants computed for Bodner's model are tabulated in Table 1.

Table 1. Material Constants Used In Bodner's Model For Hastelloy-X at 1800° F

Bodner's Constants	Numerical Value
E	13.2×10^{6} psi
ε_0	1.0×10^{4} sec^{-1}
n	0.103
m	- 0.178 psi
r	0.294
A	0.162×10^{-1} sec^{-1}
D_1	0.329×10^{7} psi
D_2	0.305×10^{7} psi
$\varepsilon^I(t=0)$	0.0
$D(t=0) = D_0$	0.317×10^{7} psi

Walker's Theory

The model proposed by Walker is a viscoelastic theory developed by modifying the constitutive relation for a three parameter viscoelastic solid. This model contains three internal state variables; the inelastic strain, the back stress, and the drag stress. The back stress introduces nonlinear kinematic hardening into the model to account for the Bauschinger effect and the drag stress introduces isotropic hardening into the model to account for cyclic hardening or softening of the material. Creep, relaxation, and strain rate effects are modeled by a power law function for the inelastic strain rate. The uniaxial-differential form of Walker's model may be written as

$$\dot{\varepsilon}^I = \frac{|\sigma - B|^{n-1}}{D^n} (\sigma - B) \tag{16}$$

$$\dot{B} = (n_1 + n_2)\, \dot{\varepsilon}^I - (B - \overset{\circ}{B} - n_1\, \varepsilon^I)\, \dot{G} \tag{17}$$

$$\dot{D} = n_8\, |\dot{\varepsilon}^I| - n_9\, |\dot{\varepsilon}^I|\, D - n_{10}\, (D - D_0)^q\ , \tag{18}$$

where the value of $\dot{G}$ is defined to be

$$\dot{G} \equiv |\dot{\varepsilon}^I|\, \frac{\partial}{\partial R} \left[(n_3 + n_4 R)\, \ln\left(\frac{n_5 R}{1 + n_6 R} + 1 \right) \right] + n_7 |B - \overset{\circ}{B}|^{m-1} \tag{19}$$

and R is the cumulative inelastic stran

$$R \equiv \int_0^t \left| \frac{\partial \varepsilon^I}{\partial t'} \right| dt' \ . \tag{20}$$

Walker made several simplifying assumptions to equations (17) and (18),

including D = constant for the Hastelloy-x material. Therefore, history dependence in this model is exhibited entirely by a simplified growth law for the back stress.

$$\dot{B} = (n_1 + n_2)\,\dot{\varepsilon}^I - (B-\overset{\circ}{B}-n_1\dot{\varepsilon}^I)(n_9\dot{\varepsilon}^I + n_7\,|B-\overset{\circ}{B}|^{m-1}) \quad (21)$$

Thus, the material parameters to be determined are E, n, m, n_1, n_2, n_7, n_9, $\overset{\circ}{B}$, and D.

Determination of Material Parameters. The material parameters for Walker's model are determined through a series of constant strain rate steady state hysteresis loops under fully reversed strain controlled conditions at a constant temperature.

The first step in the evaluation of the material constants, as described by Walker [41], is to determine the value of $\overset{\circ}{B}$. The asymptotic steady state value of B may be obtained under conditions of uniaxial tension loading at a known constant strain rate because the back stress will saturate to a constant value as $\varepsilon^I \to \infty$ if $n_1 = 0$.

$$\lim_{\varepsilon^I \to \infty} B = \overset{\circ}{B} + \frac{n_2\,\dot{\varepsilon}^I}{n_9\dot{R} + n_7|B-\overset{\circ}{B}|^{m-1}} \quad (22)$$

The back stress becomes rate-independent and will saturate to a maximum value for rapid monotonic loading in tension and compression when $\dot{R} = \dot{\varepsilon}^I$. Thus, the static thermal recovery term involving n_7 in (22) may be neglected and maximum values of the back stress, in tension and compression, may be obtained by

$$B^t_{max} = \overset{\circ}{B} + n_2/n_9 \quad (23)$$

and

$$B^{c}_{max} = \overset{\circ}{B} - n_2/n_9 \quad . \tag{24}$$

For large strains, stress is assumed to approach an asymptotic such that $\dot{\varepsilon}^{I} = \dot{\varepsilon}$; therefore, equation (16) may be rewritten as

$$\sigma = B + D\,\dot{\varepsilon}^{1/n} \quad . \tag{25}$$

The maximum values of stress in rapid tension and compression loading are then obtained as

$$\sigma^{t}_{max} = \overset{\circ}{B} + n_2/n_9 + D\,\dot{\varepsilon}^{1/n} \tag{26}$$

and

$$\sigma^{c}_{max} = \overset{\circ}{B} - n_2/n_9 - D\,\dot{\varepsilon}^{1/n} \quad . \tag{27}$$

Hence, $\overset{\circ}{B}$ may be obtained using the relation

$$\overset{\circ}{B} = \frac{1}{2}\left(\sigma^{t}_{max} + \sigma^{c}_{max}\right) \quad . \tag{28}$$

To determine the constants n and D equation (25) may be rewritten in terms of steady state values of σ and B in tenson as

$$\dot{\varepsilon} = \left(\frac{\sigma^{t}_{max} - B^{t}_{max}}{D}\right)^{n} \quad . \tag{29}$$

If σ_1 and σ_2 denote the corresponding maximum tensile stresses at the two maximum strain rates, $\dot{\varepsilon}_1$ and $\dot{\varepsilon}_2$ where B attains its maximum saturated value, then equation (29) gives

$$n = \ln\left(\dot{\varepsilon}_1/\dot{\varepsilon}_2\right)/\ln\left\{(\sigma_1 - B^{t}_{max})/(\sigma_2 - B^{t}_{max})\right\} \tag{30}$$

and

$$D = (\sigma_1 - B^t_{max})\ \dot{\varepsilon}_1^{-1/n} \quad . \tag{31}$$

The value of B^t_{max} used in equations (29)-(31) is determined from stress drop tests. If the material is cycled under steady state strain controlled conditions around a closed hysteresis loop as depicted in Fig. 2, positive creep will occur at point C if the stress is held constant and alternately if the stress is held constant at point I, negative creep will occur. Since the saturation stress in tension, B^t_{max}, is desired, a point F on the hysteresis loop between points C and I must be found such that the creep rate ceases instantaneously when the stress is held at a constant value. Walker indicates that it is difficult to estimate the value of B^t_{max} using the above procedure because the creep rates are usually small on the unloading branch. He suggests that a better estimate may be obtained by a relaxation test, noting the point at which initial relaxation changes from positive (stress decreases) to negative (stress increases), since relaxation progresses more rapidly than creep.

Values for the material parameters n_2 and n_9 may be determined from the initial monotonic stress-strain curve. For rapid loading rates $n_1 = 0$ and $\dot{G} = n_9 \dot{R}$, therefore the back stress may be expressed as

$$B = \overset{\circ}{B} + (B^t_{max} - \overset{\circ}{B})\ (1 - e^{-n_9(\varepsilon - \sigma/E)}) \quad . \tag{32}$$

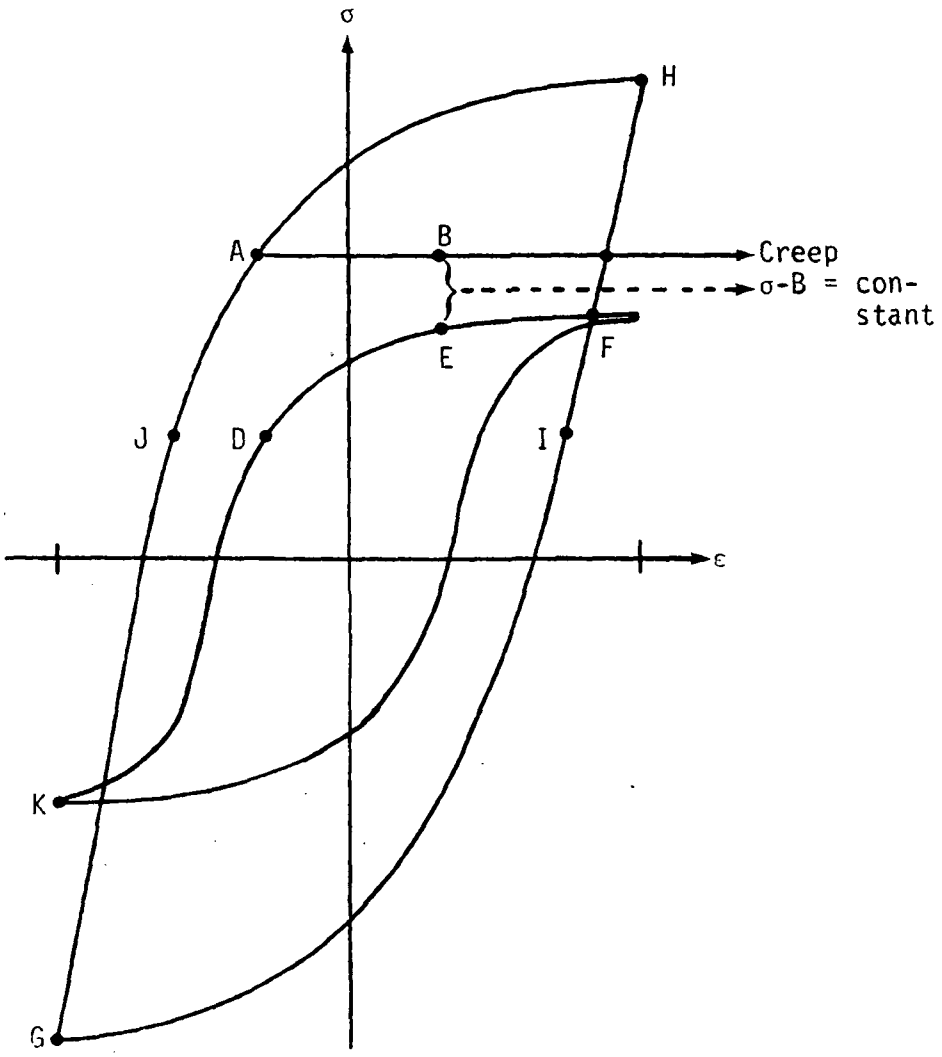

- GJAHI - True Stress Curve, σ/ϵ
- KDEF - Back Stress Curve, B/ϵ

Fig. 2. Back Stress and True Stress-Strain Curve Used in Walker's Theory.

For tensile loading equation (16) may be written as

$$\dot{\varepsilon} - \frac{\dot{\sigma}}{E} = \dot{\varepsilon} - \frac{1}{E}\frac{d\sigma}{d\varepsilon}\dot{\varepsilon} = \gamma\left(1 - \frac{1}{E}\frac{d\sigma}{d\varepsilon}\right) = \left(\frac{\sigma - B}{D}\right)^{n} \tag{33}$$

and combined with equation (32) to give

$$n_9 = (\varepsilon - \sigma/E)^{-1} \ln\left\{\frac{B^t_{max} - \overset{\circ}{B}}{B^t_{max} - \sigma + D\gamma^{1/n}\left(1 - \frac{1}{E}\frac{d\sigma}{d\varepsilon}\right)^{1/n}}\right\} \tag{34}$$

where γ is the applied strain rate and $d\sigma/d\varepsilon$ denotes the instantaneous slope of the uniaxial monotonic stress-strain curve at the point where the stress is σ and the strain is ε. An estimate of the constant n_2 can then be made by rewriting equation (23) as

$$n_2 = \frac{(B^t_{max} - \overset{\circ}{B})}{n_9} \tag{35}$$

The final two constants to be determined are m and n_7. Equation (21), with $n_1 = 0$, yields the expression for the back stress rate for tensile loading as

$$\dot{B} = n_2 \dot{\varepsilon}^I - (B - \overset{\circ}{B})(n_9 \dot{\varepsilon}^I + n_7|B - \overset{\circ}{B}|^{m-1}) \quad . \tag{36}$$

At the peaks of the hysteresis loops B saturates to a constant value, $\dot{B} = 0$ and $\dot{\sigma} = 0$ for tensile loading, so that equation (36) gives

$$n_2 \dot{\varepsilon}_4 = (B_4 - \overset{\circ}{B})n_9 \dot{\varepsilon}_4 + n_7(B_4 - \overset{\circ}{B})^m \tag{37}$$

or

$$n_2 \dot{\varepsilon}_5 = (B_5 - \overset{\circ}{B})n_9 \dot{\varepsilon}_5 + n_7(B_5 - \overset{\circ}{B})^m \quad . \tag{38}$$

If σ_4 and σ_5 denote the maximum tensile stresses at the two smallest strain rates $\dot{\varepsilon}_4$ and $\dot{\varepsilon}_5$, then B_4 and B_5, which represent the saturated back stresses for these two strain rates, may be determined by equation (25). By combining equations (37) and (38) m is obtained in the form

$$m = \frac{\ln \left\{ \frac{n_2 \dot{\varepsilon}_4 - n_9 \dot{\varepsilon}_4 (B_4 - \overset{\circ}{B})}{n_2 \dot{\varepsilon}_5 - n_9 \dot{\varepsilon}_5 (\overset{\circ}{B_5} - B)} \right\}}{\ln \left\{ \frac{B_4 - \overset{\circ}{B}}{B_5 - \overset{\circ}{B}} \right\}} \quad . \tag{39}$$

Knowing m, equation (37) may be solved for n_7. Note that n_1 is assumed to be zero in these applications.

The material constants computed for Walker's model, simulating Hastelloy-X, were evaluated by Walker [41] and are tabulated in Table 2.

Krieg, Swearengen, and Rohde's Theory

The model proposed by Krieg, Swearengen, and Rohde uses a power law function to model the inelastic strain rate and is based upon the microstructural aspects of deformation mechanics. This model contains three internal state variables; the inelastic strain, the back stress, and the drag stress. The growth laws for the back stress and drag stress are formulated as the differences in hardening and recovery rates. The back stress is a kinematic hardening state variable which is used to model the Bauschinger effect and the drag stress is an isotropic hardening state variable which attempts to account for the dislocation density or mechanical

Table 2. Material Constants Used In Walker's Model For Hastelloy-X at 1800°F

Walker's Constants	Numerical Value
E	13.2×10^6 psi
n	4.49
m	1.16
n_1	0.0 psi
n_2	1.0×10^6 psi
n_7	2.73×10^{-3} psi^{1-m} sec^{-1}
n_9	312.5
$\overset{\circ}{B}$	- 1,200 psi
D	59,292 psi
$\varepsilon^I(t=0)$	0.0
B(t=0)	0.0
D(t=0)	59,292 psi

strength of the material. The uniaxial-differential form of Krieg's model may be written as

$$\dot{\varepsilon}^I = \frac{|\sigma - B|^{n-1}}{D^n} (\sigma - B) \tag{40}$$

$$\dot{B} = A_1 \dot{\varepsilon}^I - A_2 (B - \overset{\circ}{B}) |B - \overset{\circ}{B}| (e^{A_3(B-\overset{\circ}{B})^2} - 1) \tag{41}$$

$$D = A_4 |\dot{\varepsilon}^I| - A_5 (D - D_0)^n \quad . \tag{42}$$

It should be noted that equations (16) thru (18) vary in form from those originally proposed by Krieg [33], instead the notation adopted by Walker [42] is presented. The material parameters to be determined are E, n, A_1, A_2, A_3. A_4, A_5, $\overset{\circ}{B}$, and D_0.

Determination of Material Parameters. The material parameters for Krieg's model are determined through a series of constant strain rate cyclic tests and stress drop tests.

The constants n, D_0, $\overset{\circ}{B}$, and A_1 in Krieg's model are analogous to the material parameters n, D, $\overset{\circ}{B}$, and $(n_1 + n_2)$ respectively, in Walker's Theory. Therefore, the interested reader is referred back to Walker's model for a detailed explanation of their determination.

Under steady state conditions where $\dot{\sigma} = 0$, equation (40) shows that B = constant for constant strain rates. That is,

$$B_1 = \sigma_1 - D \dot{\varepsilon}_1^{1/n} \tag{43}$$

or

$$B_2 = \sigma_2 - D \dot{\varepsilon}_2^{1/n} \quad . \tag{44}$$

Where B_1 and B_2 are saturated values of the back stress for strain rates $\dot{\varepsilon}_1$ and $\dot{\varepsilon}_2$ respectively. Therefore, by equating equation (41) to zero and noting that $\dot{\varepsilon} = \dot{\varepsilon}^I$ if $\dot{\sigma} = 0$, gives (for $\dot{\varepsilon}$ positive)

$$\left(\frac{A_1}{A_2}\right) = \frac{(B - \overset{\circ}{B})^2}{\dot{\varepsilon}} \left(e^{A_3(B - \overset{\circ}{B})^2} - 1\right) \quad . \tag{45}$$

By applying known values of the back stress (B_1 and B_2) for the given strain rates ($\dot{\varepsilon}_1$ and $\dot{\varepsilon}_2$) to equation (45) to give two equations with the unknowns, (A_1/A_2) and A_3, the constant (A_1/A_2) may be eliminated so that A_3 is determined by

$$A_3 = \frac{\ln\left\{1 + \frac{\dot{\varepsilon}_1}{\dot{\varepsilon}_2}\left(\frac{B_2 - \overset{\circ}{B}}{B_1 - \overset{\circ}{B}}\right)^2 \left(e^{A_3(B_2 - \overset{\circ}{B})^2} - 1\right)\right\}}{(B_1 - \overset{\circ}{B})^2} \quad , \tag{46}$$

which can be solved using an interative technique.

The constant A_2 may be determined from steady state hysteresis loops where $\dot{B} = 0$. Under these conditions, equation (41) may be written as

$$A_2 = \frac{A_1 \dot{\varepsilon}}{(B - \overset{\circ}{B})^2 \left\{e^{A_3(B - \overset{\circ}{B})^2} - 1\right\}} \quad . \tag{47}$$

The final two constants to be determined are A_4 and A_5. The parameter A_4 controls the amount of isotropic hardening produced by a given amount of strain. As such, it plays an important role in three different transient situations: 1) When a tensile

test is simulated, A_4 controls the rate of work hardening; 2) When a creep test is simulated, A_4 controls the amount of primary creep; and 3) When a fatigue test is simulated, A_4 controls the rate of cyclic hardening (or softening). A best-fit value for A_4 can be tried and the resulting simulations compared with the test data for the same loading, to select the one which causes the closest agreement. Once a value for A_4 has been selected, the constant A_5 may be determined from the following relation

$$A_5 = \frac{A_4 \dot{\varepsilon}}{(D_1 - D_0)^n} \quad , \tag{48}$$

where D_1 is the steady state value of the drag stress at a constant strain rate, $\dot{\varepsilon}_o$.

The material constants computed for Krieg's model, simulating Hastelloy-X at 1800° F, were evaluated by Walker [42] and are tabulated in Table 3.

Miller's Theory

The model proposed by Miller [35] is a phenomenologically based theory which uses a hyperbolic sine function for the inelastic strain rate. This model contains three internal state variables; the inelastic strain, the back stress, and the drag stress. The theory is capable of simulating many of the structurally significant deformation phenomena including cyclic hardening/softening, Bauschinger effect, strain rate effects, and annealing, among others. The growth laws for the back stress and drag stress are formulated as the difference between hardening and recovery rates.

Table 3. Material Constants Used In Krieg's Model For Hastelloy-X at 1800° F

Krieg's Constants	Numerical Value
E	13.2×10^6 psi
n	4.49
A_1	1.0×10^6 psi
A_2	6.21×10^{-6} psi^{-1} sec^{-1}
A_3	4.027×10^{-7} psi^{-2}
A_4	100 psi sec$^{1/n}$
A_5	4.365 psi^{1-n} sec$^{1/n-2}$
B°	- 1,200 psi
D_0	59,292 psi sec$^{1/n}$
$\varepsilon^I(t=0)$	0.0
$B(t=0)$	0.0
$D(t=0)$	59,292 psi

C-2

The uniaxial-differential form of Miller's model may be written as

$$\dot{\varepsilon}^I = B_C\Theta' \left\{ \sinh \left(\frac{\sigma-B}{D} \right)^{1.5} \right\}^n \operatorname{sgn}(\sigma-B) \qquad (49)$$

$$\dot{B} = H_1\dot{\varepsilon}^I - H_1 B_C\Theta' \{ \sinh A_1 |B| \}^n \operatorname{sgn}(B) \qquad (50)$$

$$\dot{D} = H_2|\dot{\varepsilon}^I| (C_2 + |B| - A_2D^3/A_1) - H_2C_2B_C\Theta'\{\sinh(A_2D^3)\}^n \quad . \qquad (51)$$

The material parameters to be determined are E, $B_C\Theta'$, n, H_1, H_2, A_1, A_2, C_2, and D_0. The only constants which depend on temperature are the coefficients $B_C\Theta'$ and D_0.

Determination of Material Parameters. The material parameters for Miller's model are determined through a series of constant strain rate steady state hysteresis loops under fully reversed strain controlled conditions at a constant temperature.

The starting point for the calculation of the constants is to find the values of $B_C\Theta'$, n, and A that satisfy one following steady state equations

$$\dot{\varepsilon}^I_{SS} = B\Theta' [\sinh (A\, \sigma_{SS})]^n \quad , \qquad (52)$$

The constant A does not appear explicitly in the final equations, but it enters into the calculation of A_1 and A_2.

During monotonic loading under steady state conditions the back stress and drag stress reach their saturated values, thus $\dot{B}$ and $\dot{D}$ are zero. Therefore, by equating equations (50) and (51) to zero and solving for the resulting steady state plastic strain rate gives

$$\dot{\varepsilon}^I_{SS} = B_C\Theta' [\sinh(A_1B_{SS})]^n \quad , \qquad (53)$$

$$\dot{\varepsilon}^{I}_{SS} = B_C\Theta' \left\{ \sinh \left(\frac{\sigma_{SS}-B_{SS}}{D_{SS}} \right)^{1.5} \right\}^{n} , \quad (54)$$

$$\dot{\varepsilon}^{I}_{SS} = \frac{C_2\, B_C\Theta' \,[\sinh(A_2 D_{SS}{}^3)]^n}{C_2 + B_{SS} - A_2 D_{SS}{}^3/A_1} . \quad (55)$$

Thru separation of variables in equations (52) through (55), it may be seen that

$$A_1 B_{SS} = \left[\frac{\sigma_{SS} - B_{SS}}{D_{SS}} \right]^{1.5} = A_2\, D_{SS}{}^3 = A\sigma_{SS} . \quad (56)$$

Hence, from equation (56) explicit relations for the constants A_1 and A_2 may be obtained:

$$A_1 = \frac{A\ \sigma_{SS}}{B_{SS}} \quad (57)$$

and

$$A_2 = \left(\frac{A}{1-B_{SS}/\sigma_{SS}} \right)^3 . \quad (58)$$

By linearizing equation (52) one obtains the relation

$$\ln(\dot{\varepsilon}^{I}_{SS}) = n \ln [\sinh(A\sigma_{SS})] + \ln (B_C\Theta') . \quad (59)$$

The constant A is chosen so that a plot of $\ln (\dot{\varepsilon}^{I}_{SS})$ versus $\ln [\sinh(A\sigma_{SS})]$ falls on a straight line. If the test data points fall on a straight line for a particular value of A, then Fig. 3 shows that (CD/AB)/(EC/EB) = 1, or

$$\left| \frac{\ln \dot{\varepsilon}_4 - \ln \dot{\varepsilon}_5}{\ln \dot{\varepsilon}_1 - \ln \dot{\varepsilon}_5} \right| = \left| \frac{\ln[\sinh(A\sigma_4)] - \ln[\sinh(A\sigma_5)]}{\ln[\sinh(A\sigma_1)] - \ln[\sinh(A\sigma_5)]} \right| . \quad (60)$$

Where σ_1, σ_4, and σ_5 are the steady state asymptotic stress

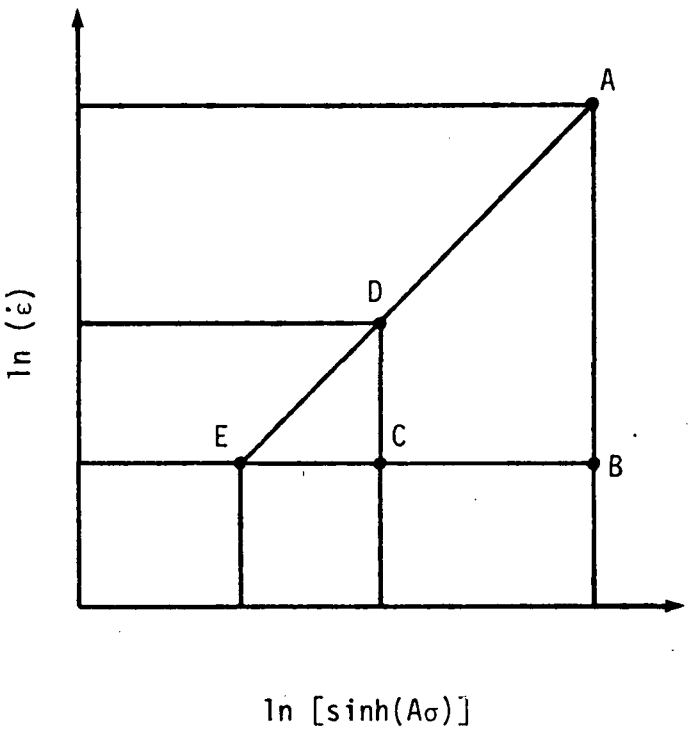

Fig. 3. Plot Used to Determine The Material Constant A For Miller's Model.

obtained from hystresis loops executed at strain rates $\dot{\varepsilon}_1$, $\dot{\varepsilon}_4$, and $\dot{\varepsilon}_5$ respectively. Once a value for A has been chosen, then from equation (59) the slope of $\ln(\varepsilon^I_{SS})$ versus $\ln[\sinh(A\sigma_{SS})]$ plot is n and the intercept is $\ln(B_C\Theta')$.

From stress drop creep tests the value of B_{SS} can be established and the constants A_1 and A_2 may be computed from equations (57) and (58) respectively. In additon, once A_1 and A_2 are known, then $D_{SS} = D_0$ may be found from equation (56).

The constant H_1 in equation (50) governs the hardening rate of the back stress. This constant is analogous to the constants $n_1 + n_2$ in Walker's model; therefore, the interested reader is referred back to Walker's model for a detailed explanation of their determination.

The final two constants yet to be determined are H_2 and C_2. The parameter H_2 controls the mount of isotropic hardening produced by a given amount of strain. A best-fit value for H_2 can be tried and the resulting simulations compared with the test data for the same loading, to select the one which causes the closest agreement. The constant C_2 sets a "floor" under the drag stress and its value is estimated by a best-fit procedure to the actual test data.

The material constants computed for Miller's model, simulating Hastelloy-X at 1800° F, were evaluated by Walker [42] and are tabulated in Table 4.

Table 4. Material Constants Used In Miller's Model For Hastelloy-X at 1800° F

Miller's Constants	Numerical Value
E	13.2×10^{6} psi
n	2.363
$B_{C\Theta}'$	2.616×10^{-5} sec^{-1}
H_1	1.0×10^{6} psi
A_1	1.4053×10^{-3} psi^{-1}
H_2	100 psi $sec^{1/n}$
C_2	5,000.0 psi
A_2	4.355×10^{-12} psi^{-3}
$\varepsilon^{I}(t=0)$	0.0
$B(t=0)$	0.0
$D(t=0)$	8,642 psi

CHAPTER IV

EVALUATION OF SELECTED THEORIES

Evaluation of the unified constitutive theories considered herein is based upon numerical simulations of Hastelloy-X at 1800° F in uniaxial form by specifying input strain histories and comparing output stress histories. Since this thesis addresses two separate problems, a section on the numerical time integration study is presented first, followed by a section detailing the material parameter sensitivity study.

Numerical Time Integration Study

Accurate integration of the constitutive relationship given by equations (1) through (4) is extremely important to the numerical solution of a nonlinear field problem. However, the integration process is somewhat hindered because the coupled system of ordinary differential equations defining the state variables may be "locally" stiff and thus is sensitive to the time step size and numerical algorithm. The instability problems associated with integrating stiff O.D.E.'s can be minimized through proper selection of time step size, when using standard integration techniques, or through the use of specially tailored algorithms which check for stiffness and automatically take the appropriate action.

In general, equation (5) may be integrated between time t and $t + \Delta t$ by writing

$$\Delta\varepsilon^I = \int_{\varepsilon^I(t)}^{\varepsilon^I(t+\Delta t)} d\,\varepsilon^I = \int_t^{t+\Delta t} \dot{\varepsilon}^I\, dt \qquad (61)$$

or

$$\Delta\,\varepsilon^I = \varepsilon^I\,(t+\Delta t) - \varepsilon^I(t) = \int_t^{t+\Delta t} \dot{\varepsilon}^I\, dt \quad , \qquad (62)$$

where $\dot{\varepsilon}^I$ is defined by the particular constitutive theory being employed.

Integration Algorithms Considered. Four of the more commonly used integration schemes were selected for use in this study. These include: Explicit Euler Forward Difference Method, Implicit Trapezoidal Method, Runge-Kutta 4th Order Method, and Trapezoidal Predictor-Corrector (Iterative) Method.

The basic presumption of the Euler method is that the inelastic strain rate function is assumed to be a constant over an interval of interest. For all but the highly-nonlinear portion of the stress strain curve, this assumption is quite reasonable at constant strain rates. However, when the material response is nonlinear, the assumption may no longer be valid unless a sufficiently small time interval is chosen. In addition, the Euler method is sensitive to numerical round-off. The major advantage of using the Euler technique is its ease of implementation. The approximation to the solution of equation (5) using Euler's method may be written as

$$\Delta\,\varepsilon^I = \Delta t\,\dot{\varepsilon}^I\,(t) \quad . \qquad (63)$$

The Implicit Trapezoidal Method is another commonly used integration strategy from the family of single step schemes. Overall solution accuracy is improved by averaging the evaluated function over the desired interval assuming a small enough time increment has been selected. The Implicit Trapezoidal Method approximates the inelastic strain variable as

$$\Delta\varepsilon^I = \frac{\Delta t}{2} [\, \dot{\varepsilon}^I(t) + \dot{\varepsilon}^I(t+\Delta t)] \tag{64}$$

The Runge-Kutta Method, which is also a single step scheme, provides a straight forward high order approximation for computing $\Delta\varepsilon^I$ for various locations along the interval in question. The self-starting characteristic and small error per step of this algorithm has made it popular among researchers for numerically integrating differential equations. It is pointed out that, like most other numerical procedures for solving differential equations, the methods of Runge-Kutta are sensitive to variations in the selected interval. Too small a value leads to an excessive number of computations; on the other hand, too large of an interval may well lead to an answer that differs significantly from the true one. The 4th order Runge-Kutta integration method approximates the solution to equation (5) as

$$\Delta\varepsilon^I = 1/6\ [K_1 + 2K_2 + 2K_3 + K_4] \quad , \tag{65}$$

where

$$K_1 = \Delta t\ \dot{\varepsilon}^I(t,\ \varepsilon^I(t))$$

$$K_2 = \Delta t\ \dot{\varepsilon}^I(t + \tfrac{1}{2}\Delta t,\ \varepsilon^I(t) + \tfrac{1}{2}K_1)$$

$$K_3 = \Delta t\ \dot{\varepsilon}^I(t + \tfrac{1}{2}\Delta t,\ \varepsilon^I(t) + \tfrac{1}{2}K_2)$$

$$K_4 = \Delta t\ \dot{\varepsilon}^I(t + \Delta t,\ \varepsilon^I(t) + K_3) \quad .$$

The last integration algorithm selected for use in this study is the multi-step Trapezoidal Predictor-Corrector method. The objective of this strategy is to predict $\Delta\varepsilon^I$ as accurately as possible using an iterative procedure. As a first guess, $\varepsilon^I(t+\Delta t)$ is computed by the Euler method

$$\text{Predictor:}\quad \varepsilon^I(t+\Delta t) = \varepsilon^I(t) + \Delta t\ \dot{\varepsilon}^I(t,\ \varepsilon^I(t)). \tag{66}$$

This value is then substituted into the Trapezoidal scheme

$$\text{Corrector:}\quad \varepsilon^I(t+\Delta t)_j = \varepsilon^I(t) + \frac{\Delta t}{2}\left[\dot{\varepsilon}^I(t,\varepsilon^I(t)) + \dot{\varepsilon}^I(t+\Delta t,\varepsilon^I(t+\Delta t)_j)\right], \tag{67}$$

which may also be written as

$$\Delta\varepsilon^I_j = \frac{\Delta t}{2}\left[\dot{\varepsilon}^I(t) + \dot{\varepsilon}^I(t+\Delta t)\right]. \tag{68}$$

The subscript j in equations (67) and (68) refers to the j^{th} iteration. If the values for $\Delta\varepsilon^I$ determined by (66) and (67) differ too greatly, equation (67) is re-evaluated using the most recent computed value of $\varepsilon^I(t+\Delta t)j$. This iterative process is continued until the convergence criterion,

$$\left|\frac{\Delta\varepsilon^I_j}{\Delta\varepsilon^I_{j+1}}\right| \leq r_{tol}\ , \tag{69}$$

is satisfied. Selection of an appropriate r_{tol} is important because it governs solution accuracy, number of iterations per interval, and ultimate solution time. For this study r_{tol} was chosen to be 0.000001. While the error of this iterative procedure is greatly reduced, it is still sensitive to numerical round-off.

Strain Histories Considered. All numerical simulations were performed under strain control conditions using one of four input histories. These included: An alternating square-wave strain rate; a ramp up and ramp down strain rate; and two complex multi-step strain rate histories. Restrictions which were arbitrarily imposed on each loading sequence included: 1) the total response time would be 35 seconds; 2) the total strain would not exceed 0.5%; 3) all simulations would begin with a positive (or tensille) load; and 4) the numerical experiments would end with a 10 to 15 second relaxation period. While these strain rate histories (see Fig. 4) were not developed to model any specific physical phenomena, they are representative of conditions under which a material could be strained either in the laboratory or the field.

Qualitative and Quantitative Comparisons. The integration investigation was divided into two tasks. The first task included a comparison of the numerical stability of each constitutive theory in order to access the degree of nonlinearity of the prescribed growth laws. The comparisons were based upon predicted stress-strain behavior for constant strain rate tests simulating monotonic loading. Explicit Euler forward integration was used to obtain the stress

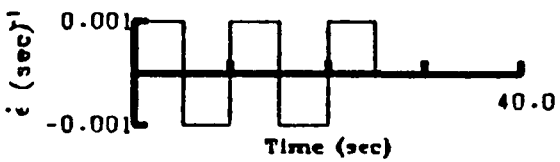

1) Alternating Square Wave Strain Rate History.

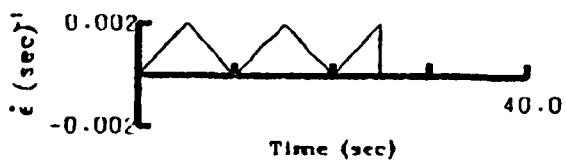

2) Ramp-up-ramp-down Strain Rate History.

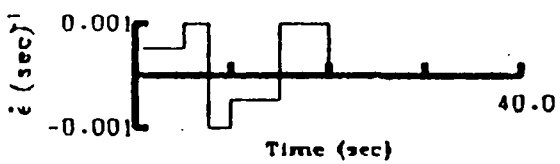

3) Complex Strain Rate History - 1.

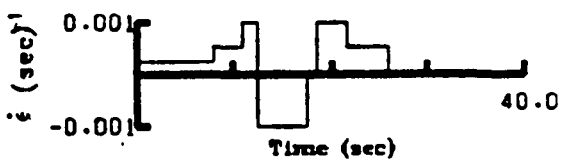

4) Complex Strain Rate History - 2.

Fig. 4. Input Strain Rate Histories.

histories presented in Fig.'s 5 through 8 for various time steps. From Fig. 8 it may be concluded that Miller's model is the most sensitive to step size variation because of the oscillatory response of the stress-strain curve for the larger Δt values.

The oscillatory nature of Miller's model can be traced back to the hyperbolic sine function that is used to characterize the inelastic strain rate and other growth laws. In contrast, the power law function used by Bodner, Walker, and Krieg, to model a material's response appears to be much more stable for a wide range of time increments.

Figures 5 through 8 also reveal that as the step size is increased, all of the constitutive theories tend to overestimate the stress history in the 0.1 to 0.2 percent strain region and then automatically correct themselves as deformation continues. The "self-correcting" phenomenon of predicted stress appears to be an intrinsic property of the prescribed growth laws as is illustrated in Fig's. 9 and 10. Figure 9 is a plot of the inelastic strain computed by Walker's model for Δt's of 0.0005 and 0.1 seconds. If the smaller time step is defined to predict the correct results, then the inelastic strain computed when using the larger Δt is initially underestimated. Because of the coupled nature of equations (1) through (4), subsequent integration reverses this trend and results in an over prediction of the inelastic strain. While not shown in Fig. 9, the difference between the two curves assumes a more constant value as the total strain is increased. That is, the difference (or error) does not grow. Figure 10 shows the identical situation

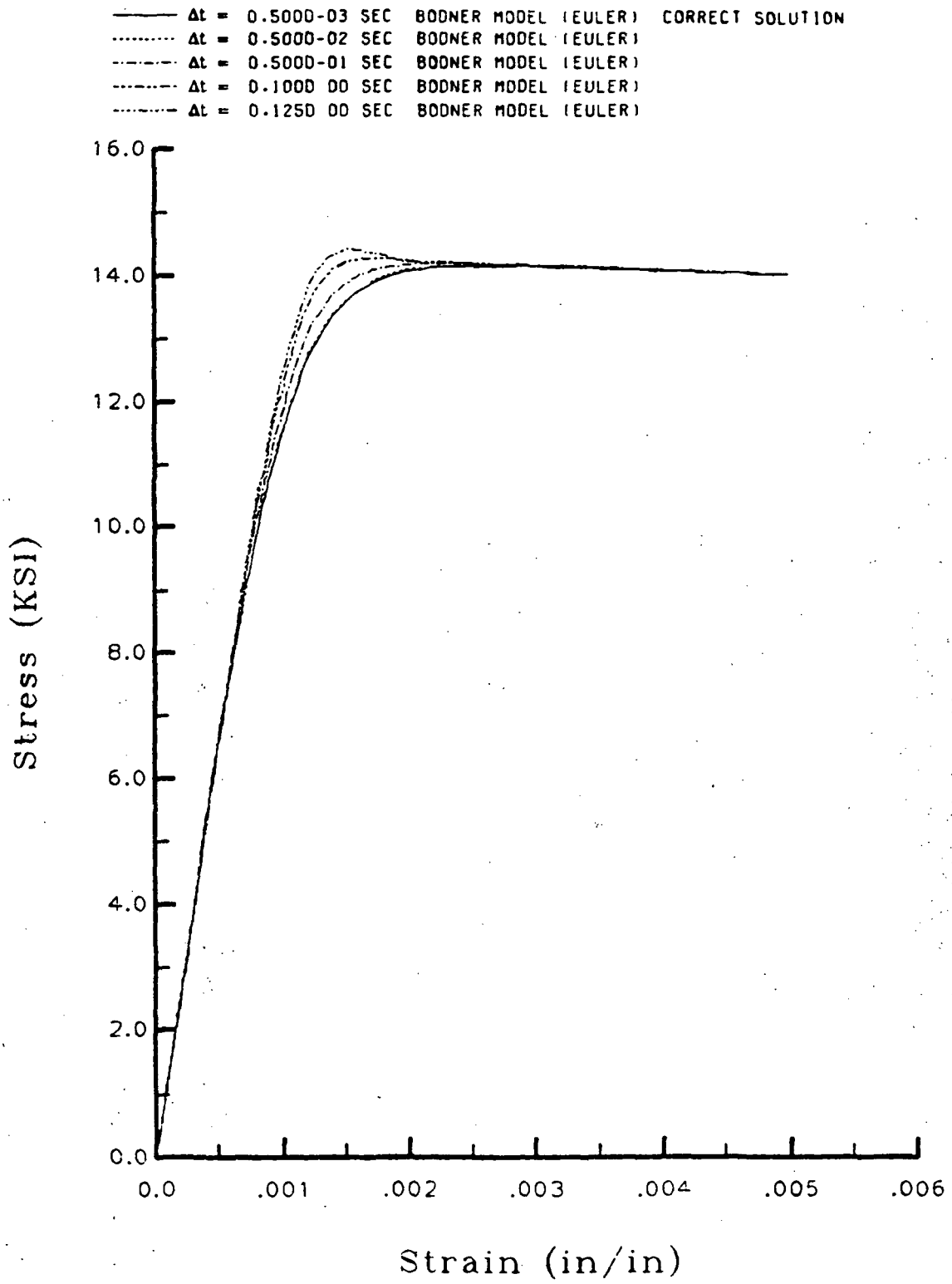

Fig. 5. Monotonic Loading of Hastelloy-X at 1800° F Predicted by Bodner's Model ($\dot{\varepsilon} = 0.001\ sec^{-1}$).

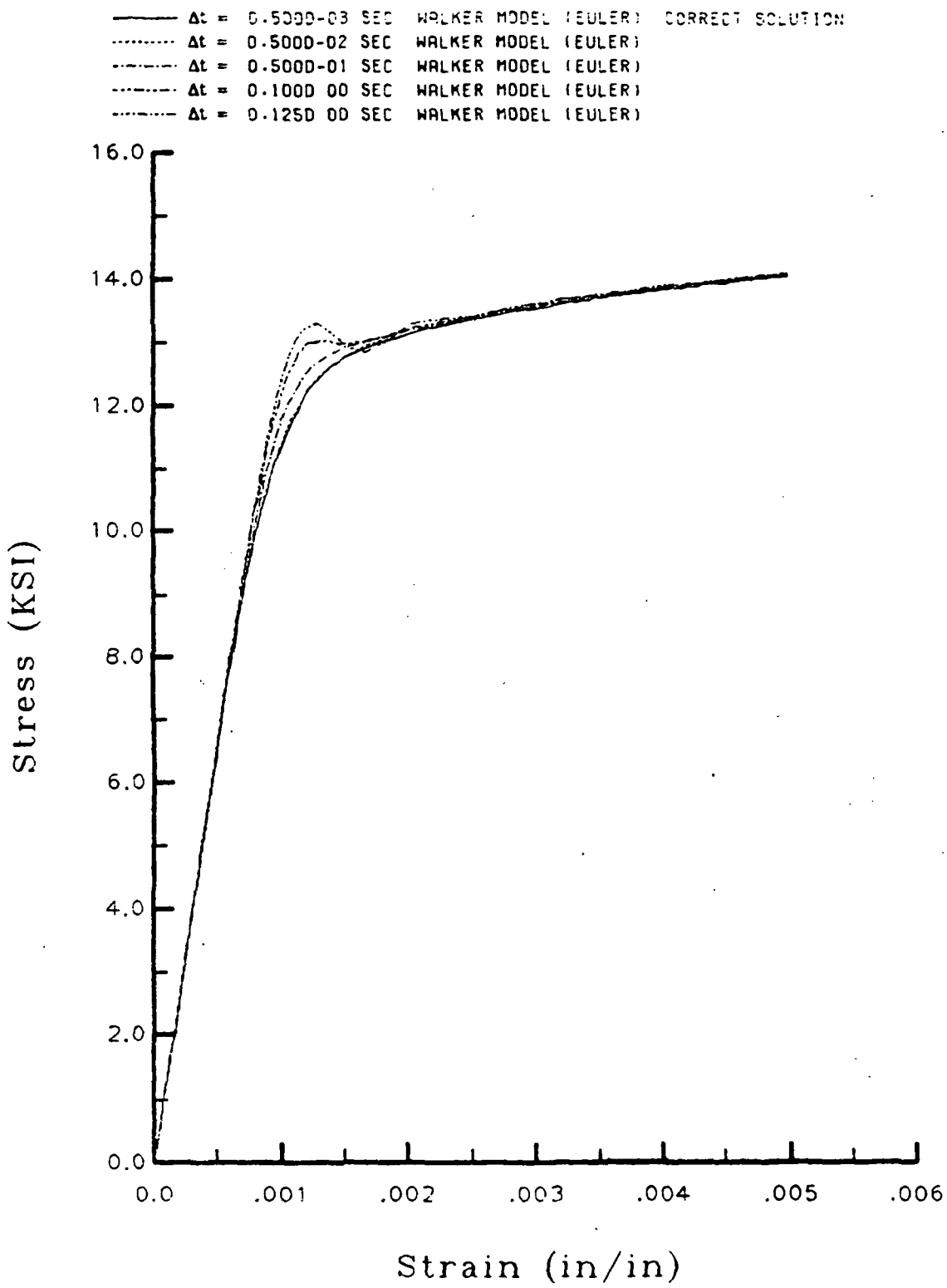

Fig. 6. Monotonic Loading of Hastelloy-X at 1800° F Predicted by Walker's Model ($\dot{\varepsilon} = 0.001\ \text{sec}^{-1}$).

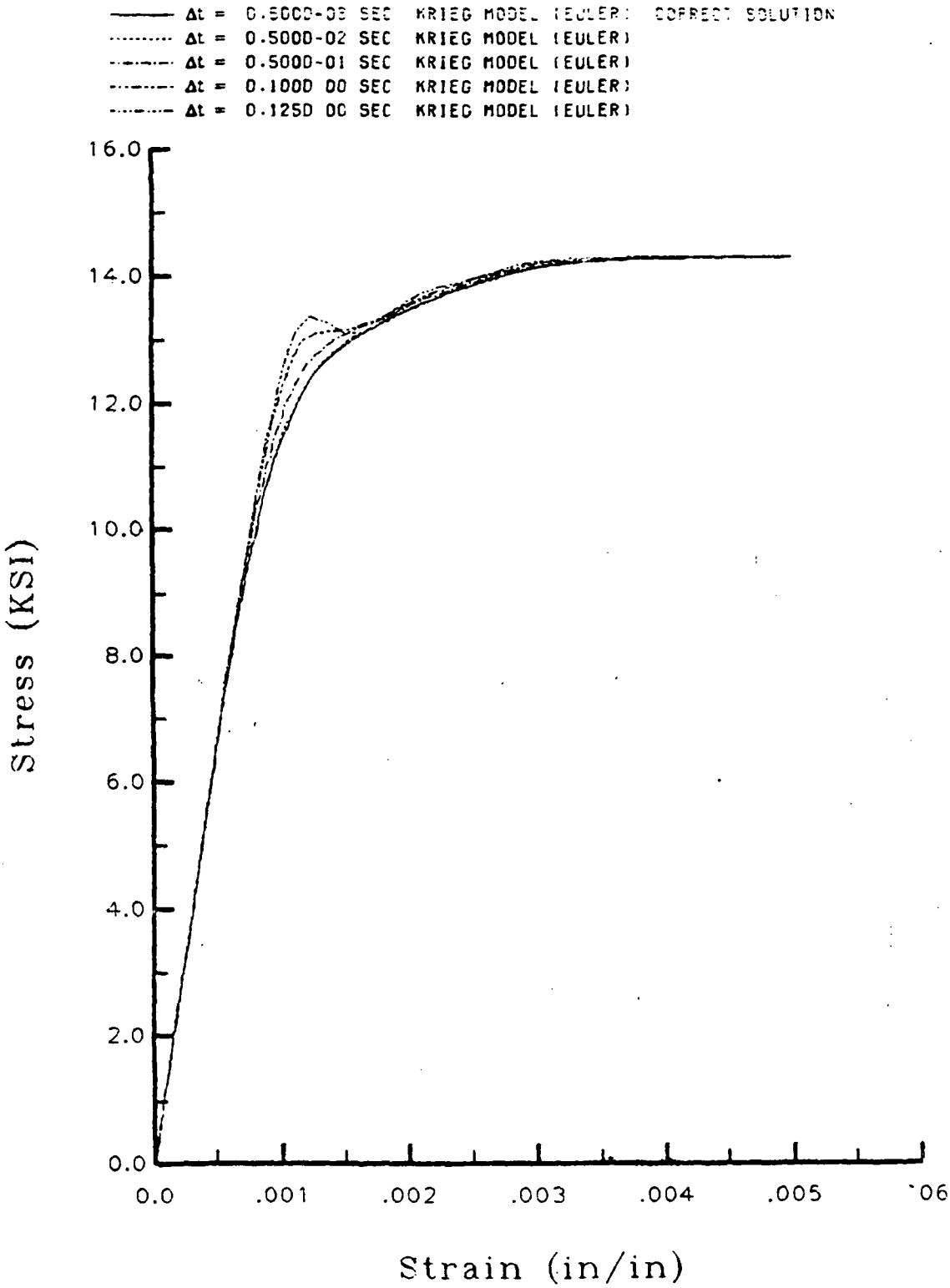

Fig. 7. Monotonic Loading of Hastelloy-X at 1800° F Predicted by Krieg's Model ($\dot{\varepsilon}$ = 0.001 sec^{-1}).

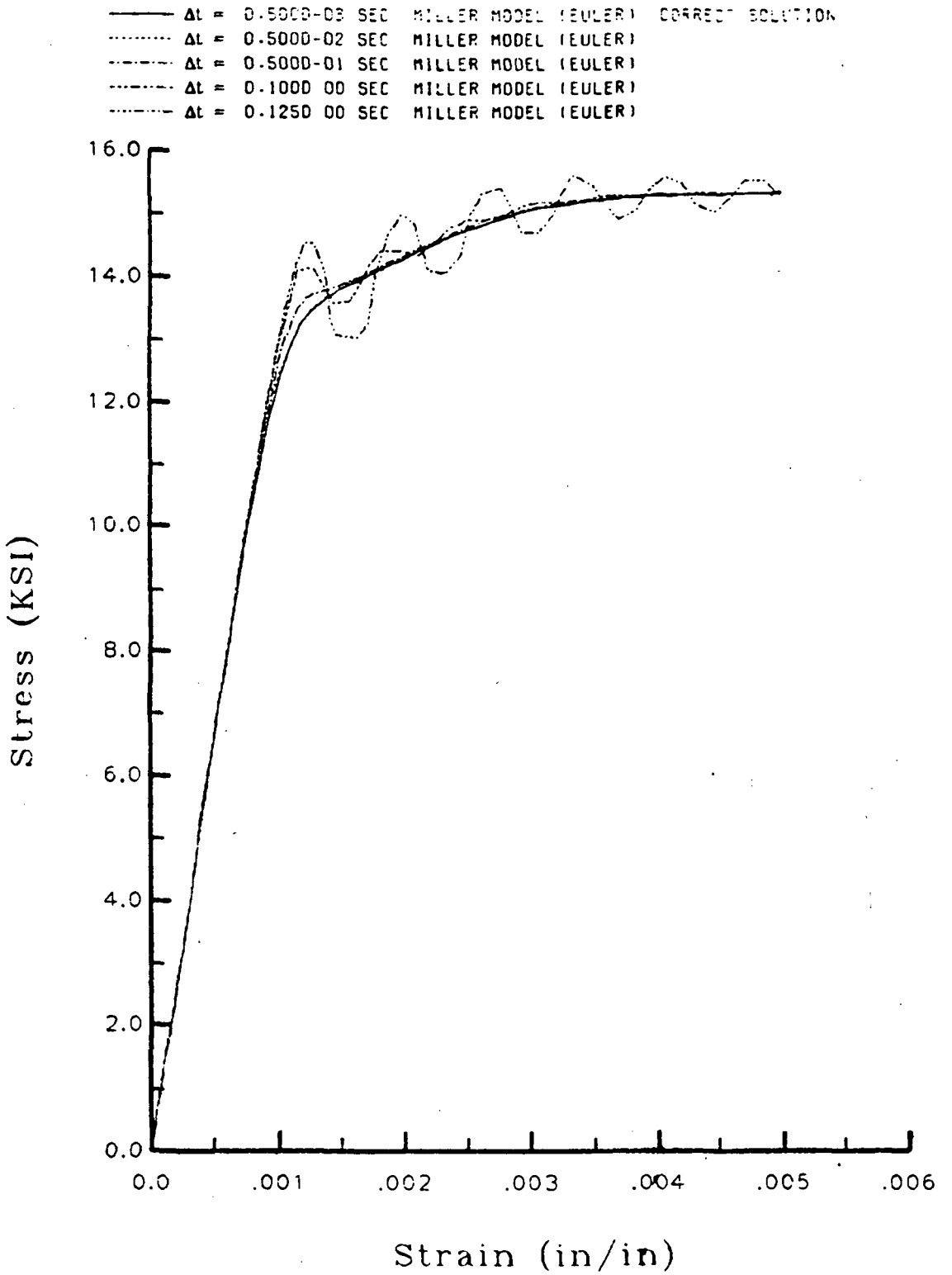

Fig. 8. Monotonic Loading of Hastelloy-X at 1800° F Predicted by Miller's Model ($\dot{\varepsilon}$ = 0.001 sec^{-1}).

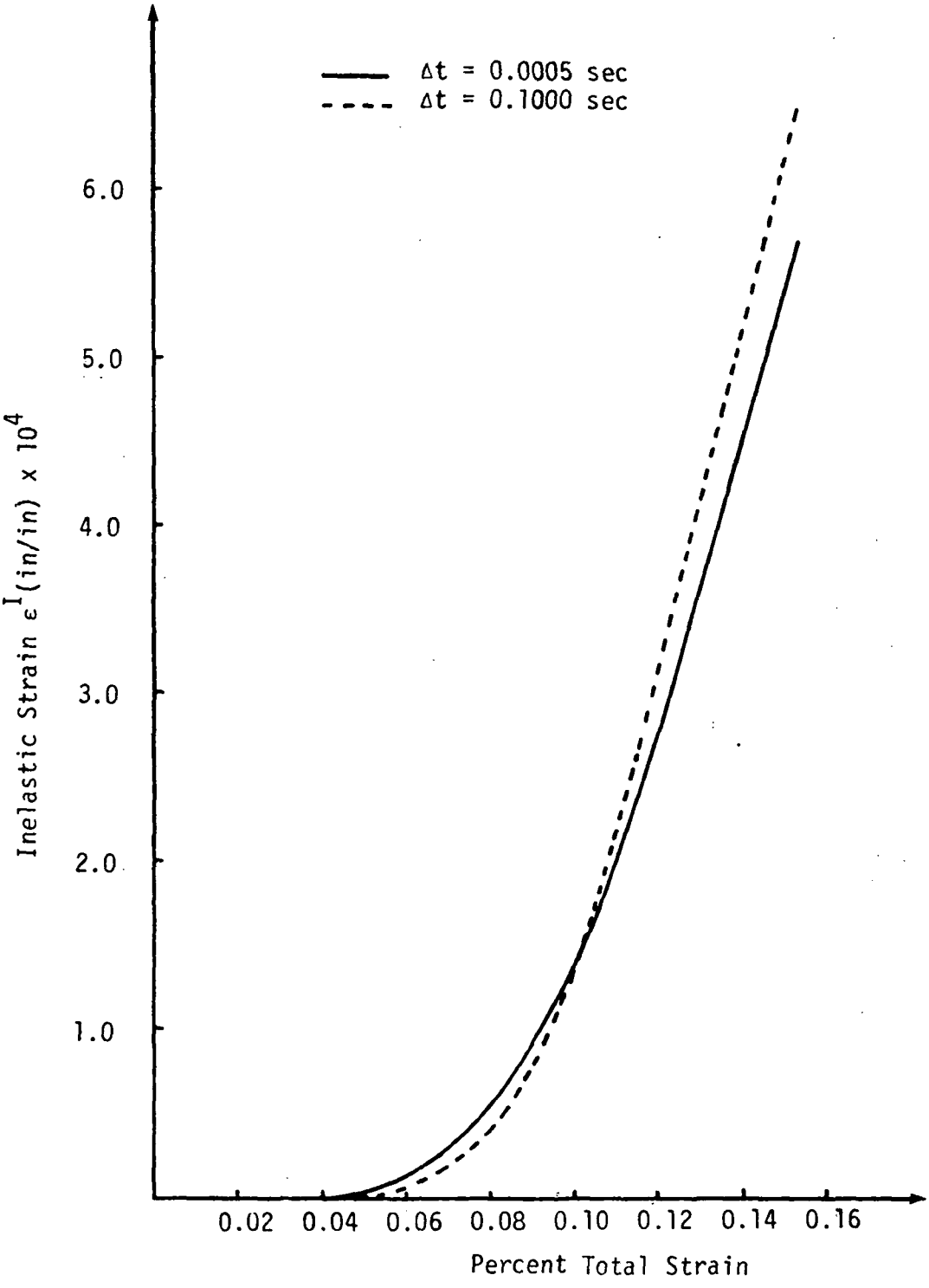

Fig. 9. Inelastic Stain Predicted by Walker's Model For Hastelloy-X at 1800° F.

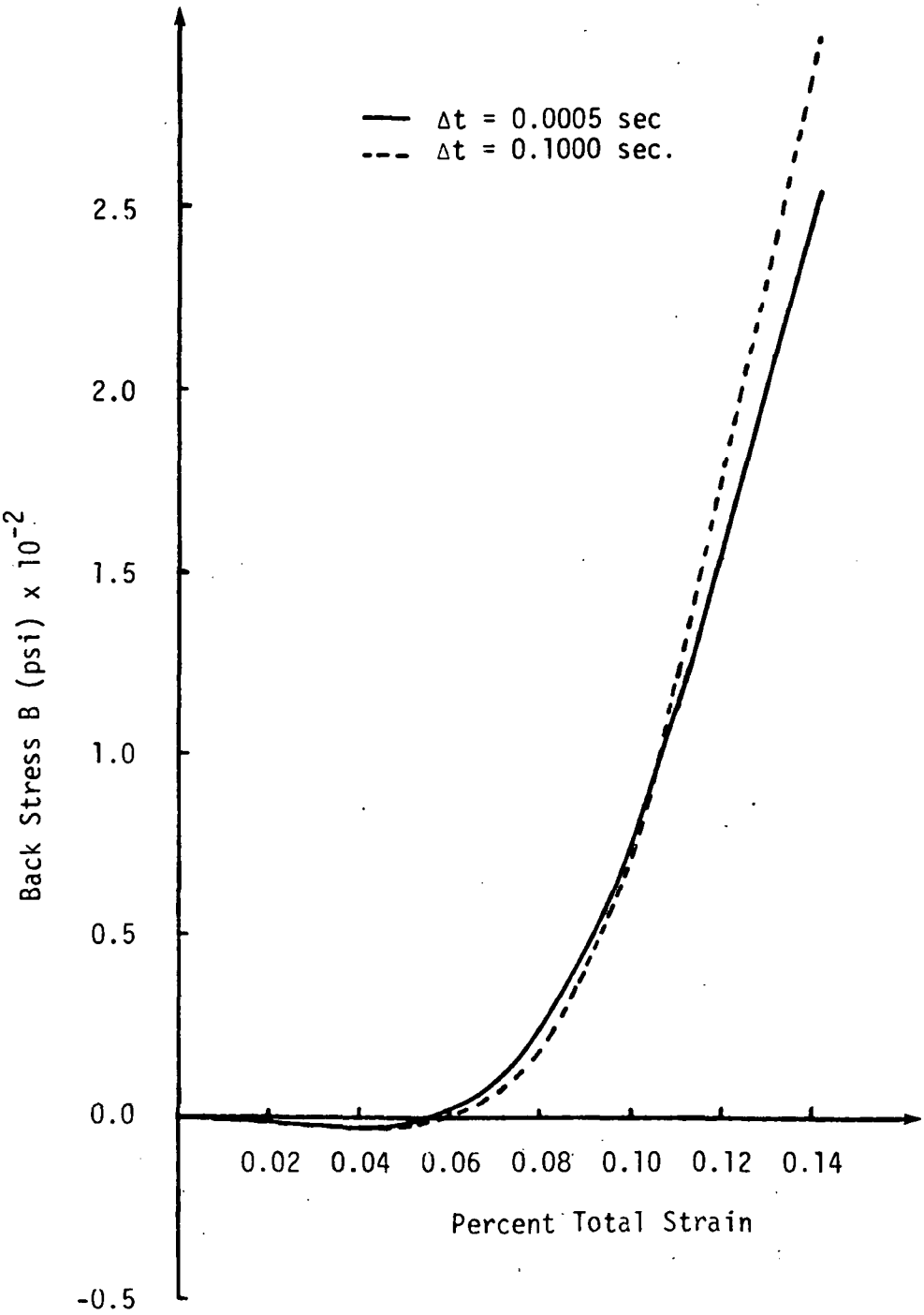

Fig. 10. Back Stress Predicted by Walker's Model For Hastelloy-X at 1800° F.

arises in the prediction of the back stress. The over/under estimation of computed stress continues until the equations ((1) through (4)) naturally dampen themselves out, as is shown in Fig. 6. It should be noted that the "self-correcting" nature of the constitutive models was only apparent when the Euler method was used to numerically integrate the prescribed growth laws. Figure 11 shows that when either the 4th order Runge-Kutta or Trapezoidal method was used, the peak values of stress were simply over- or under- predicted and there was no self-correcting tendency observed.

The second task of the integration investigation was to evaluate the constitutive theories considered herein in terms of solution stability, accuracy, and computational efficiency when numerically integrated using various algorithms. A test matrix consisting of integration methods, time step sizes, and strain input histories was established in order to make qualitative and quantitative comparisons. However, before this phase of testing could begin both a baseline or "pseudo correct" solution for each input history was needed and the integration algorithms needed to be functionally verified so that, in the limit, they would predict the same response.

For each strain history considered, a baseline or "pseudo correct" solution was obtained analytically, since no experimental data were available. The Euler method was used to numerically integrate the prescribed growth laws for each constitutive model until successive changes in step size predicted an identical response.

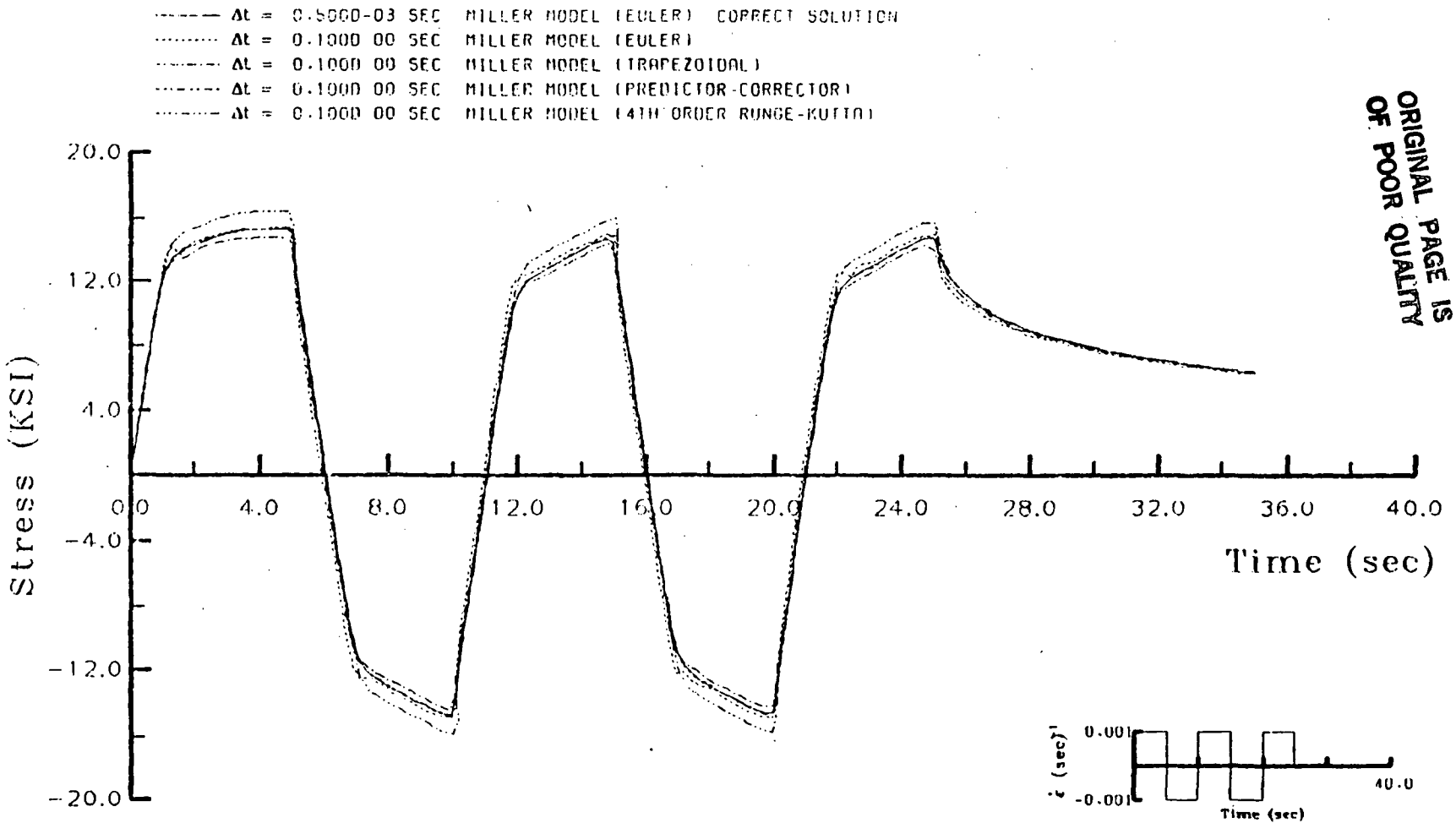

Fig. 11. Comparison of Integration Methods For Miller's Model For Equivalent Time Steps (Hastelloy-X at 1800° F).

This process was repeated for the various input histories, thus developing a family of baseline solutions.

Verification of the integration algorithms was accomplished by using an a priori assumption that all numerical approximation procedures would yield the same output stress histories if the step size was small enough. Results of this investigation indicate that the various integration schemes converge to the same solution for the strain histories and constitutive theories considered herein. In addition, the computational efficiency of each method was obtained through selection of equivalent Δt's. Euler's method was observed to be the most efficient (in terms of execution time on an Amdahl 470V/8 computer), followed by the implicit Trapezoidal method (a factor of 2 slower), then the 4th order Runge-Kutta method (a factor of 4 slower), and finally the Trapezoidal Predictor-Corrector method (a factor of 12 slower). A plausible explanation for the relative slowness of the Predictor-Corrector method was the selection of an inappropriate convergence criterion.

In the ensuing paragraphs qualitative and quantitative comparisons are made for the various test matrix parameters presented earlier. Since the amount of data generated during this study was voluminous, only a representative sample of the results will be presented.

Figure 11 demonstrates the response predicted by Miller's model for a uniaxial, alternating square-wave strain rate input history. The growth laws were integrated using four different numerical approximations and a constant step size of 0.1 seconds.

The results indicate, for monotonic loading and unloading, that integration by the 4th order Runge-Kutta method consistently over-predicts the state of stress by as much as 15%. Conversely, the Trapezoidal method generally underestimates the stress history by 4%. The Euler and Predictor-Corrector methods appear to provide accurate results at any point in the experiment. Similar observations were made for Walker's, Krieg's, and Bodner's model, when subjected to the same strain rate history. These results indicate that for equal time steps, the 4th order Runge-Kutta method provides the least accurate results.

Figures 12 and 13 illustrate that various constitutive models may differ appreciably when the same integration method is used (in this case the Euler method). In Fig. 12 it can be seen that Miller's theory gives a considerable oscillatory response for time steps greater than 0.05 seconds, while Walker's theory shown in Fig. 13 gives a much smoother response for the same time step. Figures 12 through 15 also demonstrate that numerical stability and stress-overshoot are strain rate dependent. Note that in Fig's. 12 and 14 the oscillatory response of Miller's model does not occur until a strain rate of 0.001 in/in/sec is applied. In Fig's. 13 and 15 the amount of stress-overshoot (for the larger step sizes) appears to grow with increasing strain rate.

Figures 16 and 17 present results predicted by Walker's model for a ramp-up-ramp-down strain rate history. Unlike the constant strain rate histories, this type of loading appears to affect the predictive capabilities of the model. As is illustrated, the

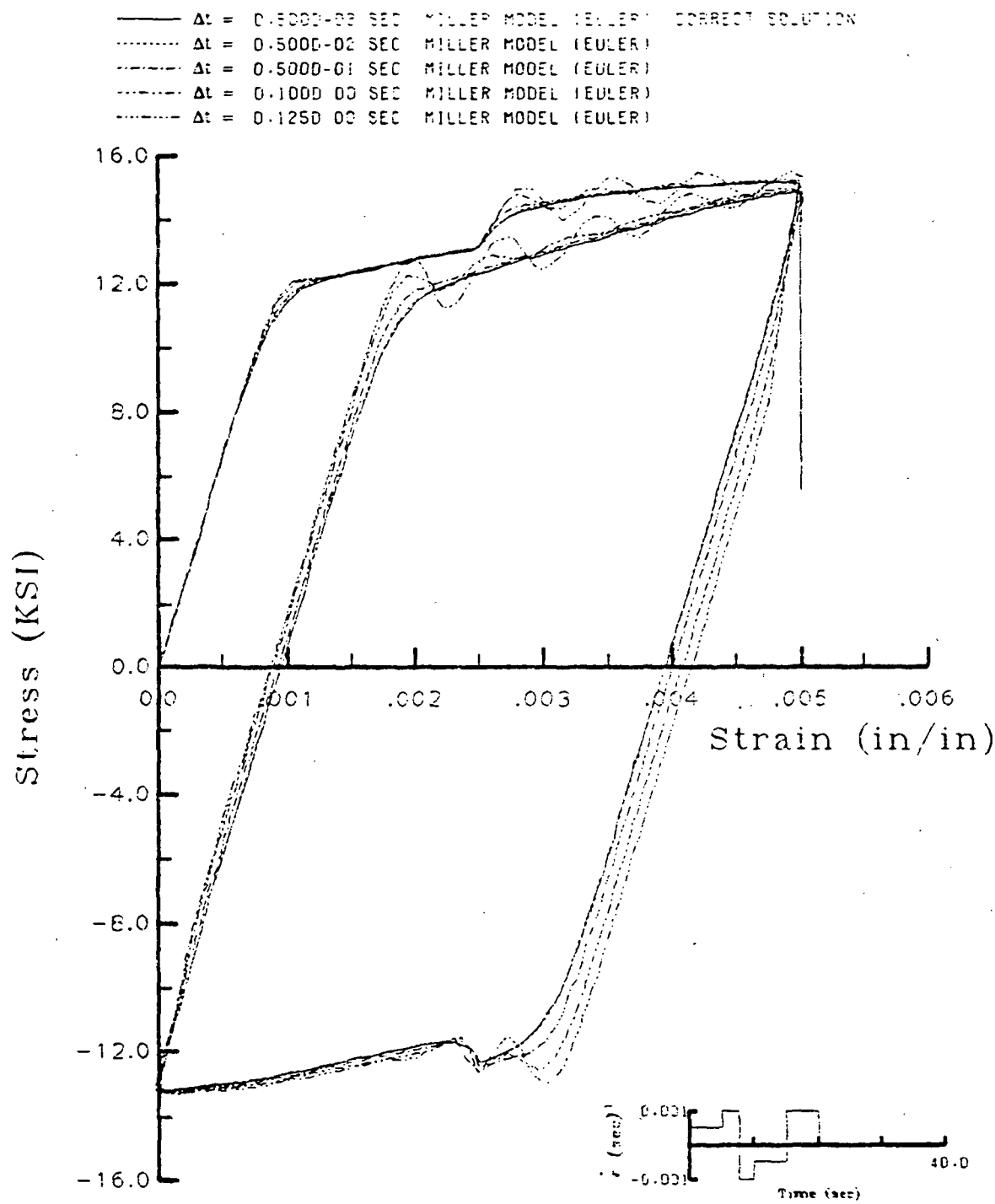

Fig. 12. Stability and Accuracy of Euler Integration For Miller's Model Using Various Step Sizes (Hastelloy-X at 1800° F).

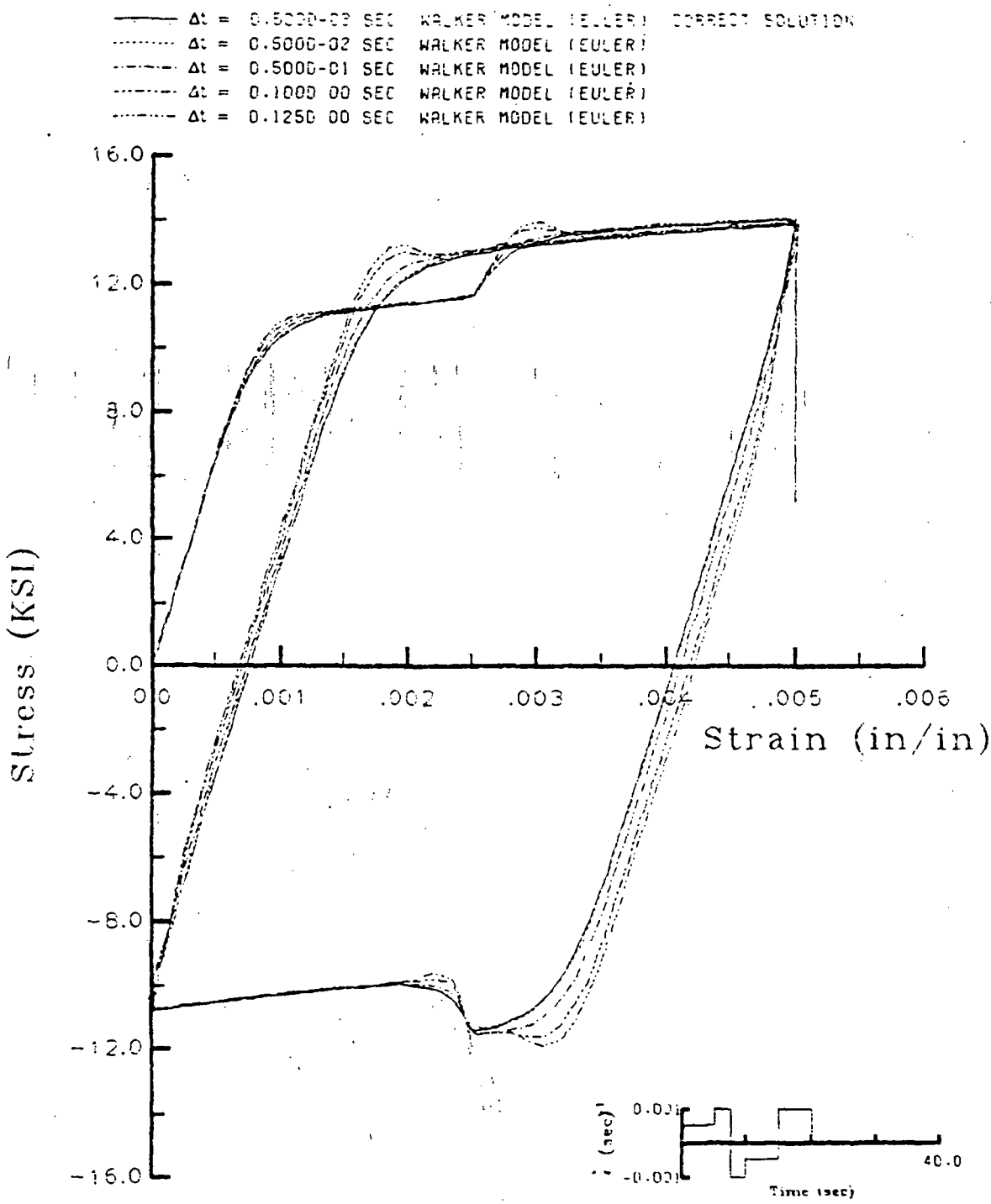

Fig. 13. Stability and Accuracy of Euler Integration For Walker's Model Using Various Step Sizes (Hastelloy-X at 1800° F).

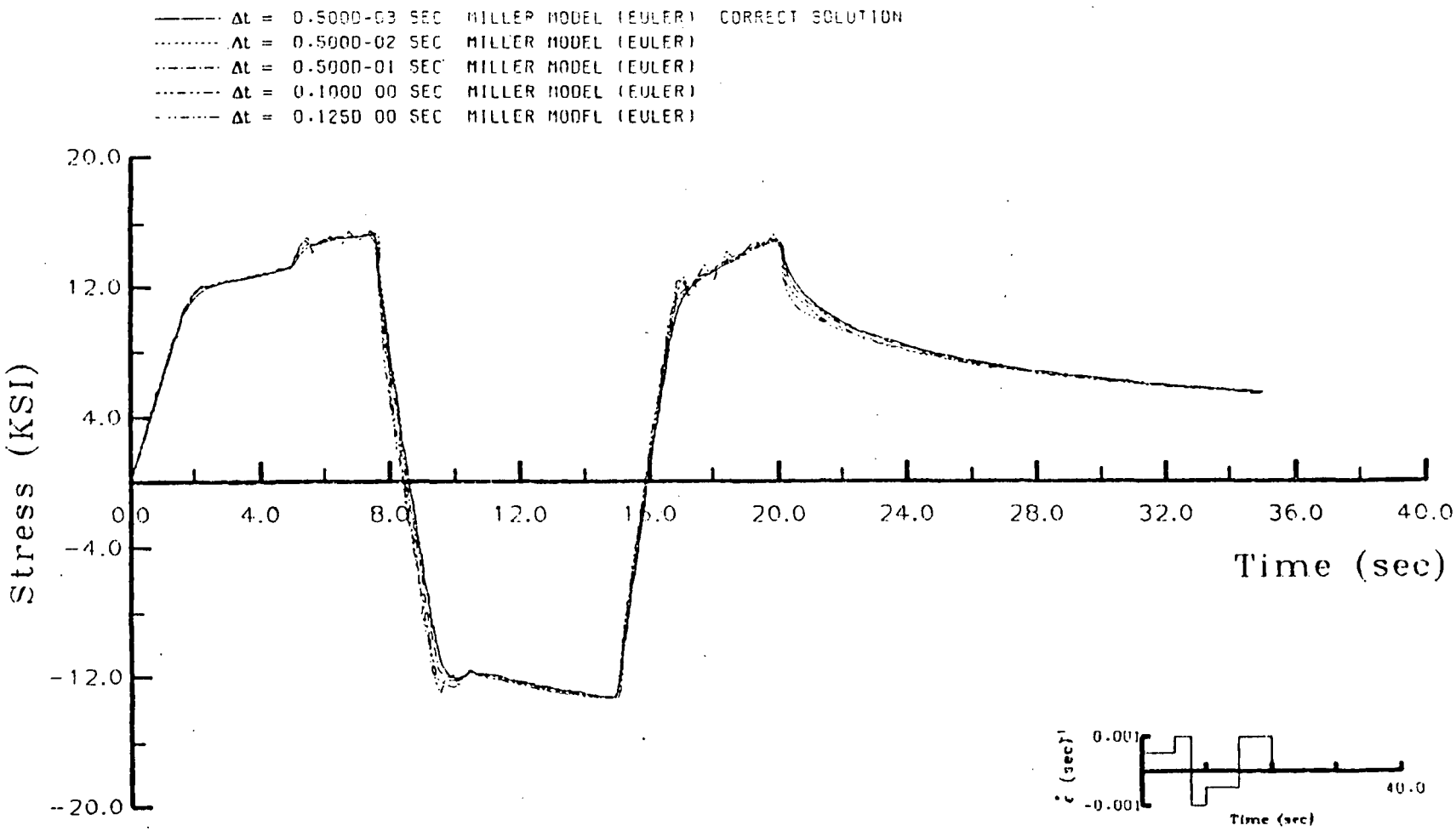

Fig. 14. Stress-time Predictions of Miller's Model Using Euler Integration (Hastelloy-X at 1800° F).

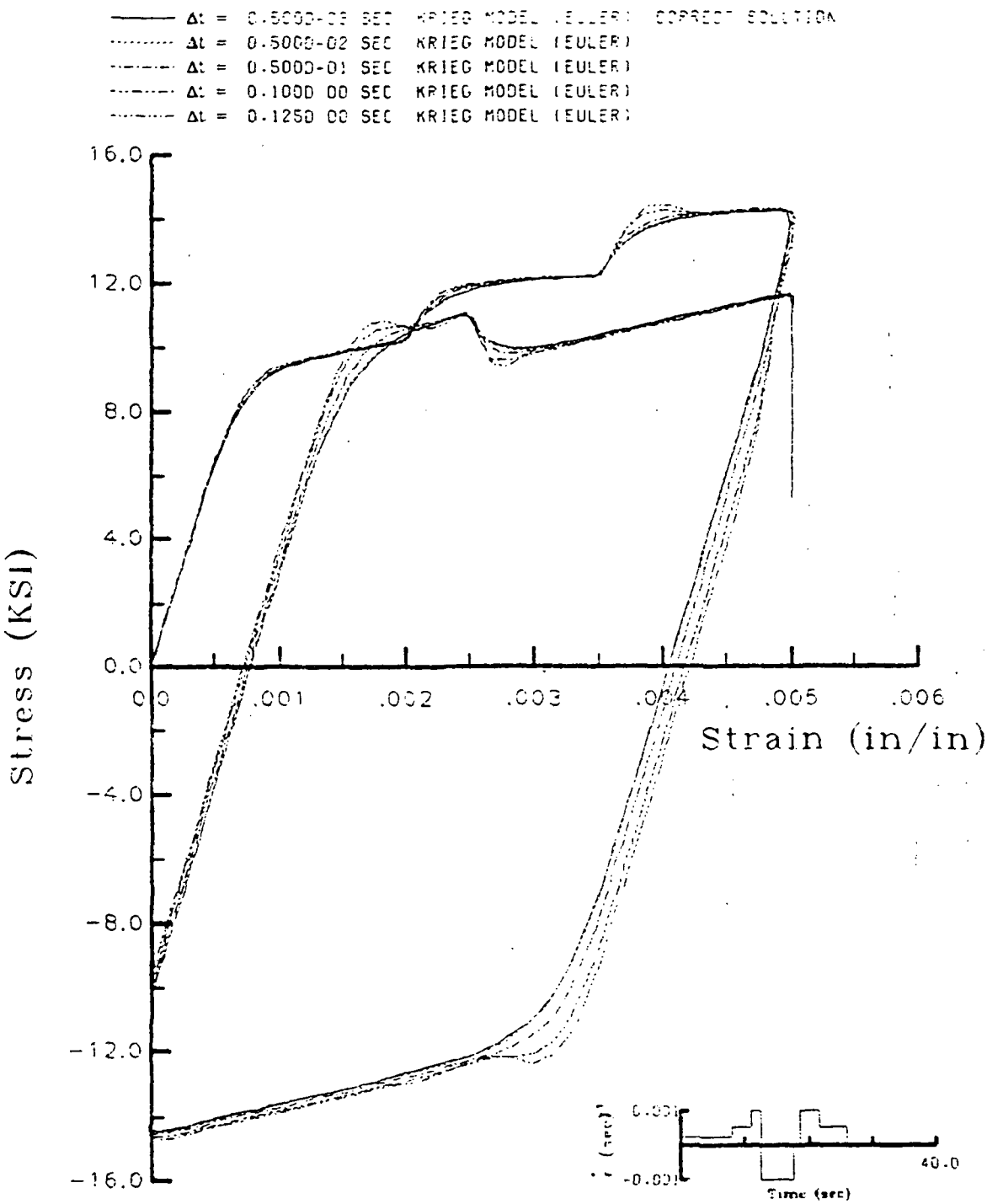

Fig. 15. Stability and Accuracy of Euler Integration for Krieg's Model Using Various Step Sizes (Hastelloy-X at 1800° F).

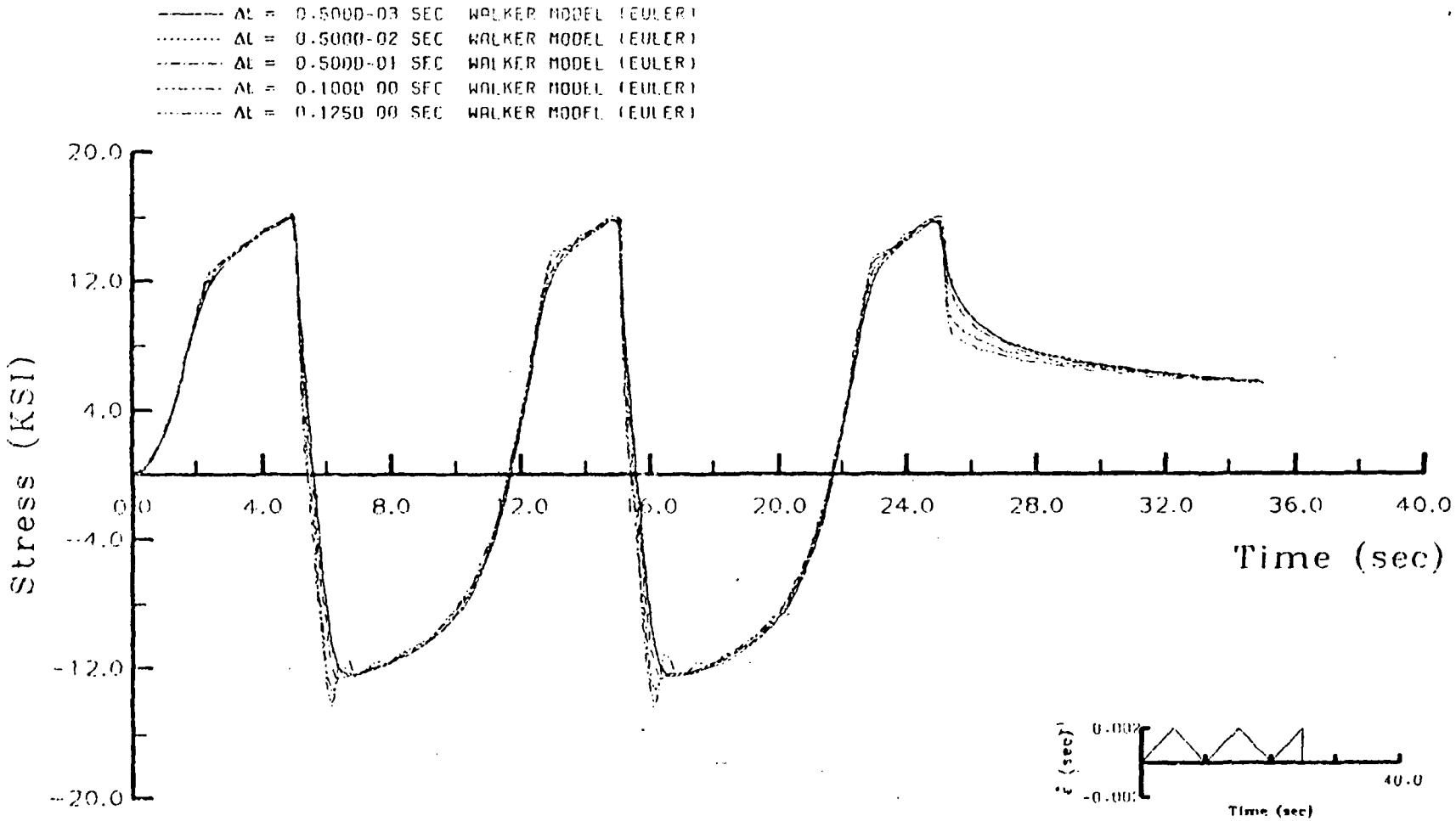

Fig. 16. Stress-time Predictions of Walker's Model Using Euler Integration (Hastelloy-X at 1800° F).

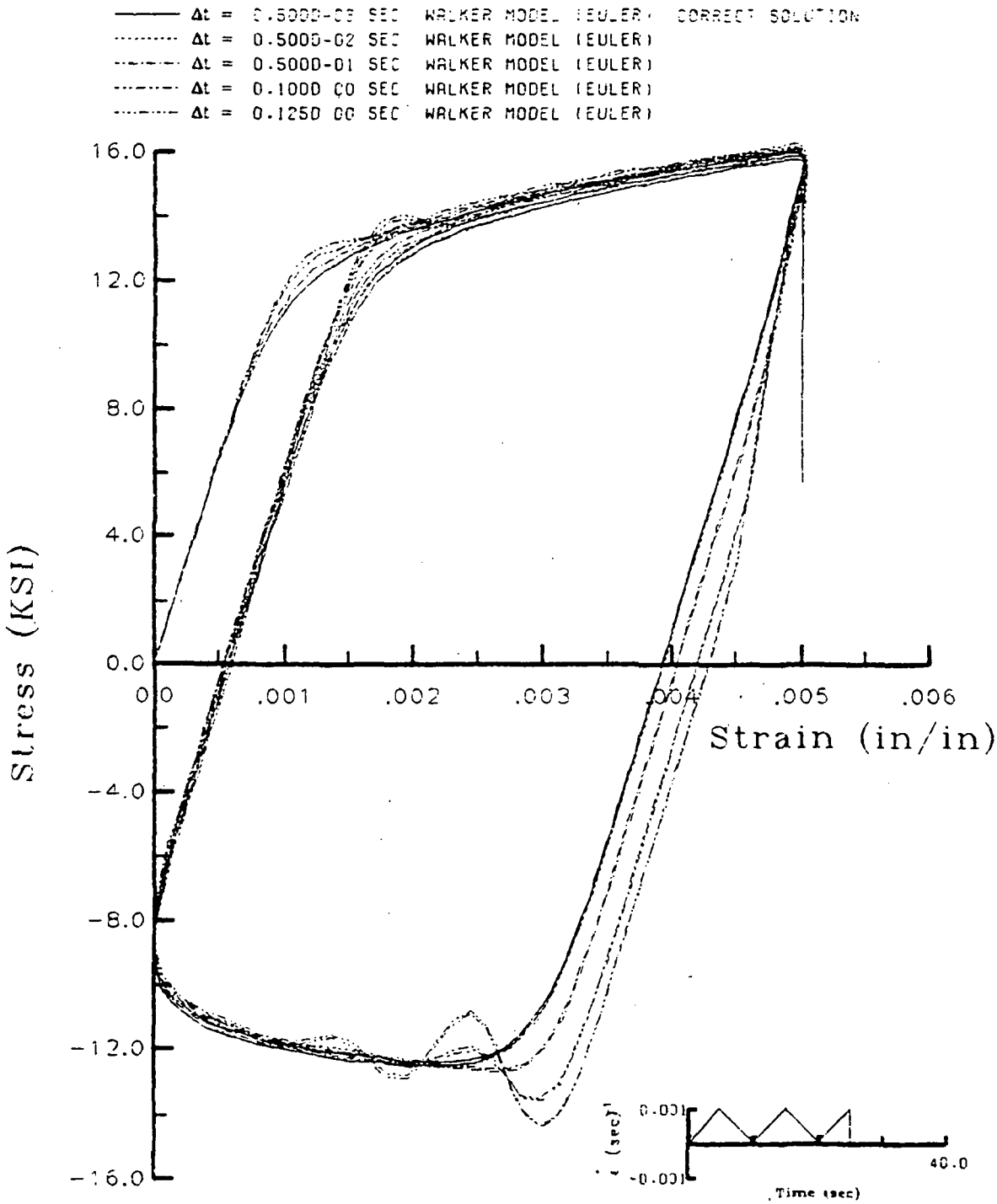

Fig. 17. Stress-strain Predictions of Walker's Model Using Euler Integration (Hastelloy-X at 1800° F).

tensile response is well behaved and the peak response is estimated fairly accurately for all step sizes. However, the compression response is oscillatory and inconsistent for Δt's greater than 0.05 seconds.

Figure 18 shows a 35 second response obtained with Bodner's theory using various integration algorithms. Time steps were selected to obtain solutions which required approximately equivalent computation times. As can be seen, the Euler method solution compares favorably with the baseline prediction, whereas the 4th order Runge-Kutta and Trapezoidal methods tend to over- or under- predict the peak response. Again, the time step used for the Euler method was smaller than those used in the other methods but the total computation time was the same. Similar observations were made for Walker's, Krieg's, and Miller's models when evaluated under the same conditions.

Material Parameter Sensitivity Study

Another important issue this research addressed was what amount of degradation in predicted response could be expected due to variations in material constants. Since each model has a number of material parameters which are determined through a set of complicated tests, the end user must be made aware of the effect small variations, i.e. typical experimental errors, have on the predictive capabilities of the constitutive theory in question. In addition, the experimentalist will better understand the importance of setting up and conducting accurate experiments from which the material constants are obtained.

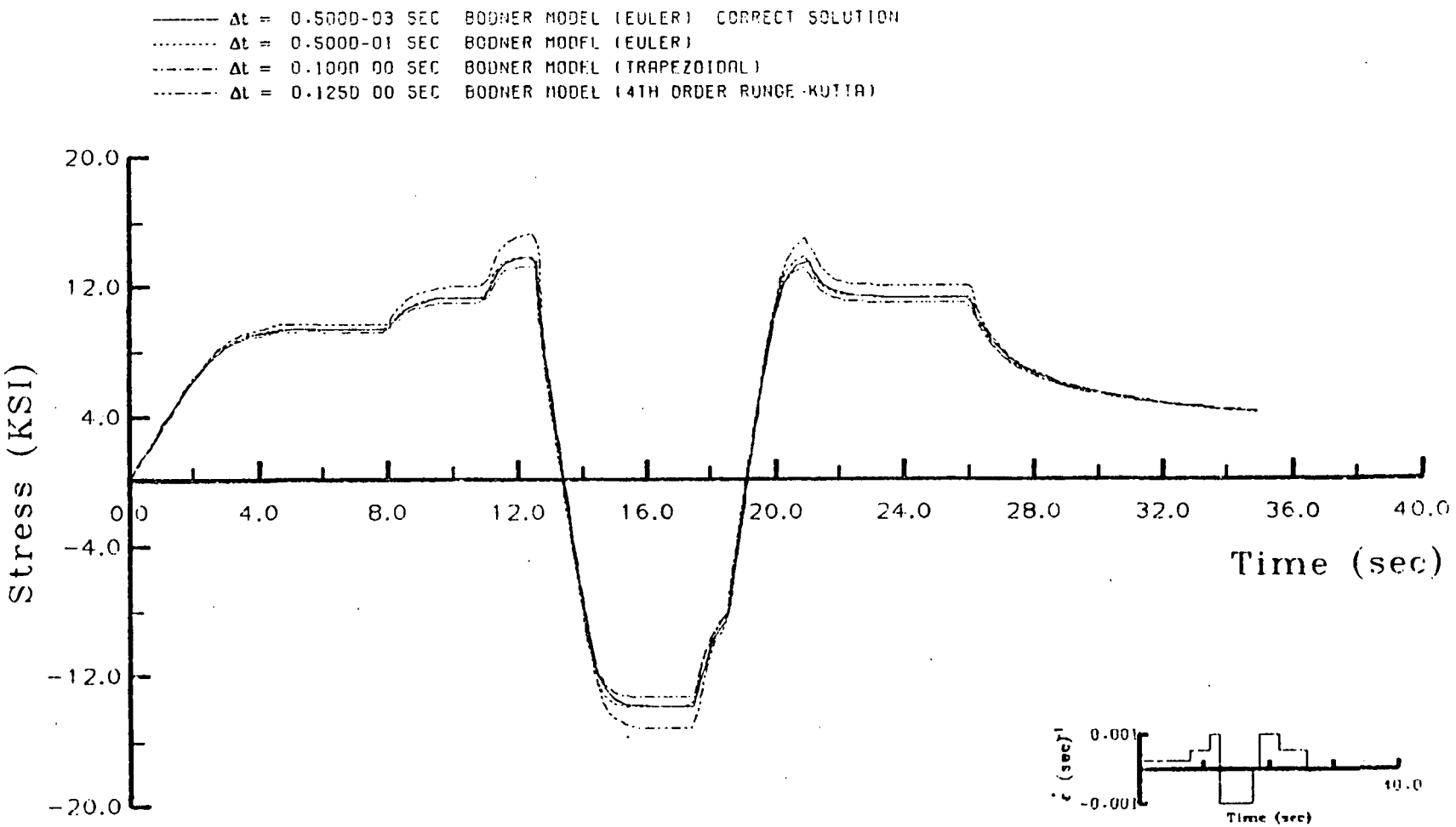

Fig. 18. Comparison of Integration Methods For Bodner's Model With Equivalent Computation Time Allowed For Each Method (Hastelloy-X at 1800° F).

Two procedures were developed to study the effect of material parameter variation. The first procedure characterizes the sensitivity of each constant within a particular constitutive model. Hence, the experimentalist will know what parameters need to be determined most accurately. Each constant's sensitivity to variation was determined by adjusting it by a prescribed amount and comparing predicted results.

The second procedure provided an "upper bound" on the effect that experimental error would have on the determination of the material parameters and ultimately, predicted response. Therefore, the experimentalist will know to what degree of accuracy the test data need to be obtained in order to insure accurate results. The effect of experimental uncertainty was studied by adjusting test data by a prescribed amount (simulating some type of error) and then using that data to determine the material constants.

The overall material parameter sensitivity study was performed by subjecting Bodner's, Walker's, Krieg's, and Miller's models to an alternating square-wave strain rate history. Euler's method was used to numerically integrate the prescribed growth laws using a time step of 0.005 seconds.

All nine of the material constants in Bodner's model were individually adjusted by -5% in order to identify the parameters that, when changed, would have the most pronounced effect on the predicted response. Results of the sensitivity study indicate that the two most sensitive constants were the stress exponent, n, and the hardening recovery constant, D_2, with the first of the two causing

the largest deviation from the baseline solution. The predicted response, after each parameter was changed by -5%, is shown in Fig. 19.

The constant n, in Bodner's model, is determined from a series of constant strain rate tensile tests, where the stress has reached a saturated value. Through the use of equation (10) or by plotting the data as depicted in Fig. 1 (a), it can be seen that the only experimentally measured quantity that affects the value of n is the stress. The parameter D_2 is obtained primarily from constant stress creep tests. Equation (13), which is used to compute D_2, shows that the measured creep rate and the peak stress values (which are used to calculate the material constant n) can affect the determination of this parameter. Hence, the aforementioned experimental quantities must be measured very accurately in order to insure a minimal error in the predicted response.

In addition to studying the sensitivity of individual constants in Bodner's model, the effect of a ±5% change in the test data (simulating experimental error) used to compute all of the material parameters was investigated. From the procedure discussed above, the stress exponent was shown to be the most sensitive constant. Therefore, the values of stress, determined from constant strain tests, were adjusted by ±5% in order to produce the largest change in n. Then the creep rates, from constant stress creep tests, were modified by ±5% in order to obtain the largest variance in D_2. Hence, with new values of stress, creep rate, n, and D_2, the other seven material parameters were re-evaluated and the resulting stress history, as shown in Fig. 20, was predicted. However, Fig. 20

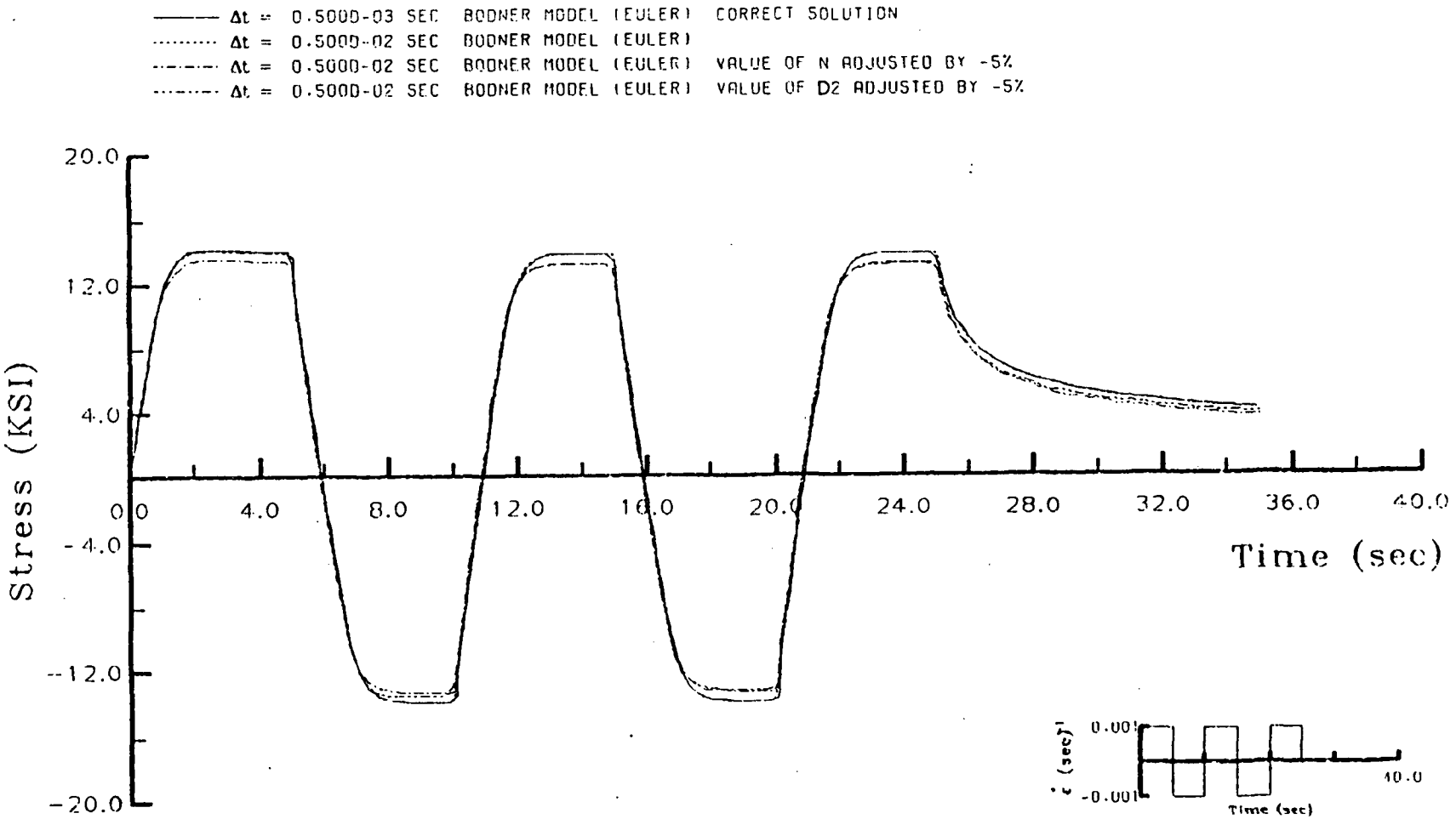

Fig. 19. Sensitivity of Bodner's Model to a -5% Change in Input Constants (Hastelloy-X at 1800° F).

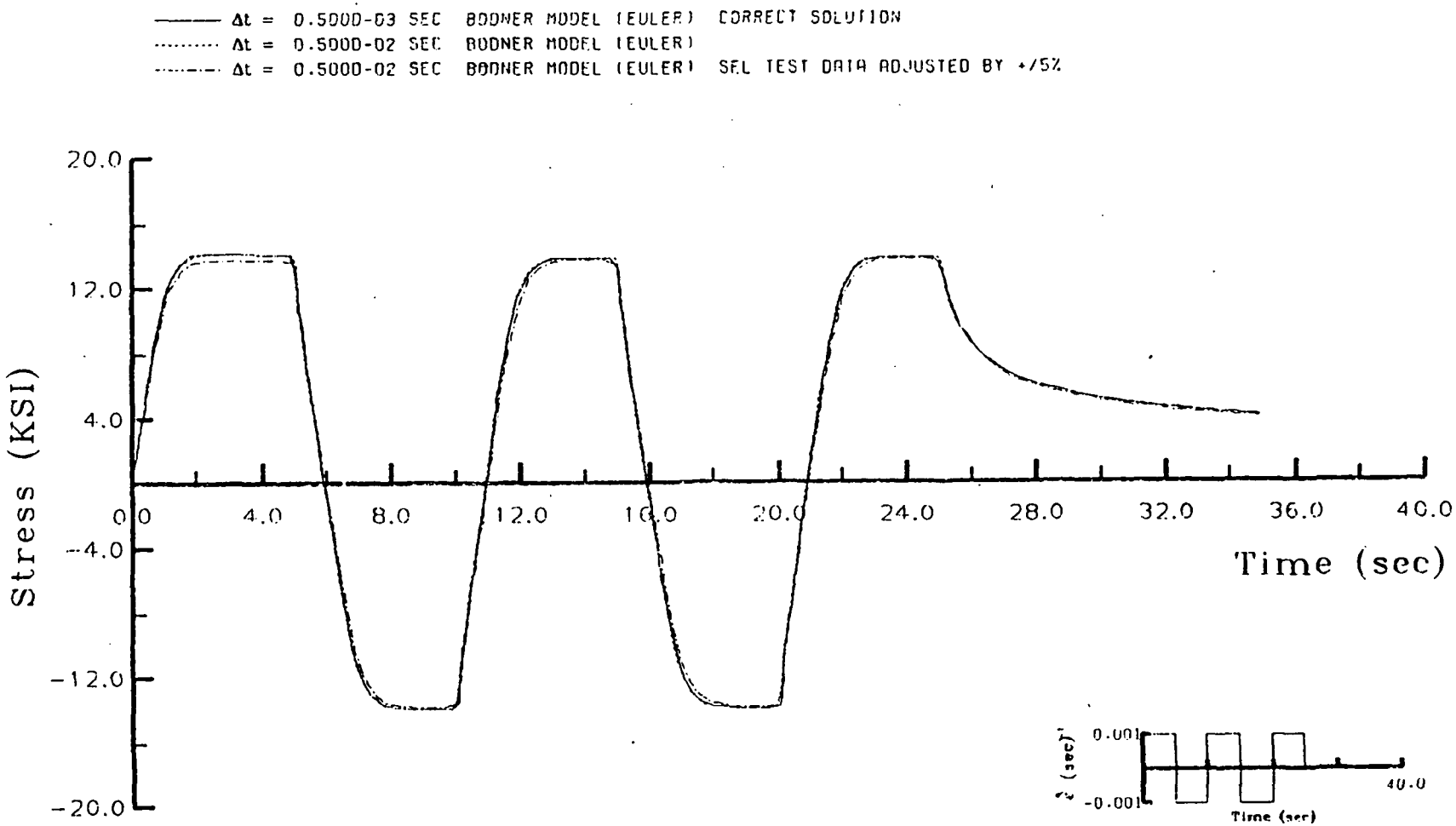

Fig. 20. Sensitivity of Bodner's Model to a ±5% Change in Experimental Test Data Used to Generate Input Constants (Hastelloy-X at 1800° F).

indicated that as a result of the way the constants are determined in Bodner's model, a ±5% change in the test data used to compute the material parameters has little effect on the predicted response.

The sensitivity of the nine constants used in Walker's model were evaluated by individually changing each parameter by -5% and comparing the predicted stress history to a baseline solution. Identified as the two most critical constants were the drag stress (assumed to be a constant value in this model), D, and the stress exponent, n, with the latter of the two being the most sensitive. Shown in Fig. 21 is the predicted response when each parameter (D and n) was adjusted by -5%.

To compute both the stress exponent and the constant valued drag stress, the two maximum tensile stresses at the two highest strain rates (from steady state hysteresis loops) are needed. In addition to the above data, the saturated back stress in tension (B^t_{max}), obtained from stress drop tests, is required. Values for n and D may then be determined from equations (30) and (31), respectively. In order to insure accurate output stress history predictions, precise experimental measurements of σ and B^t_{max} are necessary. It should be noted that Walker [42] indicated that it is difficult to estimate the value of B^t_{max} because the creep rates are usually small and it is very difficult to discern when the creep rate ceases instantaneously.

The effect that experimental error would have on the determination of the material parameters and ultimately, predicted response, was investigated for Walker's model. By adjusting the experimentally

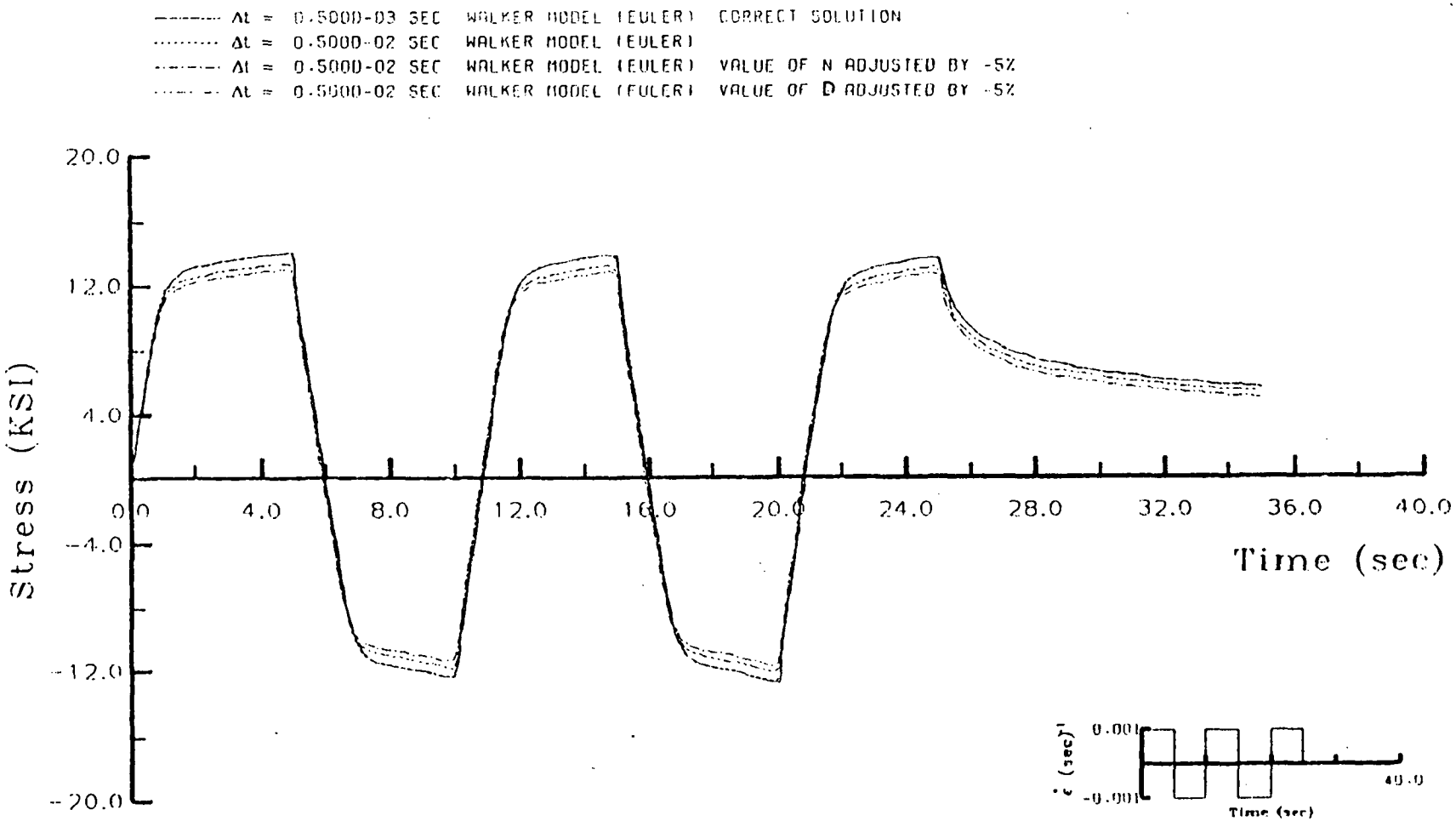

Fig. 21. Sensitivity of Walker's Model to a -5% Change In Input Constants (Hastelloy-X at 1800° F).

measured values of stress from constant strain rate hysteresis loops and saturated back stress by ±5% to create a worst case scenario, each of the nine constants were sequentially recomputed. The effect of experimental uncertainty on the output stress history for Walker's theory is shown in Fig. 22. It can be seen that a ±5% error in all the test data required to compute the material parameters results in significant predicted response errors, with up to 30% over-prediction in the stress during the relaxation period.

In a similar fashion, Fig. 23 illustrates the sensitivity of the stress exponent, n, and initial drag stress, D, to a -5% change in Krieg's model. Since these constants are analogous to the parameters, n and D, used in Walker's model, it is simply reiterated that the measured values of σ and B^t_{max} must be determined very precisely in order to insure an accurate estimation of the predicted response. However, from Fig. 24 it can be seen that even after the constants are re-evaluated to reflect a ±5% change in the experimental test data, the output stress history is virtually unaffected. Hence, Krieg's theory appears to be more tolerant to experimental uncertainty than any of the models previously discussed.

The nine constants in Miller's model were individually varied by -5% in order to characterize their sensitivity. However, unlike the preceding models, selectively changing any one parameter in this set of constitutive equations had little effect on the predicted response. In any event, the most sensitive constants were found to be n and A_2. Figure 25 illustrates the effect that a -5% change in each of these parameters had on the computed stress history.

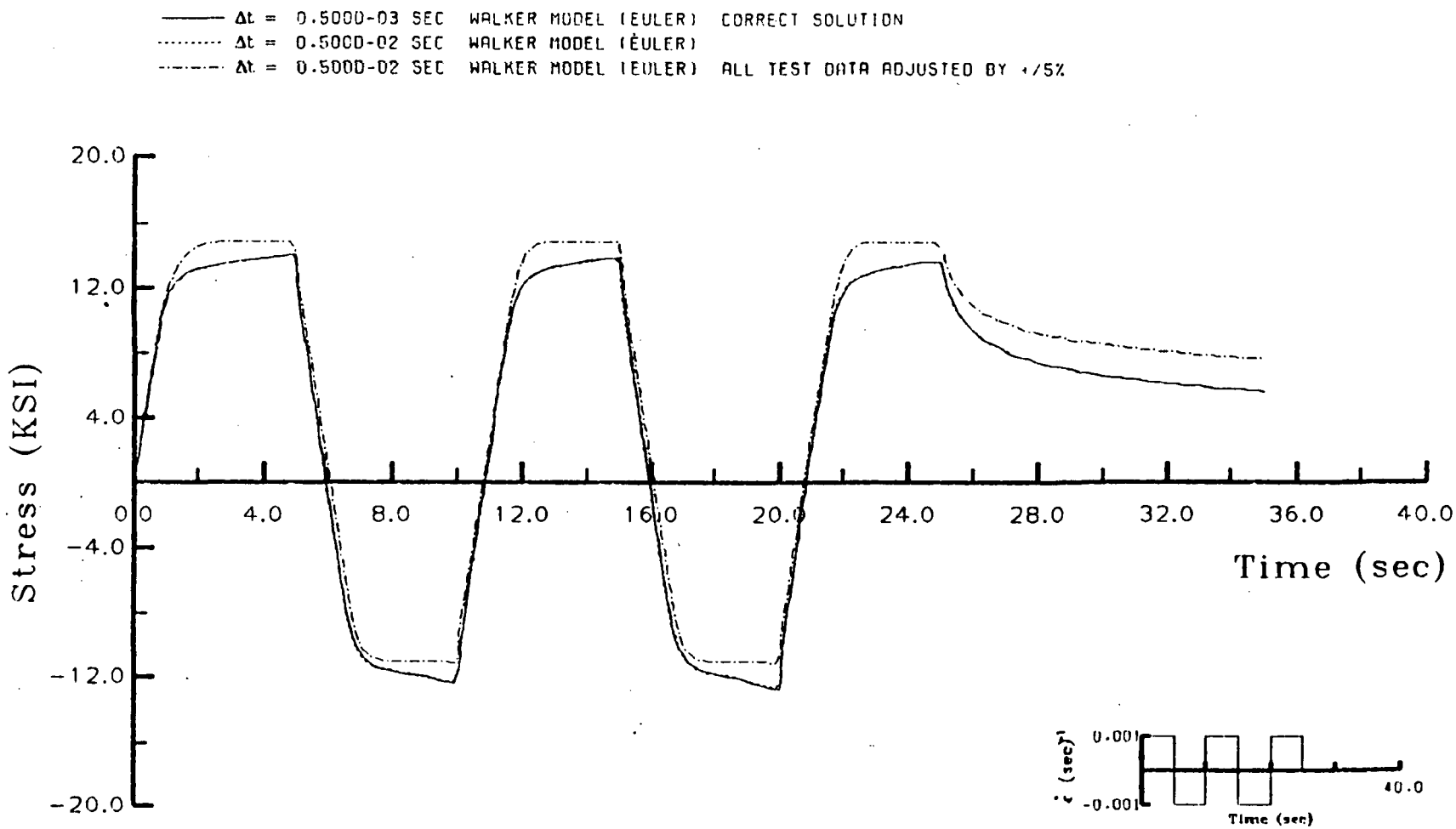

Fig. 22. Sensitivity of Walker's Model to a ±5% Change In Experimental Test Data Used to Generate Input Constants (Hastelloy-X at 1800° F).

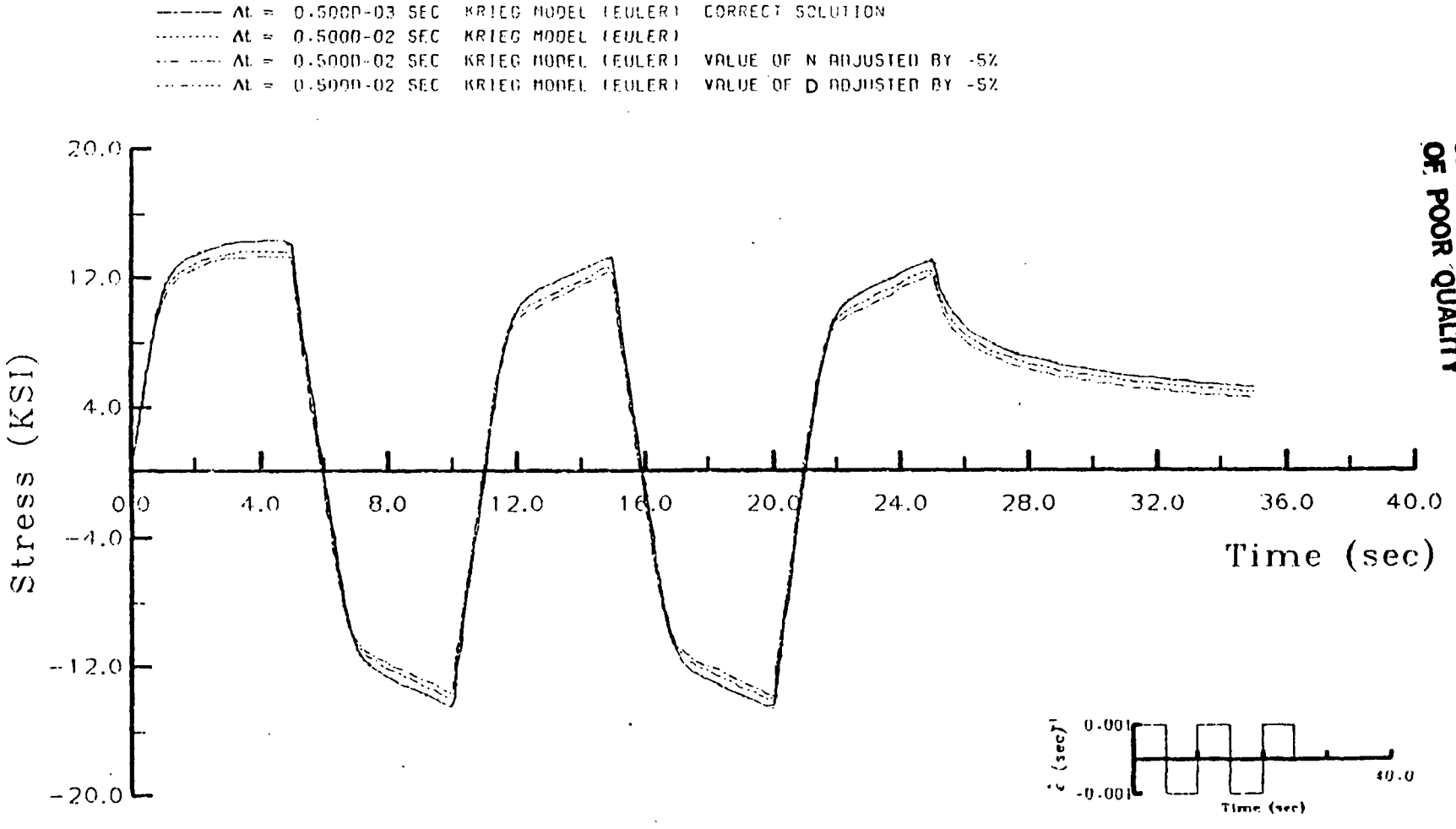

ORIGINAL PAGE IS
OF POOR QUALITY

Fig. 23. Sensitivity of Krieg's Model to a -5% Change In Input Constants (Hastelloy-X at 1800° F).

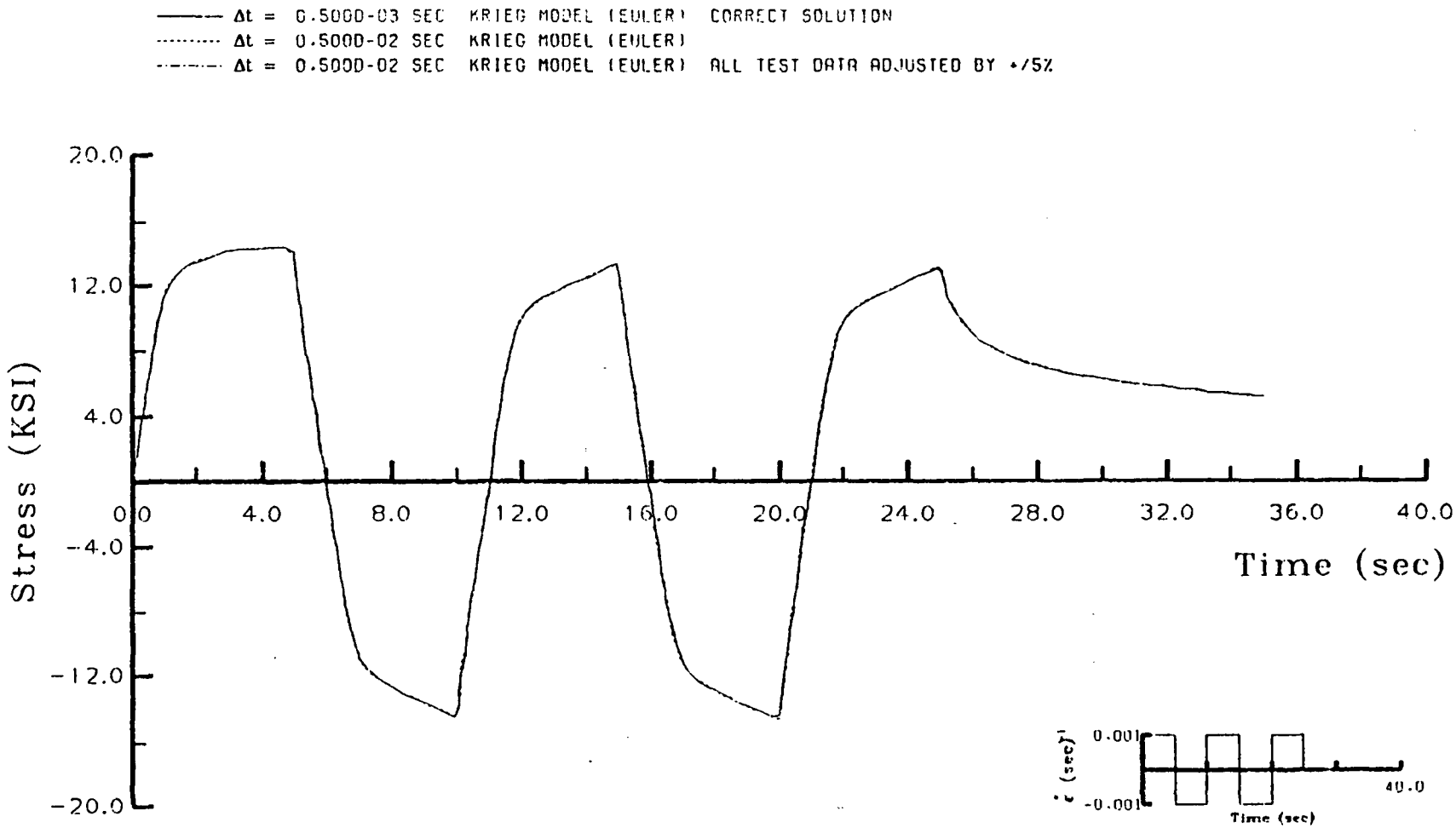

Fig. 24. Sensitivity of Krieg's Model to a ±5% Change In Experimental Test Data Used to Generate Input Constants (Hastelloy-X at 1800° F).

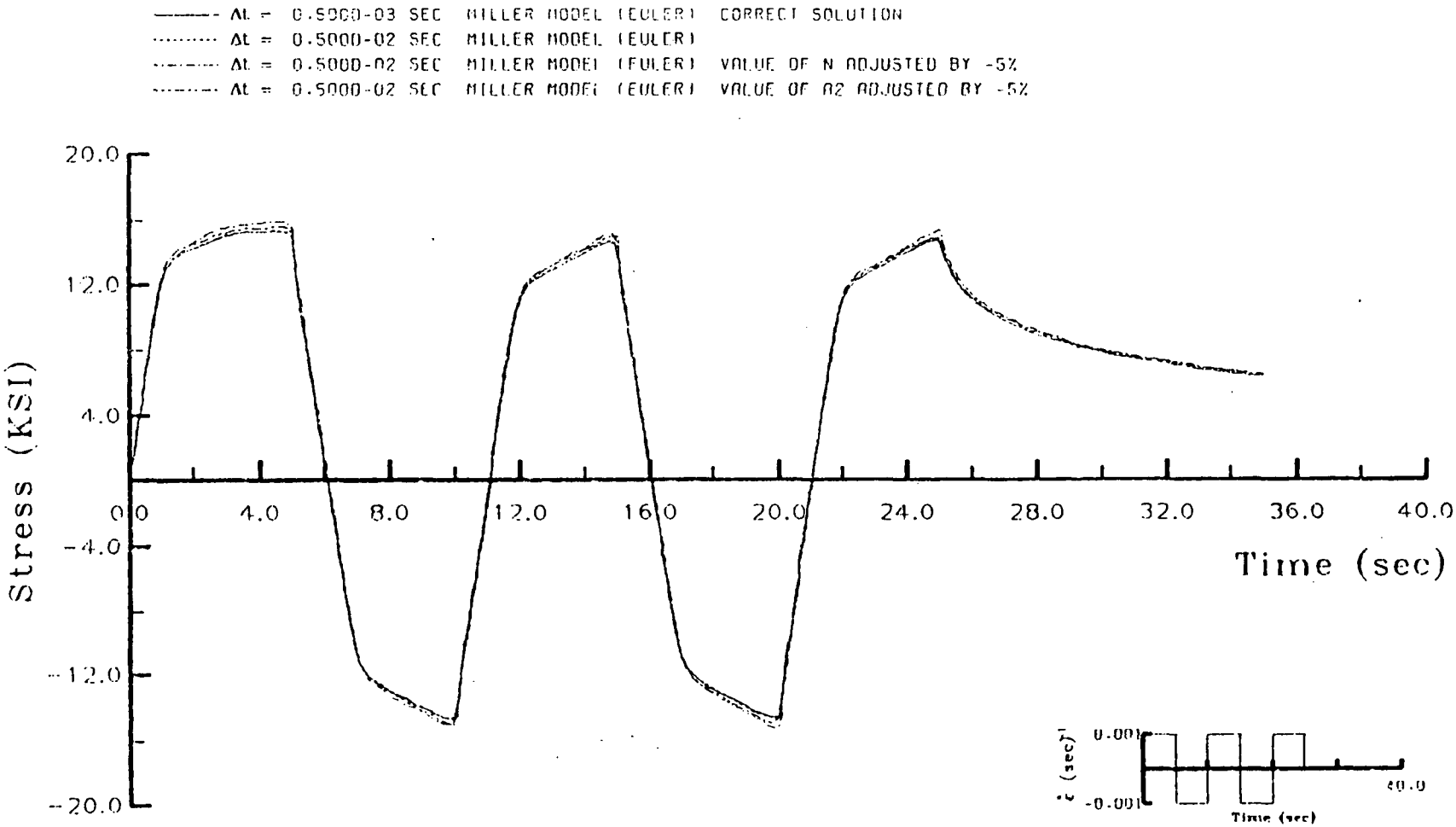

Fig. 25. Sensitivity of Miller's Model to a -5% Change In Input Constants (Hastelloy-X at 1800° F).

In order to minimize the error in the computation of n, the steady state asymptotic stresses obtained from hysteresis loops executed at several strain rates must be measured very accurately. In addition, to determine the parameter A_2, one must precisely establish the value of the steady state back stress from stress drop creep tests.

While Miller's model appears to be fairly insensitive to small variations in particular material constants, when the parameters were collectively re-evaluated (to simulate experimental error in the test data) an appreciable deviation from the baseline solution was noticed. Shown in Fig. 26 is the output stress history resulting from a ±5% change in the steady state stresses and back stresses that were used to recompute the respective constants. As can be seen, a significant over-prediction in peak stresses occurs.

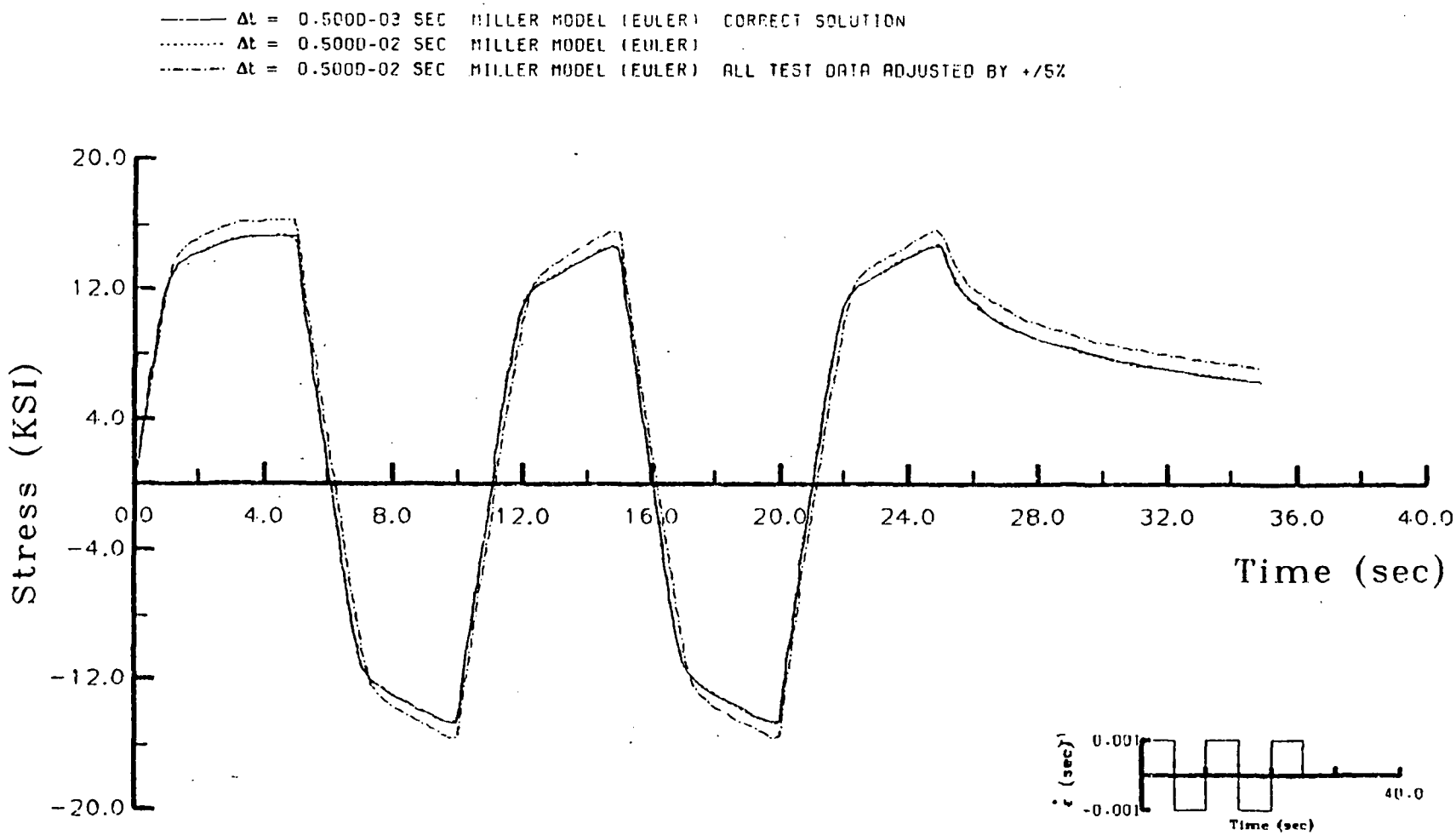

Fig. 26. Sensitivity of Miller's Model to a ±5% Change In Experimental Test Data Used to Generate Input Constants (Hastelloy-X at 1800° F).

CHAPTER V

CONCLUSIONS

In conclusion, the sensitivity of the unified constitutive theories proposed by Bodner, Walker, Krieg, and Miller, to numerical integration techniques and slight changes in material parameters was investigated. The integration sensitivity study involved the use of the Explicit Euler Forward Difference method, the Implicit Trapezoidal method, the Runge-Kutta 4th Order method, and the Trapezoidal Predictor-Corrector method. From the results of this study, the following observations were made:

1) It appears that a simple integration scheme, like the Euler Forward Difference Method, is preferable to more complex schemes from the standpoint of accuracy, computation time, and ease of implementation. The results also indicate that under the conditions tested, the 4th Order Runge-Kutta method provided the least accurate results.
2) The constitutive models may differ appreciably, in terms of numerical stability, when the same integration method and strain input history is used. Miller's model was shown to be the most sensitive to time step variation, which is apparently due to the hyperbolic sine function that is used to characterize the inelastic strain rate function and other growth laws.
3) The predicted stress response appears to be "self correcting" for large time increments when the constitutive equations are integrated by the Euler method. However, when either

the 4th Order Runge-Kutta or Trapezoidal method was used, the peak values of stress were simply over- or under- predicted and no self-correcting tendency was observed.

The material parameter sensitivity study involved the characterization of the sensitivity of each constant within a particular constitutive theory and provides an "upper bound" on the effect that experimental error would have on the determination of the material parameters and ultimately, predicted response. From the results of this sensitivity study, the following observations were made:

1) Small changes (5%) in the material constants may produce significant and unacceptable errors in the predicted stress, particularly the peak stress amplitudes during cyclic loading, and the amount of residual stress during stress relaxation.

2) From this numerical study, it would appear that more precise predictions can be achieved if the experimentally obtained data can be measured more accurately. The type of tests and data that are required to determine the material parameters for each model vary, however some generalizations can be made. For example, most theories require either monotonic or cyclic loading of the specimen in order to obtain peak or saturated values of stress for several constant strain rates. In addition, most models require a stress drop or constant stress creep test in order to determine the steady state or saturated back stress. While other specific

experiments may need to be performed, those mentioned above are probably the most critical to obtaining accurate analytical predictions.

It should be noted that the conclusions reached herein are based on the use of uniaxial simulations. It is expected that the conclusions would hold for multi axial situations; however, further evaluation is needed in this area.

REFERENCES

1. Beek, J.M., Allen, D.H., and Milly, T.M., "A Qualitative Comparison of Current Models for Nonlinear Rate-Dependent Material Behavior of Crystalline Solids," MM 4246T-83-14, Mechanics and Materials Research Center, Texas A&M University, 1983.

2. William, K.J., "Numerical Solution of Inelastic Rate Processes," Computers & Structures, Vol. 8, p. 511, 1978.

3. Shih, C.F., Delorenzi, H.G., and Miller, A.K., "A Stable Computational Scheme for Stiff Time-Dependent Constitutive Equations," Transactions of the 4th International Conference on Mechanics in Reactor Technology, Vol. L2/2, 1977.

4. Chan, K.S., Bodner, S.R., Walker, K.P., and Lindholm, U.J., "A Survey of Unified Constitutive Theories," 2nd Symposium on Nonlinear Constitutive Relations for High-temperature Applications - Cleveland, OH, 1984.

5. Chang, T.Y. and Chang, J.P., "On Numerical Integration and Computer Implementation of Viscoplastic Models," 2nd Symposium on Nonlinear Constitutive Relations for High-Temperature Applications - Cleveland, OH, 1984.

6. Miller, A.K. and Shih, C.F., "An Improved Method for Numerical Integration of Constitutive Equations of the Work Harding Recovery Type," Journal of Engineering Materials and Technology, Vol. 99, p. 275, 1977.

7. Gear, C.W., "The Automatic Integration of Stiff Ordinary Differential Equations," Information Processing 68 - North Holland Publishing Company, Vol. 1, p. 187, 1968.

8. Gear, C.W., "The Automatic Integration of Ordinary Differential Equations," Numerical Mathematics, Vol. 14, No. 3, p. 176, 1971.

9. Gear, C.W., "Algorithm 407 -- DIFSUB for Solution of Ordinary Differential Equations [D2]", Numerical Mathematics, Vol. 14, No. 3, p. 185, 1971.

10. Kumar, V., Morjaria, M., and Mukherjee, "Numerical Integration of Some Stiff Constitutive Models of Elastic Deformation," Journal of Engineering Materials and Technology, Vol. 102, p. 101, 1980.

11. Cormeau, I.C., "Numerical Stability In Quasi-Static Elasto/Viscoplasticity," International Journal for Numerical Methods in Engineering, Vol. 9, p. 109, 1975.

12. Zienkiewicz, O.C. and Cormeau, I.C., "Visco-Plasticity-Plasticity and Creep in Elastic Solids—A Unified Numerical Solution Approach," International Journal for Numerical Methods in Engineering, Vol. 8, p. 821, 1974.

13. Argyris, J.H., Vaz, L.E., and William, K.J., "Improved Solution Methods for Inelastic Rate Problems," Computer Methods in Applied Mechanics and Engineering, Vol. 16, p. 231, 1978.

14. Zirin, R.M. and Kremple, E., "A Finite Element Time Integration Method for the Theory of Viscoplasticity Based on Infinitesimal Total Strain," Journal of Pressure Vessel Technology, Vol. 104, p. 130, 1982.

15. Hughes, J.R., and Taylor, R.L., "Unconditionally Stable Algorithms for Quasi-Static Elasto/Visco-Plastic Finite Element Analysis," Computers & Structures, Vol. 8, p. 169, 1978.

16. Krieg, R.D., "Numerical Integration of Some New Unified Plasticity-Creep Formulations," Transactions of the 4th International Conference on Structural Mechanics in Reactor Technology, Vol. M 6/4, 1977.

17. Tresca, H., "Notes on Yield of Solid Bodies Under Strong Pressures," Comptes Renduz del' Academie des Sciences, Vol. 59, p. 754, 1864.

18. Levy, M., "Memorie sur les equations generales des mourements interieurs des corps solides ductiles au dela des limites ou l' elasticite pourrait les ramener a leur premier eata.," C.R. Acad. Scl. (Paris), Vol. 70, p. 1323, 1870.

19. von Mises, R., "Mechanik der Festen Koerper im plastisch deformablen Eustant, "Goettinger Nachr., Math-Phys. KL," p. 582, 1913.

20. Hencky, H., "Zur Theorie Plastischer Deformationen und die Hierduch im Material Hervorgerufenen Nach-Spannungen," Z. ang. Math, Mech., Vol. 4, p. 323, 1924.

21. Prandtl, L., "Spannungsverteilurg in Plastischen Koerpen," Proceedings of the First International Congress on Applied Mechanics, Delft, Technische Boekhandel en Druckerij, Jr., Waltman, Jr., p. 43, 1925.

22. Prager, W., "The Theory of Plasticity: A Survey of Recent Achievements," Proceedings of The Institution of Mechanical Engineers, Vol. 169, p. 41, 1955.

23. Ziegler, H., "A Modification of Prager's Hardening Rule," Quarterly of Applied Mathematics, Vol. XVIII, p. 55, 1959.

24. Bodner, S.R. and Partom, Y., "Constitutive Equations for Elastic—Viscoplastic Strain—Hardening Materials," Journal of Applied Mechanics, Vol. 42, No. 2, p. 285, 1975.

25. Merzer, A. and Bodner, S.R., "Analytical Formulation of a Rate and Temperature Dependent Stress-strain Realtion," Journal of Engineering Materials and Technology, Vol. 101, p. 254, 1979.

26. Bodner, S.R., "Representation of Time Dependent Mechanical Behavior of Rene 95 by Constitutive Equations," Air Force Materials Laboratory, AFML-TR-4116, 1979.

27. Cernocky, E.P. and Krempl, E., "A Nonlinear Uniaxial Integral Constitutive Equation Incorporating Rate Effects, Creep, and Relaxation," International Journal of Nonlinear Mechanics, Vol. 14, p. 183, 1979.

28. Cernocky, E.P. and Krempl, E., "A Theory of Thermoviscoplasticity Based on Infinitesimal Total Strain," International Journal for Solids and Structures, Vol. 16, p. 723, 1980.

29. Cescotto, S. and Leckie, F., "Determination of Unified Constitutive Equations For Metals at High Temperature," Proceedings of the International Conference on Constitutive Laws for Engineering Materials, p. 105, 1983.

30. Cailletaud, G. and Chaboche, J.L., "Macroscopic Description of the Microstructural Changes Induced By Varying Temperature: Example of IN100 Cyclic Behavior," Third International Conference on Mechanical Behavior of Materials, Vol. 2, p. 22, ICM3, Cambridge, England, 1979.

31. Hart, E.W., "Constitutive Relations for the Nonelastic Deformation of Materials," ASME Journal of Engineering Materials and Technology, Vol. 98-H, p. 193, 1976.

32. Kremple, E., "On the Integration of Rate and History Dependence in Structural Materials," Alta Mechanica, Vol. 22, p. 53, 1975.

33. Krieg, R.D., Swearengin, J.C., and Rohde, R.W., "A Physically-Based Internal Variable Model for Rate-dependent Plasticity," Proceedings ASME/CSME/PVP Conference, p. 15, 1978.

34. Kocks, U.F., "Laws for Work-hardening and Low-temperature Creep," Journal of Engineering Materials and Technology, Vol. 98-H, p. 76, 1976.

35. Miller, A.K., "An Inelastic Constitutive Model for Monotonic, Cyclic, and Creep Deformation: Part I - Equations, Development, and Analytical Procedures" and "Part II - Application to Type 304 Stainless Steel," ASME Journal of Engineering Materials and Technology, p. 97, 1976.

36. Robinson, E.N., "A Unified Creep-Plasticity Model for Structural Metals at High Temperatures," ORNL-TM-5969, 1978.

37. Stouffer, D.C., "A Constitutive Representation for IN100," Air Force Materials Laboratory, AFWAL-TR-81-4039, 1981.

38. Stouffer, D.C. and Bodner, S.R., "A Relationship Between Theory and Experiment for a State Variable Constitutive Equation," ASTM Special Technical Publication 785, 1982 (Also AFWAL-TR-80-4194, 1981).

39. Valanis, K.C., "A Theory of Viscoplasticity Without a Yield Surface: Part I - General Theory," and "Part II - Application to Mechanical Behavior of Metals," Archives of Mechanics, Vol. 23, p. 517, 1971.

40. Valanis, K.C., "On the Foundation of the Endochronic Theory of Viscoplasticity," Archives of Mechanics, Vol. 27, p. 857, 1975.

41. Walker, K.P., "Representation of Hastelloy-X Behavior at Elevated Temperature with a Functional Theory of Viscoplasticity," presented at the ASME Pressure Vessels Conference, San Francisco, CA, 1980.

42. Walker, K.P., "Research and Development Program for Nonlinear Structural Modeling with Advanced Time-temperature Dependent Constitutive Relationships," PWA-5700-50, United Technologies Research Center, East Hartford, CT, 1981.

43. Milly, T.M. and Allen, D.H., "A Comparative Study of Nonlinear Rate-Dependent Mechanical Constitutive Theories for Crystalline Solids at Elevated Temperature," VPI-E-82-5, Virginia Polytechnic Institute and State University, 1982.

44. Ralston, Anthony and Rabinowitz, Philip, "A First Course in Numerical Analysis," 2nd edition, McGraw-Hill Book Company, p. 228, 1978.

APPENDIX 6.3

ON THE USE OF INTERNAL STATE VARIABLES IN THERMOVISCOPLASTIC CONSTITUTIVE EQUATIONS

D.H. Allen and J.M. Beek
Aerospace Engineering Department
Texas A&M University

ABSTRACT

The use of internal state variables in modeling of inelastic solids is gaining widespread usage in current research. Therefore, it is useful to construct a well-defined framework for internal state variable models which is based in continuum mechanics. The objective of this paper is to review and clarify the general theory of internal state variables and to apply it to inelastic metals currently in use in high temperature environments. In this process, certain constraints and clarifications will be made regarding internal state variables.

It will be shown that the Helmholtz free energy can be utilized to construct constitutive equations which are appropriate for metallic superalloys. Furthermore, internal state variables will be shown to represent locally averaged measures of dislocation arrangement, dislocation density, and intergranular gracture. Finally, the internal state variable model will be demonstrated to be a suitable framework for comparison of several currently proposed models for metals and can therefore be used to exhibit history dependence, nonlinearity, and rate as well as temperature sensitivity.

INTRODUCTION

The prediction of inelastic behavior of structural materials at elevated temperature is a problem of great importance which has accordingly been given a great deal of interest by the research community in recent years. These materials exhibit substantial complexity in their thermomechanical constitution. In fact, so complex is their material response that it could be argued that without useful *a priori* information, experimental characterization is futile. The purpose of this paper is to show how the thermodynamics with internal state variables can be utilized to emplace certain constraints on the allowable form of thermomechanical constitutive equations, thus providing some limited insight regarding experimental requirements.

Historically, there have been two distinct approaches to the modelling of inelastic materials: 1) the functional theory [1], in which all dependent variables are assumed to depend on the entire history of independent variables; and 2) the internal state variable (ISV) approach [2], wherein history dependence is postulated to appear implicitly in a set of internal state variables. Lubliner [3] has shown that in most circumstances ISV models can be considered to be special cases of functional models. For experimental as well as analytic reasons numerous recently proposed models for the classes of materials

discussed herein have been proposed in ISV form. Therefore, in this paper the ISV method will be reviewed as well as clarified and it will be shown that this general framework is useful in modeling metals at elevated temperature.

The paper begins with a review of ISV theory, and this is supplemented with a section describing the procedure for constructing macroscopically averaged internal state variables. These concepts are then applied to metals at elevated temperatures. Finally, applications to boundary value problem solving techniques are discussed.

REVIEW OF THE INTERNAL STATE VARIABLE (ISV) APPROACH

The concept of internal state variables, sometimes called hidden variables, was apparently first utilized in thermodynamics by Onsager [4,5] and numerous applications are recorded since the second world war [2,6-14]. Although not originally described for application to solids, the approach which will be discussed herein is due to Coleman and Gurtin [2].

In the theory of internal state variables applied to solids the following state variables are required in order to fully characterize the state of the body at all points x_j and at all times t:*

1) the displacement field $u_i = u_i(x_k,t)$; (1)

2) the stress tensor $\sigma_{ij} = \sigma_{ij}(x_k,t)$; (2)

3) the body force per unit mass $f_i = f_i(x_k,t)$; (3)

4) the internal energy per unit mass $u = u(x_k,t)$; (4)

5) the heat supply per unit mass $r = r(x_k,t)$; (5)

6) the entropy per unit mass $s = s(x_k,t)$; (6)

7) the absolute temperature $T = T(x_k,t)$; (7)

8) the heat flux vector $q_i = q_i(x_k,t)$; (8)

and

9) $\alpha^k_{ij} = \alpha^k_{ij}(x_m,t)$, $k = 1, 2, \ldots, n$; (9)

where α^k_{ij} are a set of n internal state variables which are necessary to account for inelastic material behavior. Although they are listed here as second order tensors, they may be tensors of other rank as well [15].

---

* For convenience, only infinitesimal deformations will be considered here, although the general theory applies to finite deformations as well.

The method of Coleman and Noll [16] may be used to obtain the spatial and time distribution of the body force f_i and heat supply r from the conservation of linear momentum and energy, respectively, assuming the displacements u_i and the temperature T are specified independent variables. Subsequently, it is hypothesized that constitutive equations of state may be constructed for the state variables described in (1) through (8) in terms of u_i and T and their spatial derivatives:

$$\sigma_{ij}(x_k,t) = \sigma_{ij}(\varepsilon_{mn}(x_k,t),\ T(x_k,t),\ g_m(x_k,t),\ \alpha^p_{mn}(x_k,t)) \quad ; \quad (10)$$

$$u(x_k,t) = u(\varepsilon_{mn}(x_k,t),\ T(x_k,t),\ g_m(x_k,t),\ \alpha^p_{mn}(x_k,t)) \quad ; \quad (11)$$

$$s(x_k,t) = s(\varepsilon_{mn}(x_k,t),\ T(x_k,t),\ g_m(x_k,t),\ \alpha^p_{mn}(x_k,t)) \quad ; \quad (12) \text{ and}$$

$$q_i(x_k,t) = q_i(\varepsilon_{mn}(x_k,t),\ T(x_k,t),\ g_m(x_k,t),\ \alpha^p_{mn}(x_k,t)) \quad ; \quad (13)$$

where g_m is the spacial temperature gradient $T_{,m}$ and

$$\varepsilon_{ij} \equiv \tfrac{1}{2}(u_{i,j} + u_{j,i}) \quad . \quad (14)$$

The form of equations (11) through (13) implies that all constitutive equations are evaluated in the specified state (x_k,t). For this reason σ_{ij}, u, s, and q_i are termed observable state variables since they can be determined from equations of state even though there is implicit history dependence via the internal state variables α^p_{mn}, which are defined to be of the form:

$$\dot{\alpha}^k_{ij} \equiv \Omega^k_{ij}(\varepsilon_{mn},\ T,\ g_m,\ \alpha^\ell_{mn}) \quad ; \quad (15)$$

where time and spacial dependence have been dropped for notational convenience. If equations (15) are at all times integrable in time, then the following form is equivalent to (15):

$$\alpha^k_{ij}(x_m,t) = \int_{-\infty}^{t} \Omega^k_{ij}(x_m,t')dt' \quad ; \quad (16)$$

where t is the time of interest and t' is a dummy variable of integration. Therefore, it is apparent that α^k_{ij} are not directly observable at any time and must therefore be considered to be hidden or internal.

Although the above framework has been shown to be applicable to rate dependent crystalline solids [17,18], it is often misconstrued that the absence of explicit strain-rate dependence renders the model inappropriate for use in viscoplasticity theories. It is alternatively hypothesized that

$$\sigma_{ij} = \sigma_{ij}(\varepsilon_{mn},\ \dot{\varepsilon}_{mn},\ T,\ g_m,\ \alpha^\ell_{mn}) \quad (17)$$

is an appropriate form of thermomechanical constitutive equations (10). Although metals at elevated temperature certainly exhibit strain-rate dependence, there are several reasons why equations (17) are less desirable than equations (10). First, equations (17) are not actually equations of state since the inclusion of strain rate implies knowledge is required at some time other than the current time t. Secondly, as demonstrated in discussions of

materials similar to (17) but without internal state variables [19], very little useful information will come from thermodynamic constraints. Finally, explicit strain rate dependence is actually redundant for the materials discussed herein, as will be shown later. Therefore, although this is certainly a semantical issue, equations (10) through (13) and (15) are utilized as the constitutive model in the balance of this paper.

It should also be pointed out that internal state variable growth laws (15) could contain explicit strain-rate dependence:

$$\dot{\alpha}_{ij} = \Omega^{k}_{ij}(\varepsilon_{mn}, \dot{\varepsilon}_{mn}, T, g_m, \alpha^{\ell}_{mn}) \quad , (18)$$

as in the example of a rate independent elastic-plastic material, in which equations of the above form are linear in strain rate:

$$\dot{\alpha}^{\ell}_{ij} = \Omega^{k}_{ijpq}(\varepsilon_{mn}, T, g_m, \alpha^{\ell}_{mn})\dot{\varepsilon}_{pq} \quad . (19)$$

Such a form, although not excluded by the principle of equipresence [20], is only necessary in the circumstance wherein specific rate independence is required, as can be demonstrated by direct substitution of (19) into (16). Furthermore, although the thermodynamic constraints will vary somewhat when (19) are utilized [21,22], the results will be quite similar to those described below.

On the basis of the Coleman-Mizel procedure [23] it can be shown that satisfaction of the first and second laws of thermodynamics for the class of materials detailed above will lead to the following conclusions:

$$h \equiv u - Ts = h(\varepsilon_{mn}, T, \alpha^{k}_{mn}) \quad ; (20)$$

where h is the specific Helmholtz free energy;

$$\sigma_{k\ell} = \rho \frac{\partial h}{\partial \varepsilon_{k\ell}} \quad ; (21)$$

$$s = -\frac{\partial h}{\partial T} \quad ; (22)$$

and

$$q_i = -k_{ij} g_j + 0(g_i) \quad . (23)$$

Equations (21) should not be interpreted as defining as hyperelastic material since the Helmholtz free energy, described by (20), is dependent on the internal state and therefore path dependent.

Although not directly related to our problem, it is useful to note that the path dependence of the Helmholtz free energy precludes the usefulness of equations (21) in Rice's J-integral for fracture mechanics [24]. However, in the case wherein the loading path is radial:

$$\varepsilon_{ij} = k_{ij}\bar{\varepsilon} \; ; \; \alpha^{\ell}_{ij} = k^{\ell}_{ij}\bar{\varepsilon} \; ; \; \bar{\varepsilon} \equiv \sqrt{\varepsilon_{ij}\varepsilon_{ij}} \quad , (24)$$

where k_{ij} and k^{2}_{ij} are constant coefficients, then it is well known that equations (15) are directly integrable so that the free energy can be described by

$$h = h(\varepsilon_{mn}, T, \alpha^{i}_{pq}) = h(\varepsilon_{mn}, T, \alpha^{i}_{pq}(\varepsilon_{mn})) = h(\varepsilon_{mn}, T) \quad . \quad (25)$$

Thus, for the case of proportional loading only, the constitutive equations are derivable directly from a potential function and the J-integral method is applicable.

THE LOCAL AVERAGING PROCESS

Constitutive equations (10) through (13) and (15) are theoretically pointwise in nature; that is, they are applicable to fixed infinitesimal material points. However, practically speaking, there is no way to construct experiments on material points since at the microscopic level the continuum assumption becomes invalid. Rather, it is considered acceptable to construct constitutive equations by subjecting local specimens to surface deformations (or tractions) which lead to spacially homogeneous stresses and strains so that some local average of the pointwise observable state variables can be determined directly from the effects on the boundaries of the specimens.

As shown in Fig. 1, the scale of the smallest dimension of a local specimen is generally constructed so as to be at least an order of magnitude larger than the scale of the largest material inhomogeneity. This sizing helps preserve the continuum assumption while at the same time averaging out the effects of point defects such as crystal lattice dislocations. Conversely, the scale of the largest dimension of a typical specimen should be as small as possible compared to the scale of the global boundary value problem of interest. This constraint is necessary in order to preserve the notion that constitutive equations are indeed pointwise in nature, but it is pragmatic in that it is a simple matter of economy.

The local rather than pointwise constitutive equations that result from experimentation are assumed to be of the same form as pointwise equations (10) through (13) and (15). For example, in the uniaxial test described in Fig. 1 it is customary to define

$$\bar{\sigma}_{11} \equiv \frac{1}{A} \int_{B_1} \sigma_{11} dx_2 dx_3 \quad , \quad (26)$$

$$\bar{\varepsilon}_{11} \equiv \frac{1}{L} \int_{L} \varepsilon_{11} dx_1 \quad , \quad (27)$$

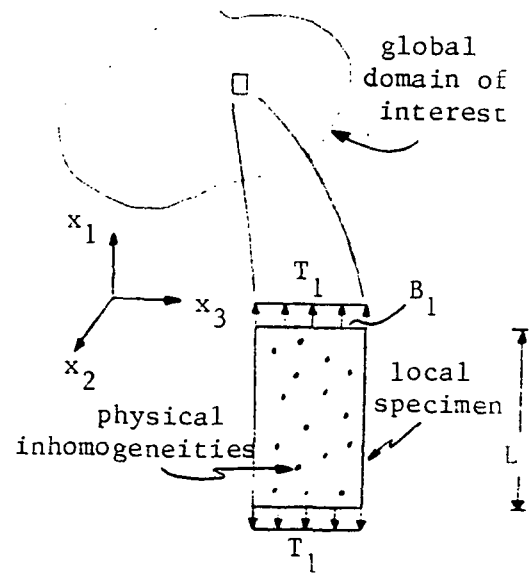

Figure 1

and

$$\bar{T} \equiv T(a_1, a_2, a_3) \quad , (28)$$

where L is the local specimen gage length, A is the cross-sectional area in the x_2-x_3 plane, and (a_1, a_2, a_3) is some arbitrary point on the surface of the specimen. Utilizing these quantities, it is then hypothesized that

$$\sigma_{11}(\varepsilon_{11}, T, \alpha^{\ell}_{mn}) \equiv \bar{\sigma}_{11}(\bar{\varepsilon}_{11}, \bar{T}, \bar{\alpha}^{\ell}_{mn}) \quad , (29)$$

where

$$\bar{\alpha}^{\ell}_{mn} \equiv \frac{1}{V} \int_V \alpha^{\ell}_{mn} \, dx_1 \, dx_2 \, dx_3 \quad , (30)$$

and all quantities with bars represent the locally measured state variables.

Although equations (29) represent an often used way of relating pointwise equations to experimental results, the local averaging process is nevertheless fraught with shortcomings since definitions (26) through (28) all reresent nonunique relations between pointwise state variables σ_{ij}, ε_{ij}, T, α^{k}_{ij} and their locally defined counterparts $\bar{\sigma}_{ij}$, $\bar{\varepsilon}_{ij}$, $\bar{T}$, and $\bar{\alpha}^{k}_{ij}$. There are in fact an infinite number of distributions $\alpha^{\ell}_{mn}(x_1, x_2, x_3)$ which will result in identical values of $\bar{\alpha}^{\ell}_{mn}$. However, assuming that the scale of inhomogeneities is small and that the distribution of α^{ℓ}_{mn} is random the specimen will be statistically homogeneous and the relation between $\bar{\alpha}^{\ell}_{mn}$ and α^{ℓ}_{mn} will be reasonably one to one.

For example, suppose that during some monotonically increasing local strain history $\bar{\varepsilon}_{11}$ a particular internal state variable α^{1}_{11} such as a single dislocation arrangement is governed on a pointwise basis by the almost discontinuous behavior shown in Fig. 2. Suppose further that the time t at which the internal state begins to change is determined by the pointwise stress state. Then the number of dislocation rearrangements occurring in the local specimen as a function of time might be distributed as shown in Fig. 3. If the local specimen is large compared to the scale of the dislocation, and there are numerous dislocation rearrangements, as is usually the case in testing of metals, then the peak of the curve shown in Fig. 3 will be several orders of magnitude greater than unity. It follows from equations (30) that the locally averaged value of the internal state variable represented in Fig. 2 will be as qualitatively shown in Fig. 4.

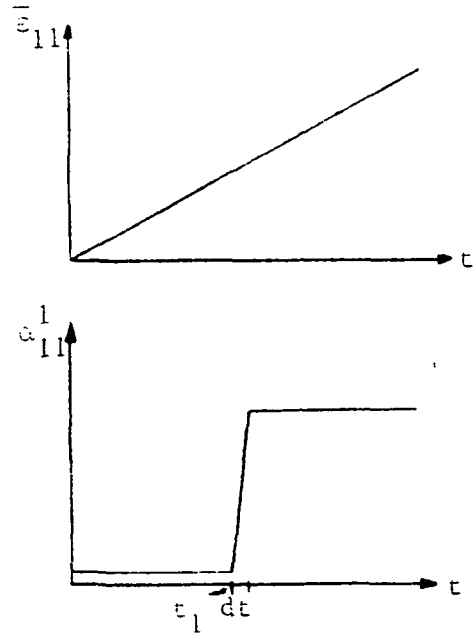

Figure 2

APPLICATION TO METAL CONSTITUTION

In order to describe the class of metals discussed herein, the free energy maybe expanded in terms of the elastic strain tensor ε^E_{kl} and the temperature T in a second order Taylor series expansion as follows:

$$\varepsilon^E_{ij} \equiv \varepsilon_{ij} - \varepsilon^I_{ij} - \varepsilon^T_{ij} \quad , (31)$$

where ε^T_{ij} is the thermal strain tensor and ε^I_{ij} is the inelastic strain tensor, considered to be an internal state variable [17,18,22,25], and

$$h = h_R + \frac{1}{2\rho}\varepsilon^E_{ij}D_{ijkl}\varepsilon^E_{kl} - \frac{C_v}{2T}(T - T_R) \quad , (32)$$

where the subscript R refers to quantities in the reference state, D_{ijkl} is the linear elastic modulus tensor, and $C_v \equiv -T\left(\frac{\partial^2 h}{\partial T^2}\right)$ is the specific heat at constant elastic strain. Substitution of equation (32) into (21) will result in

$$\sigma_{kl} = D_{klmn}(\varepsilon_{mn} - \varepsilon^I_{mn} - \varepsilon^T_{mn}) \quad . (33)$$

The above equations, together with internal state variable growth laws (15), will be shown to be a suitable framework for comparison of all of the models to be discussed herein.

Internal State Variables in Metals

It is now generally agreed in the literature that in single crystals there are two locally averages internal state variables: the back stress ($\alpha_{1_{ij}}$) representing dislocation arrangement; and the drag stress (α_2) representing dislocation density; where the bars have been dropped for convenience and the superscript has been converted to a subscript in order to avoid the confusion which would arise if a state variable were raised to some power. For obvious reasons the back stress is a second order tensor, whereas the drag stress is a scalar. In specimens composed of multiple crystals it is generally agreed that a third internal state variable loosely termed damage ($\alpha_{3_{ij}}$) is necessary in order to account for intergranular mechanisms such as grain boundary sliding and microvoid growth and coalescence that may occur at high temperature and/or large strain. Although damage is obviously a directionally related quantity and therefore tensorial in nature, it is difficult to distinguish phenomenologically between damage and drag stress since both are primarily stiffness reducing mechanisms.

Within the thermodynamic framework described earlier it is also possible to define the inelastic strain tensor to be an internal state variable. However, this interpretation is not generally utilized within the materials

literature. It is hypothesized that the rate of growth of the internal state variables does not depend on the inelastic strain tensor so that

$$\dot{\alpha}^k_{ij} = \Omega^k_{ij}(\varepsilon_{mn}, T, g_m, \alpha_{1_{mn}}, \alpha_2, \alpha_{3_{mn}}) \quad . \quad (34)$$

Due to the form of equations (34) it is said that since the inelastic strain tensor does not appear on the right hand side it is not an internal state variable. However, within the framework defined herein, it is still possible to construct an internal state variable growth law of the form

$$\dot{\varepsilon}^I_{ij} \equiv \Omega^I_{ij}(\varepsilon_{mn}, T, g_m, \alpha_{1_{mn}}, \alpha_2, \alpha_{3_{mn}}) \quad , \quad (35)$$

which is precisely in agreement with definitions (15).

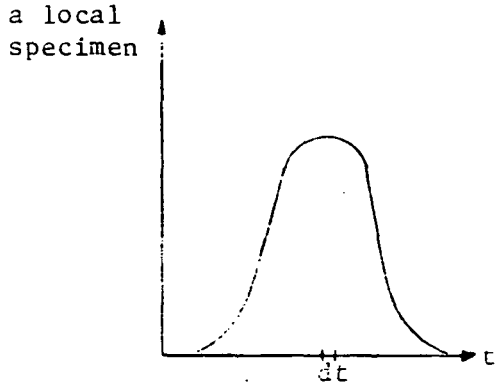

Figure 3

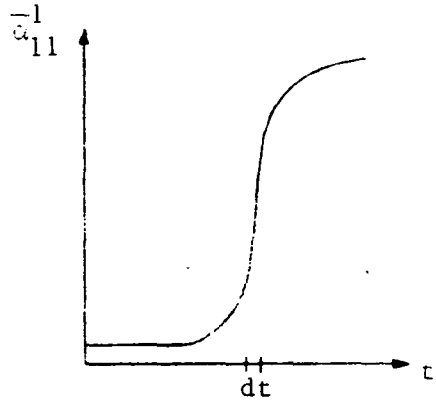

Figure 4

In order to qualitatively verify the supposition that the inelastic strain tensor can be regarded to be an ISV, consider the example of a uniaxial bar subjected to applied displacements such that the end tractions will be evenly distributed. It is customary to deduce the inelastic strain in an experiment of this type by utilizing the output from a load cell to determine the stress and then making use of equations (33) to determine the elastic strain. This result and the total strain measured by an extensometer are then substituted into equations (31) to determine the inelastic strain. Nevertheless, this does not imply that the inelastic strain tensor in an observable state variable. This result can be arrived at only in constitutive experiments such as uniaxial bar tests in which the stress and strain tensors are spacially homogeneous. In heterogeneous boundary value problems, only two state variables may be input (temperature and either stress or strain), and for this case equations (31) and (33) must be supplemented with an ISV growth law of the form of equations (35) in order to determine the inelastic strain tensor. Therefore, in the context of the current thermodynamic framework the inelastic strain tensor may be interpreted to be an ISV.

A Framework for Current Metals Models

In order to establish that current models can be constructed from equations (33), consider the standard solid shown in Fig. 5. The governing differential equation for this analog is

$$\sigma + \frac{\eta_M}{E_M}\dot{\sigma} = E_\infty \varepsilon + \eta_M \left[1 + \frac{E_\infty}{E_M}\right] \dot{\varepsilon} \quad , \quad (36)$$

where by convention the stress is denoted σ and the strain is ε. Equation (36) may be written in the following equivalent form

$$\dot{\varepsilon} = \frac{\dot{\sigma}}{[E_M+E_\infty]} + \frac{E_M}{\eta_M}\frac{[\sigma-E_\infty\varepsilon]}{[E_M+E_\infty]} \quad . \tag{37}$$

In accordance with the instantaneous linear elastic behavior of metals, it is assumed that

$$E_M+E_\infty \equiv E = \text{Young's modulus} = \text{constant}, \tag{38}$$

so that it is clear that equation (37) can be integrated in time to give the following stress formulation

$$\varepsilon(t_1) = \frac{\sigma(t_1)}{E} + \varepsilon^I(t_1) \quad . \tag{39}$$

where ε^I is the inelastic strain, defined by

$$\varepsilon^I(t_1) = \int_{-\infty}^{t_1} \frac{E_M}{E}\frac{[\sigma-E_\infty\varepsilon]}{\eta_M}\,dt \quad . \tag{40}$$

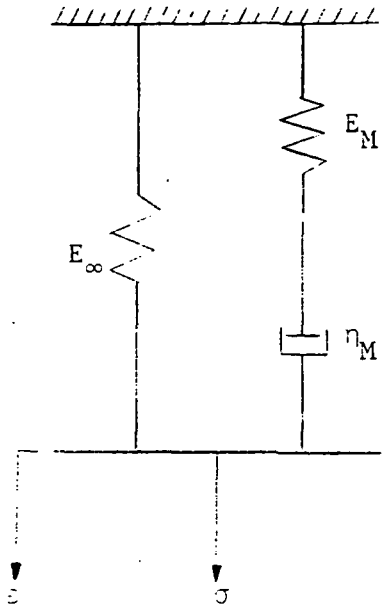

Figure 5

Equation (39) may be solved for the stress and substituted into equation (40) so that it is clear that equation (40) is in accordance with ISV growth laws (16). Further, it can be seen from the standard solid analog in Fig. 5 that since $\sigma-E_\infty\varepsilon$ represents the stress in the Maxwell element, ε^I is not observable, so that ε^I satisfies the two conditions required for it to be an internal state variable.

Equation (39) may be written equivalently in the following strain formulation:

$$\sigma(t_1) = E[\varepsilon(t_1) - \varepsilon^I(t_1)] \quad , \tag{41}$$

which is an equation of state compatible with constitutive equations (10) as well as equations (33). Since no other internal state variables are present in this equation, and also, no additional internal state variables are present in growth law (40) it is apparent that the standard solid analog with constant coefficients E_M, η_M and E_∞ is a single internal state variable model.

It has been noted by several researchers that the standard solid is an appropriate analog for thermoviscoplastic metals if the springs and dashpot are nonlinearized [26,27]. In order to demonstrate this feature, consider a multiaxial extension of equation (36):

$$\sigma_{pq} + K_{pqmn}\,\dot{\sigma}_{mn} = G_{pqmn}\,\varepsilon_{mn} + M_{pqmn}\,\dot{\varepsilon}_{mn} \quad , \quad (42)$$

where by convention the small strain tensor ε_{ij} is used in conjunction with the work conjugate stress tensor σ_{ij}. In order to model metals K_{pqmn}, G_{pqmn}, and M_{pqmn} are required to be nonlinear in some as yet undetermined way. In addition, in accordance with constraint equation (38), it is required that

$$K^{-1}_{ijmn}\,M_{mnkl} = D_{ijkl} \quad , \quad (43)$$

where D_{ijkl} is the linear elastic modulus tensor. Equations (42) may be rewritten in a strain formulation equation of state form as follows:

$$\sigma_{ij} = D_{ijkl}\,[\varepsilon_{kl} - \varepsilon^{I}_{kl}] \quad , \quad (44)$$

where ε^{I}_{kl} is the inelastic strain tensor, defined by

$$\varepsilon^{I}_{ij} \equiv \int_{-\infty}^{t_1} M^{-1}_{ijpq}\,[\sigma_{pq} - G_{pqmn}\varepsilon_{mn}]\,dt \quad . \quad (45)$$

Substituting equations (43) and (44) into equations (45) will result in

$$\varepsilon^{I}_{ij} = \int_{-\infty}^{t_1} \{K^{-1}_{ijmn}[\varepsilon_{mn} - \varepsilon^{I}_{mn}] - M^{-1}_{ijpq}\,G_{pqmn}\varepsilon_{mn}\}\,dt \quad , \quad (46)$$

so that equations (46) are in accordance with growth laws (16). The number of internal state variables contained in the model will depend on the degree of nonlinearity proposed in the nonlinear tensors K_{pqmn}, G_{pqmn}, and M_{pqmn}, and this will be discussed in the following section. However, before continuing, it should be pointed out that the constitutive equations developed in this section assume that the elastic and inelastic strain tensors may be linearly decoupled. It has been shown that this assumption is invalid for finite deformation [28]. However, even under finite deformation conditions the inelastic strain is decoupled from the elastic strain in such a way that the inelastic strain tensor may be considered to be an internal state variable.

Current Models for Metals

The framework for metals models discussed in the previous section can be used to describe numerous models currently under development [26,27,29-58]. For example, the microphysically based isothermal model proposed by Krieg, et al., [30] is of the form described by equations (33):

$$\sigma_{ij} = D_{ijkl}(\varepsilon_{kl} - \varepsilon^{I}_{kl}) \quad , \quad (47)$$

where

$$\dot{\varepsilon}^{I}_{ij} \equiv \dot{\varepsilon}_o \left\{ \frac{\left[\left(\sigma'_{kl} - \alpha'_{1_{kl}}\right)\left(\sigma'_{kl} - \alpha'_{i_{kl}}\right)\right]^{\frac{1}{2}}}{\alpha_2} \right\}^{m} \frac{\left(\sigma'_{ij} - \alpha'_{1_{ij}}\right)}{\left[\left(\sigma'_{pq} - \alpha'_{1_{pq}}\right)\left(\sigma'_{pq} - \alpha'_{1_{pq}}\right)\right]^{\frac{1}{2}}} , \quad (48)$$

and $\dot{\varepsilon}_o$ and m are material constants, and σ'_{ij} is the deviatoric stress tensor and $\alpha'_{1_{ij}}$ is the deviatoric component of the back stress tensor. Since equations (48) contain the stress tensor, substituting equations (33) into (48) will result in equations consistent eith growth laws (15). In addition, Krieg, et al., give the back stress and drag stress to be, respectively,

$$\dot{\alpha}'_{1_{ij}} = A_\alpha \dot{\varepsilon}^{I}_{ij} - r_\alpha \frac{\alpha'_{1_{ij}}}{\left(\alpha'_{1_{pq}} \alpha'_{1_{pq}}\right)^{\frac{1}{2}}} , \quad (49)$$

and

$$\dot{\alpha}_2 = A_R \left(\dot{\varepsilon}^{I}_{ij} \dot{\varepsilon}^{I}_{ij}\right)^{\frac{1}{2}} - r_R , \quad (50)$$

where A_α and A_R are hardening constants, and r_α and r_R are recovery functions of temperature and internal state variables. It can be seen that since ISV growth laws (49) and (50) are consistent with equations (15), the model proposed by Krieg, et al., contains three internal state variables: the inelastic strain tensor, the back stress tensor, and the drag stress tensor.

Furthermore, classical plasticity theories can be described by the general form

$$\sigma_{ij} = D_{ijmn} \left(\varepsilon_{mn} - \varepsilon^{I}_{mn}\right) , \quad (51)$$

where

$$\dot{\varepsilon}^{I}_{ij} = \dot{\lambda} \frac{\partial F}{\partial \sigma_{ij}} . \quad (52)$$

$\dot{\lambda}$ is a scalar valued function of state, and F is a scalar valued state function for inelastic behaviour often taken to be the yield function. If F is described by the von Mises yield criterion [53], given by

$$F(\sigma_{ij} - \alpha_{1_{ij}}) = \tfrac{1}{2}(\sigma_{ij} - \alpha_{1_{ij}})(\sigma_{ij} - \alpha_{1_{ij}}) = k^2 , \quad (53)$$

where $\alpha_{1_{ij}}$ is a tensor describing the yield surface center in stress space and k is a constant representing the yield surface size, then equations (52) can be written as

$$\dot{\varepsilon}_{ij} = \dot{\lambda}(\sigma_{ij} - \alpha_{1_{ij}}) \quad , (54)$$

resulting in a kinematic hardening model with constant yield surface size. Substitution of equations (51) into the above will yield a result consistent with rate independent ISV growth laws (19).

Furthermore, if the yield surface translation is derived from the Ziegler modification [60] of the Prager work hardening rule [61], it may be described by

$$\dot{\alpha}_{1_{ij}} = \dot{\mu}(\sigma_{ij} - \alpha_{1_{ij}}) \quad , (55)$$

where $\dot{\mu}$ is a scalar valued function of state. By use of equations (51), equations (55) can also be shown to be consistent with equations (19). Therefore, a classical plasticity-based kinematic hardening model contains two internal state variables: the inelastic strain tensor and the yield surface translation tensor representing the back stress.

In order to further illustrate the applicability of equations (33), (35) and (15) to current models for metals, ten of these models have been cast in uniaxial form in Table 1, wherein it is shown that although the framework for each model is identical (Valanis' model is in simplified form), the ISV growth laws vary widely both in number and form.

CONCLUSION

The main content of this paper has been to review and clarify the continuum and thermodynamics based internal state variable model for application to thermoviscoplastic metals. In this process the following points have been made:

1) the definition of an internal state variable utilized in this model has been clarified;

2) internal state variables in metals represent local averages of dislocation arrangement, dislocation density, and intergranular damage,

3) in the context of the ISV definition given here, inelastic strain may also be interpreted as an internal state variable;

4) the path dependent Helmholtz free energy may be expanded in a second order expansion in elastic strain and temperature in order to obtain a stress-strain equation of state;

5) rate dependence enters the constitutive equations implicitly via the inelastic strain, as demonstrated by the nonlinear standard solid analog; and

6) a three-dimensional generalization of the standard solid may be used as a means of comparison of the general form of several currently proposed models.

Further ramifications of the ISV model discussed are also of importance, although not detailed herein. For example, this model may be utilized to construct a coupled heat conduction equation which may be utilized to predict heat generation in thermoviscoplastic metals [62]. Furthermore, the concept of internal state variables may be utilized to construct models for the mechanical constitution of composites with damage [63,15,65,66].

ACKNOWLEDGEMENT

The authors gratefully acknowledge support for this research which was sponsored by NASA Lewis Research Center under grant no. NAG 3-491.

REFERENCES

1. Coleman, B.D.: Thermodynamics of Material with Memory. Archive for Rational Mechanics and Analysis, Vol. 17, pp. 1-46, 1964.

2. Coleman, B.D., and Gurtin, M.E.: Thermodynamics with Internal State Variables. Journal of Chemical Physics, Vol. 47, pp. 597-613, 1967.

3. Lubliner, J.: On Fading Memory in Materials of Evolutionary Type. Acta Mechanica, Vol. 8, pp. 75-81, 1969.

4. Onsager, L.: Reciprocal Relations in Irreversible Processes I. Physics Review, Vol. 37, pp. 405-426, 1931.

5. Onsager, L.: Reciprocal Relations in Irreversible Processes II. Physics Review, Vol. 38, pp. 2265-2279, 1931.

6. Eckart, C.: Thermodynamics of Irreversible Processes, I. The Simple Fluid. Physics Review, Vol. 58, p. 267, 1940.

7. Meixner, J.: Die thermodynamische Theorie der Relaxationserscheinungen und ihr Zusammenhang mit der Nachwirkungstheorie. Kolloid-Z., Vol. 134, p. 2, 1953.

8. Biot, M.A.: Theory of Stress-Strain Relations in Anisotropic Viscoelasticity and Relaxation Phenomena. Journal of Applied Physics, Vol. 25, p. 1385, 1954.

9. Biot, M.A.: Variational Principles in Irreversible Thermodynamics with Application to Viscoelasticity. Physics Review, Vol. 97, p. 1463, 1955.

10. Ziegler, H.: An Attempt to Generalize Onsager's Principle, and Its Significance for Rheological Problems. Z. angew. Math. Phys., Vol. 9, p. 748, 1958.

11. Valanis, K.C.: Unified Theory of Thermomechanical Behavior of Viscoelastic Materials. Mechanical Behavior of Materials Under Dynamic Loads, p. 343, Springer,1968.

12. Kestin, J., and Rice, J.R.: Paradoxes in the Application of Thermodynamics to Strained Rods. A Critical Review of Thermodynamics, p. 275, Mono Book Corp., 1970.

13. Schapery, R.A.: Application of Thermodynamics to Thermomechanical, Fracture and Birefringent Phenomena in Viscoelastic Media. Journal of Applied Physics, Vol. 35, p. 1941, 1964.

14. Schapery, R.A.: A Theory of Non-Linear Thermoviscoelasticity Based on Irreversible Thermodynamics. Proceedings 5th U.S. National Congress of Applied Mechanics, ASME, pp. 511-530, 1966.

15. Krajcinovic, D., and Fonseka, G.U.: The Continuous Damage Theory of Brittle Materials - Part I - General Theory. Journal of Applied Mechanics, Vol. 48, pp. 809-815, 1981.

16. Coleman, B.D., and Noll, W.: The Thermodynamics of Elastic Materials with Heat Conduction and Viscosity. Archive for Rational Mechanics and Analysis, Vol. 13, p. 167, 1963.

17. Kratochvil, J., and Dillon, O.W., Jr.: Thermodynamics of Crystalline Elastic-Visco-Plastic Materials. Journal of Applied Physics, Vol. 41, pp. 1470-1479, 1970.

18. Kratochvil, J., and Dillon, O.W., Jr.: Thermodynamics of Elastic-Plastic Materials as a Theory with Internal State Variables. Journal of Applied Physics, Vol. 40, pp. 3207-3218, 1969.

19. Day, W.A.: The Thermodynamics of Simple Materials with Fading Memory. Springer, New York, 1972.

20. Truesdell, C., and Noll, W.: The Nonlinear Field Theories of Mechanics. Handbuck der Physik, Vol. III/3, Springer, Berlin, 1965.

21. Lubliner, J.: On the Thermodynamic Foundations of Non-Linear Solid Mechanics. International Journal of Non-Linear Mechanics, Vol. 7, pp. 237-254, 1972.

22. Green, A.E., and Naghdi, P.M.: A General Theory of an Elastic-Plastic Continuum. Archive for Rational Mechanics and Analysis, Vol. 18, pp. 251-281, 1965.

23. Coleman, B.D., and Mizel, V.J.: Thermodynamics and Departures from Fourier's Law of Heat Conduction. Archive for Rational Mechanics and Analysis, Vol. 13, pp. 245-261, 1963.

24. Rice, J.R.: A Pathe Independent Integral and the Approximate Analysis of Strain Concentration by Notches and Cracks. Journal of Applied Mechanics, Vol. 35, pp. 379-386, 1968.

25. Allen, D.H.: Some Comments on Inelastic Strain in Thermoviscoplastic Metals. Texas A&M University Report No. MM NAG 3-31-83-8, June 1983.

26. Cernocky, E.P., and Krempl, E.: A Theory of Thermoviscoplasticity Based on Infinitesimal Total Strain. International Journal of Solids and Structures, Vol. 16, pp. 723-741, 1980.

27. Walker, K.P.: Representation of Hastelloy X Behavior at Elevated Temperature with a Functional Theory of Viscoplasticity. Presented at ASME Pressure Vessels Conference, San Francisco, Aug. 12, 1980.

28. Lee, E.H., and McMeeking, R.M.: Concerning Elastic and Plastic Components of Deformation. International Journal of Solids and Structures, Vol. 16, pp. 715-721, 1980.

29. Hart, E.W.: Constitutive Relations for the Nonelastic Deformation of Metals. ASME J. Eng. Mater. Tech., Vol. 98-H, p. 193, 1976.

30. Krieg, R.D., Swearengen, J.C., and Rohde, R.W.: A Physcially-based Internal Variable Model for Rate-Dependent Plasticity. Proceedings ASME/CSME PVP Conference, pp. 15-27, 1978.

31. Bodner, S.R., and Partom, Y.: Constitutive Equations for Elastic-Viscoplastic Strain-Hardening Materials. Journal of Applied Mechanics, Vol. 42, No. 2, pp. 305-389, 1975.

32. Bodner, S.R.: Representation of Time Dependnet Mechanical Behaviour of Rene 95 by Consitutive Equations. Air Force Materials Laboratory, AFML-TX-79-4116, 1979.

33. Stouffer, D.C., and Bodner, S.R.: A Relationship Between Theory and Experiment for a State Variable Constitutive Equation. Air Force Materials Laboratory, AFWAL-TR-80-4194, 1981.

34. Bodner, S.R., Partom, I., and Partom, Y.: Uniaxial Cyclic Loading of Elastic-Viscoplastic Materials. J. App. Mech., 1979.

35. Cescotto, S., and Leckie, F.: Determination of Unified Constitutive Equations for Metals at High Temperature. Proc. Int. Conf. on Constitutive Laws for Eng. Mater., pp. 105-111, 1983.

36. Robinson, D.N.: A Unified Creep-Plasticity Model for Structural Metals at High Temperatures. ORNL-TM-5969, October 1978.

37. Miller, A.K.: An Inelastic Constitutive Model for Monotonic, Cyclic, and Creep Deformation: Part I - Equations Development and Analytical Procedures and Part II - Application to Type 304 Stainless Steel. ASME J. Eng. Mater. Tech., Vol. 98-H, p. 97, 1976.

38. Krempl, E.: On the Interaction of Rate and History Dependence in Structural Materials. Acta Mechanica, Vol. 22, pp. 53-90, 1975.

39. Liu, M.C.M., and Krempl, E.: A Uniaxial Viscoplastic Model Based on Total Strain and Overstress. J. Mech. Phys. Solids, Vol. 27, pp. 377-391, 1979.

40. Cernocky, E.P., and Krempl, E.: A Theory of Viscoplasticity Based on Infinitesimal Total Strain. Acta Mechanica, Vol. 36, pp. 263-289, 1980.

41. Cernocky, E.P., and Krempl, E.: A Nonlinear Uniaxial Integral Constitutive Equation Incorporating Rate Effects, Creep and Relaxation. Int. J. Nonlinear Mechanics, Vol. 14, pp. 183-203, 1979.

42. Valanis, K.C.: A Theory of Viscoplasticity Without a Yield Surface Part I. General Theory. Archives of Mechanics, Vol. 23, pp. 517-533, 1971.

43. Valanis, K.C.: A Theory of Viscoplasticity Without a Yield Surface Part II. Application to Mechanical Behaviour of Metals. Archives of Mechanics, Vol. 23, pp. 535-551, 1971.

44. Valanis, K.C.: On the Foundations of the Endochronic Theory of Viscoplasticity. Arch. Mech., Vol. 27, pp. 857-868, 1975.

45. Allen, D.H., and Haisler, W.E.: A Theory for Analysis of Thermoplastic Materials. Computers and Structures, Vol. 13, pp. 124-135, 1981.

46. Allen, D.H.: Computational Aspects of the Nonisothermal Classical Plasticity Theory. Accepted for publication in Computers and Structures, 1982.

47. Kocks, U.F.: Laws for Work-hardening and Low-Temperature Creep. Journal of Engineering Materials and Technology, Vol. 98-H, pp. 76-85, 1976.

48. Cailletaud, G., and Chaboche, J.L.: Macroscopic Description of the Microstructural Changes Induced by Varying Temperature: Example of IN100 Cyclic Behaviour. Third International Conference of Mechanical Behaviour of Materials, Vol. 2, pp. 23-32, ICM3, Cambridge, England, August 1979.

49. Lee, D., and Zaverl, F., Jr.: A Generalized Strain Rate Dependent Constitutive Equation for Anisotropic Metals. Acta Metallica Vol. 26, No. 11, p. 1771, 1978.

50. Laflen, J.H., and Stouffer, D.C.: An Analysis of High Temperature Metal Creep: Part I - Experimental Definition of an Alloy and Part II - A Constitutive Formulation and Verification. ASME J. Eng. Mat. & Tech., Vol. 100, p. 363, 1978.

51. Zienkiewicz, O.C., and Cormeau, I.C.: Visco-Plasticity -- Plasticity and Creep in Elastic Solids -- A Unified Numerical Approach. Int. Journal for Numerical Methods in Engineering, Vol. 8, pp. 821-845, 1974.

52. Perzyna, P.: Fundamental Problems in Viscoplasticity. Advan. Appl. Mech., Vol. 9, pp. 243-377, 1966.

53. Perzyna, P., and Wojno, W.: Thermodynamics of Rate Sensitive Plastic Materials. Arch. Mech. Stos., Vol. 20, p. 5, 1968.

54. Perzyna, P.: The Constitutive Equations for Work-Hardening and Rate-Sensitive Plastic Materials. Proc. Vibr. Probl., Vol. 4, pp. 281-290, 1963; Bull. Acad. Polon. Sci., Ser. Sci. Tech., Vol. 12, pp. 199-206,

55. Perzyna, P.: On the Thermodynamic Foundations of Viscoplasticity. Symposium on the Mechanical Behavior of Materials Under Dynamic Loads, San Antonio, Texas, 1967.

56. Yamada, Y., and Sakurai, T.: Basic Formulation and a Computer Program for Large Deformation Analysis. Pressure Vessel Technology, Part I, ASME, pp. 341-352, 1977.

57. Yamada, Y.: Constitutive Modelling of Inelastic Behaviour and Numerical Solution of Nonlinear Problems by the Finite Element Method. Computers and Structures, Vol. 8, pp. 533-543, 1978.

58. Snyder, M.D., and Bathe, K.J.: Formulation and Numerical Solution of Thermo-Elastic-Plastic and Creep Problems. National Technical Information Service, No. 82448-3, June 1977.

59. von Mises, R.: Mechanik der Festen Koerper im Plastich Deformablen Zustand. Goettinger Nachr., Math.-Phys. Kl., pp. 582-592, 1913.

60. Ziegler, H.: A Modification of Prager's Hardening Rule. Quarterly of Applied Mathematics, Vol. XVIII, pp. 55-65, 1959.

61. Prager, W.: The Theory of Plasticity: A Survey of Recent Achivements. Proceedings of the Institution of Mechanical Engineers, London, Vol. 169, pp. 41-57, 1955.

62. Allen, D.H.: A Prediction of Heat Generation in a Thermoviscoplastic Uniaxial Bar. Texas A&M Mechanics and Materials Center, Report no. MM 4875-83-10, July, 1983 (to be published in International Journal of Solids and Structures).

63. Schapery, R.A.: On Viscoelastic Deformation and Failure Behavior of Composite Materials with Distributed Flaws. Advances in Aerospace Structures and Materials, ASME AD-01, pp. 5-20, 1981.

64. Talreja, R.: A Continuum Mechanics Characterization of Damage in Composite Materials. The Technical University of Denmark, Lyngby, to be published.

65. Allen, D.H., Groves, S.E., and Schapery, R.A.: A Damage Model for Continuous Fiber Composites. In preparation.

TABLE 1. COMPARISON OF UNIAXIAL MODELS

Theory	Stress-Strain Relaxation	Internal State Variable Growth Laws	Comments	Material Parameters
Cernocky and Krempl	(T1) $\sigma=E[\epsilon-\epsilon^I-\epsilon^T]$	(T2) $\dot{\epsilon}^I=\frac{\sigma-G}{Ek}$	1. $G=G(\epsilon,T)$ is obtained from extrapolation of relaxation data. 2. k is curve-fit to $k=R_0 e^{R_1 e^{-\left[\frac{\lvert\sigma-G\rvert}{R_2}\right]^{R_3}}}$	E, R_0, R_1, R_2, R_3
Krieg, Swearengen, and Rohde	(T3) $\sigma=E[\epsilon-\epsilon^I]$	(T4)[1] $\dot{\epsilon}^I=c_1\left[\frac{\lvert\sigma-a_1\rvert}{a_2}\right]^{c_2}\operatorname{sgn}(\sigma-a_1)$ (T5)[1,2] $\dot{a}_1=c_3\dot{\epsilon}^I-c_4 a_1^2[e^{c_5 a_1^2}-1]\operatorname{sgn}(a_1)$ (T6)[2] $\dot{a}_2=c_6\lvert\dot{\epsilon}^I\rvert-c_7[a_2-a_{2_0}]^n$		$E, c_1, c_2, c_3, c_4, c_5, c_6, c_7, a_{2_0}, n$
Bodner et al.	(T7) $\sigma=E[\epsilon-\epsilon^I]$	(T8)[1] $\dot{\epsilon}^I=\frac{2}{\sqrt{3}}D_0 e^{-\left[\frac{n+1}{2n}\right]\left[\frac{\sigma}{a_2}\right]^{2n}}\operatorname{sgn}(\sigma)$ (T9) $\dot{a}_2=[Z_1-a_2]\dot{W}_p-AZ_1\left[\frac{a_2-Z_I}{Z_1}\right]^r$	1. $\dot{W}_p=\sigma\dot{\epsilon}^I$	$E, D_0, n, m, Z_1, Z_I, A, r$
Walker	(T10) $\sigma=E[\epsilon-\epsilon^I]$	(T11)[1] $\dot{\epsilon}^I=\left[\frac{\lvert\sigma-a_1\rvert}{a_2}\right]^n\operatorname{sgn}(\sigma-a_2)$ (T12)[2] $\dot{a}_1=[n_1+n_2]\dot{\epsilon}^I-[a_1-a_{1_0}-n_1\epsilon^I][\lvert\dot{\epsilon}^I\rvert\frac{\partial}{\partial R}([n_3+n_4R][\ln(\frac{n_5R}{1+n_6R}+1)])+n_7\lvert a_1-a_{1_0}\rvert^{m-1}]$ (T13) $\dot{a}_2=n_8\lvert\dot{\epsilon}^I\rvert-n_9\lvert\dot{\epsilon}^I\rvert a_2-n_{10}[a_2-a_{2_0}]^q$	1. R is the cumulative inelastic strain: $R=\int^t\frac{\partial\epsilon^I}{\partial\tau}d\tau$. 2. The growth law for a_2, eq.(T13), is not presently used in the model; a_2 is assumed to be a constant.	$E, n, n_1, n_2, n_3, n_4, n_5, n_6, n_7, n_8, n_9, n_{10}, m, q, a_{1_0}, a_{2_0}$
Miller	(T14) $\sigma=E[\epsilon-\epsilon^I-\epsilon^T]$	(T15)[1] $\dot{\epsilon}^I=B\theta'\left[\sinh(\frac{\lvert\sigma-a_1\rvert}{a_2})1.5\right]^n\operatorname{sgn}(\sigma-a_1)$ (T16)[1,2] $\dot{a}_1=H_1\dot{\epsilon}^I-H_1B\theta'[\sinh(A_1\lvert a_1\rvert)]^n\operatorname{sgn}(a_1)$ (T17)[2] $\dot{a}_2=H_2\lvert\dot{\epsilon}^I\rvert[C_2+\lvert a_1\rvert-\frac{A_2}{A_1}a_2^3]-H_2C_2B\theta'[\sinh(A_2a_2^3)]^n$	1. $\theta'=e^{-\frac{Q}{RT}}$ for $T>0.6\,T_m$ $\theta'=e^{-\left[\frac{Q}{0.6RT_m}\right]\left[\ln(\frac{0.6T_m}{T})+1\right]}$ for $T\leq 0.6\,T_m$ T_m is the melting temp. k is the gas constant.	$E, B, n, H_1, A_1, H_2, C_2, A_2, Q$

Cescotto and Leckie	(T18) $\sigma=E[\epsilon-\epsilon^I-\epsilon^T]$	(T19)[1] $\dot{\epsilon}^I=f(\lvert\frac{\sigma-a_1}{a_2}\rvert)\ \mathrm{sgn}(\sigma-a_1)$ (T20)[2] $\dot{a}_1=\frac{3}{2}h_a\dot{\epsilon}^I - r_a a_1$ (T21) $\dot{a}_2=h_\kappa - r_\kappa$	1. f, h_a, r_a, h_κ, and r_κ are experimentally determined functions.	E
Hart	(T22) $\sigma=E[\epsilon-\epsilon^I-\epsilon^T]$	(T23)[1] $\dot{\epsilon}^I=\dot{a}^*\left[\frac{2}{3}\right]^{M/2}\left[\frac{\lvert\sigma-a_1\rvert}{\mu}\right]^M \mathrm{sgn}(\sigma-a_1)$ (T24)[2] $\dot{a}_1=\frac{3}{2}\mu\dot{\epsilon}^I - \frac{\mu\left[\frac{a_2'}{G}\right]^m f e^{-\frac{Q}{RT}}}{\left[\ln\left(\frac{3a_2'}{2\lvert a_1\rvert}\right)\right]^{1/\lambda}}$ (T25) $\dot{a}_2'=c\left[\frac{2}{3}\right]^{k/2} f e^{-\frac{Q}{RT}}\left[\frac{\sigma}{a_2'}\right]^k \frac{a_2'}{\left[\ln\left(\frac{a_2'}{\sqrt{\frac{2}{3}}\,a_1}\right)\right]^{1/\lambda}}$	1. The drag stress is taken to be a constant, μ, hence there is no a_2 as in other models. There is, however, a third internal state variable, termed a_2'. 2. T is the absolute temp. R is the gas constant.	E, $\dot{a}^*$, M, μ, G, m, f, Q, k, λ, c
Robinson	(T26) $\sigma=E[\epsilon-\epsilon^I-\epsilon^T]$	(T27) $\dot{\epsilon}^I=\frac{1}{2\mu}\left[\frac{1}{\sqrt{3}}\left\lvert\frac{\sigma-a_1}{K}\right\rvert\right]^{n-1}[\sigma-a_1]$ (T28)[2] $\dot{a}_1=\frac{2\mu H}{\left[\frac{1}{\sqrt{3}}\left\lvert\frac{a_1}{K}\right\rvert\right]^\beta}\dot{\epsilon}^I - R\left[\frac{1}{\sqrt{3}}\left\lvert\frac{a_1}{K}\right\rvert\right]^{n-\beta-1} a_1$	1. G_0 is the initial value of $\frac{a_1^2}{3K^2}$.	E, μ, K, n, β, H, R, G_0
Valanis	(T29) $\sigma=E[\epsilon-\epsilon^I-\epsilon^T]$	(T30) $\dot{\epsilon}^I=k_1 f_1(\sigma,\epsilon)\dot{\epsilon} + k_2 f_2(\sigma,\epsilon)$	1. Represents simplified form of Valanis' model.	E, k_1, k_2, f_1, f_2
Allen and Haisler	(T31) $\sigma=E[\epsilon-\epsilon^I-\epsilon^T]$	(T32) $\dot{\epsilon}^I=\dot{\lambda}[\sigma-a_1] + \dot{g}[\sigma-a_1]$ (T33) $\dot{a}_1=\dot{\mu}[\sigma-a_1]$ (T34) $\dot{a}_2=f(\dot{\epsilon}^{I^2})$	1. Considerable curve-fitting and interpolation of stress-strain and creep data required to obtain material parameters $\dot{\lambda}$, $\dot{g}$, and $\dot{\mu}$.	E, $\dot{\lambda}$, $\dot{g}$, $\dot{\mu}$, f

1 $\mathrm{sgn}(x) = \begin{cases} 1 & x > 0 \\ 0 & x = 0 \\ -1 & x < 0 \end{cases}$

2 $\dot{\epsilon}^I$ can be substituted directly into growth law for a_1 and a_2 to obtain a form consistent with internal state variable growth laws (14).

Note: parentheses ( ) imply "function of", whereas brackets [ ] imply multiplication.

APPENDIX 6.4

A COMPARISON OF CURRENT MODELS FOR NONLINEAR RATE-DEPENDENT MATERIAL BEHAVIOR OF CRYSTALLINE SOLIDS

A Thesis

by

JOACHIM MICHAEL BEEK

Submitted to the Graduate College of

Texas A&M University

in partial fulfillment of the requirements for the degree of

MASTER OF SCIENCE

May 1986

Major Subject: Aerospace Engineering

ABSTRACT

A Comparison of Current Models for Nonlinear Rate-Dependent Material Behavior of Crystalline Solids. (May 1986)

Joachim Michael Beek, B.S., Texas A&M University

Chair of Advisory Committee: Dr. D. H. Allen

This thesis reviews three theories for prediction of inelastic deformation which are based on considerations of the microstructural behavior of materials. These theories are those of Krieg, et al., Bodner, et al., and Miller, et al. The thesis opens with a review of the mechanics of continua with internal state variables and a review of the historical development of constitutive modelling. A detailed discussion, including chronological development, review of theory, and method of determination of material parameters, of each model follows. An experimental data base is established from which the material parameters of the constitutive equations are calculated. Finally, computer simulations of various load histories are performed and compared to experiment, and conclusions of the ability of each theory to model inelastic deformation are drawn.

ACKNOWLEDGMENTS

I wish to thank Dr. David H. Allen for his guidance, patience, and support throughout this research effort. I would also like to thank Dr. R. A. Schapery and Dr. W. L. Bradley for kindly consenting to join my committee and for their support. Gratitude is due to my wife for her patience and to all others, too numerous to mention here, who aided in this work.

This research was supported by NASA Lewis Research Center under Grant no. NAG3-491.

TABLE OF CONTENTS

LIST OF TABLES

LIST OF FIGURES

INTRODUCTION

The prediction of inelastic material behavior in metals is a problem of great importance which has accordingly been given a great deal of attention by the research community in recent years. Recent technological advances require materials to function in severe chemical, mechanical, and thermal environments such as nuclear reactors and gas turbines. Superalloys have been developed that are able to sustain loads at extreme temperatures; however, due to this environment, these materials exhibit substantial complexity in their material constitution in that they are highly nonlinear, rate-dependent, temperature-dependent, and history-dependent.

Numerous theories have been proposed to predict the thermomechanical behavior of inelastic solids at elevated temperatures. These theories are usually based on one of the following concepts: 1) rate-dependent extensions of classical plasticity theory retaining the concept of a yield surface, 2) thermodynamics and/or nonlinear viscoelasticity theory, and 3) considerations of the

---

The style and format of this thesis follow the Journal of Engineering Materials and Technology.

microstructural behavior of the material. It is important that each of these theories be able to model diverse phenomena associated with inelastic deformation including anelasticity (completely recoverable time-dependent strain at zero load), the Bauschinger effect, cyclic strain hardening/softening, rate sensitivity, creep, relaxation, and tensile and compressive loading and unloading. These are illustrated in Figures 1 and 2.

The purpose of this research is to review three theories based on considerations of microstructural behavior. Since each theory is proposed for a material and temperature of its authors' choosing, a set of experiments is performed by this author with a single candidate material in order to create a common experimental data base with which the mathematical representation of each model can be characterized. The theories are subsequently analyzed qualitatively and quantitatively over a range of material behavior to determine their suitability in predicting inelastic deformation.

This thesis opens with a short review of the mechanics of continua with internal state variables. This is followed by a literature review and, utilizing the framework of internal state variables, a detailed study of the models chosen for discussion. The experimental program associated with the research for this thesis is presented

as an assessment of the experimental data base requirements for each model, accompanied by the results of the experiments. A uniaxial comparison of the predictive capabilities of the models follows and, finally, conclusions from the complete survey are presented.

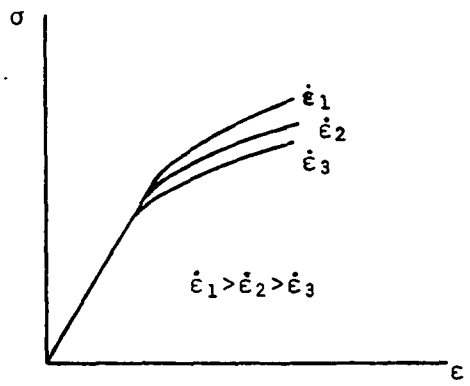

Rate sensitivity

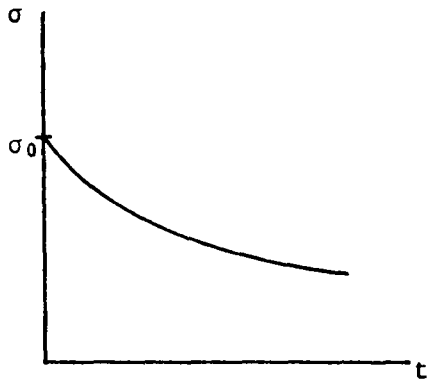

Relaxation

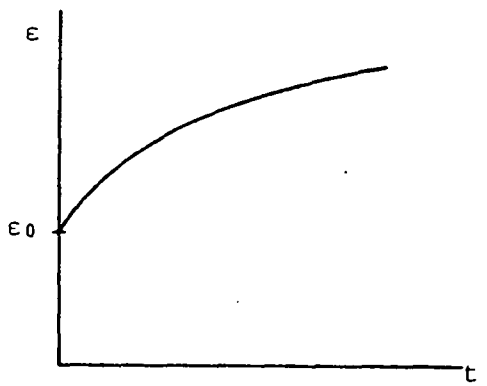

Creep

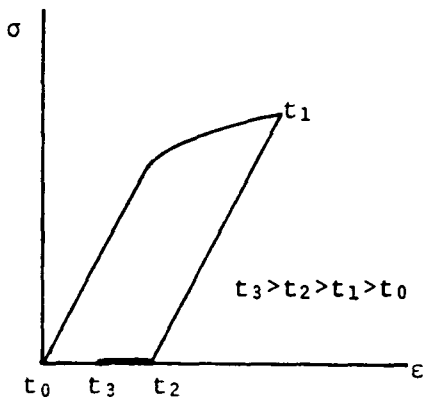

Anelasticity

Fig. 1 Phenomena associated with inelastic deformation (uniaxial loading)

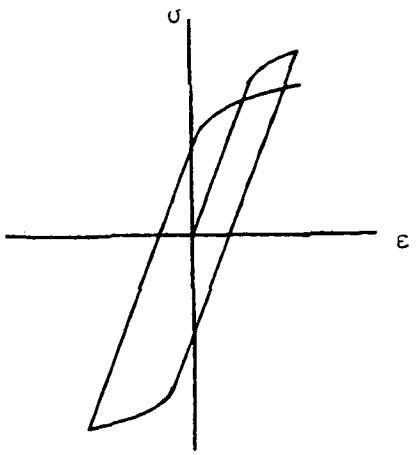

Cyclic strain softening

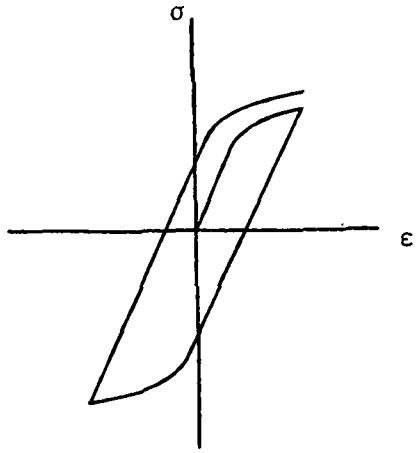

Cyclic strain hardening

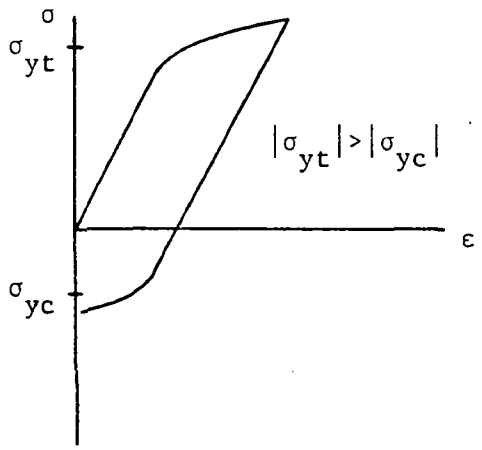

Bauschinger effect

Fig. 2 Phenomena associated with inelastic deformation (cyclic loading)

THE EQUATION OF STATE APPROACH

The concept of internal state variables, sometimes called hidden variables, is gaining widespread usage in current research on the modelling of inelastic solids. Therefore, it is useful to construct a well-defined framework for internal state variable models which is based on continuum mechanics.

The concept of internal state variables was apparently first utilized in Onsager's work in thermodynamics [1,2] and has found numerous applications since the Second World War [3-12].

In the theory of internal state variables applied to solids, Coleman and Gurtin [3] defined the elastic field problem to be one in which the following state variables are required in order to characterize fully the state of a body at all points x_j and at all times t: *

1) the displacement field $u_i = u_i(x_j,t)$; (1)

---

* For convenience, only infinitesimal deformations will be considered here, although the general theory applies to finite deformations as well.

2) the stress tensor $\sigma_{ij} = \sigma_{ij}(x_k,t)$; (2)

3) the body force per unit mass $f_i = f_i(x_j,t)$; (3)

4) the internal energy per unit mass

$u = u(x_j,t)$; (4)

5) the heat supply per unit mass $r = r(x_j,t)$; (5)

6) the entropy per unit mass $s = s(x_j,t)$; (6)

7) the absolute temperature $T = T(x_j,t)$; (7)

and

8) the heat flux vector $q_i = q_i(x_j,t)$. (8)

Thermodynamic constraints will lead to the conclusion that, for elastic bodies, entropy is generated only through heat conduction [3]. For inelastic bodies, however, this conclusion cannot be drawn because additional entropy is generated. The state cannot be characterized solely from the observable state variables; rather, a set of internal state variables α_{ij}^{k} is also necessary, and these are determined by observation of the entire past history of

states of the body:

$$\alpha_{ij}^{k} = \alpha_{ij}^{k}(x_m, t), \tag{9}$$

where the superscript k ranges from one to the number of internal state variables necessary to characterize fully the state of the body. Although listed here as second order tensors, they may be tensors of other rank as well [13].

The method of Coleman and Noll [14] may be used to obtain the spatial and time distribution of the body force f_i and the heat supply r from the conservation of linear momentum and the conservation of energy, respectively, assuming the displacements u_i and the temperature T are specified independent variables. It is hypothesized subsequently that constitutive equations may be constructed for the remaining state variables in terms of u_i and T and their spatial derivatives:

$$\sigma_{ij}(x_k, t) =$$

$$\sigma_{ij}(\varepsilon_{mn}(x_k, t), T(x_k, t), g_m(x_k, t), \alpha_{mn}^{p}(x_k, t)); \tag{10}$$

$$u(x_k,t) =$$

$$u(\varepsilon_{mn}(x_k,t),T(x_k,t),g_m(x_k,t),\alpha^p_{mn}(x_k,t)); \quad (11)$$

$$s(x_k,t) =$$

$$s(\varepsilon_{mn}(x_k,t),T(x_k,t),g_m(x_k,t),\alpha^p_{mn}(x_k,t)); \quad (12)$$

$$q_i(x_k,t) =$$

$$q_i(\varepsilon_{mn}(x_k,t),T(x_k,t),g_m(x_k,t),\alpha^p_{mn}(x_k,t)); \quad (13)$$

where g_m is the spatial temperature gradient $T_{,m}$ and

$$\varepsilon_{ij} = \frac{1}{2}(u_{i,j}+u_{j,i}) \quad (14)$$

is the infinitesimal strain tensor. The form of equations (10) through (13) implies that all constitutive equations are evaluated in the specified state x_k and t. For this reason, σ_{ij}, u, s, and q_i are termed observable state variables since they can be determined from equations of state, even though there is an implied history dependence through the internal state variables α^p_{mn}. These are defined to be of the form:

$$\dot{\alpha}^{k}_{ij} = \Omega^{k}_{ij}(\varepsilon_{mn}, T, g_{m}, \alpha^{p}_{mn}), \tag{15}$$

where time and spatial dependence have been dropped for notational convenience and the superscripts k and p range from one to the number of internal state variables necessary to characterize fully the state of the body. If equations (15) are integrable in t at all times, then they can be rewritten as

$$\alpha^{k}_{ij}(x_{m}, t) = \int_{-\infty}^{t} \Omega^{k}_{ij}(x_{m}, t')dt', \tag{16}$$

where t is the time of interest and t' is a dummy variable of integration.

The above framework has been shown to be applicable to crystalline solids [15,16] and further discussion of this subject is provided in reference [17].

On the basis of the Coleman-Mizel procedure [18] it can be shown that satisfaction of the first and second laws of thermodynamics will lead to the following conclusions:

$$h = u - Ts = h(\varepsilon_{mn}, T, \alpha^{p}_{mn}), \tag{17}$$

where h is the Helmholtz free energy;

$$\sigma_{kl} = \rho \, \partial h / \partial \varepsilon_{kl}; \tag{18}$$

$$s = -\partial h/\partial T; \tag{19}$$

and

$$q_i = -k_{ij}g_j + O(g_j), \tag{20}$$

where k_{ij} is the thermal conductivity tensor. Although further results are obtainable [3,15-17], they are not pertinent to the current research. The importance of the results above is that, in order to construct a complete description of constitutive equations (10) through (13) and (15), it is necessary only to prescribe the Helmholtz free energy. In order to describe the class of materials discussed herein, the free energy is expanded in terms of the elastic strain tensor ε^E_{ij} and the temperature T in a second order Taylor series as follows:

$$h = h_R + \varepsilon^E_{ij}D_{ijkl}\varepsilon^E_{kl}/2\rho - c_V\,(T - T_R)/2T, \tag{21}$$

where the subscript R refers to quantities in the reference state, D_{ijkl} is the linear elastic modulus tensor, $c_V = -T(\partial^2 h/\partial T^2)$ is the specific heat at constant elastic volume, and

$$\varepsilon^E_{ij} = \varepsilon_{ij} - \varepsilon^I_{ij} - \varepsilon^T_{ij}, \tag{22}$$

where ε^T_{ij} is the thermal strain tensor and ε^I_{ij} is the inelastic strain tensor, which can be considered to be an internal state variable [15,16,18-21]. Substitution of equation (21) into (18) will result in

$$\sigma_{kl} = D_{klmn} (\varepsilon_{mn} - \varepsilon^I_{mn} - \varepsilon^T_{mn}). \qquad (23)$$

The above equations, together with internal state variable growth laws (15), will be shown to be a suitable framework for comparison of all the models discussed herein.

Theoretically, constitutive equations (10) through (13) and (15) are applicable to fixed infinitesimal material points. In practical terms however, it is not possible to construct experiments on material points since the continuum assumption becomes invalid at the microscopic level. Rather, it is considered acceptable to construct constitutive equations by subjecting local specimens to surface deformations (or tractions) which lead to spatially homogeneous stresses and strains. In this manner, a local average of the pointwise observable state variables can be determined directly from the effects on the boundaries of the specimen.

As shown in Figure 3, the scale of the smallest dimension of a local specimen is generally assumed to be at least one order of magnitude larger than the scale of the

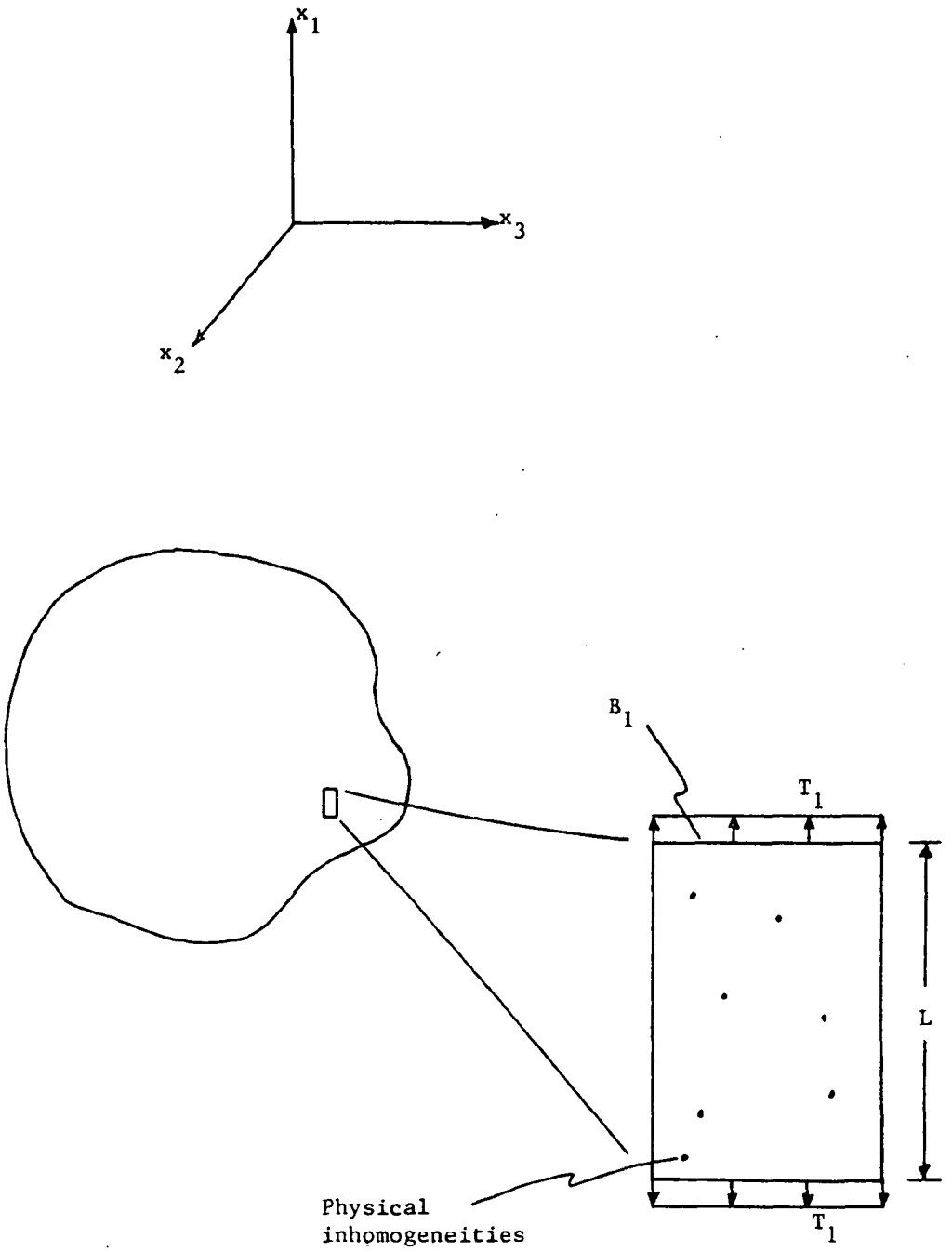

Fig. 3 The relationship between local inhomogeneities and the continuum assumption

largest material inhomogeneity, while the scale of the largest dimension of the local specimen is much smaller than the scale of the domain of interest. The former preserves the continuum assumption, while the latter conserves the notion that constitutive equations are indeed pointwise in nature. The local constitutive equations that result from experimentation are assumed to be of the same form as pointwise equations (10) through (13) and (15); for example,

$$\bar{\sigma}_{11} = \bar{\sigma}_{11}(\bar{\varepsilon}_{11}, \bar{T}, \bar{\alpha}^{p}_{mn}), \tag{24}$$

where

$$\bar{\sigma}_{11} = \frac{1}{A}\int_{B_1} \sigma_{11}\, dx_2 dx_3, \tag{25}$$

$$\bar{\varepsilon}_{11} = \frac{1}{L}\int_{L} \varepsilon_{11}\, dx_1, \tag{26}$$

and

$$\bar{T} = T(a_1, a_2, a_3), \tag{27}$$

where L is the length of the local specimen, A is the cross-sectional area in the x_2-x_3 plane, (a_1, a_2, a_3) is an arbitrary point on the surface of the specimen, and

$$\bar{\alpha}^{p}_{mn} = \frac{1}{V}\int_{V}\alpha^{p}_{mn}dx_1dx_2dx_3. \qquad (28)$$

It is then assumed that equation (24) is a suitable replacement for equation (10). There are obvious shortcomings in this assumption in that equation (24) represents a solution to a boundary value problem. This implies volume averaging of local balance laws, which violates the local nature of constitutive equations. In addition, there may be a question of uniqueness resulting from the fact that more than one global state of a given internal state variable will map into the globally averaged state variable described by equations (28). However, assuming that the scale of inhomogeneities is small and that the distribution of α^{p}_{mn} is random, the specimen will be statistically homogeneous and the relation between α^{p}_{mn} and $\bar{\alpha}^{p}_{mn}$ reasonably one-to-one. The above procedure remains the only reasonable method for constructing constitutive equations from experimental data bases.

LITERATURE REVIEW AND GENERAL DISCUSSION OF MODELS

Man's curiosity about his environment and his constant striving to harness the power and resources of nature with increasing efficiency have been the driving force behind the study of the laws of nature and the attempts to use these laws to predict the solutions of many problems.

The theory of elasticity dates to the 17th century with Robert Hooke's discovery that the tension in a spring is directly proportional to its extension. This heralded the beginning of the characterization of mechanical behavior of materials using mathematical constitutive models. Contributions to the theory of elasticity were also made by Galileo, the Bernoullis, Navier, Cauchy, Euler, and Saint-Venant, to name a few [22].

Classical Plasticity Models

Often only a small part of material deformation is elastic and, in general, a material will not behave elastically at large strains. Consequently, in 1864 Tresca [23] proposed a criterion to predict the onset of inelastic deformation in metals based on the maximum shear stress reaching a critical value. This was followed in 1913 by von Mises [24] with a yield criterion based on an equivalent

stress state reaching a critical value; this has been interpreted as the elastic shear strain energy reaching a critical value [25].

Independently of each other, Levy [26] and von Mises [24] formed the basis of classical plasticity by proposing a three-dimensional relationship between the strain increment and the stress tensor which became known as the Levy-Mises equations:

$$d\varepsilon_{ij} = d\lambda\, \sigma'_{ij}, \tag{29}$$

where $d\varepsilon_{ij}$ is the total strain increment, $d\lambda$ is a scalar, and σ'_{ij} is the deviatoric stress tensor, given by

$$\sigma'_{ij} = \sigma_{ij} - \frac{1}{3}\sigma_{kk}\delta_{ij} \tag{30}$$

where δ_{ij} is the Kronecker delta. In equations (29), the elastic strain component is assumed to be negligible; these equations consequently describe a fictitious, rigid, perfectly plastic material. Equations (29) were extended to take into account the elastic strain component by Prandtl [27] in 1924, who solved the plane stress case, and by Reuss [28] in 1930, who generalized the equations to three dimensions:

$$d\varepsilon^{P}_{ij} = d\lambda \; \sigma'_{ij}, \tag{31}$$

where $d\varepsilon^{P}_{ij}$ is the plastic strain component and $d\lambda$ is a scalar history-dependent material property. The total strain increment $d\varepsilon_{ij}$ is then assumed to be the sum of the plastic strain component $d\varepsilon^{P}_{ij}$ and the elastic strain component $d\varepsilon^{E}_{ij}$.

These developments enabled the classical plasticity theory to model elastic and rate-independent inelastic deformation fairly accurately for most metals with only a few restrictions. These were that the material be subjected to monotonically increasing loads and low non-transient homologous temperatures; that is, temperatures less than three tenths of the absolute melting temperature. At higher temperatures, however, rate dependence of material behavior becomes significant, limiting the use of the existing plasticity theory.

Rate dependence was initially treated as an extension of classical plasticity theory by Bingham [29] in 1922 by using the concept of a yield function dependent on the excess of the stress intensity over the yield stress for the case of simple shear. This was generalized by Hohenemser and Prager [30] in 1932 for the three-dimensional case. Further progress in plasticity theories was slow and advanced vastly and diversely only

after completion of World War II. Prager [31] and Ziegler [32] proposed work-hardening rules for rate-independent plasticity to allow the yield surface to translate to model kinematic hardening. Drucker's stability postulate [33] serves as a basis for the incremental theories of plasticity, in which the plastic strain increment is determined by the stress and the stress increment. Rate-dependent plasticity models proposed in the postwar period included those by Freudenthal [34], Malvern [35,36], who constructed a one-dimensional equation relating the stress increment to the strain rate, Lubliner [37], who modified Malvern's equation to include a limiting stress-strain curve, and Perzyna [38-41], who generalized Malvern's equations to three dimensions and finite strains.

Many classical plasticity models have been extended to include rate dependence by adding an uncoupled rate-dependent strain component to the rate-independent strain component. No observable difference exists between the physical mechanisms causing these phenomena, however, and it has been argued that the two terms should be combined [42]. Naghdi and Murch [43] attempted to include rate dependence by introducing interdependent, although not unified, plastic and viscoelastic strain components.

Classical plasticity theories are usually described by

$$\sigma_{ij} = D_{ijmn} (\varepsilon_{mn} - \varepsilon^{I}_{mn} - \varepsilon^{T}_{mn}), \qquad (32)$$

where D_{ijmn} is the linear elastic modulus tensor, ε^{T}_{mn} is the thermal strain, and ε^{I}_{mn}, the inelastic strain, is given by

$$\dot{\varepsilon}^{I}_{mn} = \dot{\lambda} \, \partial F/\partial \sigma_{mn}, \qquad (33)$$

where $\dot{\lambda}$ is a scalar valued function of state and F is a scalar valued function for inelastic behavior often taken to be the yield function. If F is described by the von Mises yield criterion [24], given by

$$F(\sigma_{ij} - \alpha_{ij}) = \frac{1}{2}(\sigma_{ij} - \alpha_{ij})(\sigma_{ij} - \alpha_{ij}) = k^2, \qquad (34)$$

where α_{ij} is a tensor describing the yield surface center in stress space and k is a constant representing the yield surface size, then equations (33) can be written as

$$\dot{\varepsilon}^{I}_{ij} = \dot{\lambda} \, (\sigma_{ij} - \alpha_{ij}), \qquad (35)$$

resulting in a kinematic hardening model with constant yield surface size. Furthermore, if the yield surface translation is derived from the Ziegler modification [32] of the Prager work-hardening rule [31], it may be described

by

$$\dot{\alpha}_{ij} = \dot{\mu} (\sigma_{ij} - \alpha_{ij}), \qquad (36)$$

where $\dot{\mu}$ is a scalar valued function of state.

By use of equations (32), equations (35) and (36) can be shown to be consistent with growth laws (15). It can then be seen that classical plasticity theories are consistent with the thermodynamic framework developed in the equation of state approach.

Recently proposed theories include those by Snyder and Bathe [44], Yamada and Sakurai [45], Allen and Haisler [46,47], which attempts to model transient temperature effects, Zienkiewicz and Cormeau [48], and Robinson [49]. Bodner and his associates proposed a model [50] which uses a flow law similar to equations (31), although the internal state variable growth laws are based on microstructural considerations. Robinson's model and Bodner's model are still under active development.

Nonlinear Viscoelasticity Models

Nonlinear viscoelasticity models are usually based on thermodynamics and/or mechanical analogs composed of springs and dashpot combinations such as the three parameter standard solid, shown in Figure 4. In 1954, Biot

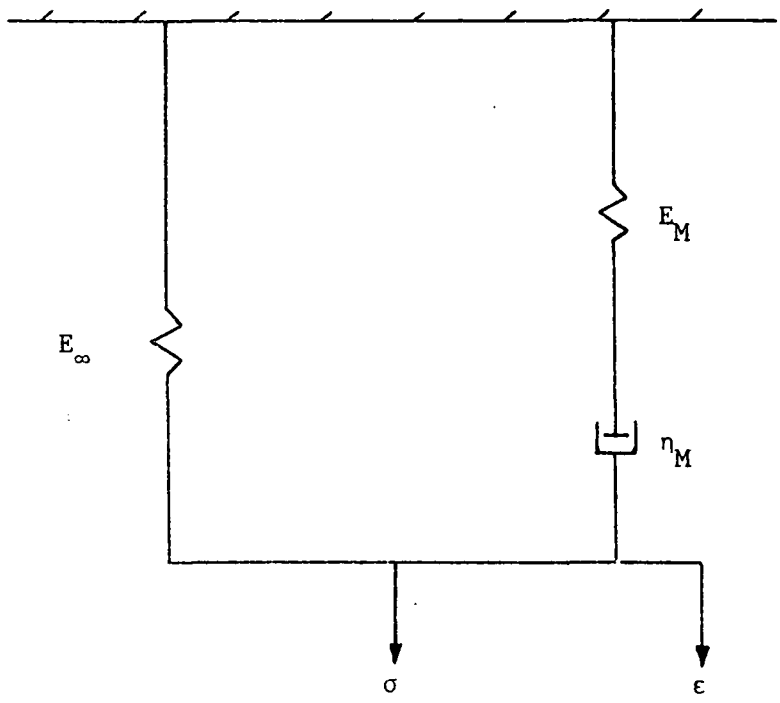

Fig. 4 The three parameter standard solid

[6,7] proposed a theory of linear thermoviscoelasticity based on the principles of irreversible thermodynamics. Schapery [12] later modified this to include nonlinear behavior and introduced a reduced time scale to solve the resulting highly nonlinear equations. Valanis [51-53] proposed a viscoplasticity theory, termed the endochronic theory, which includes a history-dependent reduced time parameter. This was later shown to be a special case of Schapery's model [54]. Some other models based on thermodynamics are those of Coleman and Noll [55,14], Green and Rivlin [56], and Green and Naghdi [57]. These tend to be quite complex in nature and difficult to solve.

Many of the recent models are based on variations of the three parameter standard solid. The standard solid shown in Figure 4 has been demonstrated to be an appropriate representation for thermoviscoplastic metals if the springs and dashpot are nonlinearized [58,59]. The governing differential equation for this solid is

$$\sigma + (\eta_M/E_M)\dot{\sigma} = E_\infty\varepsilon + (\eta_M/E_M)\,(E_M + E_\infty)\dot{\varepsilon}. \qquad (37)$$

This may be rewritten in the equivalent form

$$\dot{\varepsilon} = \dot{\sigma}/(E_M + E_\infty) + E_M/[\eta_M(E_M + E_\infty)]\,(\sigma - E_\infty\varepsilon). \qquad (38)$$

In accordance with the instantaneous linear behavior of metals, it is assumed that

$$E_M + E_\infty = E = \text{Elastic modulus} = \text{constant}, \tag{39}$$

and equation (38) becomes

$$\varepsilon = \frac{\sigma}{E} + \varepsilon^I, \tag{40}$$

where ε^I is the inelastic strain, given by

$$\dot{\varepsilon} = (E_M/\eta_M E)\ (\sigma - E_\infty \varepsilon). \tag{41}$$

The nonlinearity of the springs and dashpot can be introduced by considering a multiaxial extension of equation (37):

$$\sigma_{pq} + K_{pqmn}\dot{\sigma}_{mn} = G_{pqmn}\varepsilon_{mn} + M_{pqmn}\dot{\varepsilon}_{mn}. \tag{42}$$

In order to model metals, K_{pqmn}, G_{pqmn}, and M_{pqmn} are nonlinear material functions determined from experimental data. In addition, constraint (39) requires that

$$K^{-1}_{ijmn} M_{mnkl} = D_{ijkl}, \tag{43}$$

where D_{ijkl} is the linear elastic modulus tensor. Equations (42) and (43) lead to

$$\sigma_{ij} = D_{ijmn} (\varepsilon_{mn} - \varepsilon^{I}_{mn} - \varepsilon^{T}_{mn}), \tag{44}$$

where the inelastic strain ε^{I}_{ij} is given by

$$\dot{\varepsilon}^{I}_{ij} = M^{-1}_{ijkl} (\sigma_{kl} - G_{klmn}\varepsilon_{mn}). \tag{45}$$

Substitution of equations (44) into (45) will result in equations consistent with growth laws (15). It can then be seen that nonlinear viscoelasticity models are consistent with the thermodynamic framework developed earlier in the equation of state approach.

Some recent models which are based on nonlinear modifications of the three parameter standard solid are those of Krempl, et al. [59-66], and Walker [58,67,68].

Microstructural Models

Microstructural models have generated increased interest in recent years because their formulation is based on microphysical considerations rather than a statistically averaged macroscopic view. The primary micromechanisms which cause inelastic deformation are dislocation glide and climb, deformation twinning, diffusion, grain boundary

sliding, and microvoid growth and coalescence. These mechanisms are difficult to model individually and are usually reduced to three more general mechanisms: dislocation arrangement, dislocation density, and damage. In the concept of microphenomenology it is assumed that the three mechanisms can be characterized by internal state variables. One internal state variable represents the back stress for modelling the dislocation arrangement. Another internal state variable, termed the drag stress, models dislocation density. In addition, it can be argued that the inelastic strain represents the third internal state variable [15,16,19]. Current research is in progress to account for damage in materials using a fourth internal state variable [69-71], although it is difficult to distinguish between damage and the drag stress since both are primarily stiffness-reducing parameters.

Early research in this field was performed by Coble [72], Nabarro [73], and Herring [74] in their work on diffusion-controlled creep. Other important contributions were made by Sherby, et al. [75-77], Garofalo [78], Argon [42], Weertman [79], Alden [80], Kocks [81], and Hart [82].

Mukherjee, et al. [83], studied the effectiveness of using a power law of the following form to model dislocation climb:

$$\dot{\varepsilon}^I = D\ A\ (\sigma/E)^n, \qquad (46)$$

where D is the self-diffusivity, E is Young's modulus, and A and n are temperature-dependent material parameters. The authors concluded, however, that a model in terms of a single dislocation mechanism may not completely characterize high-temperature creep.

Gibbs [84] proposed a two-internal-state-variable theory in which the inelastic strain rate is characterized by an exponential function of temperature and an effective stress:

$$\dot{\varepsilon}^I = A^* \exp\{-[Q_c - (\sigma-\sigma_a)lb^2]/kT\}, \qquad (47)$$

where A^* is a structure factor, Q_c is the dislocation core diffusion energy, k is the activation energy, T is the absolute temperature, b is the Burger's vector, and σ_a and l are internal state variables representing, respectively, back stress and drag stress.

It is generally recognized [85] that at intermediate to high stresses and at temperatures above $0.5T_m$, where T_m is the absolute melting temperature, stress is related to the inelastic strain rate by a power law of the form

$$\dot{\varepsilon}^I = A\ \sigma^n, \qquad (48)$$

where A and n are constants. At very high stress levels, the relationship is

$$\dot{\varepsilon}^I = B \exp(m\sigma), \tag{49}$$

where B and m are constants. Power law and exponential relationships represent limiting cases for the more general empirical relationship

$$\dot{\varepsilon}^I = C [\sinh(k\sigma)]^p, \tag{50}$$

where C, p, and k are constants. Equation (50) approximates a power law when $k\sigma<0.8$, but it approximates an exponential curve when $k\sigma>1.2$. See Figure 5 for a comparison of the forms of equations (48), (49), and (50).

Microstructural models are usually similar in nature, differing only in the proposed relationship between stress and inelastic strain (that is, equations (48), (49), or (50)) and in the proposed internal state variable growth laws. The growth laws for the internal state variables representing the back stress and the drag stress usually follow the framework established by Bailey [86] and Orowan [87] in which a hardening term, proceeding with accumulated deformation, competes simultaneously with a softening or recovery term, proceeding with time. For example, the

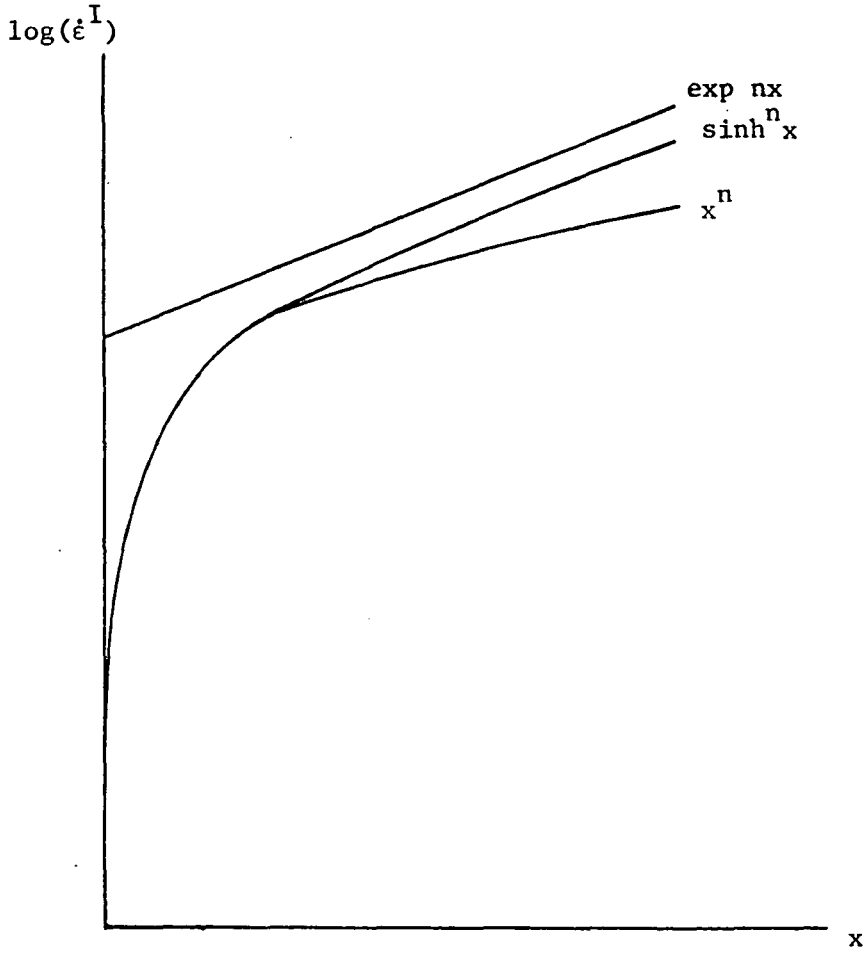

Fig. 5 A comparison of the hyperbolic sine, power law, and exponential forms of the inelastic strain rate equation

isothermal model proposed by Krieg, et al. [88], is given in its uniaxial form by

$$\sigma = E\,(\varepsilon - \varepsilon^{I}), \tag{51}$$

where the inelastic strain is given by

$$\dot{\varepsilon}^{I} = c_1\,[|\sigma - \alpha_1|/\alpha_2]\ \mathrm{sgn}(\sigma - \alpha_1), \tag{52}$$

where the growth laws for the back stress α_1 and the drag stress α_2 are given as the differences of hardening and softening rates:

$$\dot{\alpha}_1 = c_3\dot{\varepsilon}^{I} - c_4\alpha_1^2\,[\exp(c_5\alpha_1^2) - 1]\ \mathrm{sgn}(\alpha_1) \tag{53}$$

and

$$\dot{\alpha}_2 = c_6|\dot{\varepsilon}^{I}| - c_7\,(\alpha_2 - \alpha_{2_o})^{n}, \tag{54}$$

where c_1, c_2, c_3, c_4, c_5, c_6, c_7, n, and α_{2_o} are temperature-dependent material constants, and sgn() is the signum function.

Substituting equation (51) into (52) will result in equations consistent with growth laws (15). In addition, since equations (53) and (54) are consistent with growth

laws (15), it can be seen that microstructural models agree with the thermodynamic framework developed earlier in the equation of state approach. Cescotto and Leckie [89] proposed a model which has the interesting feature that no particular forms are assumed for the inelastic strain rate function and the hardening and recovery functions; only weak hypotheses are required and the functions are defined experimentally.

Other recently proposed models include those of Miller, et al. [90], in which a hyperbolic sine function is used for the stress-inelastic strain rate equation, Walker [58], in which a power law is used for the inelastic strain rate equation, and Bodner [50], in which an exponential function is used. An interesting aspect of these last two models is that, although the respective growth laws for the back stress and the drag stress are formulated from microstructural considerations, Walker's inelastic strain rate equation is based on a nonlinear modification of a three parameter viscoelastic solid, while Bodner's inelastic strain rate equation is based on a flow law similar to the Prandtl-Reuss equation of classical plasticity (see the literature reviews on nonlinear viscoelasticity models and classical plasticity models, respectively).

Since theories based on microstructural considerations

have been given a great deal of study in recent years, the theories chosen for comparison are taken from this field and are those of Krieg, et al. [88], Miller, et al. [90], and Bodner, et al. [50]. The motivation for the choice of these three models is that they are still under development; they have been cast in a common thermodynamic framework; the authors have included in their theories detailed accounts of methods of determination of the material constants; these models have received considerable attention [20,68,91-93]; and research is in progress to extend these isothermal models to include transient temperature response [68,91,94].

KRIEG, SWEARENGEN, AND ROHDE'S MODEL

Chronological Development

In 1977, Krieg [95] cast several current unified constitutive models into the common framework of a skeletal model in which general similarities, such as the use of competing hardening and recovery rates for internal state variable growth laws, are noted. These models include those of Bodner, et al., Robinson, et al., Hart, Lagneborg, Miller, Pasley and Wells, Ponter and Leckie, and an early development of Krieg's model, which is described as a composite of the aforementioned models. All hardening and softening functions are taken to be constants in the skeletal model in order to make observations about difficulties encountered in numerically integrating mathematically stiff constitutive equations. Finally, integration techniques are proposed to alleviate these difficulties.

In a development of this model, Krieg, Swearengen, and Rohde [88] proposed a power-law kinetic relation in multiaxial form to model pure aluminum at room temperature. This model has three internal state variables: the inelastic strain, the back stress and the drag stress. The growth laws of the back stress and the drag stress are formulated in the usual hardening rate/recovery rate

format. The hardening functions have not been defined and are assumed to be constant; recovery is considered to be a thermally-activated process and dynamic recovery is not included. Furthermore, the response of pure aluminum at room temperature is very nearly kinematic and, as a consequence, the drag stress (the isotropic hardening variable) is taken to be constant. Krieg, et al., present a test method in which all material constants, except Young's modulus, are calculated by determining values of the back stress from a set of stress-drop tests. In this test, a portion of the load on a specimen during secondary creep is removed and the resulting strain transient is recorded. The authors have obtained reasonable results for pure aluminum at room temperature for various load histories, although the predicted hysteresis loops are "over-square" and the model's use is limited in high strain rate ranges.

In 1982, Jones, et al. [96], noted that, while most unified creep-plasticity models require an extensive number of tests for characterization of material parameters, the model proposed by Krieg, et al., requires only a set of stress-drop tests. It is pointed out that, although simple in concept, the stress-drop test is difficult to perform in practice. The critical measurement in this test, a zero strain rate after unloading or merely the absence of a

resolvable strain rate, results in a strong dependence of the parameters on experimental resolution. The authors present the design of a test apparatus to minimize these effects. In addition, there appear to be differing opinions in the literature on the response of the creep rate immediately after unloading. Jones, et al., conclude that stress-drop testing should be performed with great care.

In subsequent research in 1983, Jones and Rohde [97] refer to a new technique to reduce stress-drop data which alleviates the difficulties mentioned above. Rather than attempting to measure a zero strain rate, this method [98] uses a comparison of the instantaneous strain change and the maximum strain change after unloading. This method appears to simplify the calculations considerably and merits further study.

General Theory

In their unified creep-plasticity model, Krieg, Swearengen, and Rohde [88] state that inelastic deformation can be caused by: 1) thermally-activated, stress-assisted penetration of short-range obstacles to dislocation motion, 2) generation and immobilization of dislocations, leading to increases in dislocation density, stored elastic energy, and the flow stress, and 3) stress-assisted thermal

rearrangement of dislocations to reduce long-range internal stresses. Krieg, et al., note that strain hardening at low to intermediate homologous temperatures (below $0.5T_m$, where T_m is the absolute melting temperature) is both isotropic and kinematic. Isotropic hardening, manifested by an increase in the height of the reversed strain hysteresis loop, has its microstructural origins in dislocation obstacle interaction, while kinematic hardening, manifested by the Bauschinger effect, has its origins in dislocation pile-ups. Mathematical descriptions of this behavior require two internal state variables.

Deformation kinetics resulting from thermally-activated processes are usually described by Arrhenius or hyperbolic sine functions; however, over a wide range of stresses, the analytically simpler power law provides a good approximation. This motivated Krieg, et al., to propose the following flow rule in multiaxial form in deviatoric stress-strain space:

$$\dot{\underline{\varepsilon}}^I = \dot{\varepsilon}_0 \, (|\underline{\xi}|/R)^m \, (\underline{\xi}/|\underline{\xi}|), \tag{55}$$

where $\dot{\underline{\varepsilon}}^I$ is the inelastic strain rate vector, $||$ is the Euclidean vector norm, $\dot{\varepsilon}_0$ and m are temperature-dependent material constants, and R is the drag stress, an internal state variable which accounts for isotropic hardening. The

effective stress $\underline{\zeta}$ is given by

$$\underline{\zeta} = \underline{s} - \underline{\alpha}, \tag{56}$$

where $\underline{\alpha}$ is the back stress, an internal state variable which accounts for kinematic hardening; and $\underline{s}$ is the applied stress. The increase in flow stress associated with an increase in hardening is taken to be proportional to inelastic strain. Recovery is associated with dislocation escape from glide planes by climb or cross-slip. In the absence of external loads, this escape reduces the internal stresses through annealing; in the presence of external loads, this escape permits additional inelastic deformation through creep or dynamic recovery. The evolution of $\underline{\alpha}$ and R is given by the difference between hardening and recovery rates as

$$\dot{\underline{\alpha}} = A_{\alpha}\dot{\underline{\varepsilon}}^{I} - r_{\alpha}\,(\underline{\alpha}/|\underline{\alpha}|) \tag{57}$$

and

$$\dot{R} = A_{R}|\dot{\underline{\varepsilon}}^{I}| - r_{R}, \tag{58}$$

where A_{α} and A_{R} are the hardening functions, and r_{α} and r_{R} are the recovery functions.

Krieg, et al., assume the hardening functions A_{α} and A_{R}

to be constant. The recovery rates are assumed to be proportional to dislocation velocity of escape and inversely proportional to the escape distance [99], where the velocity and distance depend on the magnitude of the back and drag stresses. Since annealing rate depends on hardening mechanisms, one would expect the kinetics of recovery for $\underline{\alpha}$ and for R to be different. A unique feature of this model is that it incorporates different physically-based recovery kinetics for each internal variable.

Dislocation processes associated with the drag stress are formations of dislocation tangles, or networks. Temperature-dependent changes in the networks can be described by the climb recovery model of Friedel [99]:

$$r_R = -K_1 \, (R^n/kT) \, \exp(-U/kT), \qquad (59)$$

where K_1 and n are material constants, k is the gas constant, T is the absolute temperature, and U is the activation energy associated with the particular micromechanism of softening.

Dislocation processes associated with the back stress are pile-ups or cell-wall bowing. Although both cross-slip and climb are recovery mechanisms, only screw dislocations can cross-slip and, consequently, the model's authors feel

that recovery by climb is a more complete description. The kinetics of this process are again given by Friedel [99]:

$$r_\alpha = -K_2\,\alpha^2\,[\exp(K_3\alpha^2/kT) - 1], \tag{60}$$

where K_2 and K_3 are material constants.

By use of equations (60), in multiaxial form, and (59), equations (57) and (58) become

$$\dot{\underline{\alpha}} = A_\alpha \dot{\underline{\varepsilon}}^I - |\underline{\alpha}|\,K_2\,[\exp(K_3|\underline{\alpha}^2|/kT) - 1] \tag{61}$$

and

$$\dot{R} = A_R|\dot{\underline{\varepsilon}}^I| - K_1\,[(R - R_0)^n/T]\exp(-U/kT), \tag{62}$$

where R_0 represents an isotropic annealed state.

For conditions of uniaxial stress and constant temperature, equations (55), (61), and (62) reduce to

$$\dot{\varepsilon}^I = \bar{c}_1\,|\zeta/R|^{c_2}\,\mathrm{sgn}(\zeta), \tag{63}$$

$$\dot{\alpha} = c_3\dot{\varepsilon}^I - c_4\alpha^2\,[\exp(c_5\alpha^2) - 1]\,\mathrm{sgn}(\alpha), \tag{64}$$

and

$$\dot{R} = c_6 |\dot{\varepsilon}^I| - c_7 (R - R_0)^n, \tag{65}$$

where $\bar{c}_1$, c_2, c_3, c_4, c_5, c_6, c_7, n, and R_0 are temperature-dependent material constants, sgn () is the signum function, and the effective stress ζ is

$$\zeta = \sigma - \alpha. \tag{66}$$

Krieg, et al., simplify the model further by assuming a kinematic work-hardening material so that the isotropic hardening variable R will remain constant. Equation (65) can then be omitted and the uniaxial isothermal form of the model becomes

$$\sigma = E (\varepsilon - \varepsilon^I), \tag{67}$$

where ε^I is given by

$$\dot{\varepsilon}^I = c_1 |\zeta|^{c_2} \text{sgn}(\zeta), \tag{68}$$

and

$$\dot{\alpha} = c_3 \dot{\varepsilon}^I - c_4 \alpha^2 [\exp(c_5 \alpha^2) - 1] \text{ sgn}(\alpha), \tag{69}$$

where c_1, c_2, c_3, c_4, and c_5 are-temperature dependent

material constants, and the effective stress ς is given by equation (66).

Evaluation Of Material Constants

Krieg, et al., present an experimental test and data reduction procedure which allows all constants, except the elastic modulus E, to be determined from a set of stress-drop tests, sometimes called strain transient dip tests.

Before describing the procedure to evaluate the material constants, it would be instructive to review the somewhat controversial stress-drop test. High-temperature creep can be characterized in terms of an internal stress and an effective stress [100], where the internal (or back) stress is the driving force for recovery, and the effective stress (the difference between the applied and back stress) is the driving force for dislocation glide. Consequently, it is of interest to be able to determine the back stress.

Since the back stress is a result of the dynamic balance between strain hardening and recovery, the back stress begins to change when the applied stress is changed. Therefore, the transient response examined should be of short enough duration to ensure a structure which is still reasonably representative of the steady-state structure; i.e., a structure in which the value of the back stress has

not changed appreciably from its steady-state value. A technique described by Ahlquist and Nix [100,101] involves the dynamic measurement of back stresses by rapidly reducing the applied stress from the steady-state value σ_1 and measuring the strain rate immediately after the reduction. For a small reduction in stress $\Delta\sigma$, the strain rate immediately after the reduction is positive as shown in Figure 6a. For a large reduction in stress $\Delta\sigma$, the strain rate is negative as shown in Figure 6b. For an intermediate reduction in stress $\Delta\sigma$, the strain rate is zero and the new stress level σ_2 describes the mean internal (or back) stress σ_i. After a short time, recovery events reduce the back stress, yielding a positive strain rate. As can be seen from Figure 7, it may be necessary to load and unload a sample several times during a test before finding the stress reduction that will give the back stress.

This procedure for determining the back stress applies to thermally-activated creep. However, there are different hypotheses for creep deformation where the concept of a back stress may become questionable. Consequently, these hypotheses give differing predictions of the transient response after a stress drop. Poirier [102] summarizes these into four categories, as shown in Figure 8, where the responses due to stress drops of different magnitudes have

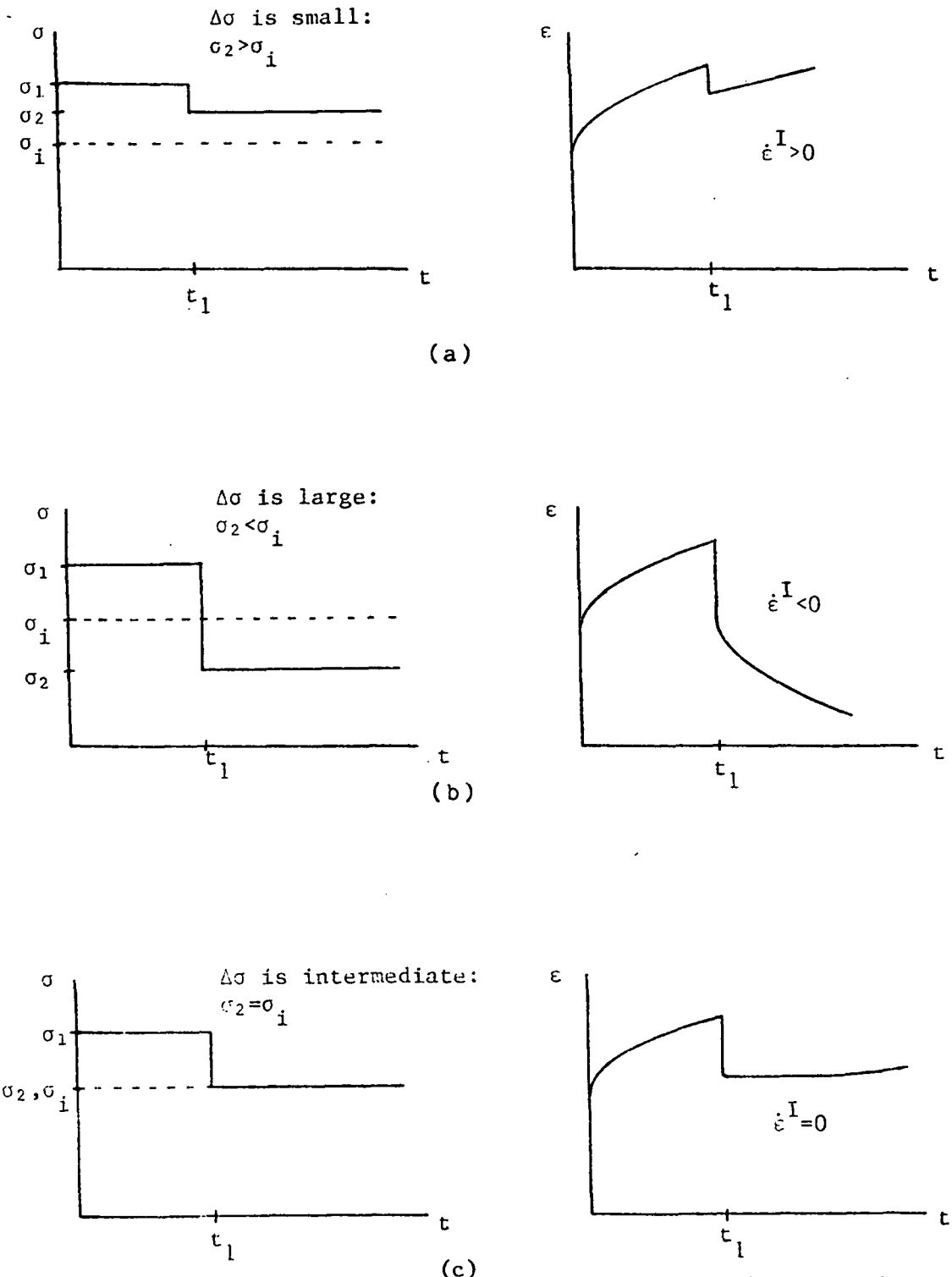

Fig. 6 Strain response for rapid stress reductions during steady-state creep

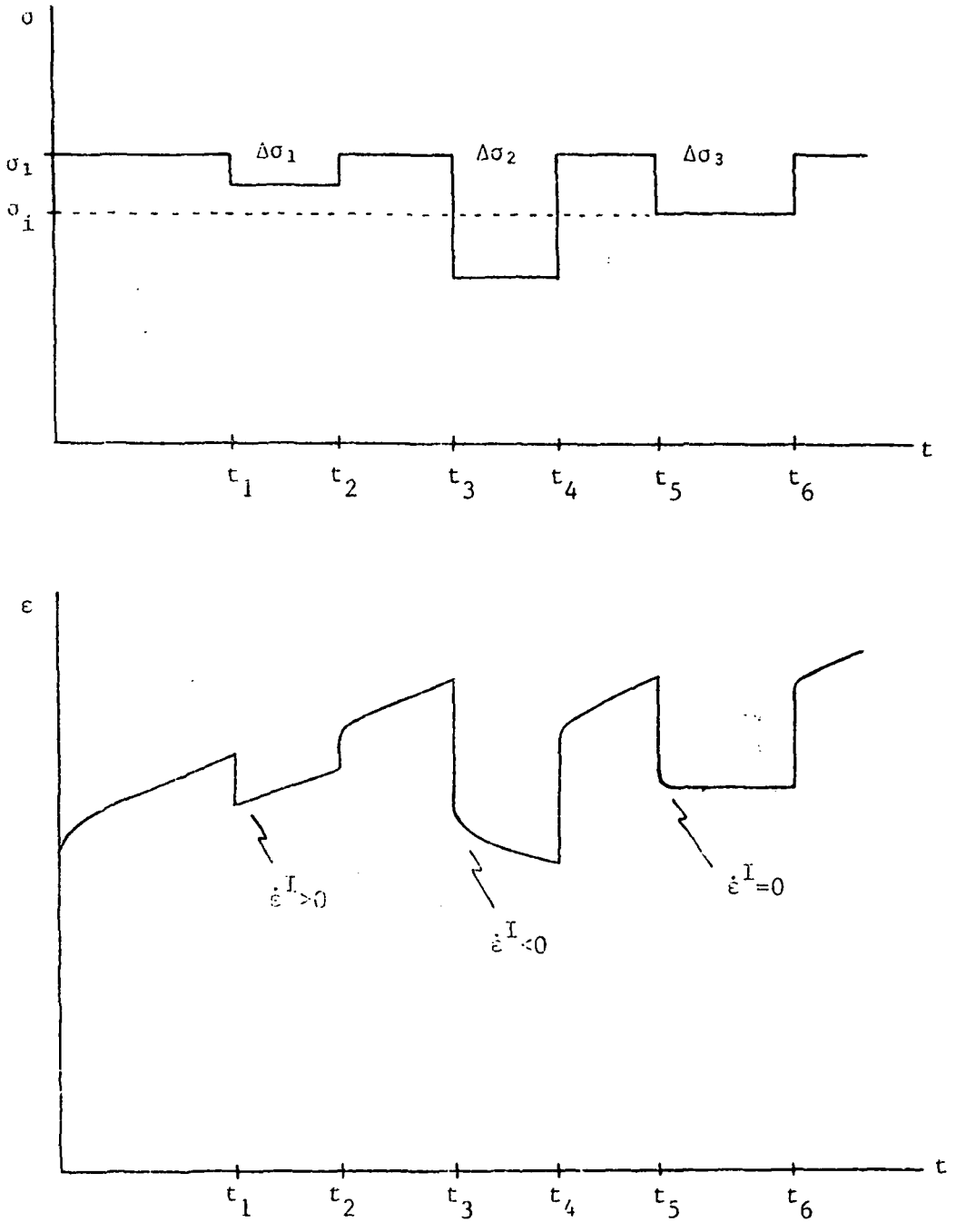

Fig. 7 A stress-drop test

been superposed.

The athermal recovery-controlled creep case is characterized by: 1) the absence of an effective stress, 2) creep proceeding only if the back stress is reduced to the applied stress level by diffusion-controlled recovery, and 3) stress reductions, regardless of magnitude, always followed by a period of zero creep rate (see Figure 8a).

The thermally-activated creep, jerky glide, case is characterized by localized obstacles to dislocation movement and, consequently, no negative creep rate after the stress reduction. However, there may be a period of zero creep or positive creep, depending on the magnitude of the stress reduction (see Figure 8b).

The thermally-activated creep, viscous glide, case is characterized by "smeared" rather than localized obstacles. Consequently, there may be positive, zero, or negative creep after the stress reduction (see Figure 8c).

Finally, the thermally-activated creep case with a combination of jerky and viscous glide is characterized by a combination of localized and smeared obstacles. The response of this case is similar to that of the previous two and depends on the magnitude of the stress reduction as well as the applied stress level (see Figure 8d).

Poirier concludes that, while the concept of a back stress cannot be rejected on experimental grounds,

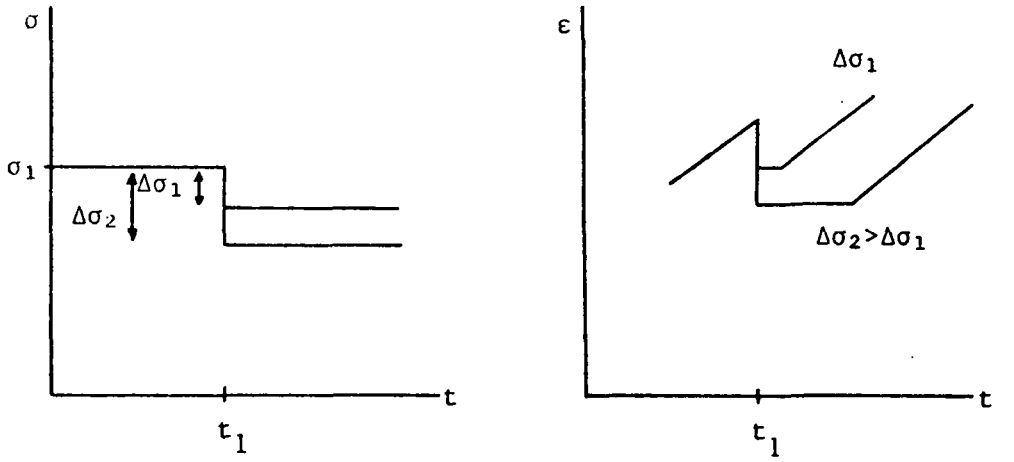

(a)

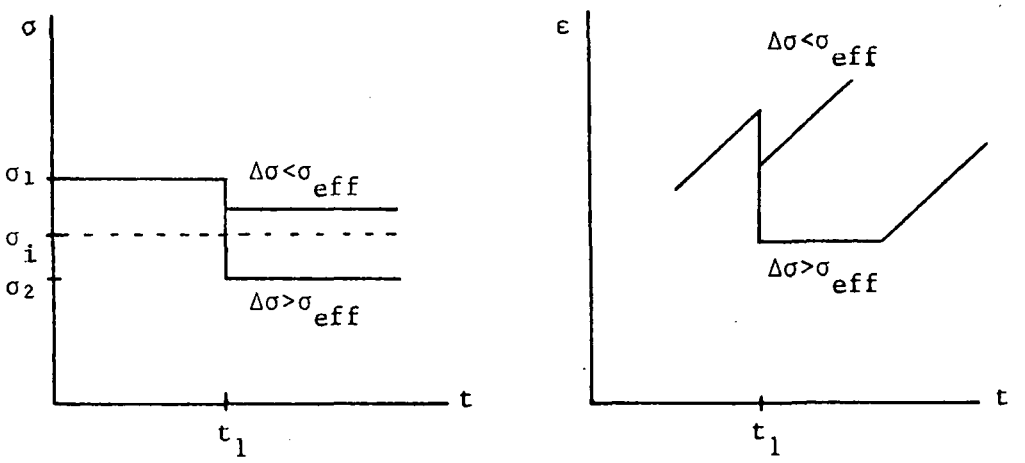

(b)

Fig. 8 Four hypotheses for creep response following a stress-drop

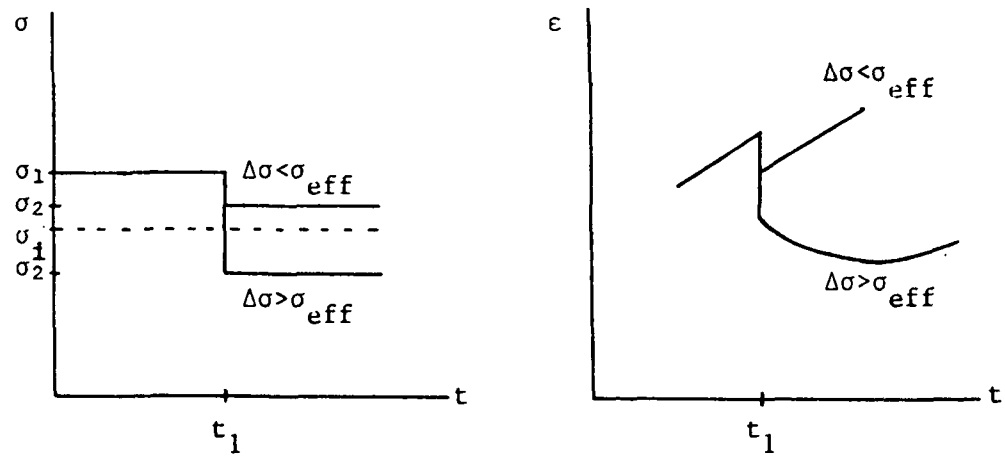

(c)

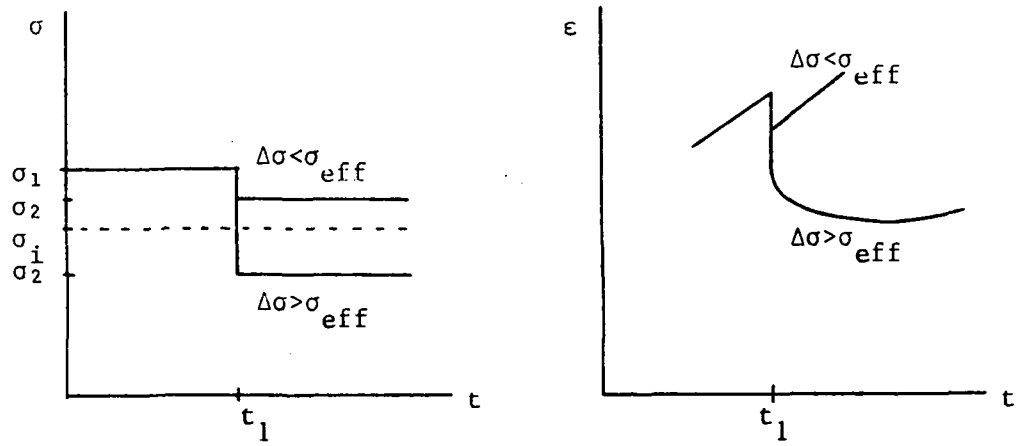

(d)

Fig. 8 (continued)

measurements of the back stress resulting from stress-drop tests should be performed with great care and are valid only for thermally-activated flow.

Similarly, Jones, et al. [96], conclude that due to ambiguity involved in attempting to determine a zero creep rate or merely the absence of a resolvable creep rate after unloading, the stress-drop test should be interpreted with great care on the basis of a specific deformation hypothesis. With this in mind, one can now proceed to evaluate the material constants c_1, c_2, c_3, c_4, and c_5.

c_1 and c_2

Equation (68), which governs inelastic strain, can be rewritten as

$$\ln(\dot{\varepsilon}^I) = \ln(c_1) + c_2 \ln|\zeta|, \qquad (70)$$

where $|\zeta|$ is the difference between the applied stress σ and the experimentally determined back stress α, and $\dot{\varepsilon}^I$ is the creep rate immediately preceding the particular stress reduction associated with that value of α. The left hand term of (70) must be linear in $\ln|\zeta|$ if it is an adequate representation of experimental data. A plot of data in the form of (70) is shown in Figure 9. Graphical means or a least-squares analysis of the data will give the values of

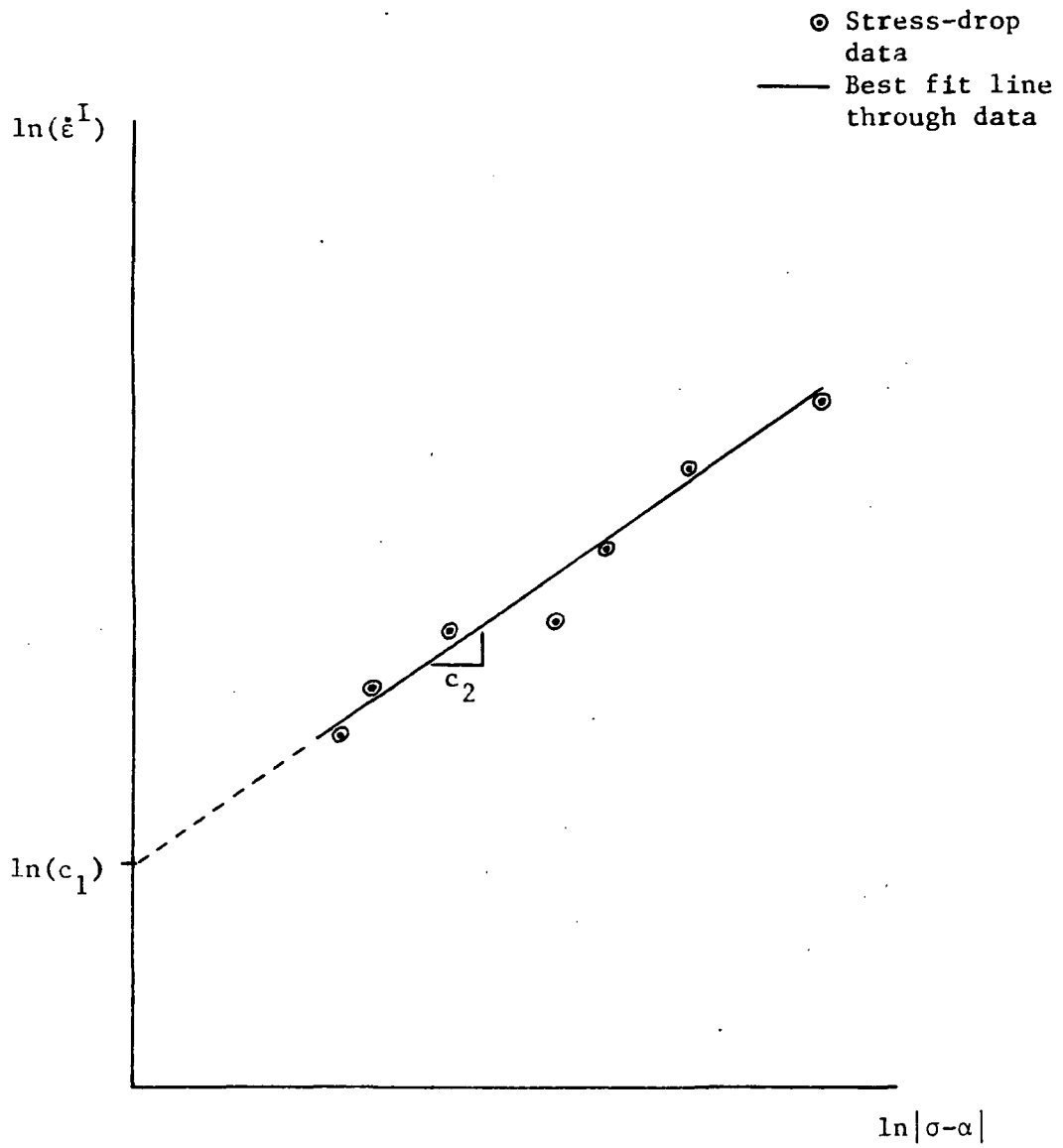

Fig. 9 A qualitative graph of $\ln(\dot{\varepsilon}^I)$ v. $\ln|\sigma-\alpha|$ for determining c_1 and c_2

c_1 and c_2.

c_5 and (c_3/c_4)

During steady-state creep, the creep rate $\dot{\varepsilon}^I$ is constant and, as a consequence of equation (68), ζ must also be constant. Since the applied stress σ is constant in a creep test, this implies that the back stress α is also constant. With $\dot{\alpha} = 0$, equation (69) reduces to:

$$(c_3/c_4) = [\alpha^2/(c_1|\zeta|^{c_2})]\,[\exp(c_5\alpha^2) - 1], \qquad (71)$$

where the fitted form $c_1|\zeta|^{c_2}$ has been used for the term $\dot{\varepsilon}^I$ to reduce experimental scatter. The experimental pairs (ζ_1,α_1) and (ζ_2,α_2), where the subscripts 1 and 2 refer to the highest and lowest values of α, may be used in equation (71) to give two nonlinear equations in two unknowns. These are then solved by iterative means to give the values of c_5 and the ratio (c_3/c_4).

c_3 and c_4

It now remains to determine either c_3 or c_4, since only their ratio is known at this point. In order to accomplish this, information from a point on the primary creep curve (where $\dot{\alpha}$ is not zero) must be used since the available steady-state information has been exhausted. Substituting

equation (68) into (69), separating variables, and integrating leads to

$$c_3 t = \int_0^{\alpha_1} \{c_1 |\sigma_1 - \alpha|^{c_2} - (c_4/c_3)\alpha^2 [\exp(c_5\alpha^2) - 1]\}^{-1} d\alpha, \quad (72)$$

where σ_1 is the creep stress, α is the variable of integration, α_1 and t are the back stress and time, respectively, at which the primary creep rate $\dot{\varepsilon}_1^I$ is still twice the eventual steady-state value. The value for α_1 at this data point can be determined by inverting equation (68):

$$\alpha_1 = \sigma_1 - (\dot{\varepsilon}_1^I/c_1)^{1/c_2}. \quad (73)$$

Since all the quantities inside the integral now have known values, equation (72) can be integrated numerically to give a value for $c_3 t$. Since t is known, c_3 and, consequently, c_4 can be calculated easily. Although not explained by Krieg, et al., a primary-to-steady-state creep rate ratio of two appears to represent a transition point between the region of rapidly decreasing primary creep rate and the region in which the creep rate slowly approaches its steady-state value, as shown in Figure 10.

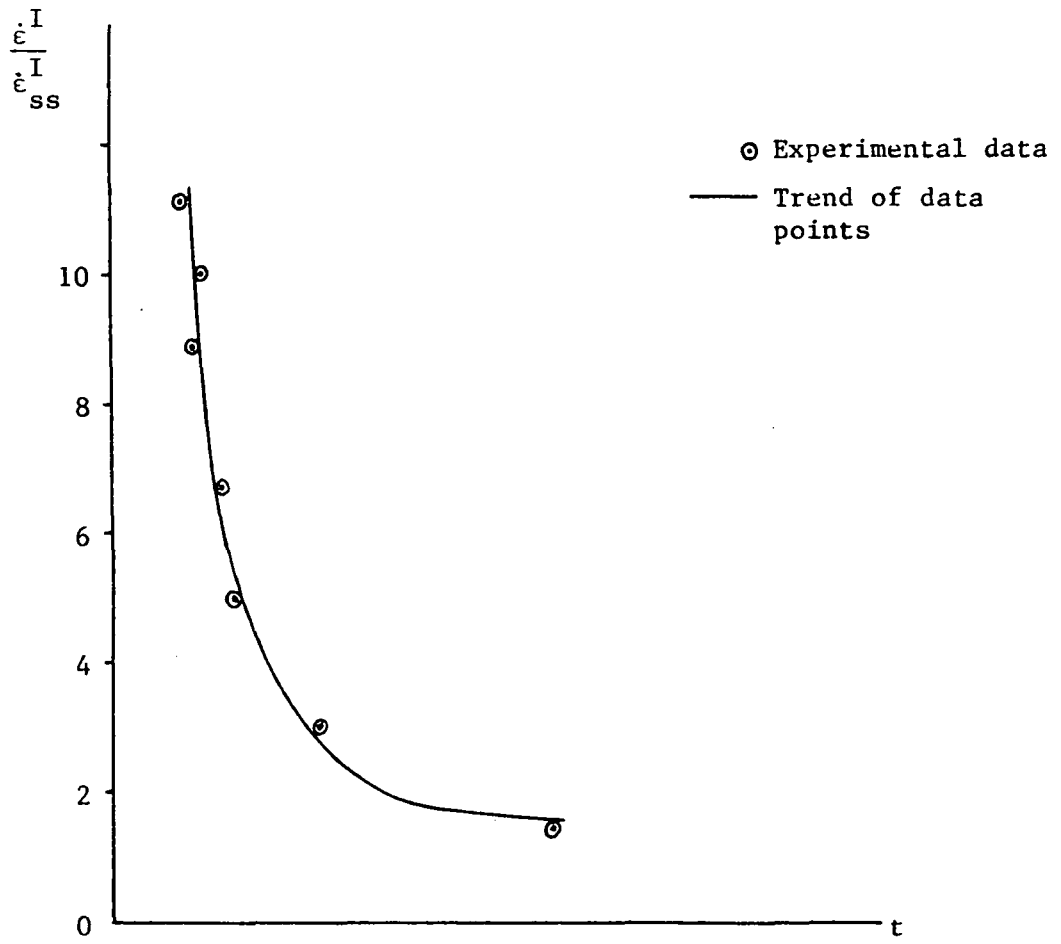

Fig. 10 A qualitative graph of the primary-to-secondary creep ratio used in determining c_3 and c_4

In summary, the Krieg, Swearengen, and Rohde theory requires a constant strain rate test (for the elastic modulus E), several stress-drop tests in the steady-state creep region (constants c_1, c_2, c_5, and the ratio c_3/c_4) and a creep curve complete with primary and secondary regions (constants c_3 and c_4). This concludes the determination of the material constants for the Krieg, Swearengen, and Rohde model.

BODNER AND PARTOM'S MODEL

Chronological Development

In 1975, Bodner and Partom [50] expanded an earlier model, capable of modelling elastic-perfectly plastic behavior only [103], to include strain-hardening by introducing plastic work as the measure of the hardened state. The formulation of the inelastic strain rate equation is based on a generalization of the flow rule of classical plasticity and is motivated partly by dislocation dynamics. The inelastic strain rate is proposed as an exponential function of stress and an internal state variable representing hardness, where the hardness parameter is an exponential function of plastic work. The proposed formulation corresponds to isotropic hardening and therefore would not characterize the Bauschinger effect. Bodner and Partom found good agreement of their theory with experimental results for commercially pure aluminum.

In noting that most constitutive theories consider isotropic and directional hardening effects as completely separable and thereby controlled by different internal state variables, Bodner and his colleagues [104] extended their isotropic theory in 1979 to model uniaxial cyclic loading by proposing an alternative approach. This

approach uses separate values of the hardening parameter in order to account for the directional character of hardening during cyclic loading; one value corresponds to tensile loading, the other corresponds to compressive loading. Bodner, et al., found good agreement with uniaxial experimental data for OFHC copper and commercially pure titanium and aluminum at room temperature in modelling phenomena such as cyclic strain hardening and softening.

The Bodner-Partom theory subsequently was generalized to a framework for the multidimensional stress case by using a general anisotropic form of the flow law [105].

In another development of the theory [106], an additional term was introduced to the constitutive equations in order to account for the thermal recovery of hardening, a term essential for modelling secondary creep. This development was used to model the superalloy Rene 95 at high temperatures.

A parameter to account for damage was introduced in 1980 [71]. Bodner examined the isotropic case first and then generalized the damage parameter to the anisotropic case in a manner similar to his earlier treatment of anisotropic hardening [105].

A preliminary method to determine the material constants of the uniaxial constitutive equations directly from experimental data rather than from trial-and-error

curve-fitting was presented in 1981 in a study of Rene 95 at high temperatures [69]. This was further developed into a detailed systematic method and applied to IN100 at elevated temperatures [107] for the case of isotropic hardening with thermal recovery and no damage.

In an earlier paper [105], anisotropy was introduced in a manner not automatically leading to plastic incompressibility. Bodner and Stouffer revised the theory in 1983 [108] to enforce plastic incompressibility in order to make the theory consistent with stability and thermodynamic principles. Results from the revised theory are essentially unchanged from the original work except that plastic volume changes become zero.

An incrementally isotropic form of the flow law has been proposed [109] in order to alleviate some of the computational difficulties encountered in using the full anisotropic form. In this formulation, the scalar hardening variable is taken to be the sum of the isotropic component and a scalar effective value of the directional component. Evolutionary equations are given for both components, including thermal recovery terms, as well as for isotropic damage. It is suggested that anisotropic damage can be treated in a manner similar to anisotropic hardening.

Recent work on the Bodner-Partom theory includes

research into modelling transient temperatures [91,94], a complete detailed review of the present constitutive theory [110], and development of a systematic method for the determination of material constants for the model in its complete anisotropic form with damage [111].

General Theory

The unified creep-plasticity model of Bodner and his colleagues [107] is motivated in part by work done in dislocation dynamics in which the total deformation can be separated into elastic and plastic components which are generally non-zero at all stages of loading. A yield criterion or loading and unloading conditions are therefore not required.

The total strain rate is given by

$$\dot{\varepsilon}_{ij} = \dot{\varepsilon}^{E}_{ij} + \dot{\varepsilon}^{I}_{ij}, \tag{74}$$

where the elastic strain rate $\dot{\varepsilon}^{E}_{ij}$ is given by the time derivative of Hooke's Law and the inelastic strain rate $\dot{\varepsilon}^{I}_{ij}$ is given by the flow rule of classical plasticity:

$$\dot{\varepsilon}^{I}_{ij} = \dot{e}^{I}_{ij} = \lambda \, \sigma'_{ij}, \tag{75}$$

where $\dot{e}^{I}_{ij}$ and σ'_{ij} are the deviatoric components of the

inelastic strain rate and applied stress tensors, respectively, and λ is a scalar material function.

Squaring both sides of (75) gives

$$\lambda^2 = D_2^P / J_2, \tag{76}$$

where D_2^P is the second invariant of the inelastic strain rate deviator

$$D_2^P = \frac{1}{2} \dot{e}_{ij}^I \dot{e}_{ij}^I \tag{77}$$

and J_2 is the second invariant of the stress deviator

$$J_2 = \frac{1}{2} \sigma'_{ij} \sigma'_{ij}. \tag{78}$$

A fundamental assumption of the Bodner-Partom theory is that all inelastic deformations are governed by the kinetic equation

$$D_2^P = f(J_2, T, Z_k), \tag{79}$$

where T is the absolute temperature and Z_k are a set of internal state variables. Extensive work in the field of dislocation dynamics [112-114] has shown that dislocation velocity and, therefore, inelastic strain rate can be

represented as a power function or an exponential function of stress.

Bodner and Partom note that in order to represent material behavior D_2^P should vary inversely with the measure of strain hardening, have a limiting value for large J_2, and be almost zero for low stresses. Whereas several mathematical functions may fulfill these requirements, the function chosen by Bodner and Partom is

$$D_2^P = D_0^2 \exp[-(Z^2/3J_2)^n], \tag{80}$$

where D_0 is the limiting strain rate in shear, n is a temperature dependent material constant, and Z is interpreted as an internal state variable representing hardness. It should be noted that, in subsequent developments of the theory, an internal state variable representing damage was introduced in the following manner [71,109,110]:

$$D_2^P = D_0^2 \exp\{-[Z^2(1 - \omega)^2/3J_2]^n\}, \tag{81}$$

where ω represents damage in the material.

Equations (75),(76), and (80) can then be combined to give an expression for the inelastic strain rate:

$$\dot{\varepsilon}^I_{ij} = \{D_0^2 \exp[-(Z^2/3J_2)^n]/J_2\}^{1/2} \sigma'_{ij}. \qquad (82)$$

The work-hardened state, that is, the resistance to plastic flow, is assumed to be represented by a single variable Z which depends on the plastic work W^P, where dW^P is $\sigma d\varepsilon^I$. The plastic work rate was chosen by Bodner and Partom as the measure of hardening over the more common choice of the inelastic strain rate because Z is directly related to the stored energy of cold work and this choice leads to relative simplicity of the resulting equations [110].

It is postulated that the evolution of Z is governed by the current values of stress, hardness, and the absolute temperature:

$$\dot{Z} = F(J_2, Z, T), \qquad (83)$$

where the particular form chosen by Bodner and his colleagues is

$$\dot{Z} = m\,(Z_1 - Z)\,\dot{W}^P - A\,Z_1\,[(Z - Z_2)/Z_1]^r, \qquad (84)$$

where m, Z_1, Z_2, A, and r are temperature-dependent material constants and the constant Z_0 is designated as the initial value of Z. The constants Z_1 and Z_2 correspond to

the maximum value of Z and the minimum recoverable value of Z, respectively.

The first term in equation (84) is the hardening term, where the negative part can be interpreted as dynamic recovery, and the second term is the thermal recovery term, designed to be negligible during rapid loading histories.

This representation, equation (84), corresponds to isotropic hardening and, as a result does not predict the Bauschinger effect. The Bodner-Partom theory was later modified [109] to include directional hardening by taking the scalar hardening variable Z in the inelastic strain rate equation (82) as the sum of the scalar isotropic hardening variable Z^I and a scalar effective directional hardening variable Z^A:

$$Z = Z^I + Z^A, \tag{85}$$

where Z^I is now given by (84) and the evolution equation for Z^A has the general form of (84) but is tensorial in character.

For the purposes of this research, the isotropic hardening model with no damage [107], equations (82) and (84), is considered.

For uniaxial stress and constant temperature, equation (82) reduces to

$$\dot{\varepsilon}^I = \frac{2}{\sqrt{3}} D_0 \exp[-\tfrac{1}{2}(\sigma/Z)^{-2n}] \operatorname{sgn}(\sigma) \qquad (86)$$

and equation (84) remains unchanged due to its scalar nature:

$$\dot{Z} = m (Z_1 - Z) \dot{W}^P - A Z_1 [(Z - Z_2)/Z_1]^r. \qquad (84)$$

The material constants to be determined are D_0, n, m, Z_1, A, Z_2, r, and Z_0, the initial value of Z.

Evaluation of Material Parameters

D_0

The quantity D_0 is the maximum value of strain rate in shear and has its physical basis in the upper bound of the dislocation velocity. The value of D_0 can be set as 10^8 sec^{-1} for $\dot{\varepsilon}^I > 10^3$, 10^6 sec^{-1} for $10^1 < \dot{\varepsilon}^I < 10^3$, and 10^4 sec^{-1} for $\dot{\varepsilon}^I < 10^1$.

Z_1 and n

The first step in the evaluation of material constants is to determine the strain rate sensitivity parameter n and the maximum value of the hardness, Z_1, from tensile data. For material behavior as shown by curve (a) in Figure 11 where the stress saturates to a maximum value, in the region where both the stress and strain rate are constant Z

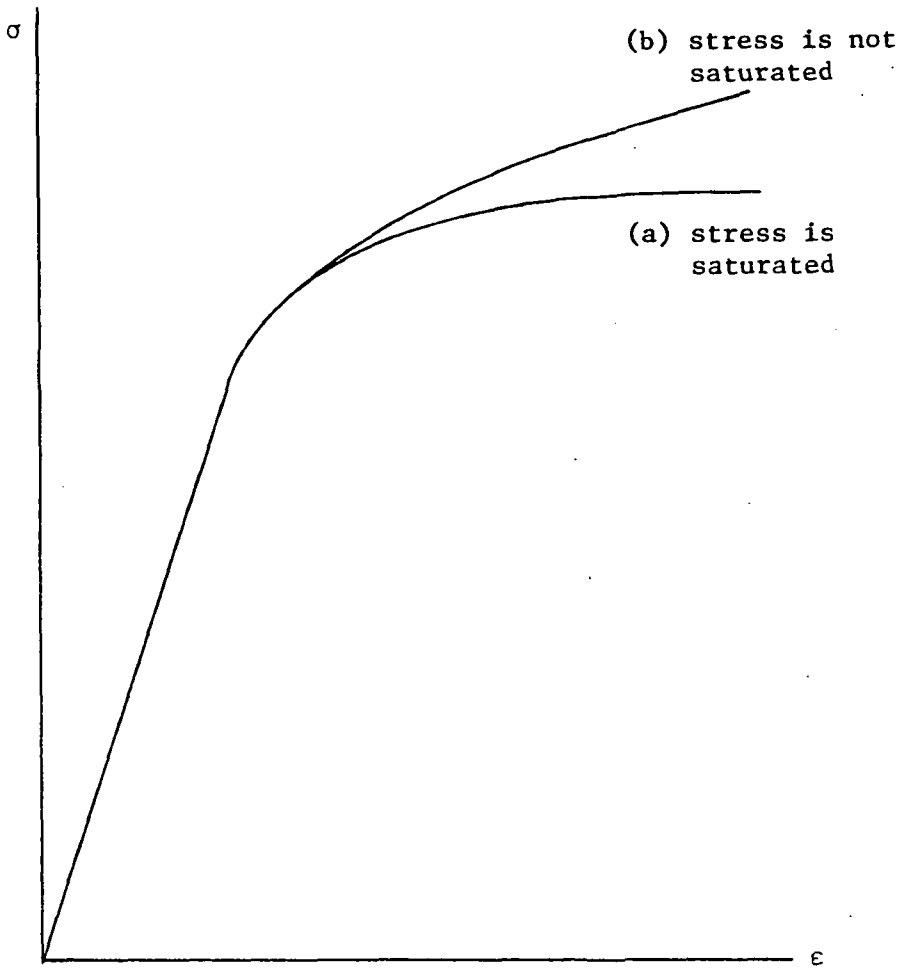

Fig. 11 A qualitative comparison of a saturated stress curve and a non-saturated stress curve

must also be constant in order to satisfy equation (86). For short duration tests with no recovery, the material must be in a fully work-hardened state to obtain the maximum value of stress; that is, Z must have its maximum value Z_1. Rewriting equation (86) for this steady flow condition gives

$$\ln[-\ln(\frac{\sqrt{3}}{2}\dot{\varepsilon}^I/D_0)] =$$

$$-2n\ln(\sigma) + [2n\ln(Z_1) + \ln(\tfrac{1}{2})]. \qquad (87)$$

The left hand term of (87) must be linear in ln (σ) if it is an adequate representation of experimental data. A plot of data in the form of equation (87) is shown in Figure 12. Graphical means or a least-squares analysis of the data will give the values for n and Z_1.

However, if the tensile curves are not quite saturated, as shown by curve (b) in Figure 11, simply using the largest value of stress attained may give incorrect values for Z_1 and n. In this case, equation (86) is solved for σ to give

$$\sigma = K_1 Z, \qquad (88)$$

where

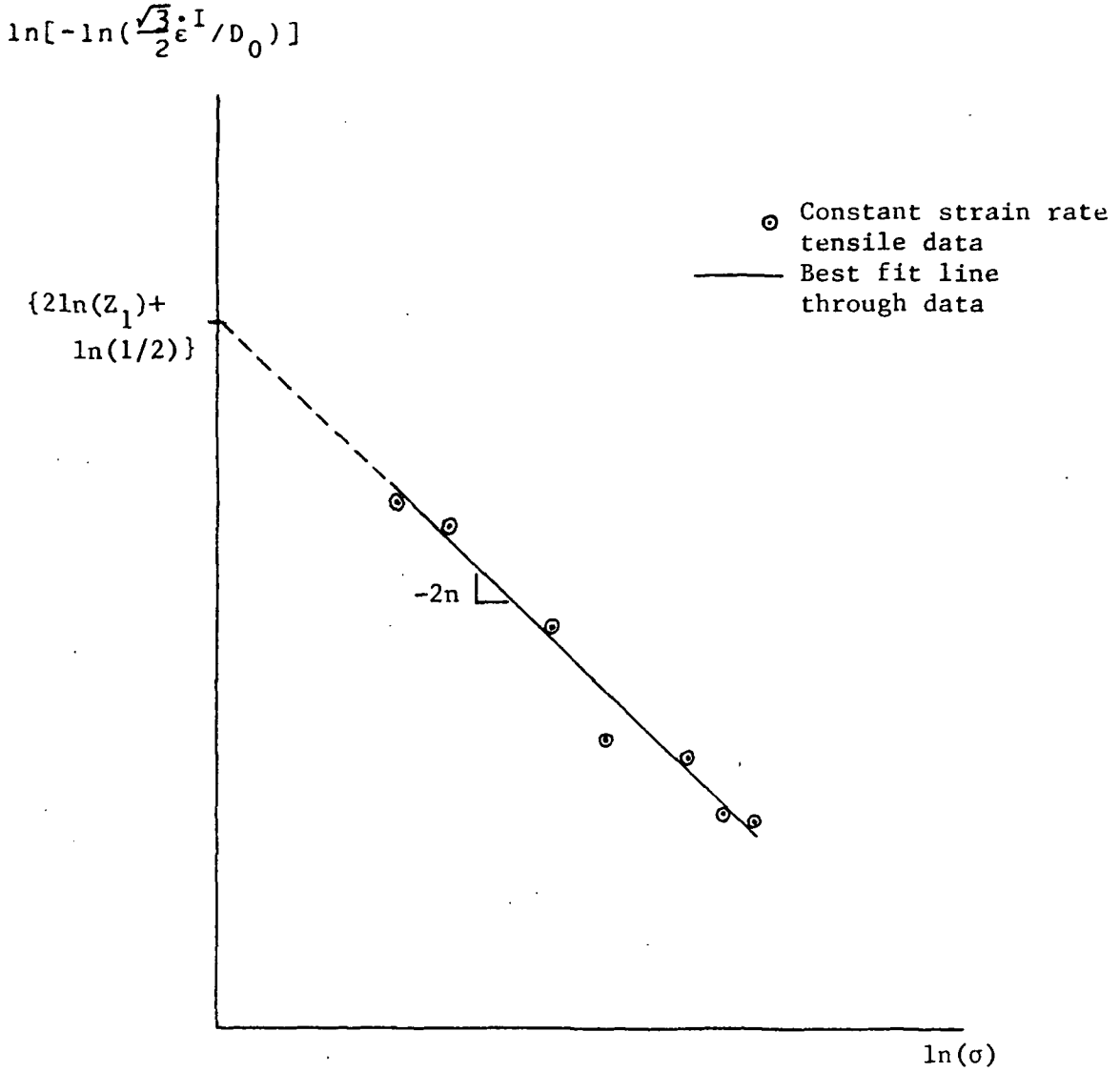

Fig. 12 A qualitative graph of constant strain rate tensile data for determining n and Z_1

$$K_1 = [2\ln(\frac{2}{\sqrt{3}}D_0/\dot{\varepsilon}^I)]^{-1/2n}. \qquad (89)$$

In the absence of hardening recovery, the hardening evolution equation (84) becomes the first order linear differential equation

$$dZ = m\ (Z_1 - Z)\ dW^P, \qquad (90)$$

which can be combined with the differential of equation (88) to give

$$d\sigma = K_1\ m\ (Z_1 - Z)\ dW^P. \qquad (91)$$

By defining a new parameter γ as

$$\gamma = d\sigma/dW^P \qquad (92)$$

and substituting equation (88) for Z, equation (91) can be rewritten as

$$\gamma = K_1\ m\ Z_1 - m\ \sigma. \qquad (93)$$

In order to be an adequate representation of experimental data, γ must be linear in σ, as shown in Figure 13. The saturation stress is given by the stress level where $\gamma=0$.

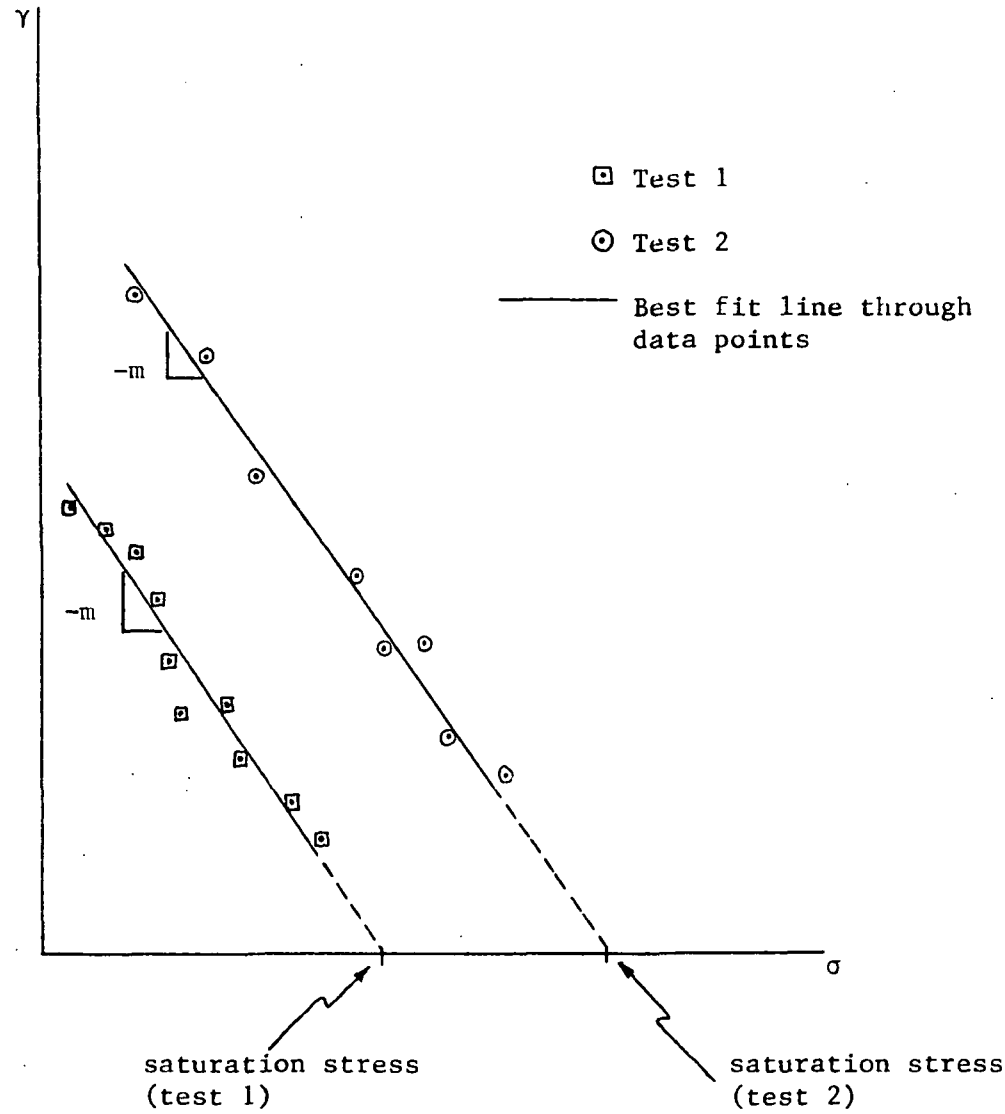

Fig. 13 A qualitative graph of γ v. σ for determining the saturated stress level

With this value of the saturation stress, one can now return to the method outlined above to determine n and Z_1.

Z_0 and m

The value of the hardening variable Z can be calculated for corresponding values of stress and inelastic strain rate by inverting equation (86):

$$Z = \sigma \left[2\ln\left(\frac{2}{\sqrt{3}}D_0/\dot{\varepsilon}^I\right)\right]^{1/2n}. \qquad (94)$$

Equation (90), the hardening evolution equation with no recovery, can be integrated to give

$$\ln(Z_1 - Z) = \ln(Z_1 - Z_0) - mW^P, \qquad (95)$$

where Z_0 is the initial value of Z. Several values of Z can be calculated for each test by using equation (94) at different stress levels and their corresponding values of $\dot{\varepsilon}^I$ taken from the region in the σ-ε graph where recovery is minimal. In this manner a plot of $\ln(Z_1 - Z)$ against W^P can be made for several constant strain rate tensile tests. Since this plot must be linear in order to represent material behavior adequately, as shown in Figure 14, the constants m and Z_0 can be calculated easily either by graphical means or by a least-squares analysis.

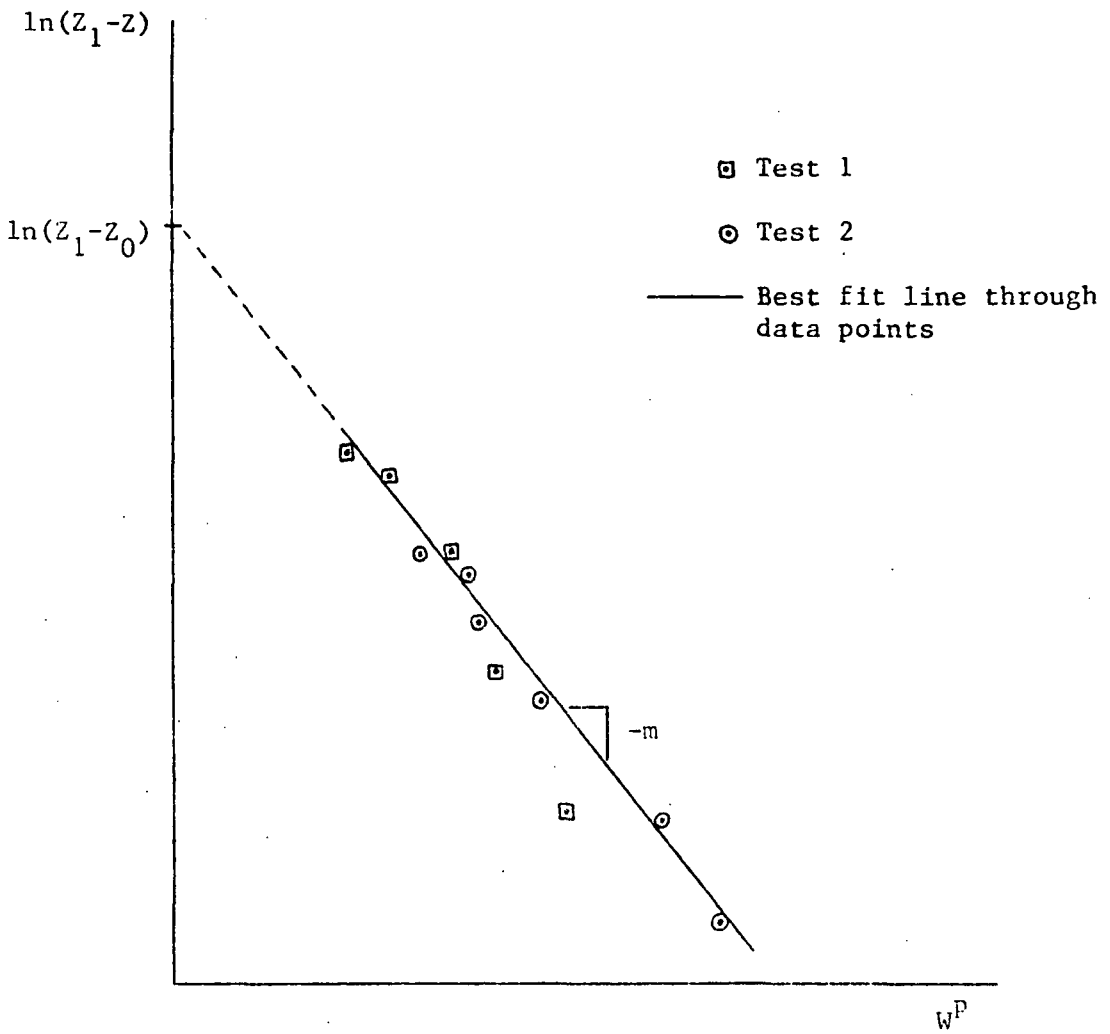

Fig. 14 A qualitative graph of $\ln(Z_1-Z)$ v. W^P for determining m and Z_0

Alternatively, if a γ-σ graph was used in the earlier determination of n and Z_1, then the average of the slopes of the linear curve-fits of the γ-σ data will be -m. Z_0 is then given by calculating values of Z in the immediate post-yield (i.e., post-elastic limit) region of a stress-strain curve.

Z_2

During secondary creep, since stress and inelastic strain rate are constant, the value of Z must also be constant in order to satisfy equation (86). These stationary values of Z can be determined from equation (94) for several creep tests. The lowest calculated stationary value of Z can be used for the value of Z_2, the minimum value of Z, although Bodner states that $Z_2 \approx Z_0$ for many applications since the initial condition (Z_0) is the fully recovered state (Z_2) [110].

A and r

Since $\dot{Z} = 0$ during secondary creep, the hardening evolution equation becomes

$$m\,(Z_1 - Z)\,\dot{W}^P = A\,Z_1\,[(Z - Z_2)/Z_1]^r. \qquad (96)$$

The values of σ, $\dot{\varepsilon}^I$, and Z used in the determination of Z_2

above may be used in a plot of $\ln[m\ (Z_1 - Z)\ \dot{W}^P]$ against $\ln[(Z - Z_2)/Z_1]$. The constants A and r can be calculated from these data by assuming a linear representation, although a bilinear representation may also be possible in some cases [107].

In summary, the Bodner-Partom theory requires several constant strain rate tensile tests (constants E, n, Z_1, m, and Z_0) and several creep tests (constants Z_2, A, and r), where the actual number of tests is dependent on the amount of data deemed necessary for accurate evaluation of the constants. This concludes the determination of material constants for the Bodner-Partom theory.

MILLER'S MODEL

Chronological Development

Miller's model [90], introduced in 1976, is based on a combination of creep phenomenology and microstructural considerations. In stressing the need to model steady-state creep rates accurately, Miller proposes to use the Garofalo hyperbolic sine relation for steady-state creep as a basis for his constitutive equations. Representing isotropic and kinematic hardening, respectively, a drag stress variable and a back stress variable are introduced to describe non-steady-state inelastic responses. The growth laws for the back stress and the drag stress follow the standard Bailey-Orowan format of competing hardening and recovery rates. Miller's growth laws feature a constant kinematic work-hardening coefficient but a variable isotropic work-hardening coefficient. A procedure for evaluation of the material constants, based partly on trial-and-error curve-fitting, is also provided. Miller found reasonably good agreement of his theory with experimental results for type 304 stainless steel at room temperature.

This model contains both kinematic and isotropic hardening terms, an arrangement which leads, in Miller's view, to a rather complex set of equations. Miller and

Sherby [115] simplified this in 1978 by eliminating kinematic hardening and allowing only isotropic hardening to be modelled. While this representation gave fairly realistic simulations for pure aluminum, it became apparent that an additional strengthening term was needed for modelling of solute-strengthened materials. The solute strengthening term, which is not an internal state variable, was added to the drag stress in the inelastic strain rate equation.

In 1980, Miller noted that several existing unified constitutive theories, including his own, predict "over-square" hysteresis loops with respect to experimentally observed behavior [116]. To eliminate this discrepancy in Miller's model, the work-hardening coefficient in the back stress growth law, previously a constant, is made an exponential function of the back stress and the direction of the effective stress. The predicted hysteresis loops using the improved equations compare more favorably with experimental results.

Schmidt and Miller further improved the model by introducing an additional solute strengthening term [117,118]. This interactive term is multiplied by the drag stress to accompany the already present non-interactive solute strengthening term (see reference [115]) which is added to this product. The non-interactive term models the

influence of solutes on yield strength while the interactive term models the influence of solutes on strain hardening. These improvements allow the model to be used over a broader range of loadings where solute effects are significant.

Miller and his colleagues have devoted much effort to research in microstructural topics which have led to the particular formulation and features of the model: the mechanisms of solutes and their effects on the yield strength and strain hardening behavior of a wide variety of alloys [119], the physical factors governing power law creep as a basis for the form of the inelastic strain rate equation [120], and experimental cyclic torsion data for support of many assumptions and predictions of the model with respect to steady-state back stresses and cyclic strain hardening/softening [121].

Recent work includes extending the theory to multiaxial form by Miller [122], and in a different manner by Kagawa and Asada [123]. In addition, it has been reported [91] that the latest form of Miller's theory contains four internal state variables in order to model the long range and short range components of the drag stress and the back stress. This form of the model may be useful in modelling transient temperature response [91].

General Theory

In attempting to model a broad spectrum of deformation phenomena, Miller uses a combination of micromechanics and creep phenomenology to derive the constitutive equations of his model [90]. It is postulated that all inelastic deformation can be characterized adequately by

$$\dot{\varepsilon}^{I} = f[(\sigma - R)/D], \tag{97}$$

where $\dot{\varepsilon}^{I}$ is the inelastic strain rate, f is the inelastic strain rate function, R is the "rest stress" (or back stress), and D is the drag stress. To complete the model, it remains to determine the best possible specific function for equation (97) and the evolution equations for R and D.

In stressing the need to model steady-state creep rates accurately, Miller uses the Garofalo hyperbolic sine relation for steady-state creep as a basis for deriving the inelastic strain rate function:

$$\dot{\varepsilon}^{I}_{ss} = B' [\sinh(A\sigma_{ss})]^{n}, \tag{98}$$

where the subscripts "ss" refer to the steady-state condition, B' is a temperature dependent parameter, and A and n are temperature-independent constants.

Since equation (97) must reduce to (98) for the special

case of steady-state creep, there must exist a function f_1 which causes the argument $(\sigma_{ss} - R_{ss})/D_{ss}$ to reduce to σ_{ss}, i.e.

$$f_1[(\sigma_{ss} - R_{ss})/D_{ss}] = \sigma_{ss}. \tag{99}$$

When this is true, equation (99) can be substituted for σ_{ss} in equation (98) to give $\dot{\varepsilon}^I_{ss}$ as a function not only of σ_{ss}, but also of R_{ss} and D_{ss}. Since steady-state creep is only a special case, the subscripts "ss" can be dropped to give

$$\dot{\varepsilon}^I = B' (\sinh\{Af_1[(\sigma - R)/D]\})^n. \tag{100}$$

By examination of warm-working data for several metals, the function f_1 is determined to be

$$f_1 = \frac{1}{A} [(\sigma - R)/D]^{1.5}. \tag{101}$$

Substituting this into equation (100) will result in the explicit equation governing the inelastic strain rate:

$$\dot{\varepsilon}^I = B' (\sinh\{[(\sigma - R)/D]^{1.5}\})^n. \tag{102}$$

The entire temperature dependence of the model lies in

the constant B', which is related to the activation energy for plastic flow. Below $0.6T_m$, where T_m is the absolute melting temperature, the activation energy decreases linearly with temperature and B' is given as

$$B' = B \exp\{[-Q/0.6kT_m] [\ln(0.6T_m/T) + 1]\}, \quad (103)$$

where B is a material constant, k is the gas constant, Q is the activation energy for plastic flow, and T is the absolute temperature. Above $0.6T_m$, the activation energy is approximately constant and B' is given as

$$B' = B \exp(-Q/kT). \quad (104)$$

In either case, the expression for B' can be abbreviated as

$$B' = B\,\theta', \quad (105)$$

where θ' is the desired temperature-dependent factor.

The evolution equations for R and D are given in the standard work-hardening/recovery format as

$$\dot{R} = H_1 \dot{\varepsilon}^I - f_2(R,T) \quad (106)$$

and

$$\dot{D} = H_2' \dot{\varepsilon}^I - f_3(D,T), \qquad (107)$$

where H_1 and H_2' are constants, and f_2 and f_3 are recovery functions.

In order to determine the recovery functions f_2 and f_3, Miller applies equations (106) and (107) to the special case of steady-state creep (where $\dot{R}=\dot{D}=0$) and substitutes equation (98) for $\dot{\varepsilon}^I_{ss}$ to obtain

$$f_2(R_{ss},T) = H_1 \dot{\varepsilon}^I_{ss} = H_1 \, B' \, [\sinh(A\sigma_{ss})]^n \qquad (108)$$

and

$$f_3(D_{ss},T) = H_2' \dot{\varepsilon}^I_{ss} = H_2' \, B' \, [\sinh(A\sigma_{ss})]^n. \qquad (109)$$

In a manner similar to the derivation of the inelastic strain rate expression, equations (97) to (100), the evolution equations become

$$\dot{R} = H_1 \dot{\varepsilon}^I - H_1 \, B \, \theta' \, [\sinh(A_1 R)]^n \qquad (110)$$

and

$$\dot{D} = H_2' \dot{\varepsilon}^I - H_2' \, B \, \theta' \, [\sinh(A_2 D^3)]^n, \qquad (111)$$

where A_1 and A_2 are material constants.

For the purposes of this research, a simplified version of this model will be used. Miller and Sherby [115] simplified the model by eliminating all kinematic hardening terms, allowing only isotropic hardening to be modelled, and incorporating a solute strengthening term:

$$\dot{\varepsilon}^I = B\ \theta'\ (\sinh\{[(\sigma/E)/(D + F_{sol})^{1/2}]^{1.5}\})^n, \quad (112)$$

where the modulus-compensated stress σ/E has replaced the stress σ from the earlier equations for mathematical convenience, F_{sol} is the solute strengthening parameter, and D and F_{sol} are placed under the square-root sign to produce parabolic hardening, since parabolic hardening is a better approximation for many materials than the linear hardening of the earlier equations. The evolution equation for D becomes

$$\dot{D} = H|\dot{\varepsilon}^I| - H\ B\ \theta'\ [\sinh(A^3 D^{1.5})]^n, \quad (113)$$

where H and A are material constants.

It should be noted that a slight modification has been introduced by this author to equation (113). In order to be able to simulate cyclic loading, the inelastic strain rate term in equation (113) has been placed in absolute

value signs. This follows the practice introduced by Miller, et al., in later works [90,116-118].

The variable F_{sol} is introduced into the equations in order to characterize the effects of solute strengthening on material behavior that are found in many solute strengthened alloys. These effects include plateaus in the yield strength versus temperature curve, local maxima and minima in the strain rate sensitivity versus temperature curve, and peaks in the apparent activation energy. By judicious selection of the functional dependence of F_{sol} upon the other variables, one can ensure that the resulting equations simulate these effects.

At low temperatures, solute atoms are so immobile that they cannot keep up with the moving dislocations and hence cannot exert any particularly strong drag force. At high temperatures, the solute atoms are so mobile that they can move easily with the dislocations and are again unable to exert a strong drag force. At intermediate temperatures, however, the average velocities of solute atoms and dislocations are approximately equal, and the two can interact strongly, producing a maximum strengthening effect. From these physical considerations, one can deduce that F_{sol} should have a low value at low temperatures, should increase with temperature and pass through a maximum, and should fall to a low value at high

temperatures.

Furthermore, experimental evidence indicates that strain rate sensitivity occurs in a fashion similar to temperature sensitivity.

The particular statistical function which satisfies the mathematical requirements is

$$F_{sol} = F_{sol,max} \exp(-\{[\log_{10}(Z) - \log_{10}(Z_{max})]/2\}^2) + 1(10)^{-7} \exp(-\{[\log_{10}(Z) - 30]/10\}^2), \quad (114)$$

where Z is $|\dot{\varepsilon}^I|/\theta'$, $F_{sol,max}$ and Z_{max} are constants, and the second term on the right hand side of the equation is included to ensure a non-zero value of F_{sol} for conditions when $Z>>>Z_{max}$.

Finally, the material constants to be determined are A, B, n, H, $F_{sol,max}$, and Z_{max}. In addition, T_m and Q must be determined for the temperature-dependent factor θ'.

Evaluation of Material Constants

Q and T_m

The values of the absolute melting temperature T_m and the activation energy for plastic flow for the material of interest may be determined from various sources in the

literature. With these values and by use of equation (103) or (104), the temperature-dependent factor θ' may be calculated for a given absolute temperature T.

A

In order to derive the relation between the constants A, B, and n and steady-state creep rates, one returns to the observation that, for the special case of steady-state creep, the inelastic strain rate equation (112) reduces to the Garofalo equation (see equation (98)):

$$\dot{\varepsilon}^{I}_{ss} = B\,\theta'\,[\sinh(A\sigma_{ss}/E)]^{n}, \qquad (115)$$

where $\dot{\varepsilon}^{I}_{ss}$ is the steady-state creep rate and σ_{ss}/E has replaced σ_{ss}. Equation (115) may be rewritten as

$$\log_{10}(\dot{\varepsilon}^{I}_{ss}/\theta') = \log_{10}(B) + n\log_{10}[\sinh(A\sigma_{ss}/E)]. \qquad (116)$$

If this equation is an adequate representation of experimental data, then the constant A can be chosen such that $\log_{10}(\dot{\varepsilon}^{I}_{ss}/\theta')$ is linear in $\log_{10}[\sinh(A\sigma_{ss}/E)]$, as shown in Figure 15.

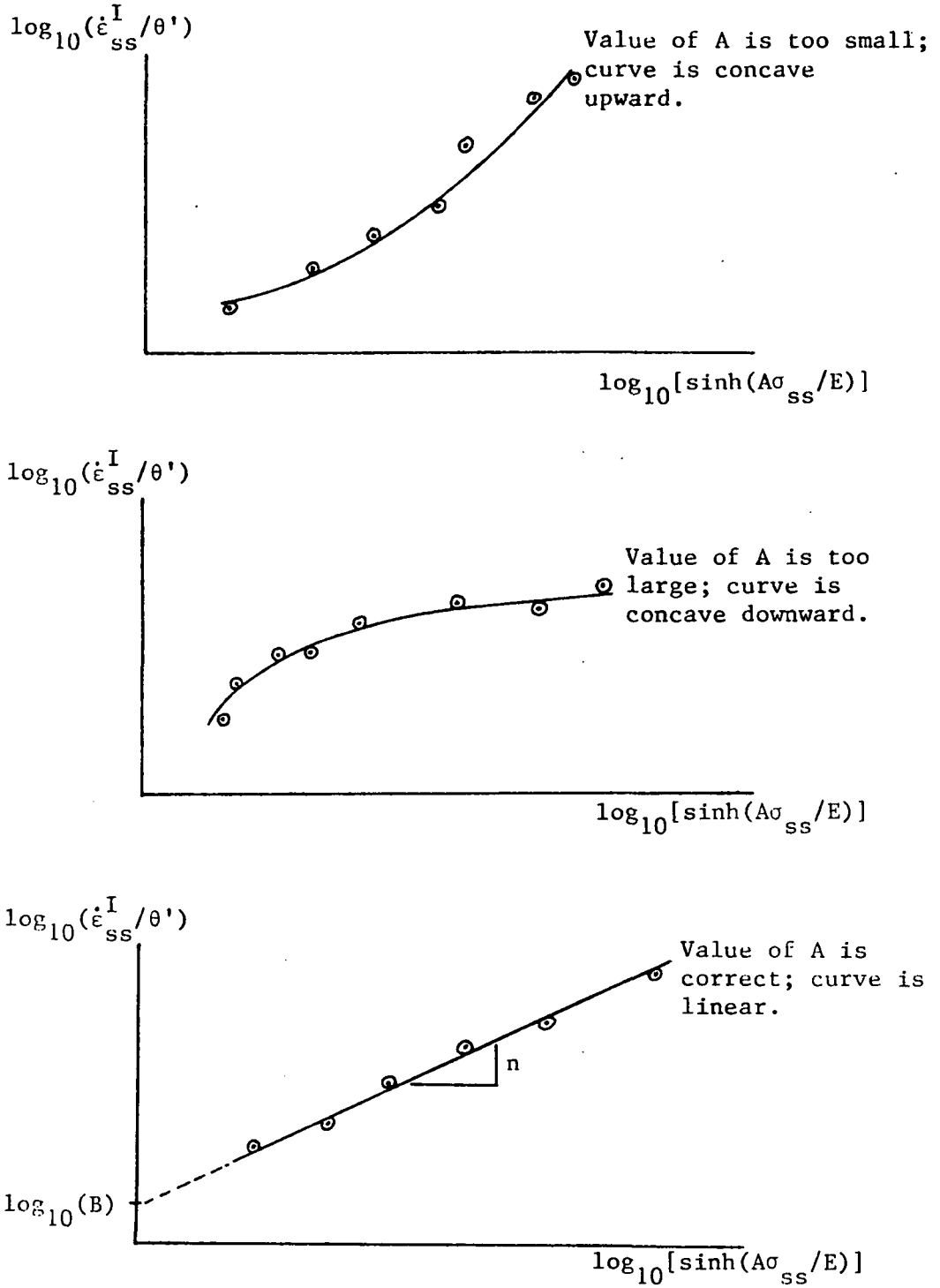

Fig. 15 The effect of A on $\log_{10}(\dot{\varepsilon}^{I}_{ss}/\theta')$ v. $\log_{10}[\sinh(A\sigma_{ss}/E)]$ data

B and n

Since the value of A is now known, one can easily determine the constants B and n from equation (116), either by graphical means or by a least-squares analysis.

$F_{sol,max}$ and Z_{max}

The maximum value for F_{sol} is assigned arbitrarily and is based on an intuitive analysis of the problem of interest. Z_{max} is set by Miller as $Z_{max} = 1(10)^{10}$ for his choice of function for F_{sol}.

H

Finally, the value of the work-hardening coefficient H is determined on a trial-and-error basis by a best fit of the model through several experimental constant strain-rate stress-strain curves.

In summary, Miller's theory requires some information about the material of interest (for T_m and Q), several creep tests (constants A, B, and n), and several constant strain rate tensile tests (for e and H). This concludes the evaluation of material constants for Miller's model.

DETERMINATION OF MATERIAL CONSTANTS

Each theory is evaluated and compared to experiment by its authors for a particular material under particular temperature conditions. In general, the choice of material and conditions varies from theory to theory. One of the objectives of the current research is to create a common experimental data base for one material at one temperature in order to characterize the mathematical representations and to compare to experiment the numerical predictions of each theory.

Many of the phenomena associated with inelastic deformation such as rate sensitivity, the Bauschinger effect, and creep become significant in crystalline structures at elevated temperatures, that is, above three tenths of the absolute melting temperature. At the start of this research it was intended to perform testing on the nickel-based superalloy IN718 at 1350°F. Testing was restricted to room temperature conditions, however, since extensive difficulties were encountered with the available equipment with testing at high temperatures. This restriction led to the choice of the aluminum alloy 5086 as the candidate material. This alloy displays many of the phenomena of inelastic deformation and is already above

three tenths of its melting temperature at room temperature. Its composition and some properties are listed in Table 1.

A review of the material test requirements of each theory is shown in Table 2. It should be noted that the stress-drop tests are performed during steady-state creep and, as such, can be combined with the creep tests. The constant strain rate tensile tests were performed on an MTS 810 hydraulic material testing system; the creep tests and the stress-drop tests were performed on a constant-load creep frame which was designed and constructed at Texas A&M University. Data acquisition in both cases was by graphical means, although a digital system was also available for the creep frame. It was decided to use a constant-load creep frame rather than a constant-stress creep frame due to difficulties associated with accurately determining the applied stress when using the latter system. As can be seen by the creep response below, the effects of this choice on the results are negligible.

The results of the constant strain rate tensile tests can be seen in Figure 16 for four applied strain rates ranging from $4(10)^{-7}$ sec^{-1} to $4(10)^{-4}$ sec^{-1}. It can be seen that the material exhibits some strain rate sensitivity and considerable work-hardening.

Table 1

Composition and Material Properties of Al 5086

Material: Al 5086 H111

Composition: 0.15%Cr, 0.40% Mn, 4.0% Mg, remainder Al

Melting temperature T_m: 858K

Elastic modulus E: $10.313(10)^3$ ksi

Ultimate stress σ_u: 40 ksi

Activation energy for plastic flow Q (at room temp.):
27,500 cal/mole

Form of specimens: uniaxial bar with $\frac{1}{2}$-inch diameter gauge section and threaded ends.

Table 2

Review of Material Test Requirements

Type of test	Krieg	Bodner	Miller	Total
Constant strain rate tensile test	1	3-4	3-4	3-4
Creep	1	3-4	3-4	3-4
Stress-drop	3-4	-	-	3-4

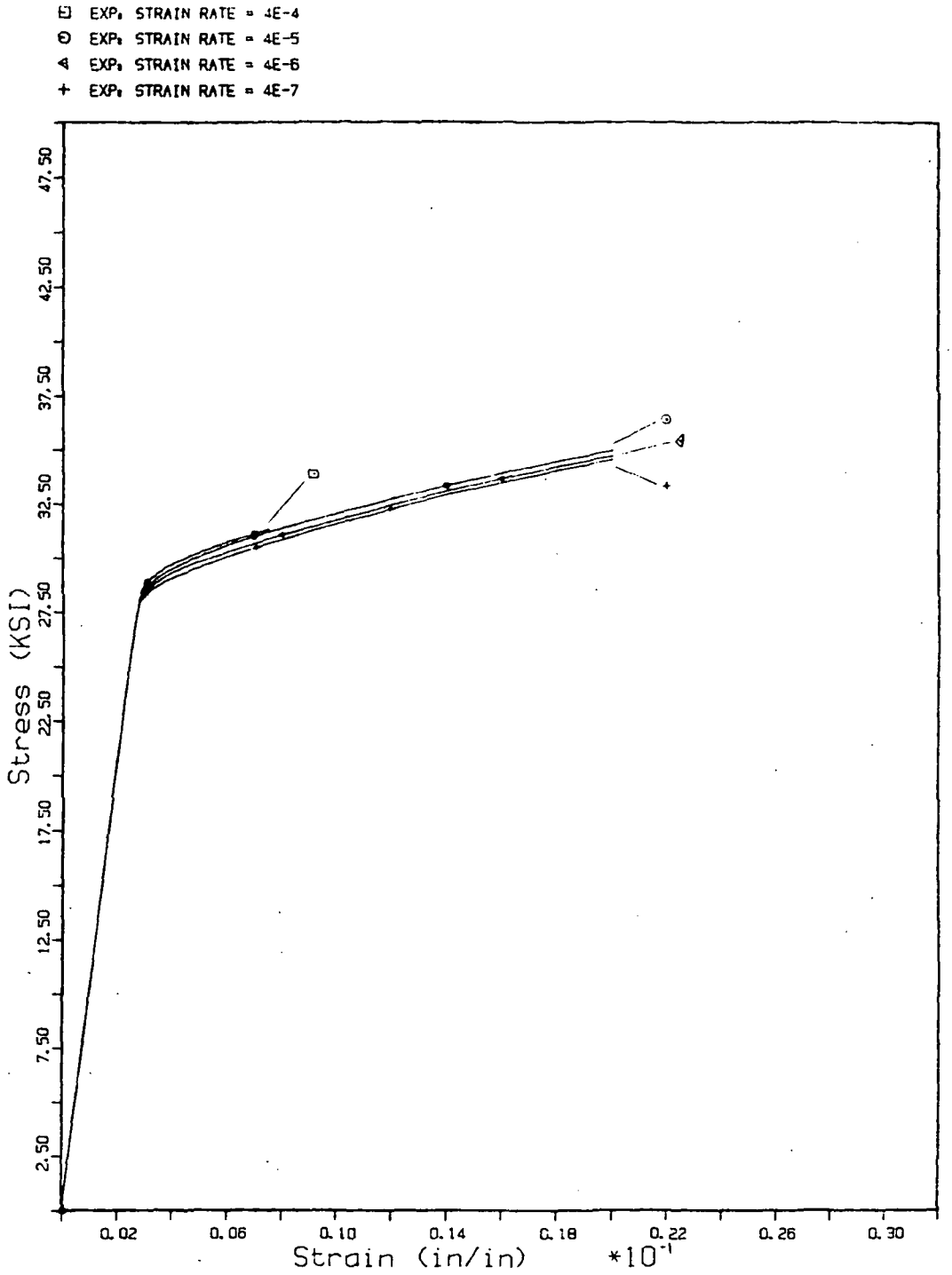

Fig. 16 Experimental constant strain rate tensile test response

The results of the constant-load creep tests can be seen in Figure 17 for five applied stresses ranging from 32.725 ksi to 38.850 ksi. Pertinent results of the constant strain rate tensile tests and the creep tests, as well as the stress-drop tests, are summarized in Table 3.

Material Constants for Krieg, et al.

In determining the material constants for this and the other theories under consideration, the procedures discussed in a previous section are followed. The reader may consult that section for greater detail.

The values of c_1 and c_2 are found by applying a linear curve-fit to a graph of $\ln(\dot{\varepsilon}^I)$ v. $\ln|\sigma - \alpha|$ data, where $\dot{\varepsilon}^I$ is the strain rate immediately preceding the stress-drop, σ is the applied stress, and α is the back stress. This is shown in Figure 18; the slope of the linear fit is c_2 and the vertical intercept is $\ln(c_1)$. In this manner, c_1 is calculated to be 7.177 and c_2 is $1.459(10)^{-9}$.

Under steady-state creep, the growth law for the back stress becomes (equation (71) repeated)

$$(c_3/c_4) = [\alpha^2/(c_1|\zeta|^{c_2})]\,[\exp(c_5\alpha^2) - 1]. \qquad (71)$$

Applying this equation to two experimental cases results in

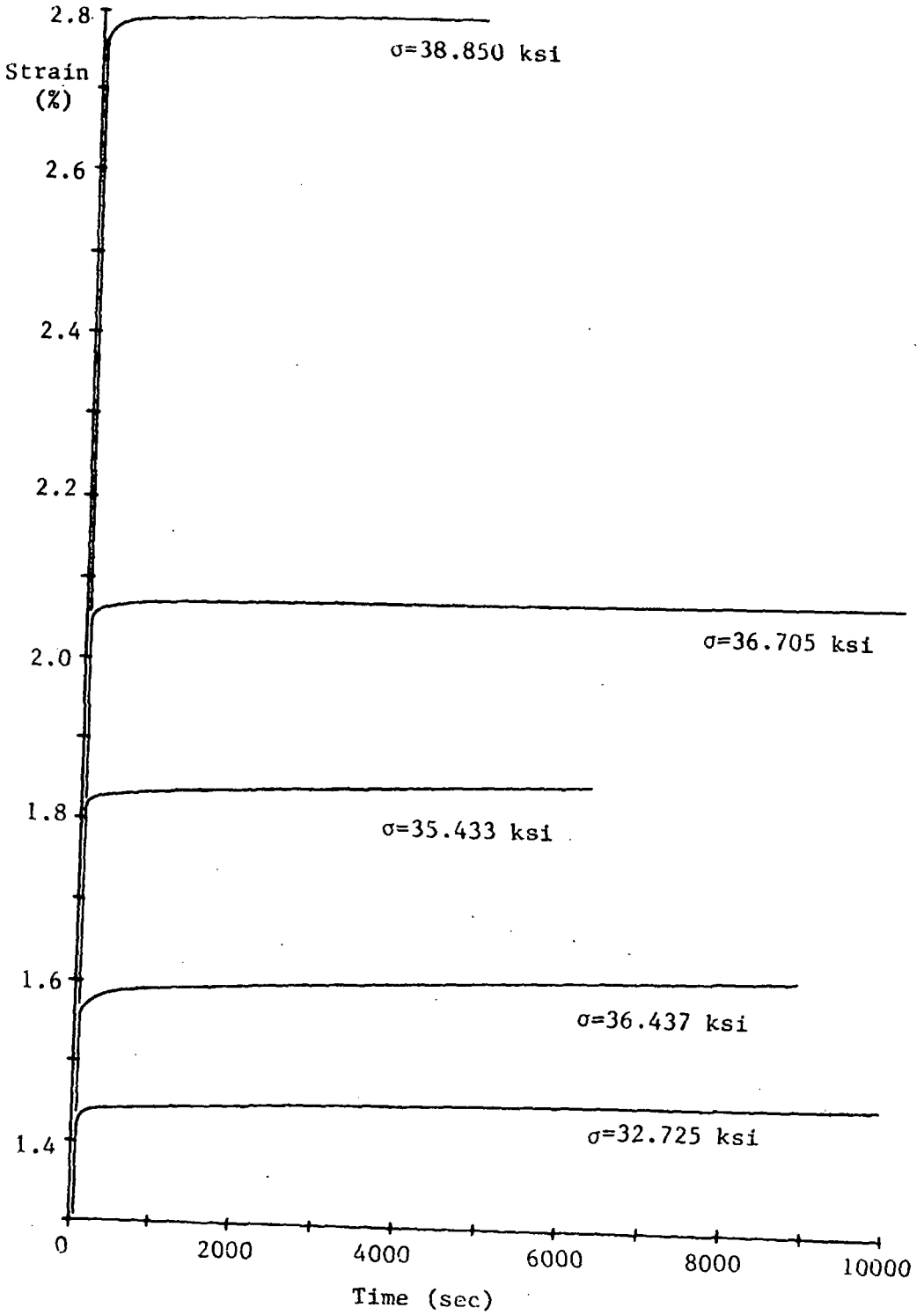

Fig. 17 Experimental Creep Test Response

Table 3

Pertinent Results of Experimental Tests

Constant strain rate tensile tests

Elastic modulus = $10.313(10)^{3}$ ksi

Elastic limit = 28.000 ksi

0.2% offset yield stress = 30.250 ksi for $4(10)^{-4}$ sec^{-1}

30.000 ksi $4(10)^{-5}$ sec^{-1}

29.750 ksi $4(10)^{-6}$ sec^{-1}

29.500 ksi $4(10)^{-7}$ sec^{-1}

Creep tests

Steady-state creep rate =

$1.205(10)^{-8}$ sec^{-1}	for 32.725 ksi
$4.167(10)^{-8}$ sec^{-1}	35.433 ksi
$3.125(10)^{-8}$ sec^{-1}	36.437 ksi
$4.435(10)^{-8}$ sec^{-1}	36.705 ksi
$4.546(10)^{-8}$ sec^{-1}	38.850 ksi

Stress-drop tests

Strain rate before stress drop	applied stress	back stress
$0.1000(10)^{-7}$ sec^{-1}	34.402 ksi	33.107 ksi
$0.4243(10)^{-7}$ sec^{-1}	35.433 ksi	33.804 ksi
$2.658(10)^{-7}$ sec^{-1}	36.705 ksi	34.659 ksi

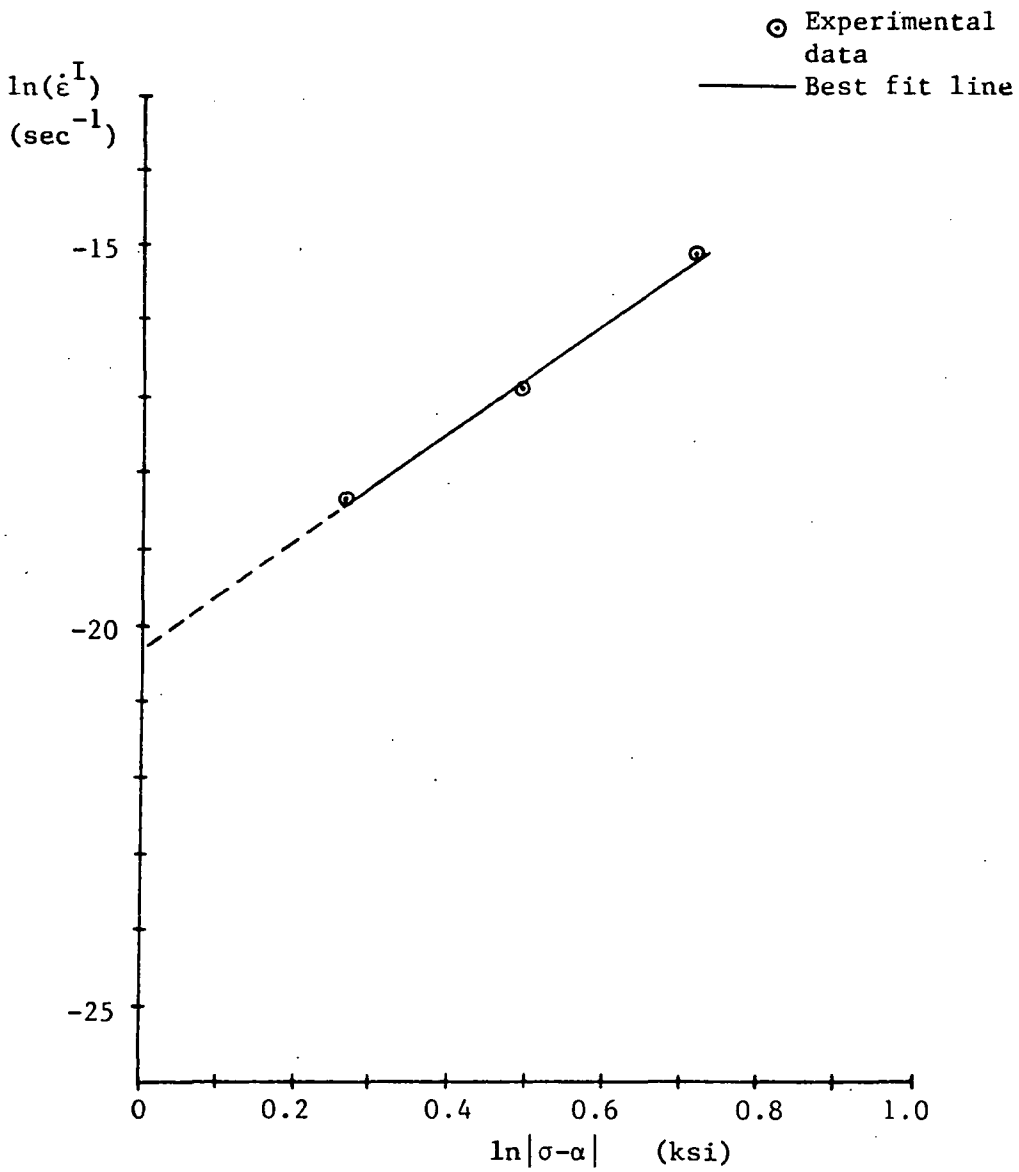

Fig. 18 Graph of $\ln(\dot{\varepsilon}^I)$ v. $\ln|\sigma-\alpha|$ for Krieg's Model

two nonlinear equations in two unknowns which can be solved for (c_3/c_4) and c_5 by iteration. Solving for the cases with the highest and lowest values of α (see Table 3) yields $(c_3/c_4) = 3.255(10)^{25}$ ksi^{2}sec and $c_5 = 0.03030$ ksi^{-2}.

To determine c_3, a point is chosen on the primary creep curve where the creep rate is still twice the eventual steady-state rate. The effective stress ζ at this point is calculated by inverting the inelastic strain rate equation (68) (equation (73) repeated here):

$$\zeta = (\dot{\varepsilon}^I/c_1)^{1/c_2}. \qquad (73)$$

The value of the back stress is then given by $\alpha = \sigma - \zeta$. Using the creep test with $\sigma = 35.433$ ksi gives the following information:

$$\sigma_1 = 35.433 \text{ ksi},$$
$$\dot{\varepsilon}^I_1 = 8.333(10)^{-8} \text{ sec}^{-1},$$
$$t_1 = 450 \text{ sec}.$$

This gives $\zeta_1 = 1.717$ ksi and $\alpha_1 = 33.716$ ksi, where the subscript 1 refers to the point on the primary creep curve. The growth law for α, equation (69), can be integrated numerically by separating variables (equation (72) repeated):

$$c_3 t_1 = \int_0^{\alpha_1} \{c_1 |\sigma_1 - \alpha|^{c_2} - (c_4/c_3)\alpha^2 [\exp(c_5\alpha^2) - 1]\}^{-1} d\alpha. \quad (72)$$

With α_1 and σ_1 known, $c_3 t$ is calculated as $2.126(10)^8$ ksi sec. From this, $c_3 = 5.185(10)^4$ ksi and $c_4 = 1.593(10)^{-21}$ $ksi^{-1} sec^{-1}$.

This concludes the material parameter determination for the theory of Krieg, et al.

Material Constants for Bodner, et al.

For the present strain rate range of interest, D_0 is set as $1(10)^4$ sec^{-1}.

To determine n and Z_1, a saturation stress must be determined analytically since the experimental stress-strain curves are not saturated (see Figure 16). This is accomplished by extrapolating to the point of zero γ on the γ v. σ graph, where $\gamma = d\sigma/dW^P$ and is given by differentiating a curve-fit of $W^P = W^P(\sigma)$. It is found that quadratics provide the best curve-fit for $W^P = W^P(\sigma)$:

$$W^P = 4.679 - 0.3679\sigma + 0.7462(10)^{-2}\sigma^2 \quad (117)$$

for $\dot{\varepsilon} = 4(10)^{-7}$ sec^{-1}, and

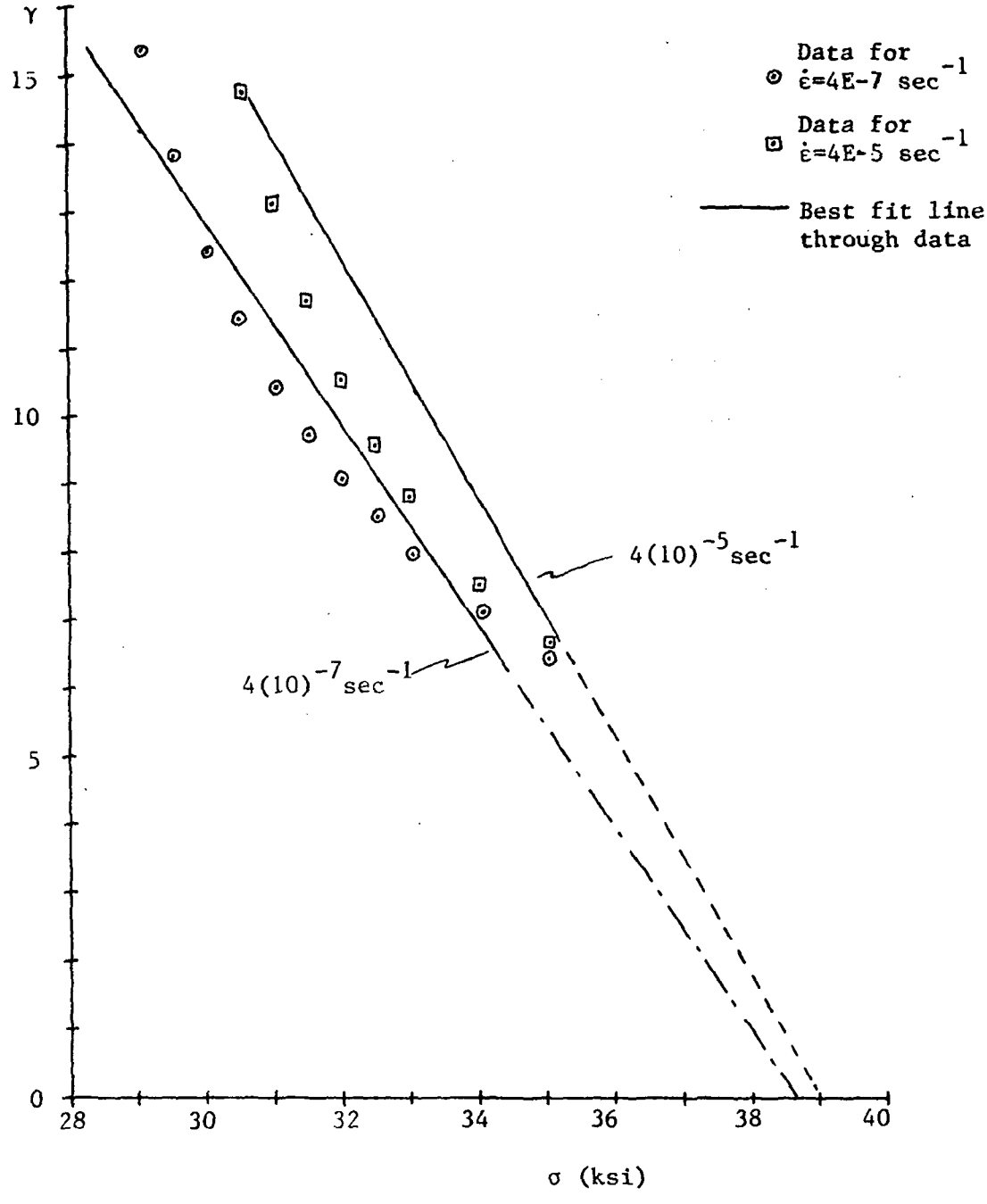

Fig. 19 Graph of Y v. σ for Bodner's Model

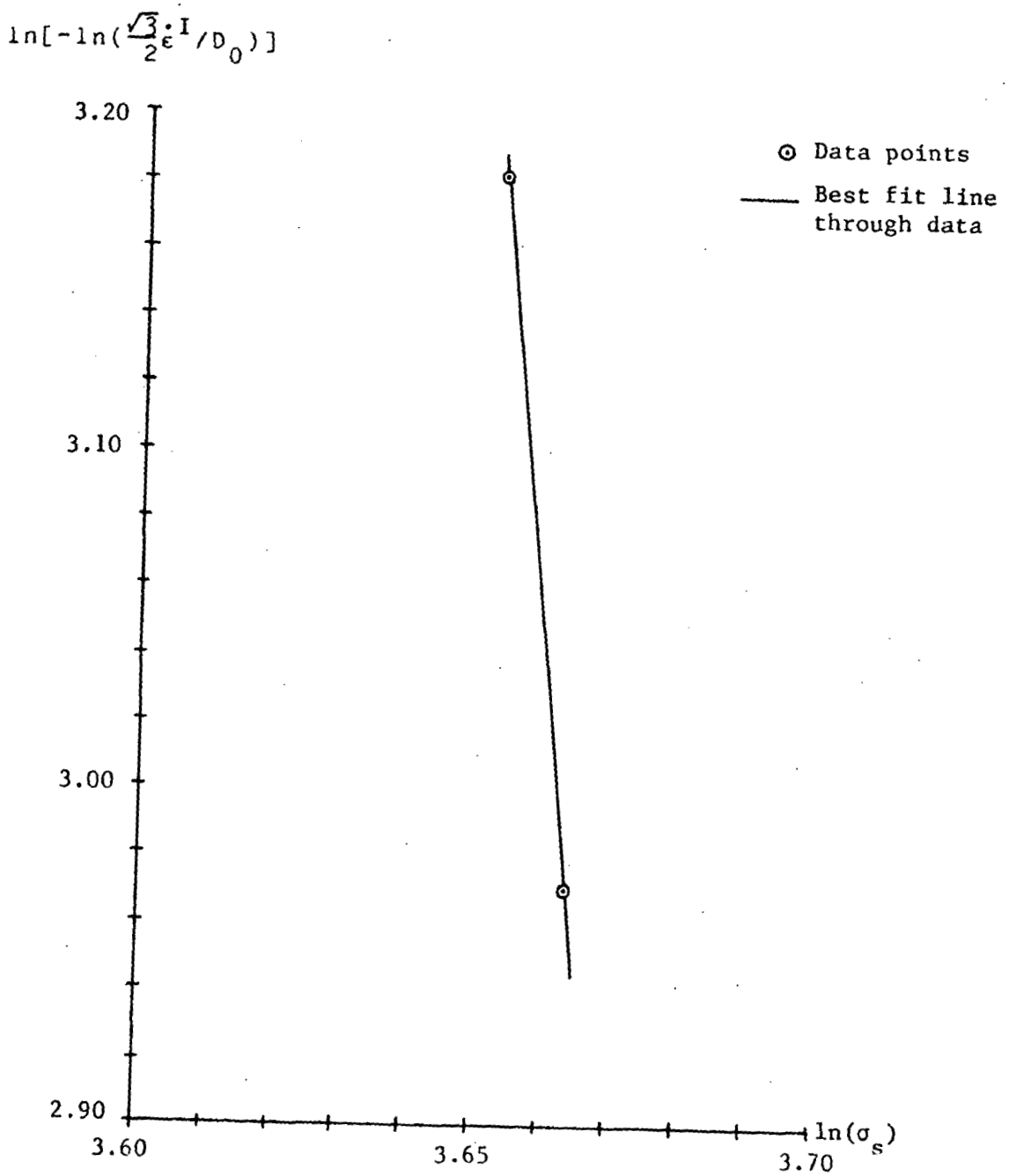

Fig. 20 Graph of $\ln[-\ln(\frac{\sqrt{3}}{2}\dot{\epsilon}^I/D_0)]$ v. $\ln(\sigma_s)$ for Bodner's Model

Values of $\dot{\varepsilon}^I$ are calculated from $\dot{\varepsilon}^I = \dot{\varepsilon}\ (1 - \frac{1}{E}\frac{\Delta\sigma}{\Delta\varepsilon})$ and the resulting values of Z are shown in Table 4 below.

Table 4. Calculated Values of Z used in the Determination of Z_0

$\dot{\varepsilon}$ (sec^{-1})	σ (ksi)	$\dot{\varepsilon}^I$ (sec^{-1})	Z (ksi)
$4(10)^{-7}$	28.250	$3.6474(10)^{-7}$	34.102
$4(10)^{-6}$	28.375	$3.5152(10)^{-6}$	34.090
$4(10)^{-5}$	28.500	$3.3536(10)^{-5}$	34.060
$4(10)^{-4}$	28.688	$3.2243(10)^{-4}$	34.081

An average value of 34.00 ksi is taken for Z_0.

The value of Z_2, the minimum value of Z, is taken to be the lowest value of Z for steady-state creep, although one may simply set $Z_2 \approx Z_0$. The latter is chosen, giving $Z_2 = 33.50$ ksi.

The values of the recovery coefficient A and the recovery exponent r are determined by calculating a value of Z for the steady-state region of each creep test by using equation (94) (see above). Calculated values of Z are shown in Table 5 below.

Table 5. Calculated Values of Z used in the Determination of A and r

σ_{ss} (ksi)	$\dot{\varepsilon}^I_{ss}$ (sec^{-1})	Z (ksi)	$\ln[m\,(Z_1-Z)\dot{W}^P]$	$\ln[(Z-Z_2)/Z_1]$
32.725	$1.205(10)^{-8}$	39.758	-2.091	-12.38
36.437	$3.125(10)^{-8}$	44.192	-1.520	-12.37
36.705	$4.435(10)^{-8}$	44.489	-1.491	-12.14

These values of Z are then used to construct a $\ln[m\,(Z_1 - Z)\,\dot{W}^P]$ v. $\ln[(Z - Z_2)/Z_1]$ graph, as shown in Figure 21. The slope of a linear curve-fit for this graph is r; the vertical intercept is $\ln(AZ_1)$. In this manner, A is calculated to be $1.447(10)^{-7} sec^{-1}$ and r is 0.2290.

This concludes the material constant determination for the theory of Bodner, et al.

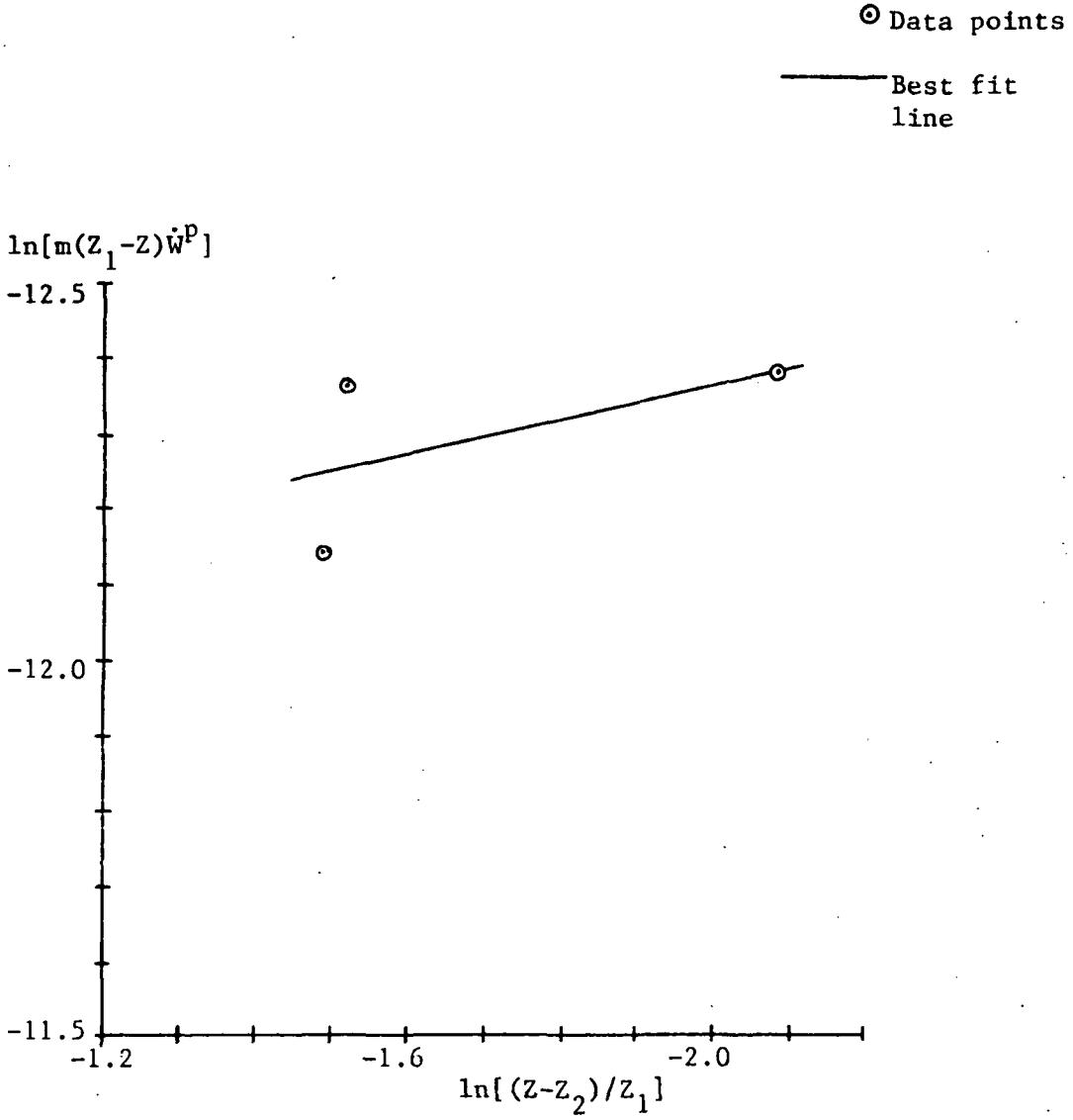

Fig. 21 Graph of $\ln[m\ (Z_1-Z)\ \dot{W}^P]$ v. $\ln[(Z-Z_2)/Z_1]$ for Bodner's Model

Material Constants for Miller, et al.

The values of the activation energy for plastic flow Q and the melting temperature T_m can be found in a materials handbook. For Al 5086 at room temperature, Q is 27500 cal/mole and T_m is 858K.

Since room temperature is less than $0.6T_m$ for Al 5086, equation (103), repeated below, is used to calculate the temperature-dependent factor θ':

$$\theta' = \exp\{[-Q/0.6kT_m]\,[\ln(0.6T_m/T) + 1]\}, \qquad (103)$$

where T and T_m are absolute temperatures. This gives θ' as $8.74(10)^{-19}$.

The value of A is chosen such that a graph of $\log_{10}(\dot{\varepsilon}^I_{ss}/\theta')$ v. $\log_{10}[\sinh(A\sigma_{ss}/E)]$ for steady-state creep data is linear. This is shown below in Table 6 and in graphical form Figure 22 for several values of A.

Table 6. Calculations for Various Values of A

$\dot{\varepsilon}^I_{ss}$ (sec^{-1})	$\log_{10}(\dot{\varepsilon}^I_{ss}/\theta')$	σ_{ss} (ksi)	$\log_{10}[\sinh(A\sigma_{ss}/E)]$ A=50	A=200	A=1000
$1.205(10)^{-8}$	10.14	32.725	-0.7977	-0.1687	1.076
$4.167(10)^{-8}$	10.68	35.443	-0.7628	-0.1292	1.191
$3.125(10)^{-8}$	10.55	36.437	-0.7506	-0.1153	1.233
$4.435(10)^{-8}$	10.71	36.705	-0.7474	-0.1116	1.244
$4.546(10)^{-8}$	10.72	38.850	-0.7225	-0.0826	1.335

As can be seen in Figure 22, the curve is nearly linear for A = 50, with no significant improvement for A < 50.

With this value of A, the values of B and n can be determined by constructing a linear curve-fit for the data in Figure 22. The slope of the curve-fit is n; the vertical intercept is $\log_{10}(B)$. In this manner, n is calculated to be 7.701 and B is $2.410(10)^{16}$ sec^{-1}.

The maximum value of F_{sol} is set arbitrarily as $F_{sol,max} = 1(10)^{-7}$. Simulations of experimental tests have shown that the choice of this value does not influence the results significantly.

The work-hardening coefficient H is set arbitrarily to give the best fit of simulations of constant strain rate tensile tests to experimental data. This value is set as $7.5(10)^{-4}$ ksi.

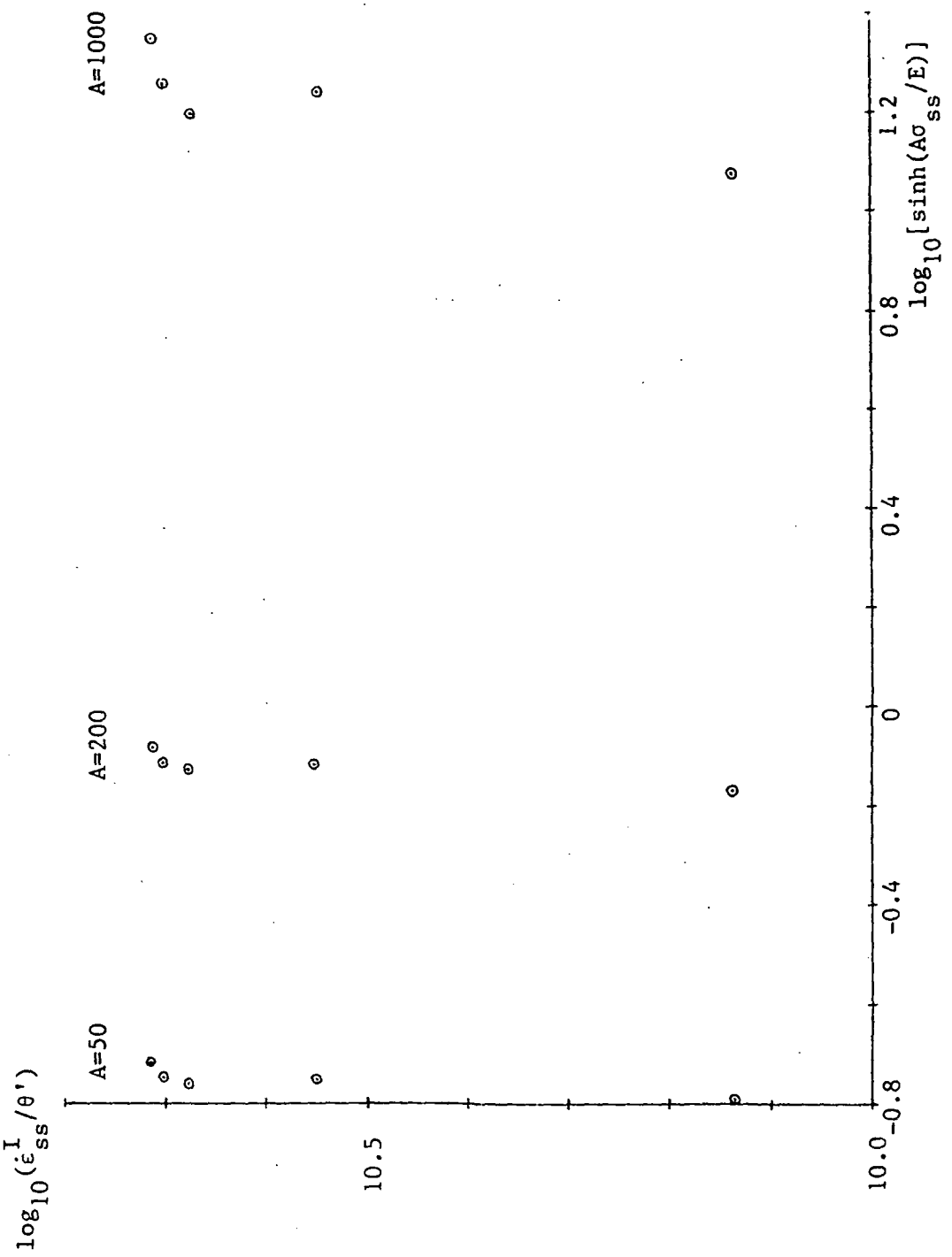

Fig. 22 Graph of $\log_{10}(\dot{\varepsilon}^{I}_{ss}/\theta')$ v. $\log_{10}[\sinh(A\sigma_{ss}/E)]$ for Miller's Model

Finally, the initial value of the drag stress, D_{init}, is calculated by inverting the inelastic strain rate equation (112) and using values of $\dot{\varepsilon}^I$ and σ at yield. In this manner, D_{init} is calculated to be $3.386(10)^{-5}$.

This concludes the material constant determination for the theory of Miller, et al.

A summary of the material constants for each theory is given in Table 7.

Table 7. Summary of Material Constants for all Models

Krieg, et al.	$E = 10.313(10)^{3}$ ksi
	$c_1 = 7.177$
	$c_2 = 1.459(10)^{-9}$
	$c_3 = 5.185(10)^{4}$ ksi
	$c_4 = 1.593(10)^{-21}$ ksi^{-1}sec^{-1}
	$c_5 = 0.03030$ ksi^{-2}
Bodner, et al.	$E = 10.313(10)^{3}$ ksi
	$n = 10.30$
	$Z_1 = 46.59$ ksi
	$m = 1.558$ ksi^{-1}
	$Z_0 = 34.00$ ksi
	$Z_2 = 33.50$ ksi
	$A = 1.447(10)^{-7}$ sec^{-1}
	$r = 0.2290$
Miller, et al.	$E = 10.313(10)^{3}$ ksi
	$\theta' = 8.74(10)^{-19}$
	$A = 50$
	$n = 7.701$
	$B = 2.410(10)^{16}$ sec^{-1}
	$F_{sol,max} = 1(10)^{-7}$
	$H = 7.5(10)^{-4}$ ksi
	$D_{init} = 3.386(10)^{-5}$

COMPARISON OF THEORY TO EXPERIMENT

The third and final objective of this research is to compare the numerical predictions of each theory to experiment by integrating the constitutive equations subject to specific load histories. Before proceeding to the quantitative comparisons, however, there follows a brief qualitative review of the predictive capabilities of each theory.

Qualitative Review of Predictive Capabilities

All the theories under consideration are similar in that they are unified theories; that is, the rate-dependent creep and the rate-independent plasticity components have been combined into one inelastic strain term. Each theory, in the form under consideration, is isothermal in that it is not able to model transient temperature response. Furthermore, each model is able to exhibit strain rate sensitivity through the exponent in the inelastic strain rate equation.

The theory of Krieg, et al., contains two internal state variables: the inelastic strain and the back stress. The back stress represents kinematic hardening, which allows the Bauschinger effect to be modelled. Krieg,

et al., have assumed the hardening function in the back stress growth law to be constant, which may cause "over-square" hysteresis loops. This may be alleviated by introducing a dependence of the hardening function on the current value of the stress or back stress. Due to the lack of a representation for isotropic hardening (the drag stress), this theory may not be able to model cyclic strain hardening. Finally, it can be seen that anelasticity (strain recovery at zero load) can be predicted by this theory by setting $\sigma = 0$ in the inelastic strain rate equation (68); relaxation is predicted by setting $\dot{\varepsilon} = 0$; and creep is predicted by setting $\dot{\sigma} = 0$.

The theory of Bodner, et al., also contains two internal state variables: the inelastic strain and a term representing isotropic hardening. The isotropic hardening growth law contains dynamic as well as thermal recovery. The presence of isotropic hardening allows cyclic strain hardening to be modelled, although the absence of kinematic hardening may preclude the ability to model the Bauschinger effect. Finally, it can be seen that anelasticity cannot be modelled since $\dot{\varepsilon}^I$ is zero when setting $\sigma = 0$ in the inelastic strain rate equation (86); creep and relaxation can be predicted, however, by setting $\dot{\sigma} = 0$ and $\dot{\varepsilon} = 0$, respectively.

The theory of Miller, et al., contains two internal

state variables: the inelastic strain and the drag stress. The drag stress represents isotropic hardening, which allows cyclic strain hardening to be modelled. This model is similar to that of Krieg, et al., in that the hardening function in the drag stress growth law is assumed to be constant, which produces "over-square" hysteresis loops. The model is similar to that of Bodner, et al., in that the lack of a back stress may preclude the ability to model the Bauschinger effect as well as anelasticity. Finally, creep and relaxation are modelled in a manner similar to that of the other two theories.

Review of Integration Technique

Each theory is represented mathematically by a set of differential equations. Since these differential equations are numerically "stiff", causing higher-order integration schemes to become unstable [124], a first-order forward integration scheme with small, variable time steps was used. For example, Krieg's inelastic strain rate equation ((68) repeated here)

$$\dot{\varepsilon} = c_1 |\sigma - \alpha|^{c_2} \operatorname{sgn}(\sigma - \alpha) \qquad (68)$$

becomes

$$\varepsilon^I(t + \Delta t) = c_1 |\sigma(t) - \alpha(t)|^{c_2 \Delta t} + \varepsilon^I(t) \qquad (119)$$

where t represents an initial state and t + Δt represents the incremented state. Similarly, the growth law for the back stress (equation (69)) becomes

$$\alpha(t + \Delta t) = \{c_3 [(\varepsilon^I(t + \Delta t) - \varepsilon^I(t))/\Delta t] -$$

$$c_4 \alpha^2(t)[\exp(c_5 \alpha^2(t)) - 1]\mathrm{sgn}(\alpha(t))\}\Delta t + \alpha(t). \qquad (120)$$

Finally, the stress is updated by

$$\sigma(t + \Delta t) = E \{\dot{\varepsilon} - [(\varepsilon^I(t + \Delta t) - \varepsilon^I(t))/\Delta t]\}\Delta t + \alpha(t). \qquad (121)$$

This concludes the review of the integration technique used in this research.

Comparison of Numerical Predictions to Experiment

In this section, the ability of each model to predict the response to a specific load history is analyzed. The first experimental test to be modelled is a constant strain rate tensile test with $\dot{\varepsilon} = 4(10)^{-5}$ sec^{-1}, shown in Figure 23.

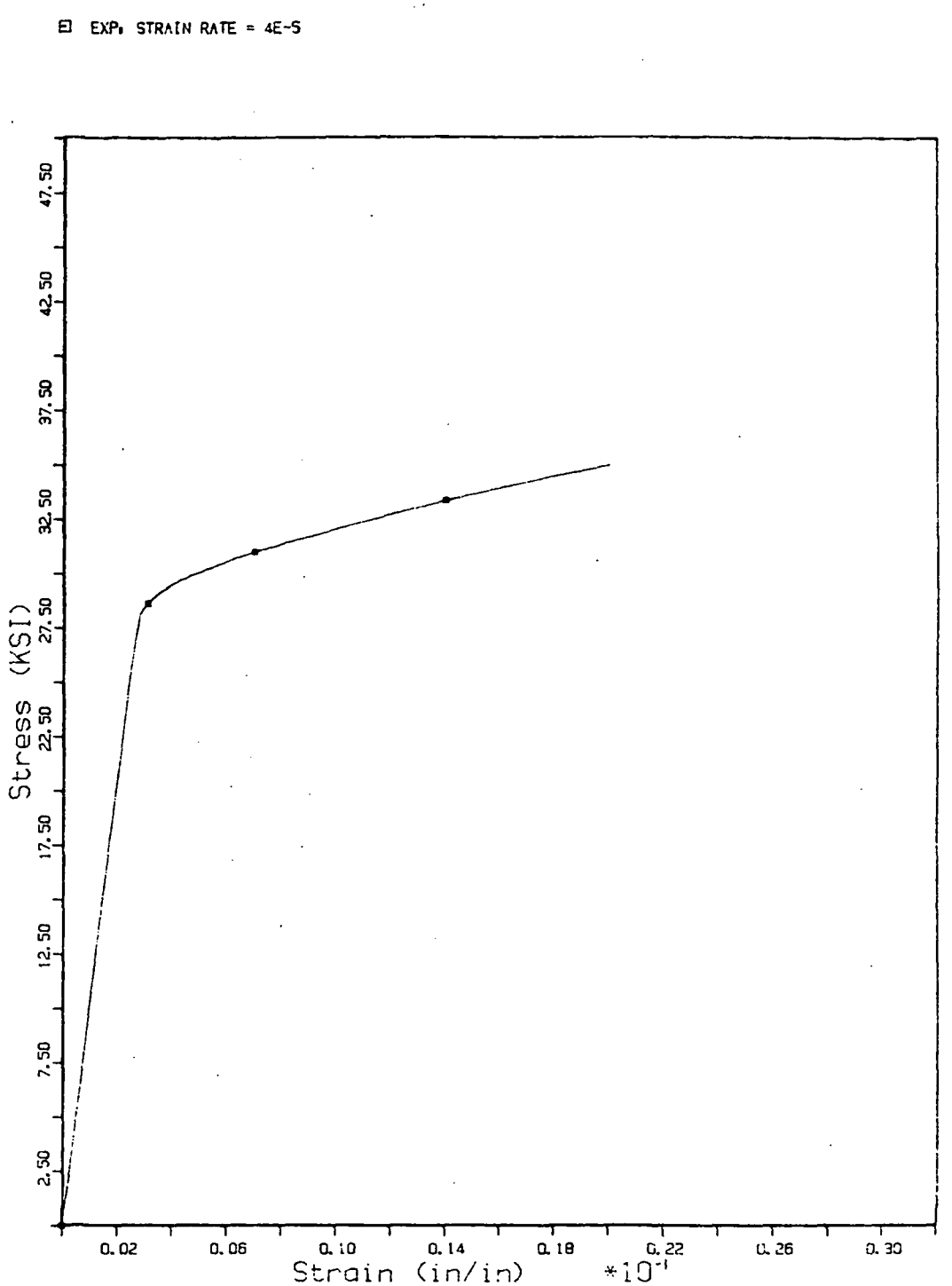

Fig. 23 Experimental constant strain rate tensile test: $\dot{\varepsilon} = 4(10)^{-5}\ \text{sec}^{-1}$

Krieg, et al.: Constant Strain Rate Tensile Test

It can be seen from Figure 24 that this theory does not compare favorably with experiment for this constant strain rate tensile test. It is believed by this author that this is due largely to the method of determining the material constants. As discussed in an earlier section, the ability to determine a zero creep rate or merely the absence of a resolvable creep rate in a stress-drop test depends greatly on the resolution of the data acquisition equipment and is extremely difficult and time consuming at best. A parameter variation study showed slight improvements in the stress-strain curve in Figure 24 but led to computational difficulties in simulating cyclic load histories and complex load histories. It can be concluded from this that improvements in the measurement of back stresses are required. For example, the methods of Blum and Finkel [98], in which the instantaneous strain change and the maximum strain change after unloading are compared, and of Walker [58], in which one applies hold times on the unloading side of a saturated hysteresis loop and extrapolates to the point of zero relaxation, merit further study.

Bodner, et al.: Constant Strain Rate Tensile Test

The theory of Bodner, et al., compares favorably to

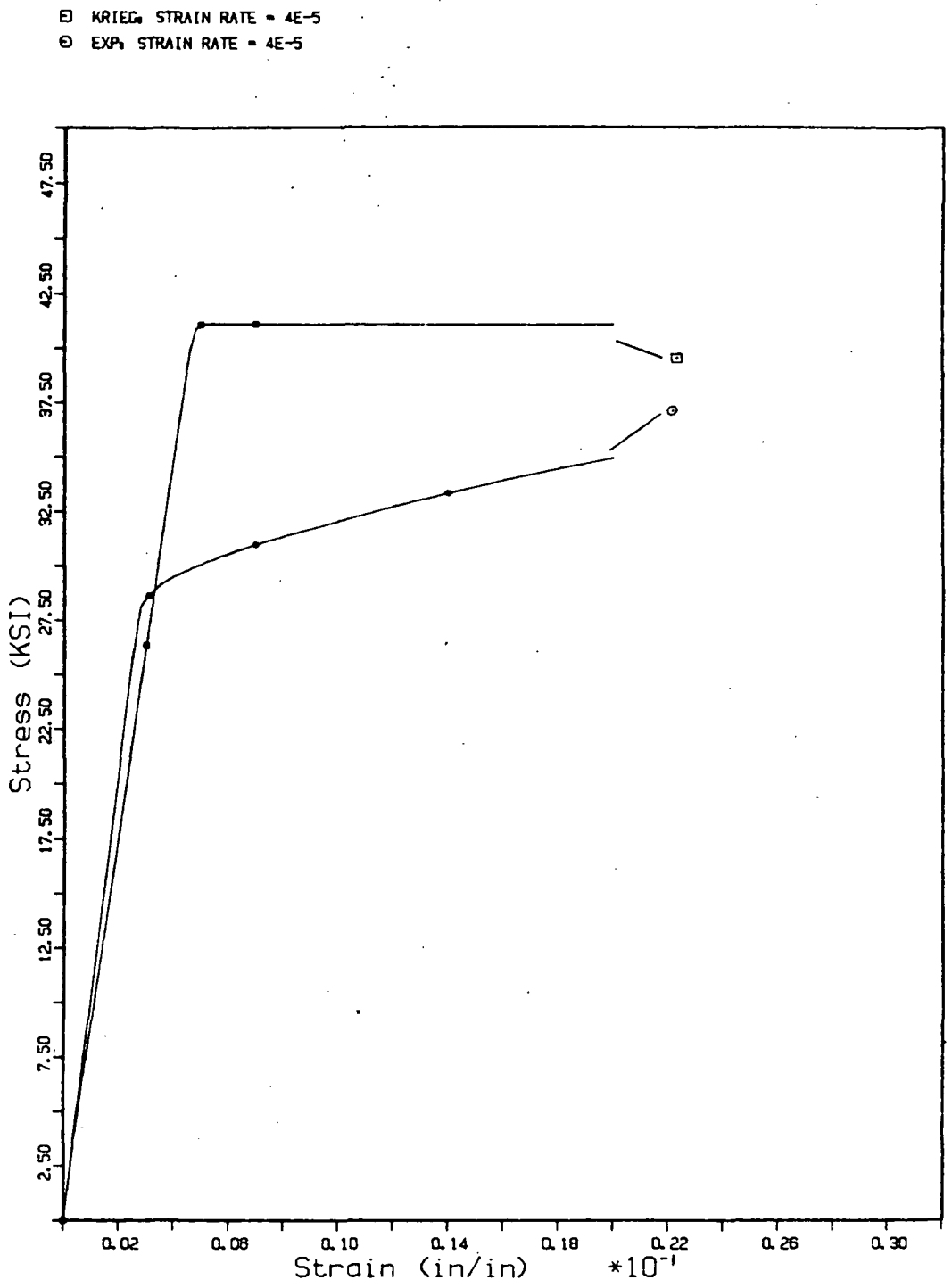

Fig. 24 Constant strain rate tensile test. Comparison of theory of Krieg, et al., to experiment.

C-4

experiment, as can be seen in Figure 25. Work-hardening is predicted well although the elastic-inelastic behavior transition is too sharp. It is found that this is due to the theory predicting values of Z that are too high at low stresses, possibly requiring a modification of the hardening term in the growth law for Z.

Miller, et al.: Constant Strain Rate Tensile Test

In determining the material constants for this theory, the strain rate exponent n was calculated to be 7.7, resulting in the response shown in Figure 26. A parameter variation study indicated that a value of n = 6 appeared to fit the experimental data much better. This indicates a problem inherent in many constitutive theories: the determination of material constants is not rigorous and the difficulties are compounded by the fact that many constants are interdependent and, in fact, may be assigned arbitrary values. In the interests of further numerical comparisons, a value of n = 6 is chosen for this model. With this choice, this theory predicts the yield point and work-hardening fairly well.

Finally, a comparison of all the models for a constant strain rate tensile test can be seen in Figure 27.

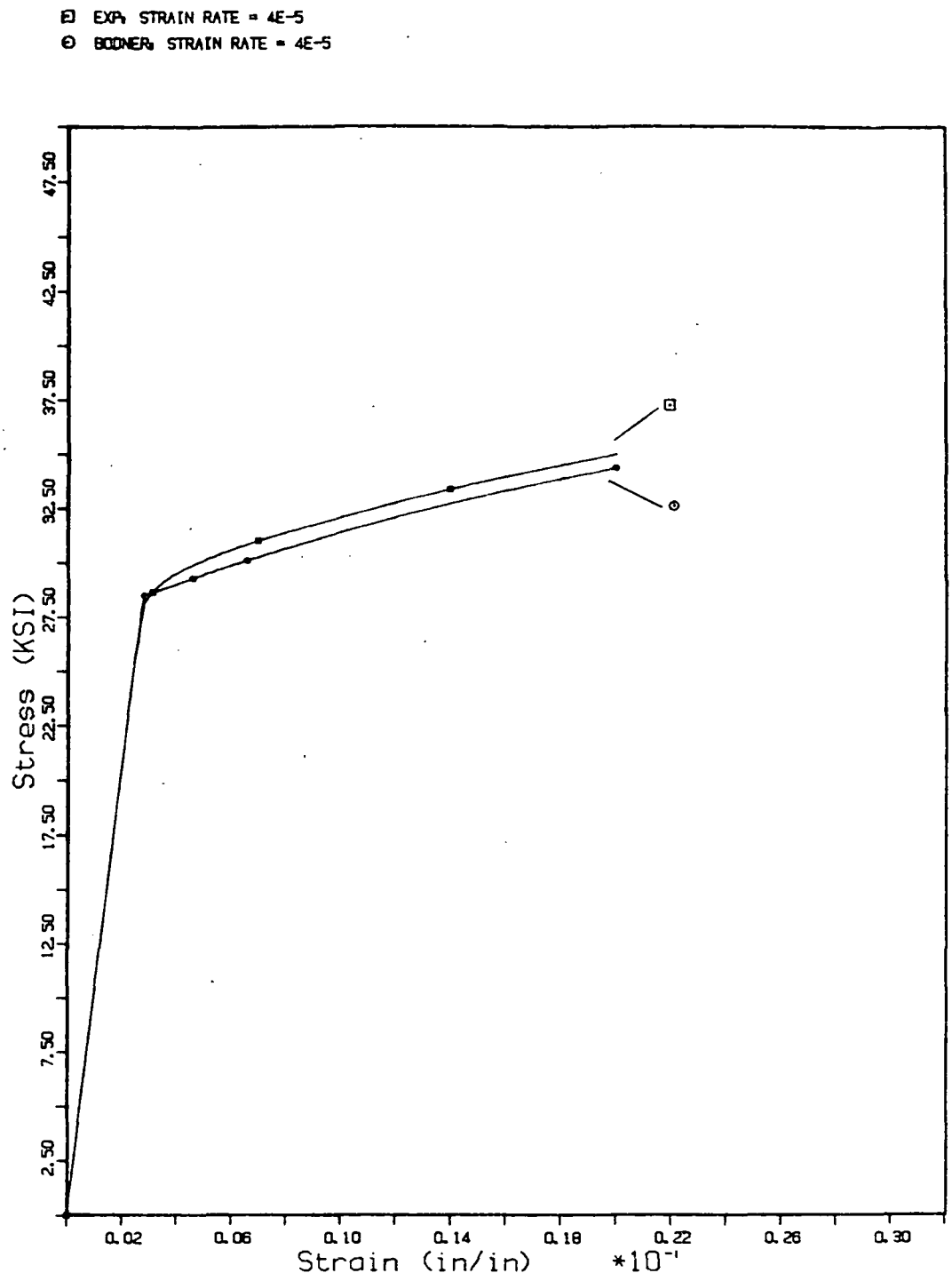

Fig. 25 Constant strain rate tensile test. Comparison of theory of Bodner, et al., to experiment.

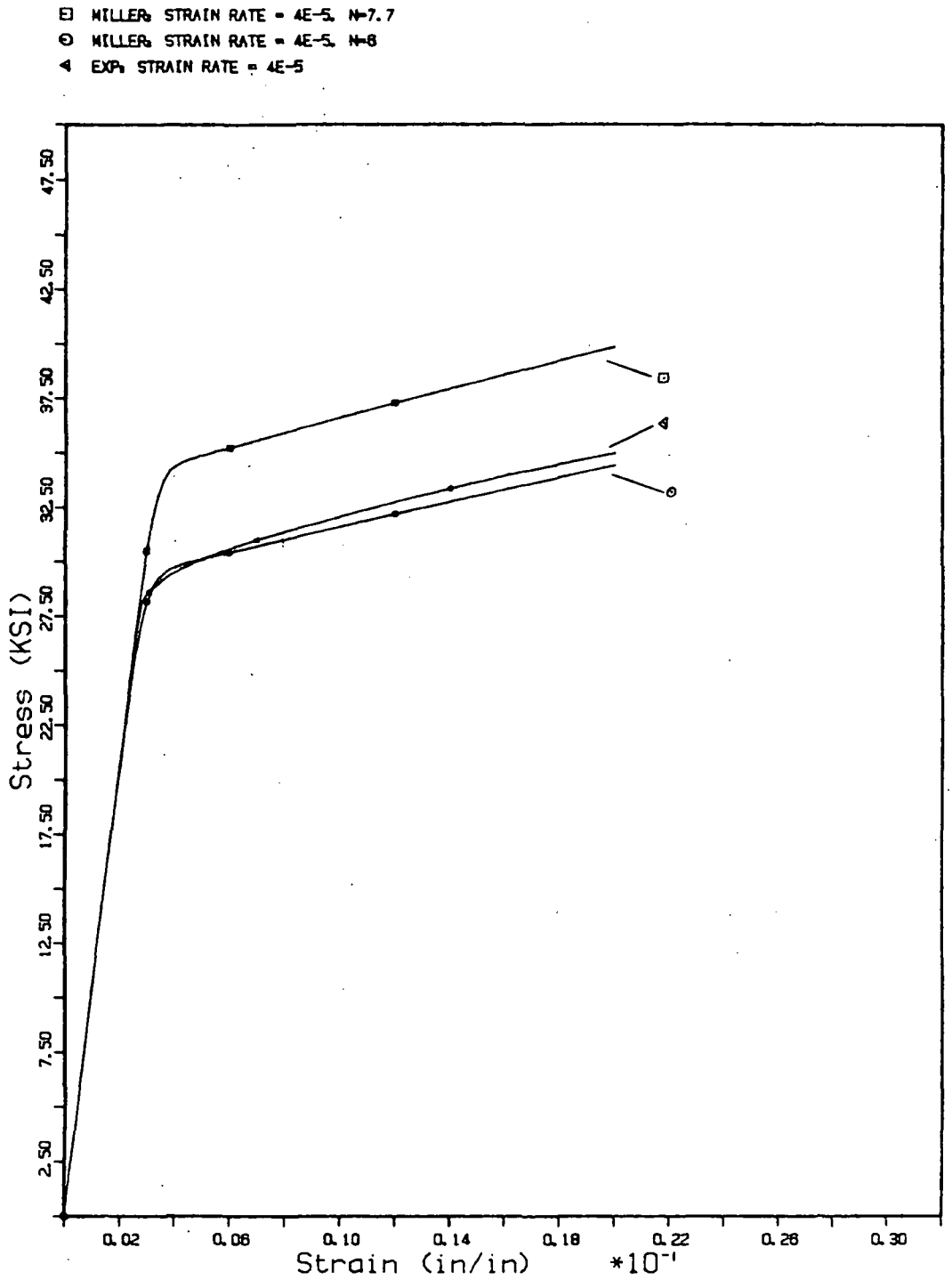

Fig. 26 Constant strain rate tensile test. Comparison of theory of Miller, et al., to experiment.

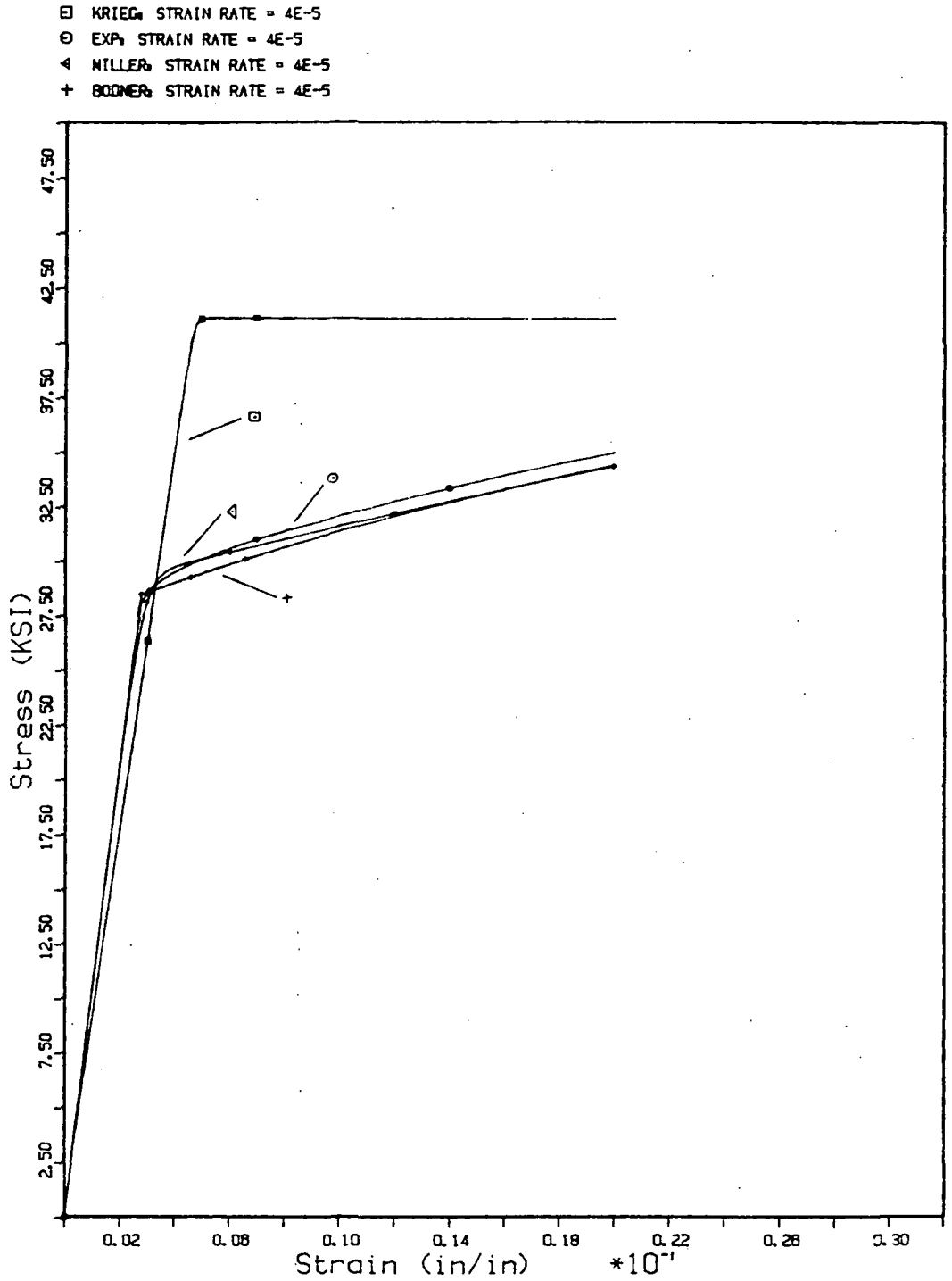

Fig. 27 Constant strain rate tensile test. Comparison of all theories to experiment.

Many theories use creep tests or constant strain rate tensile tests as information for the material parameter determination; consequently, one would expect fairly accurate simulations of these types of load histories. A more rigorous comparison, however is a cyclic load history, as shown in Figure 28 with $\dot{\varepsilon} = \pm 1(10)^{-4}$ sec^{-1} for cycles 1-10. The experimental data exhibit a pronounced Bauschinger effect and considerable cyclic strain hardening, although it appears that the hysteresis loop saturates fairly quickly.

Krieg, et al.: Cyclic Loading Test

The cyclic response of the theory of Krieg, et al., is shown in Figure 29 for cycle 1. It can be seen that the theory does indeed predict a Bauschinger effect, although it is not as pronounced as the experimental data. The model predicts a harder material than is the actual case, resulting in the very thin and, as expected, "over-square" hysteresis loop. This may be due to the ratio c_3/c_4 (calculated from stress-drop data) being too large.

A comparison of the prediction for cycles 1 and 10 can be seen in Figure 30, where, as expected, the model does not display significant cyclic strain hardening. However, since the material exhibits cyclic strain hardening, the difference between the saturated experimental and

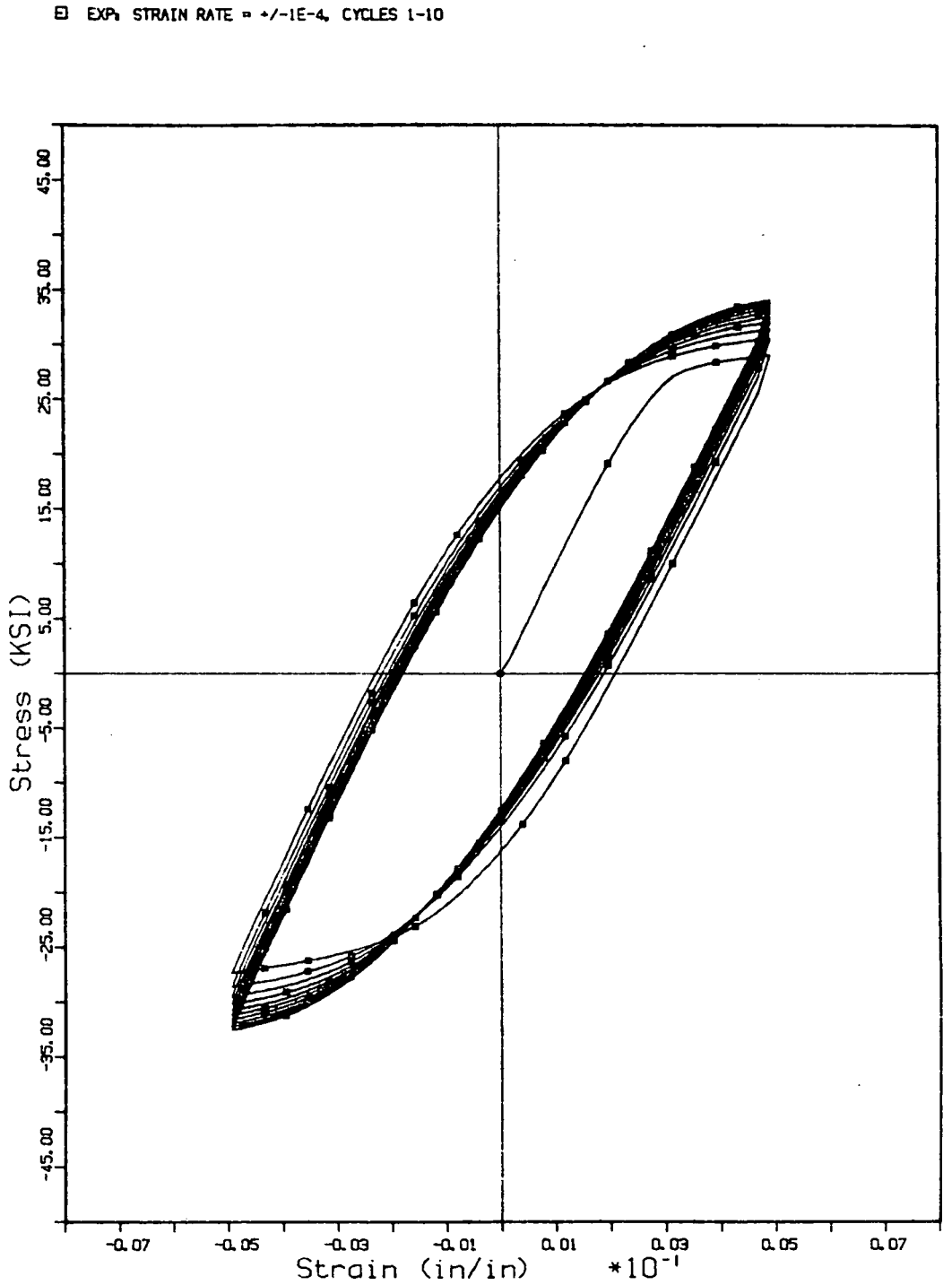

Fig. 28 Experimental cyclic loading test: cycles 1-10

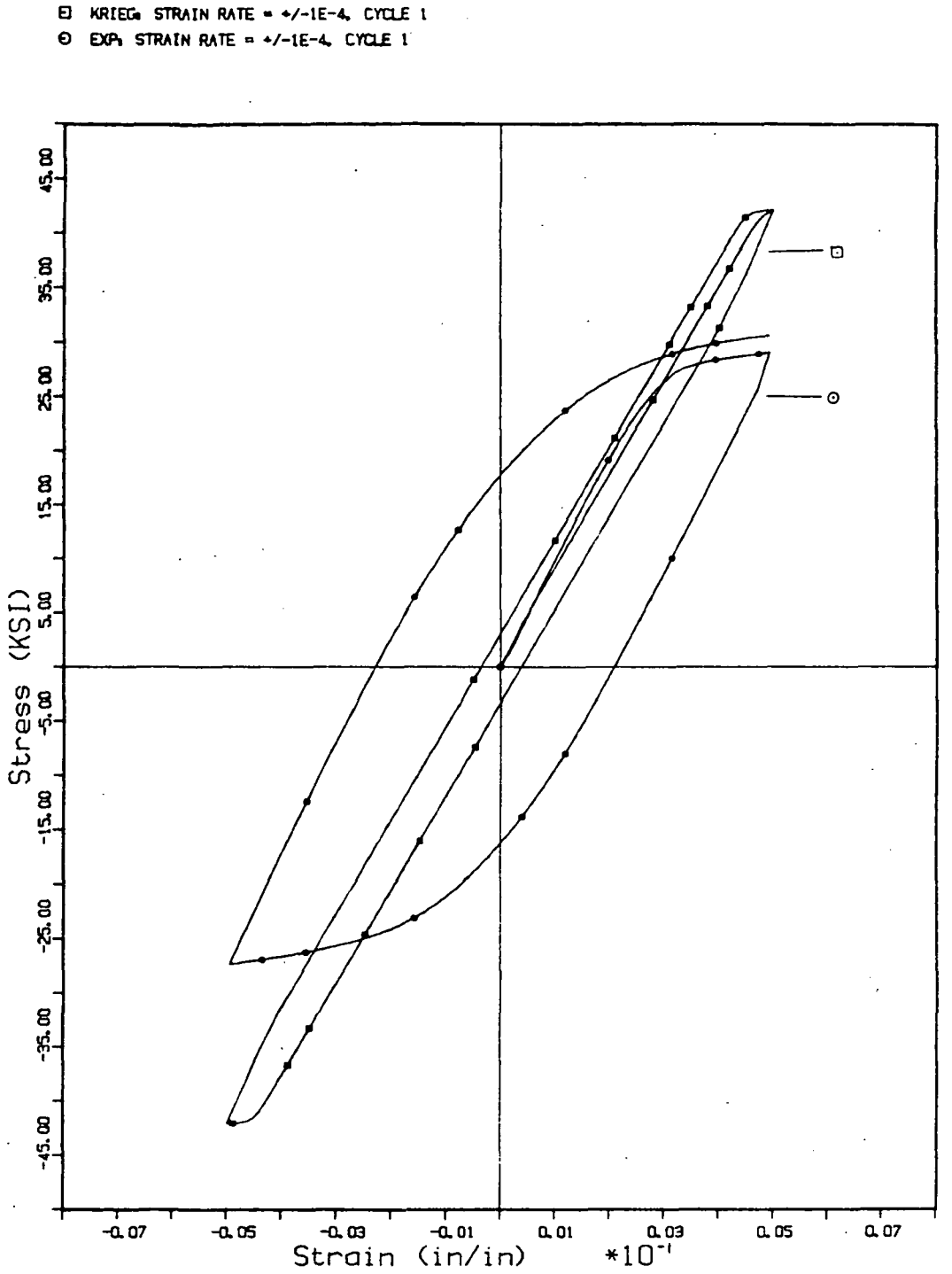

Fig. 29 Cyclic loading test: Cycle 1. Comparison of theory of Krieg, et al., to experiment.

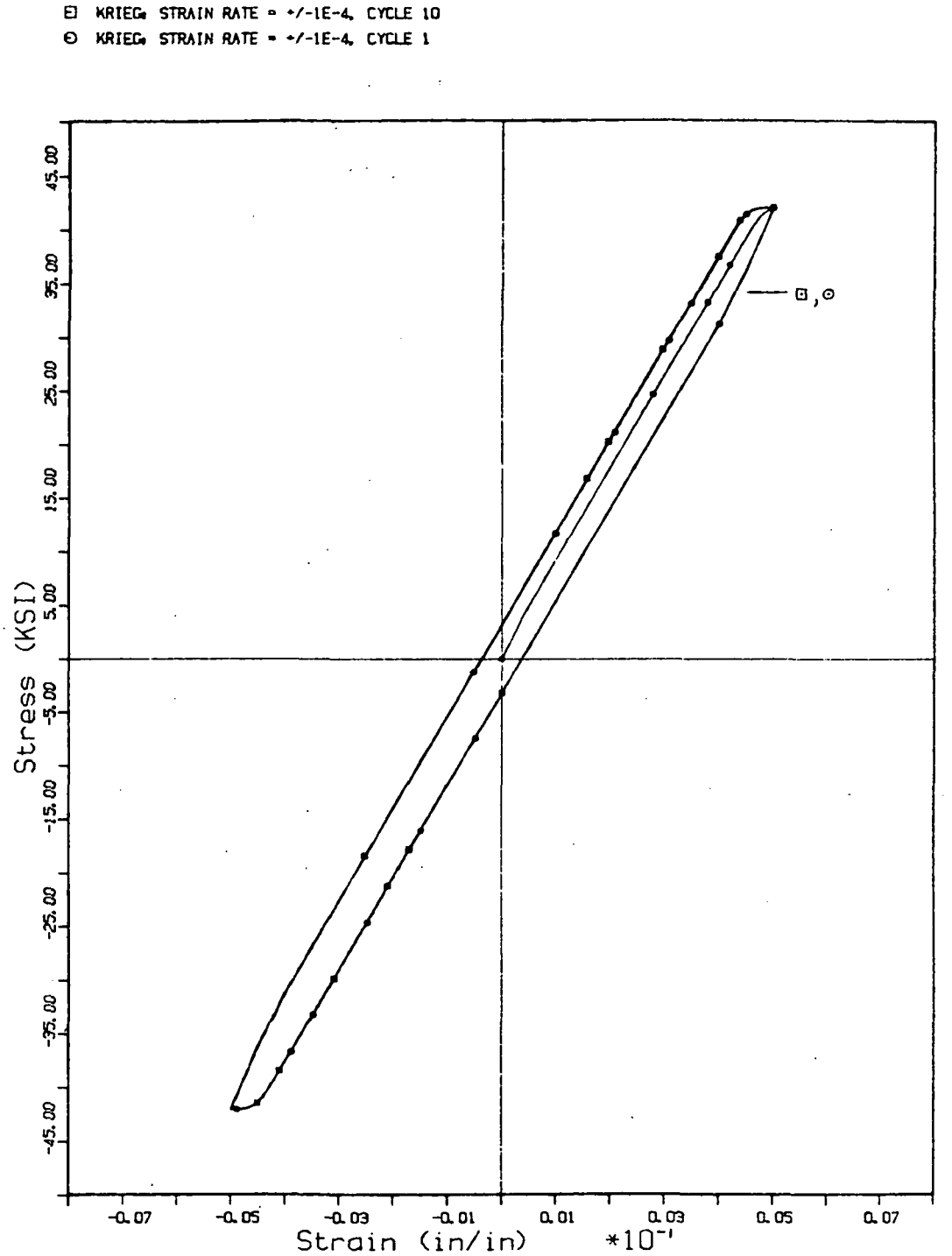

Fig. 30 Cyclic loading test: cycles 1 and 10. Prediction of theory of Krieg, et al.

predicted loops diminishes somewhat, as shown in Figure 31.

Bodner, et al.: Cyclic Loading Test

Figure 32 shows that this theory models cycle 1 fairly well, although the elastic-inelastic behavior transition is too sharp (as noted in earlier tensile data also). The absence of the Bauschinger effect suggests that a directional hardening term is necessary. This can also be seen when examining the γ v. σ graph used earlier in calculating some of the material constants. Although the theory assumes a linear relationship between γ and σ, the experimental data suggest a bilinear relationship. This is examined in greater detail by Bodner, et al., in recent work [109-111]. The upper slope in this bilinear relationship governs directional hardening and the lower slope governs isotropic hardening. It can be seen easily that including such a directional hardening term could provide the Bauschinger effect and also decrease the height of the hysteresis loop.

The aforementioned observations can also be seen in Figures 33 and 34, which compare prediction for cycle 1 to prediction for cycle 10 and prediction to experiment for cycle 10, respectively.

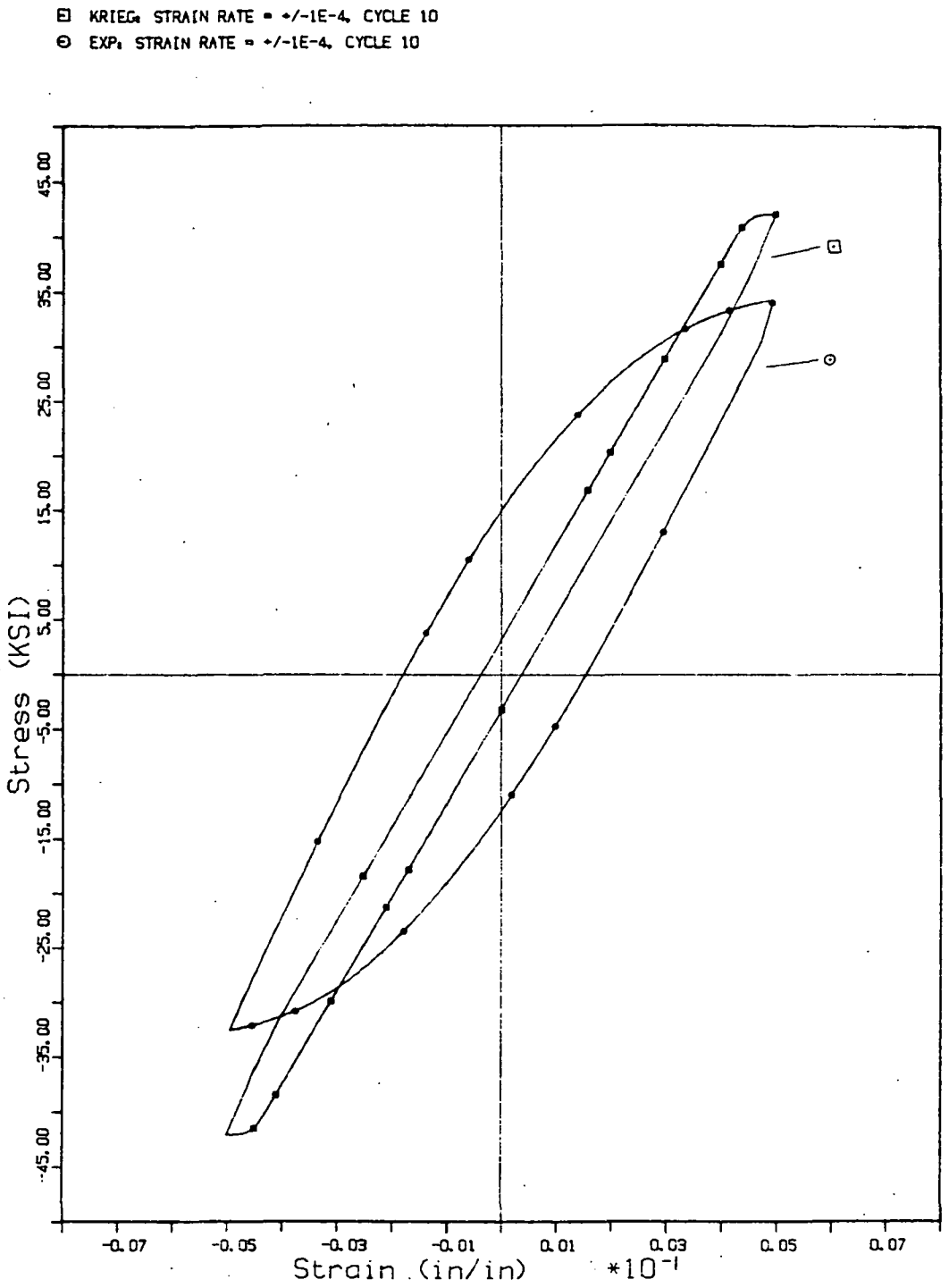

Fig. 31 Cyclic loading test: cycle 10. Comparison of theory of Krieg, et al., to experiment.

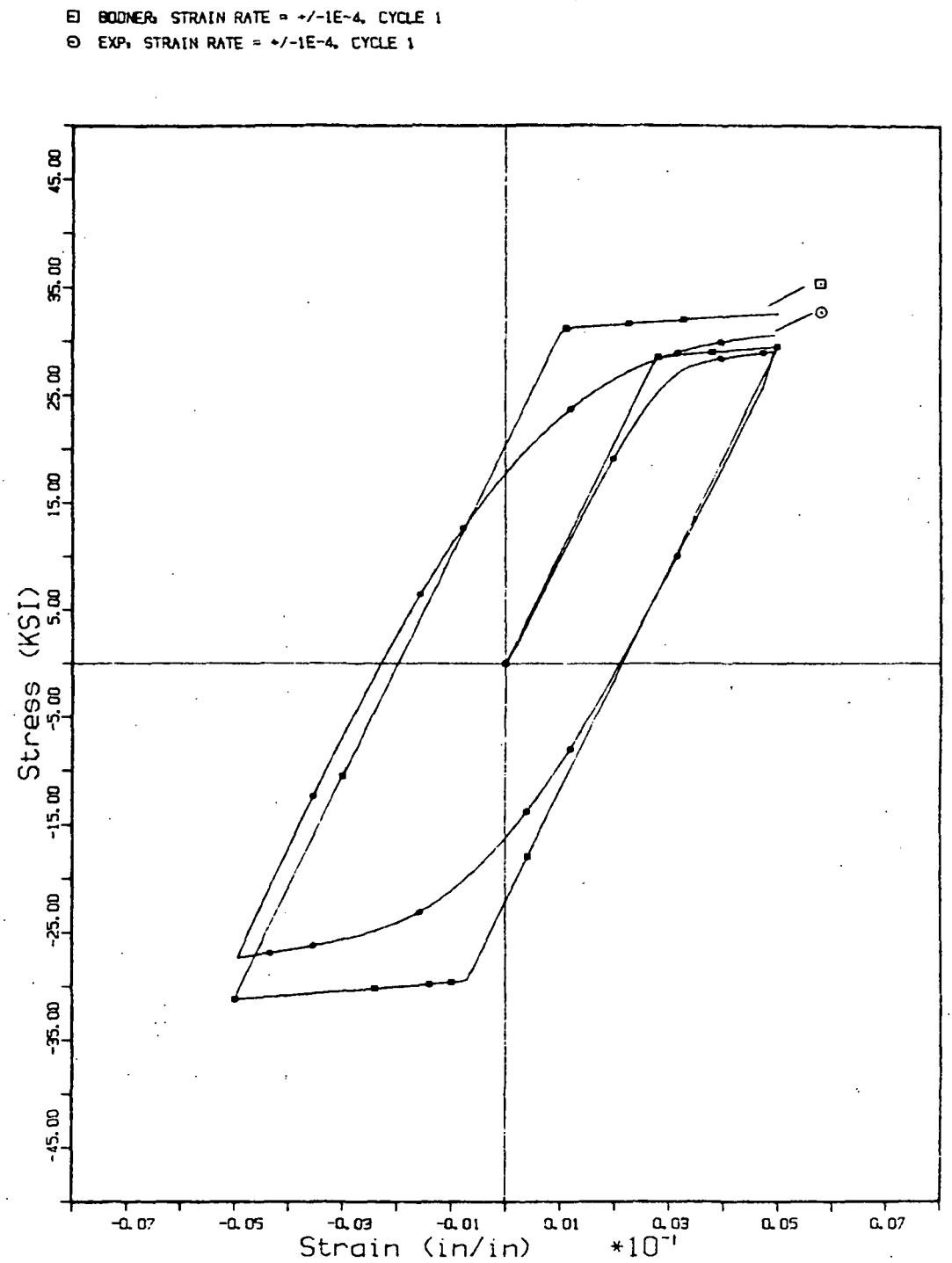

Fig. 32 Cyclic loading test: cycle 1. Comparison of theory of Bodner, et al., to experiment.

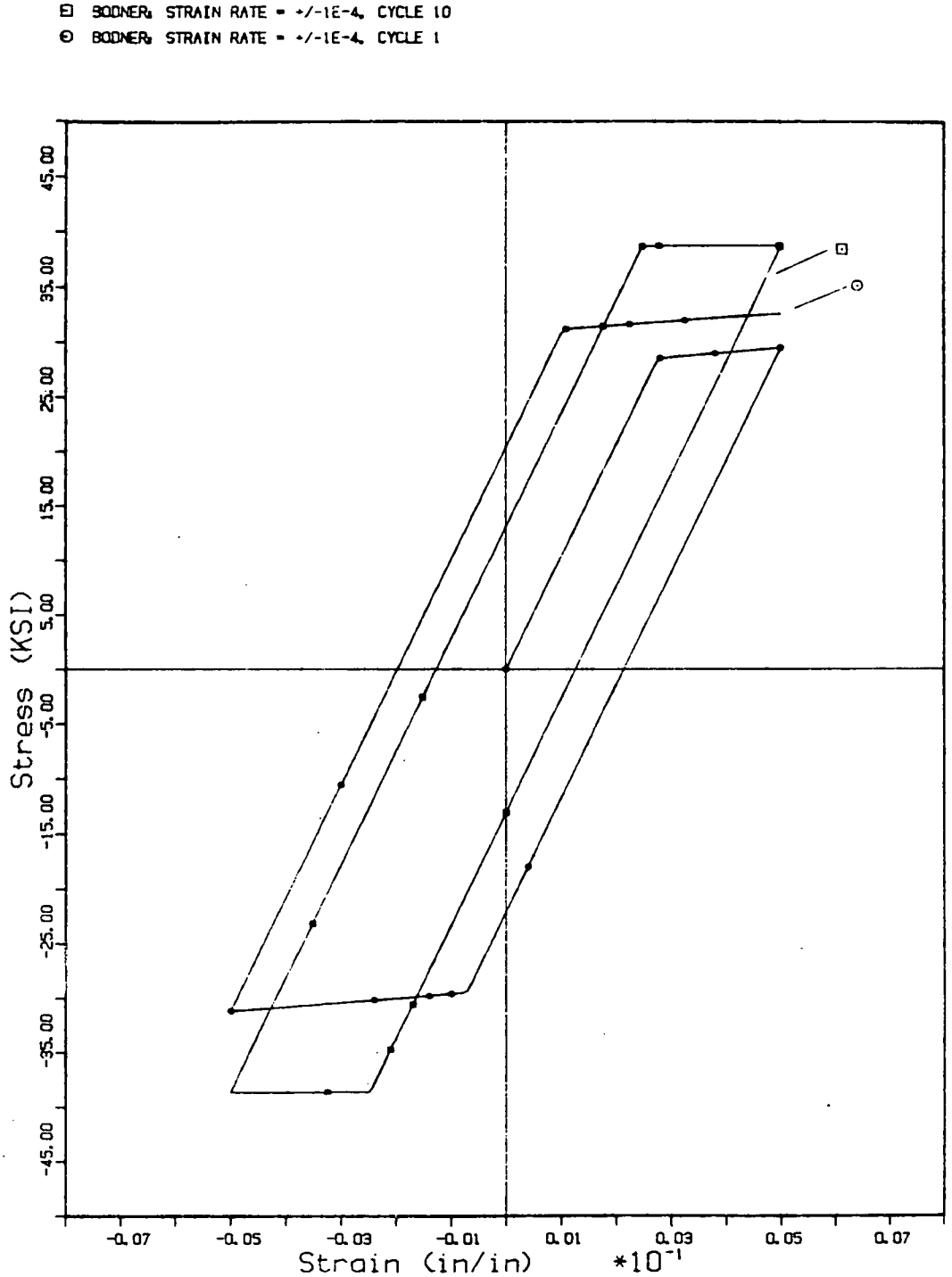

Fig. 33 Cyclic loading test: cycles 1 and 10. Prediction of theory of Bodner, et al.

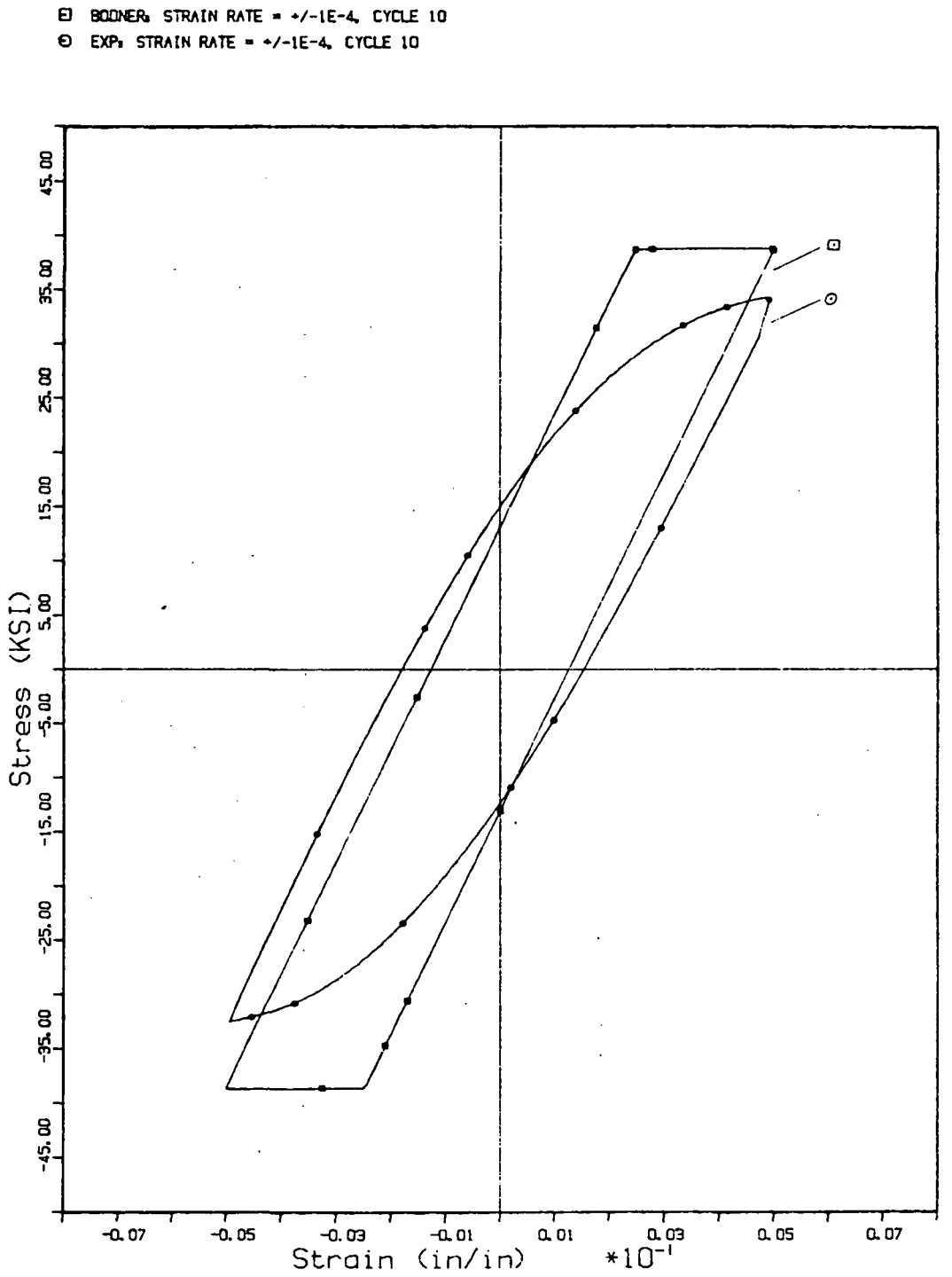

Fig. 34 Cyclic loading test: cycle 10. Comparison of theory of Bodner, et al., to experiment.

Miller, et al.: Cyclic Loading Test

The similarities between this model and that of Bodner, et al., can be seen in Figure 35 in that the theory does not model the Bauschinger effect due to the absence of a directional hardening term. It can also be seen that the assumption of a constant hardening function for the drag stress causes an "over-square" loop, although this is not as pronounced here as with the other two models.

Comparing the predictions of cycle 10 and cycle 1 shows extensive cyclic strain hardening (see Figure 36). This is much more apparent in the theory-to-experiment comparison for cycle 10, as shown in Figure 37, and suggests a need for a revision of the hardening function.

Finally, a comparison of all models for cycles 1 and 10 is shown for completion in Figures 38 and 39, respectively.

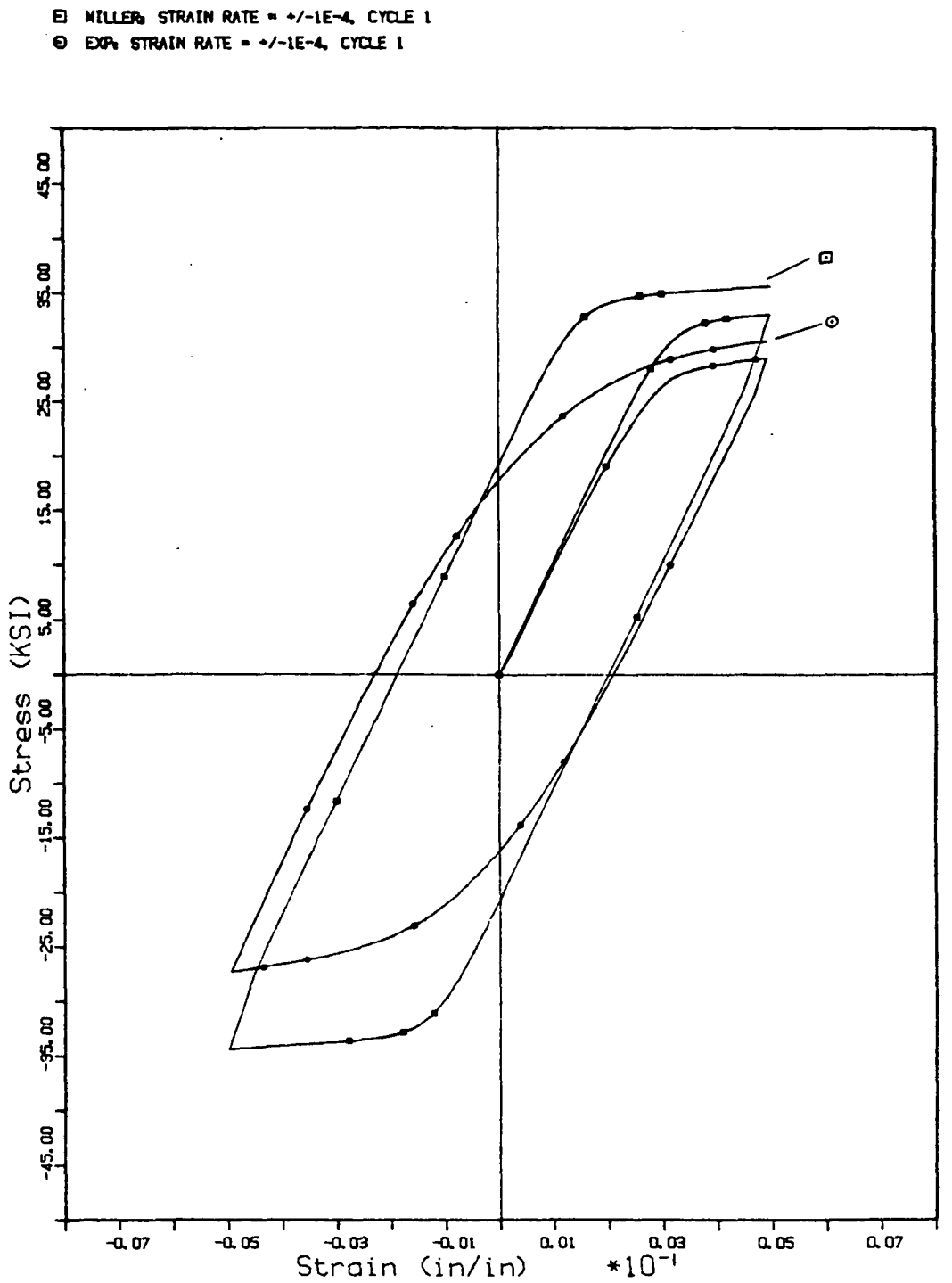

Fig. 35 Cyclic loading test: cycle 1. Comparison of theory of Miller, et al., to experiment.

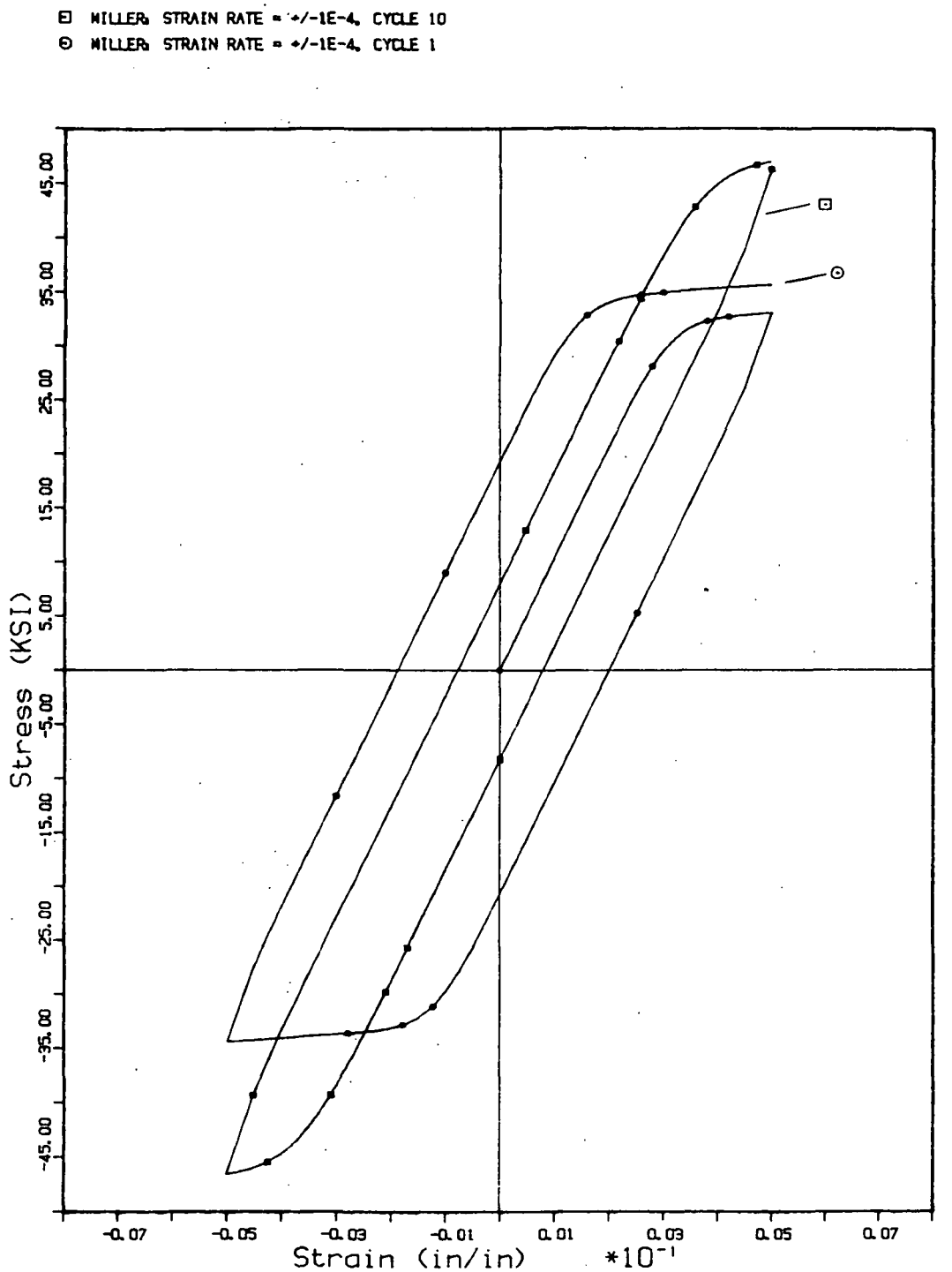

Fig. 36 Cyclic loading test: cycles 1 and 10. Prediction of theory of Miller, et al.

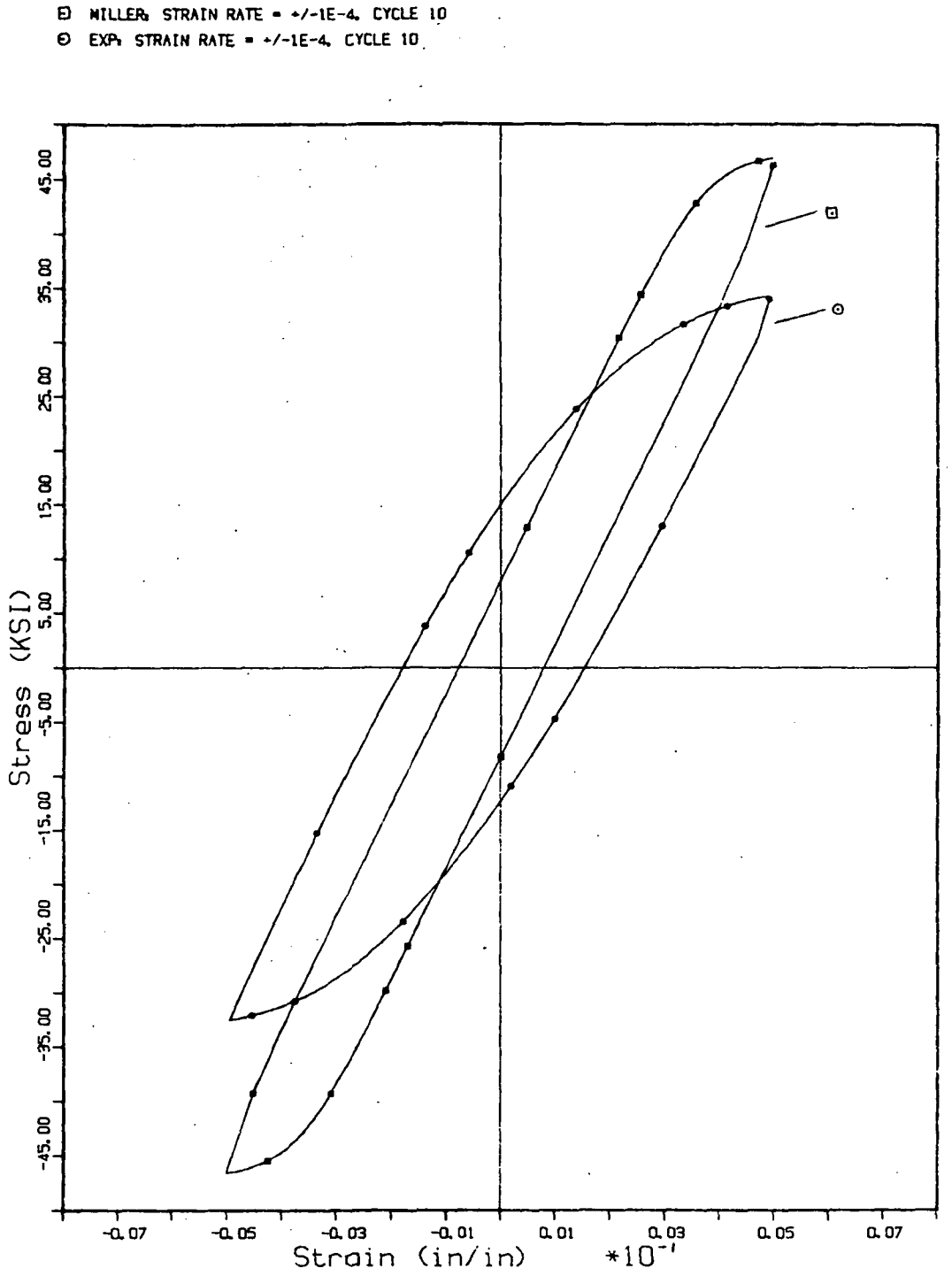

Fig. 37 Cyclic loading test: cycle 10. Comparison of theory of Miller, et al., to experiment.

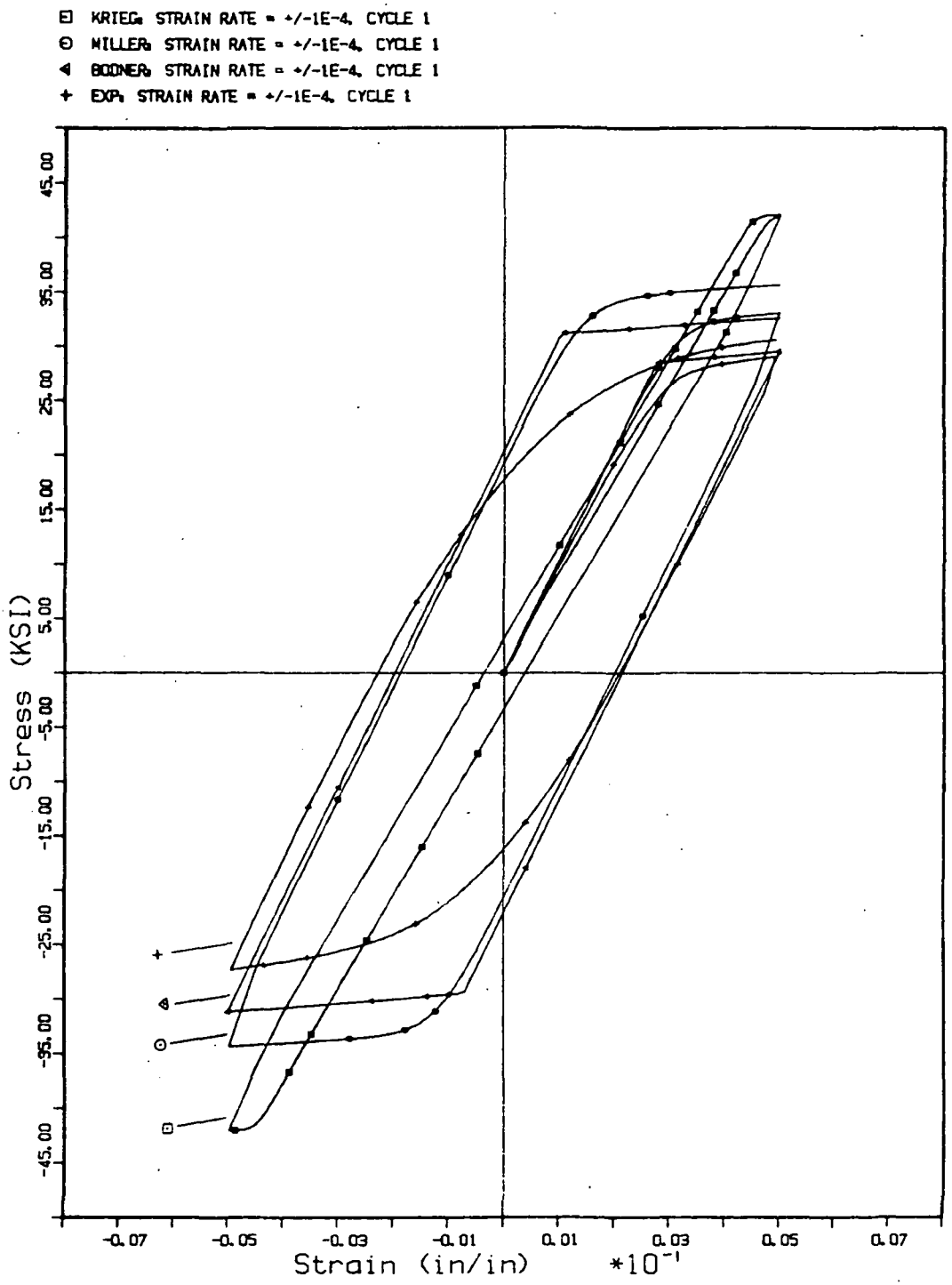

Fig. 38 Cyclic loading test: cycle 1. Comparison of all theories to experiment.

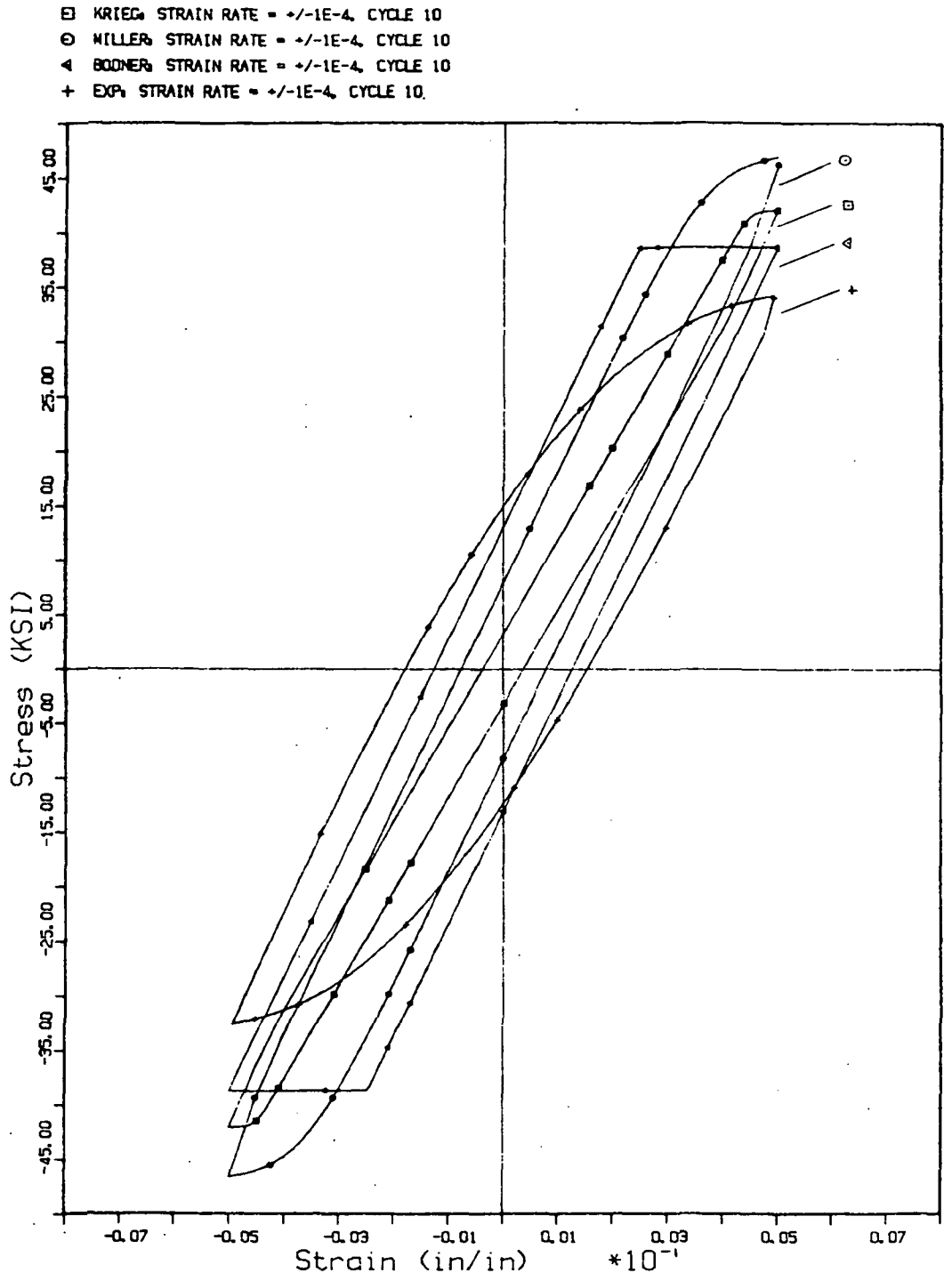

Fig. 39 Cyclic loading test: cycle 10. Comparison of all theories to experiment.

The final set of comparisons involves the prediction of the response to a complex loading history. Many models are designed specifically for creep response or cyclic response with somewhat limited capability for a general, complex response. The loading history is shown in Figure 40; the experimental response is shown in Figure 41.

Krieg, et al.: Complex Loading History

Figure 42 shows that this model over-predicts the stress, indicating that the inelastic strain is growing too slowly. This implies that the back stress is growing too quickly and that the hardening/recovery ratio is too large. Further evidence of this is demonstrated by the considerable amount of relaxation in compression. As before, this discrepancy may be due to the method of material constant determination.

Bodner, et al.: Complex Loading History

Figure 43 shows that this theory predicts the complex loading response very well. The model appears to predict a harder material with less relaxation than the experiment, again suggesting that the hardness Z is too large. A large Z causes a large $\dot{\varepsilon}$, leading to an over-prediction of stress. Similarly, during relaxation (when $\dot{\varepsilon} = 0$), a large Z causes a small $\dot{\sigma}$, leading to little relaxation.

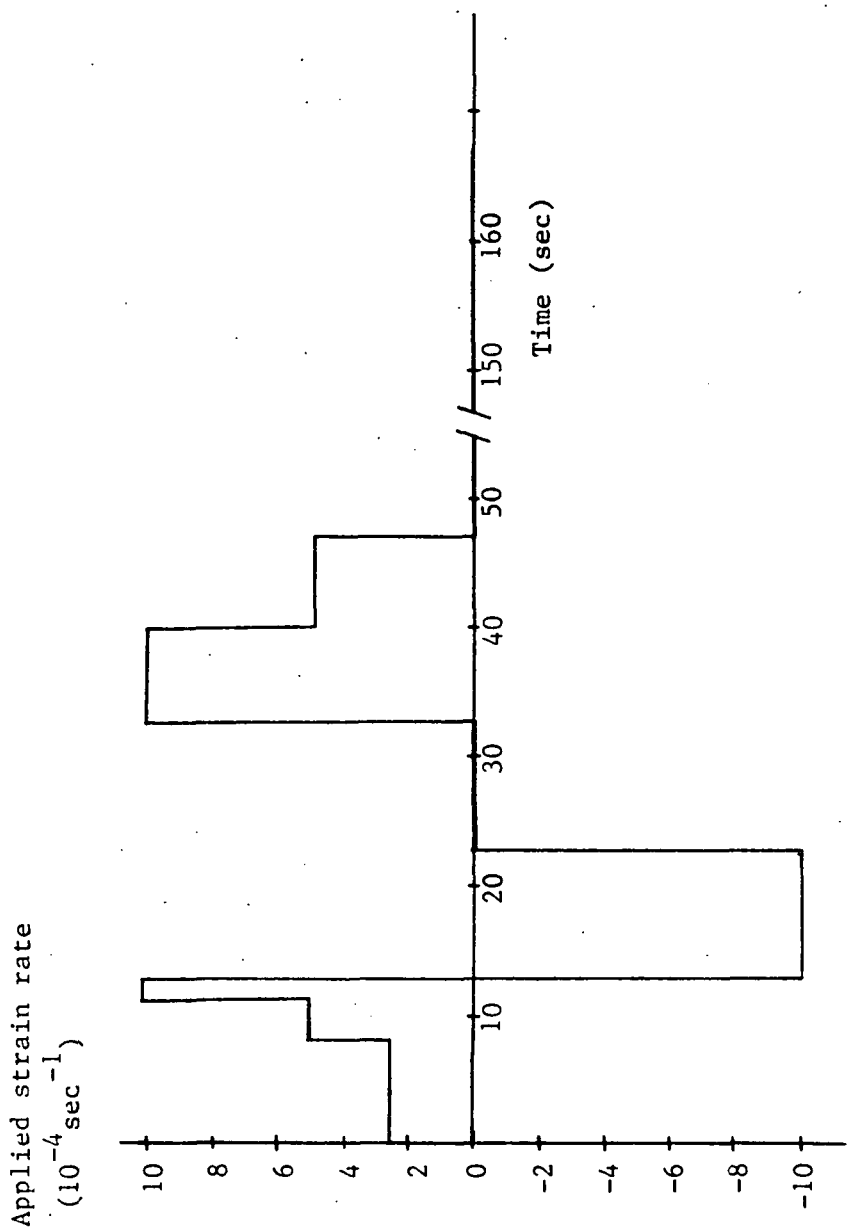

Fig. 40 Experimental complex loading history

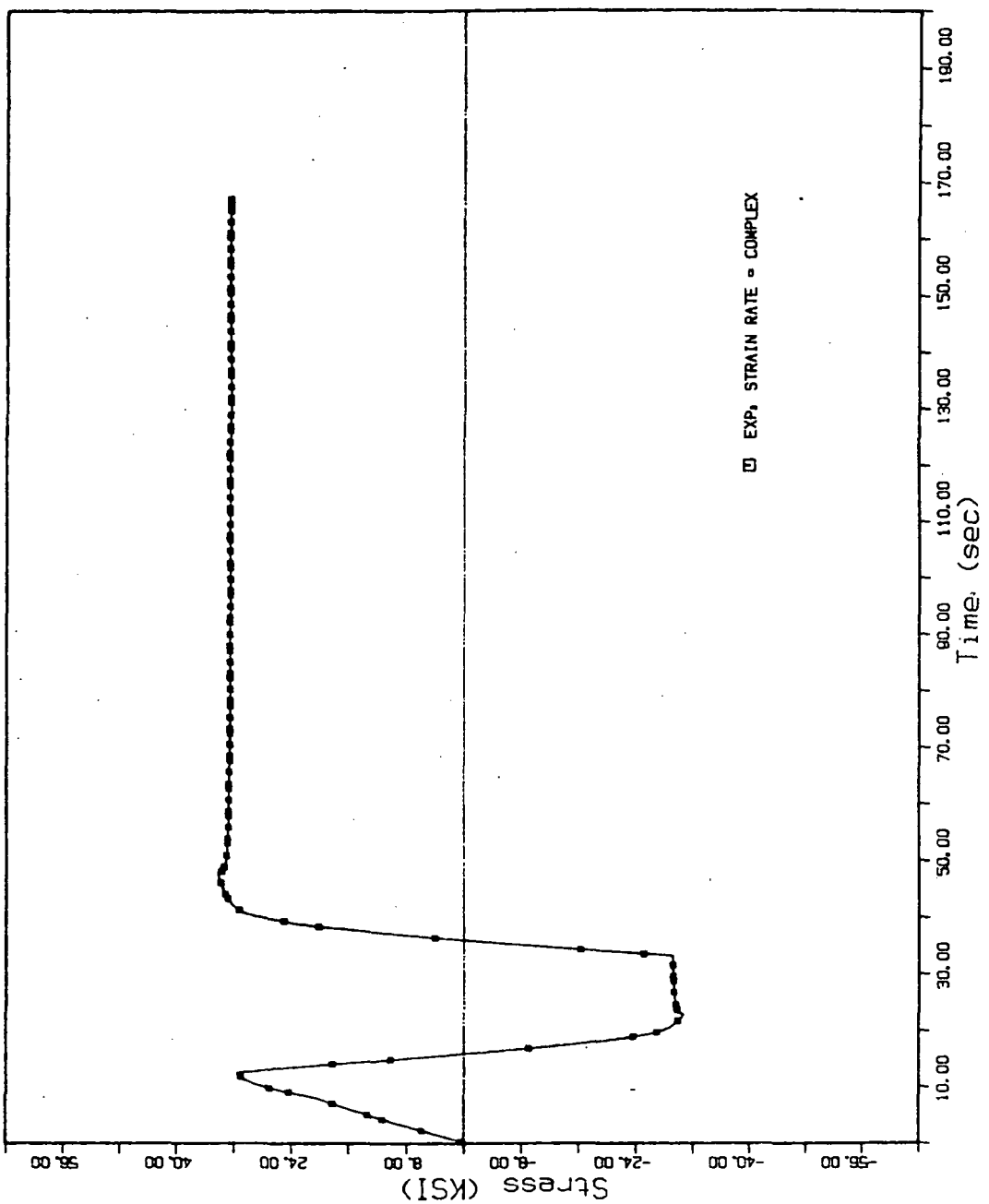

Fig. 41 Experimental complex loading response

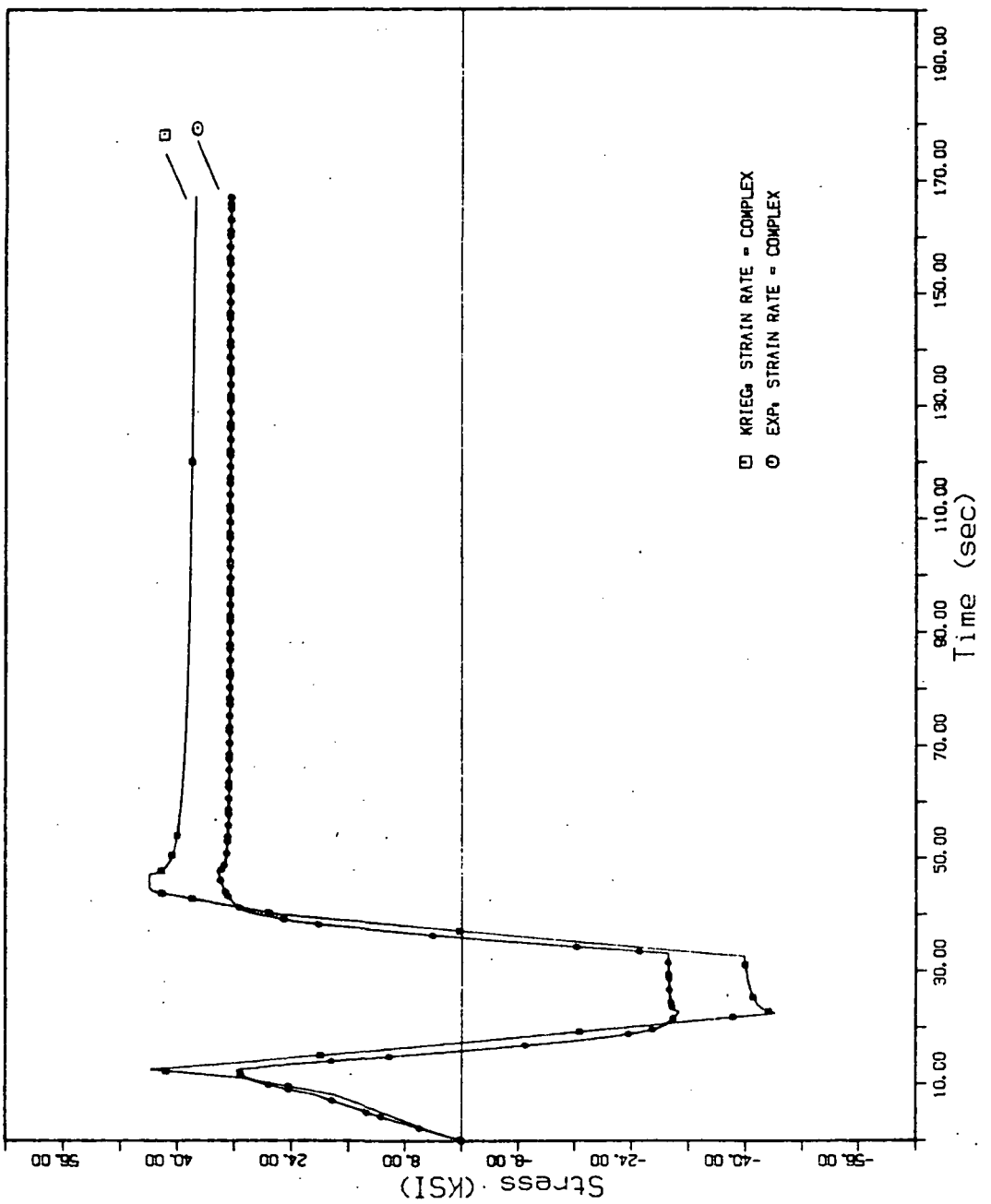

Fig. 42 Complex loading test. Comparison of theory of Krieg, et al., to experiment.

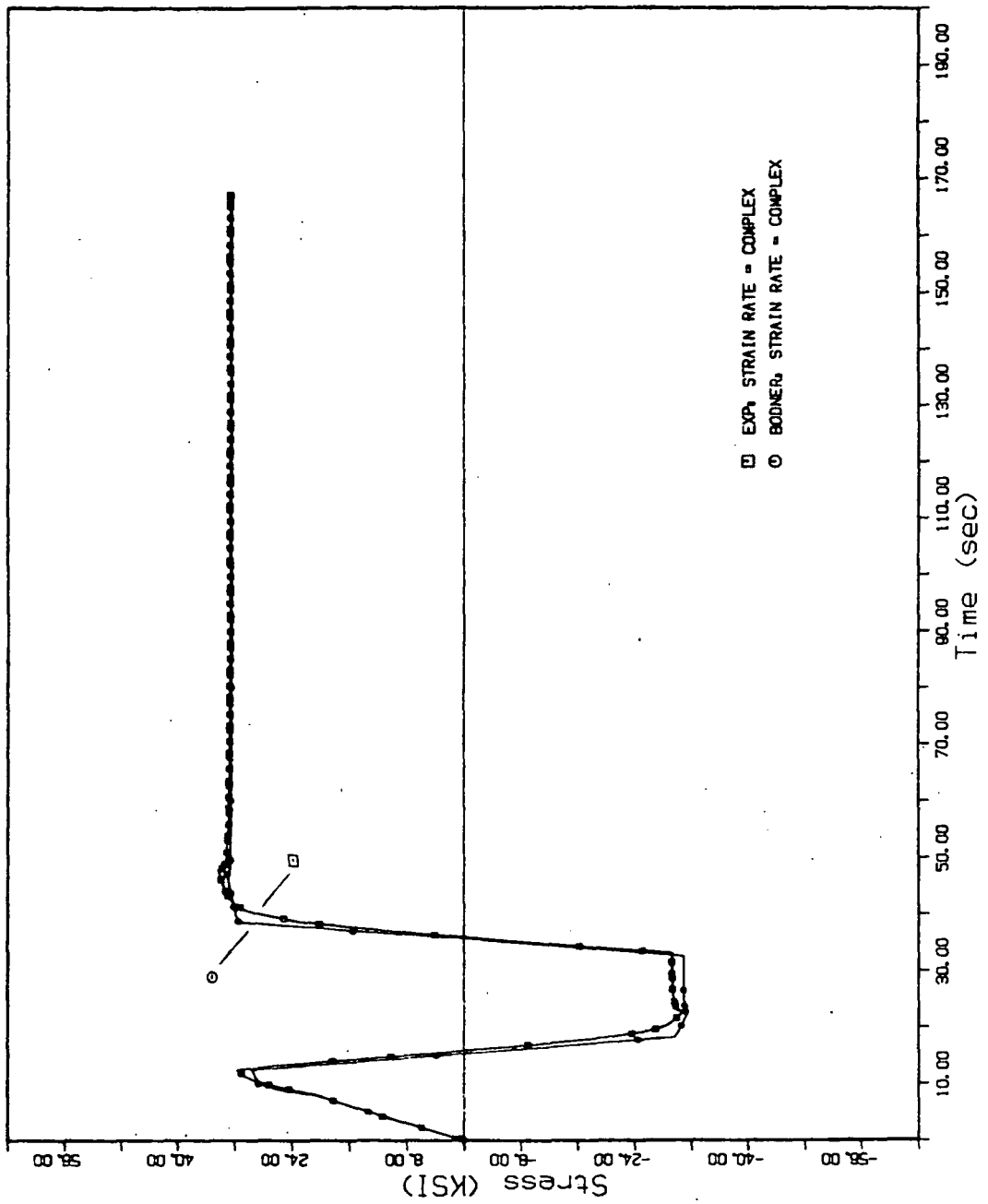

Fig. 43 Complex loading test. Comparison of theory of Bodner, et al., to experiment.

Miller, et al.: Complex Loading History

Figure 44 shows that this model over-predicts the stress during loading and unloading. This may be due to the fact that the hardening constant was set arbitrarily by fitting theory to experiment for a given strain rate, whereas the complex loading test involves strain rates upto two orders of magnitude higher. The large amount of relaxation is then brought on by the large value of stress.

Furthermore, it should be noted that, at approximately 40 seconds, the model experiences a negative stress rate immediately after the applied total strain rate is reduced. Again, this is due to the large value of stress causing the inelastic strain rate momentarily to be larger than the total strain rate. This decreases σ until $\dot{\varepsilon}^I$ is less than $\dot{\varepsilon}$, at which point the response returns to normal.

A solution to this could be an improved method for determining H, as well as a more complex hardening law for the drag stress.

Finally, a comparison of all theories to experiment for the complex loading history is shown in Figure 45 for completion.

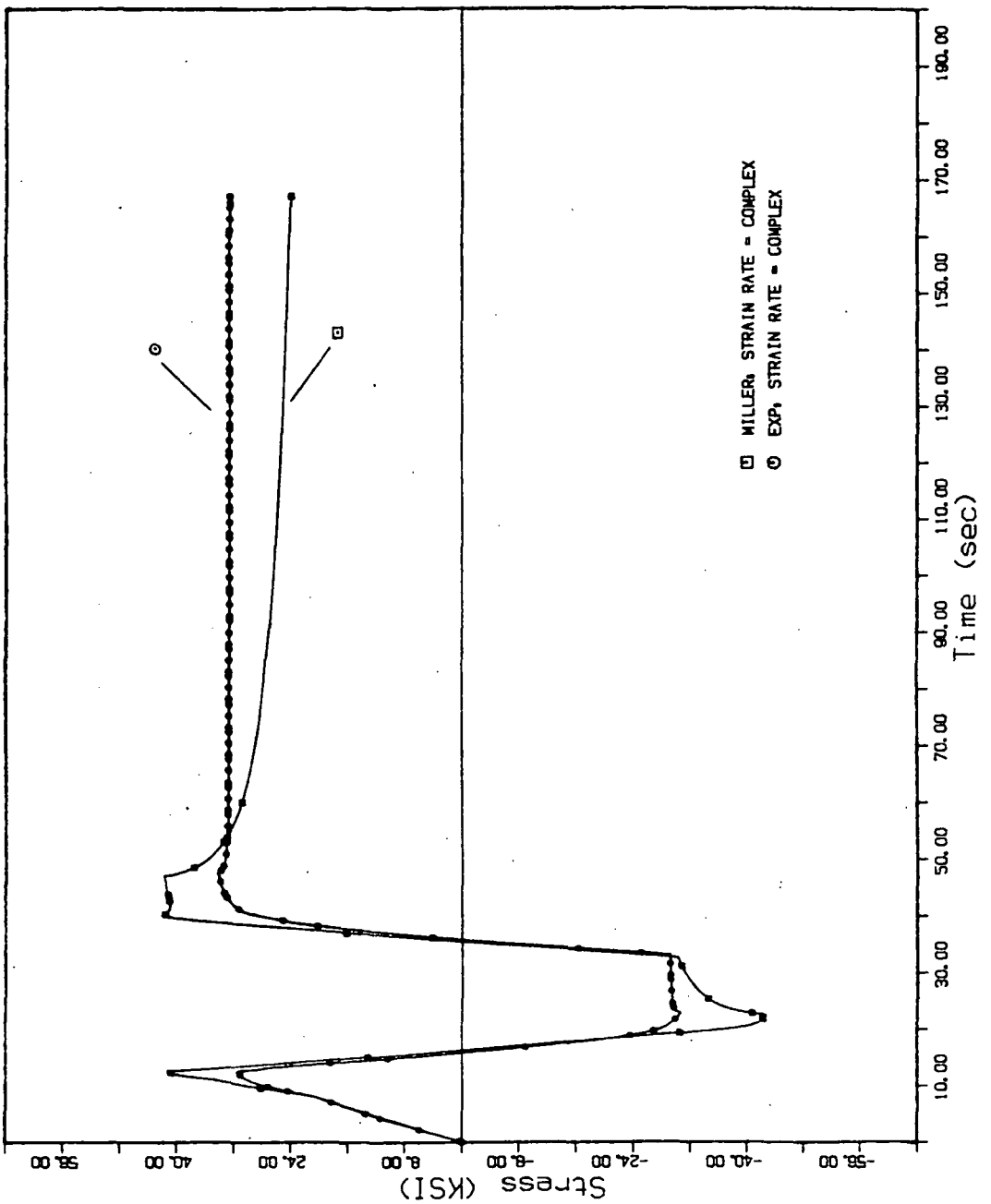

Fig. 44 Complex loading test. Comparison of theory of Miller, et al., to experiment.

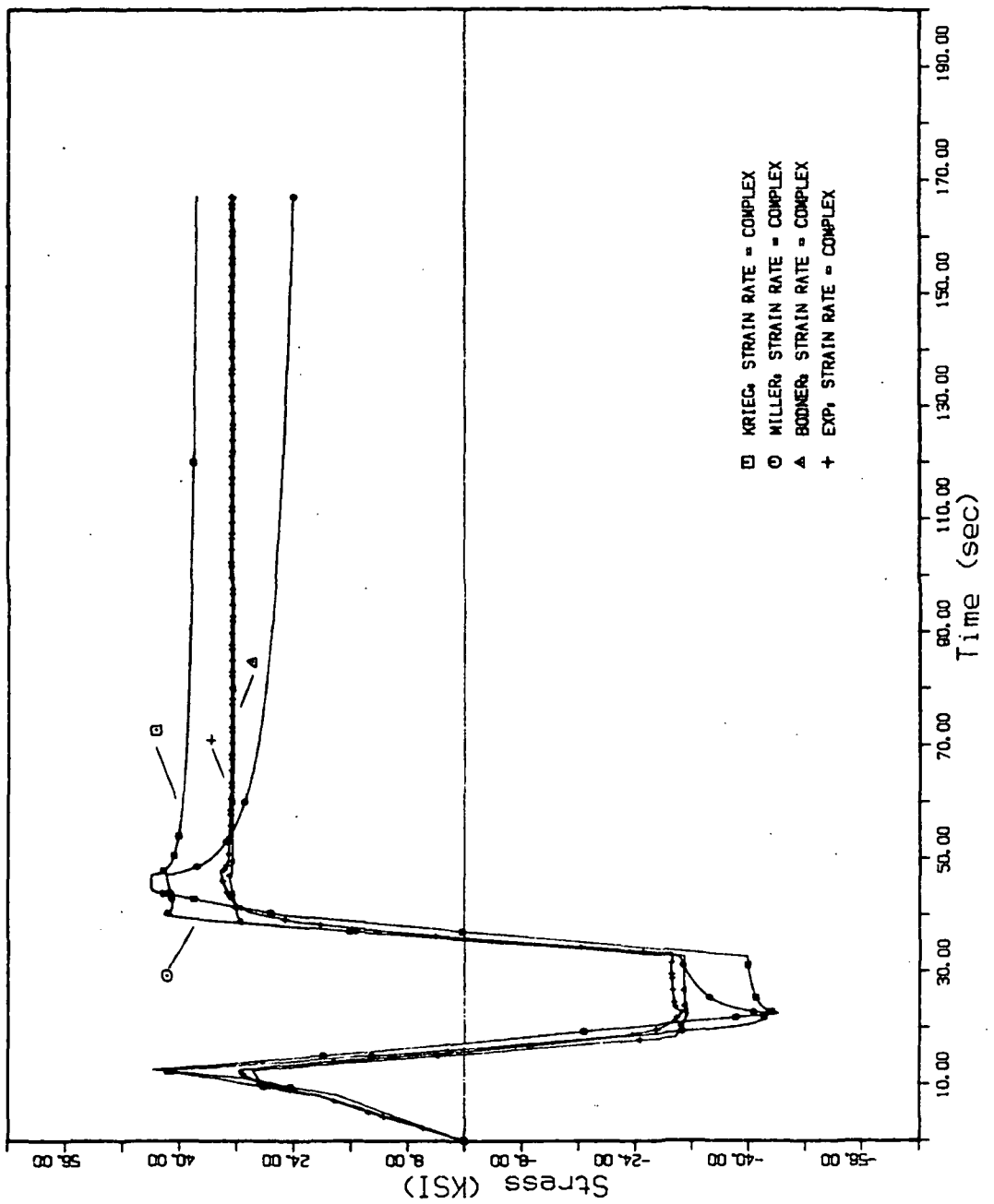

Fig. 45 Complex loading test. Comparison of all theories to experiment.

OMIT TO END 141

SUMMARY AND CONCLUSIONS

The objective of the research in this thesis has been to review and implement three theories for the prediction of inelastic deformation in crystalline structures. These theories are based on considerations of the microstructural behavior of the material and are the theories of Krieg, et al., Bodner, et al., and Miller, et al.

The thesis opens with a review of the mechanics of continua with internal state variables and a review of the historical development of constitutive modelling. It was shown that the concept of internal state variables is a suitable framework for comparison of all the models discussed herein and that the primary differences in these models are only in the number of internal state variables chosen and the growth laws used to obtain these variables.

A detailed discussion of each model chosen for comparison follows, in which the chronological development of the model is given and the theory on which the model is based is reviewed. This section closes with a description of the method of determination of material parameters and an assessment of the material test requirements of each model.

In order to perform a numerical comparison of the

models, the aluminum alloy Al 5086 was chosen as the candidate material. An experimental data base was established, from which the material constants for each model were calculated.

Finally, the uniaxial mathematical representations of each model have been encoded and implemented in computer programs in order to simulate various load histories. These simulations are compared to experimental data and comments are made on their accuracy.

In conclusion, it has been demonstrated that the theories discussed herein are suitable models for the prediction of inelastic deformation in crystalline solids. It is also apparent, however, that further research is necessary in several areas in the development of these theories.

For example, the theories lack, to varying degrees, clear, concise, and rigorous methods to determine material constants from simple experiments. The theory of Krieg, et al., uses the somewhat controversial and difficult to implement stress-drop test, although the calculation of constants is simple. This dependence on stress-drop test results may adversely affect the performance of this model. The theory of Miller, et al., uses standard creep tests, but values of several constants are set arbitrarily to obtain an optimum curve-fit. Although this is also true to

a lesser degree for the theory of Bodner, et al., it is found that this theory provides the best balance between ease of testing and determination of material constants for the theories discussed herein. In addition, it is found that all three theories exhibit substantial material parameter sensitivity to small variations in input.

It can be seen in the previous section that the models in general compare favorably to experiment. However, it is clear that the full representations of the models, incorporating both isotropic and directional hardening terms, may be more appropriate for modelling phenomena such as the Bauschinger effect and cyclic strain hardening than the simplified versions examined herein. In addition, these theories are proposed mainly for intermediate to high temperature conditions and may have failed to model fully the phenomena at the temperature used in this research ($0.3T_m$).

Another area of improvement is in the use of internal state variables. Many hardening functions are taken to be constants, whereas functions of the current stress level or back stress level may be warranted to prevent an overprediction of stress and an "over-square" transition from elastic to inelastic behavior.

Based on these assessments, it is felt that the theory of Bodner, et al., provides the best balance between ease

of implementation and accuracy of results for the material and test conditions of interest for this research. The theory of Krieg, et al., is affected adversely by the complexity of the required material tests, while the theory of Miller, et al., is affected adversely by the lack of rigor in calculating constants.

As a result of this research, it is the experience of this researcher that data acquisition and control equipment of the highest resolution and accuracy is an absolute necessity to ensure credible experimental results, particularly in specialized tests such as the stress-drop test.

Finally, it is hoped that the research presented in this thesis may answer questions relating to the modelling of inelastic deformation in crystalline solids and lead to further research in this field.

REFERENCES

1. Onsager, L., "Reciprocal Relations in Irreversible Processes I," Physical Review, Vol. 37, 1931, pp. 405-426.

2. Onsager, L., "Reciprocal Relations in Irreversible Processes II," Physical Review, Vol. 38, 1931, pp. 2265-2279.

3. Coleman, B.D., and Gurtin, M.E., "Thermodynamics with Internal State Variables," Journal of Chemical Physics, Vol. 47, 1967, pp. 597-613.

4. Eckart, C., "Thermodynamics of Irreversible Processes, I: The Simple Fluid," Physical Review, Vol. 58, 1940, pp. 267-269.

5. Meixner, J., "Die thermodynamische Theorie der Relaxationserscheinungen und ihr Zusammenhang mit der Nachwirkungstheorie," Kolloid-Z., Vol. 134, 1953, pp. 3-20.

6. Biot, M.A., "Theory of Stress-Strain Relations in Anisotropic Viscoelasticity and Relaxation Phenomena," Journal of Applied Physics, Vol. 25, 1954, pp. 1385-1391.

7. Biot, M.A., "Variational Principles in Irreversible Thermodynamics with Application to Viscoelasticity," Physical Review, Vol. 97, 1955, pp. 1463-1469.

8. Ziegler, H., "An Attempt to Generalize Onsager's Principle, and Its Significance for Rheological Problems," Zeitschrift fuer Angewandte Mathematik und Mechanik, Vol. 9, 1958, pp. 748-752.

9. Valanis, K.C., "Unified Theory of Thermomechanical Behavior of Viscoelastic Materials," Mechanical Behavior of Materials Under Dynamic Loads, Springer-Verlag, Berlin, 1968, pp. 343-364.

10. Kestin, J., and Rice, J.R., A Critical Review of Thermodynamics, Mono Book Corp., 1970.

11. Schapery, R.A., "Application of Thermodynamics to Thermomechanical, Fracture, and Birefringent Phenomena in Viscoelastic Media," Journal of Applied Physics, Vol. 35, 1964, pp. 1941-1944.

12. Schapery, R.A., "A Theory of Non-Linear Thermoviscoelasticity Based on Irreversible Thermodynamics," Proc. 5th U.S. National Congress of Applied Mechanics, ASME, 1966, pp. 511-530.

13. Krajcinovic, D., and Fonseka, G.U., "The Continuous Damage Theory of Brittle Materials - Part I - General Theory," Journal of Applied Mechanics, Vol. 48, 1981, pp. 809-815.

14. Coleman, B.D., and Noll, W., "The Thermodynamics of Elastic Materials with Heat Conduction and Viscosity," Archive for Rational Mechanics and Analysis, Vol. 13, 1963, pp. 167-178.

15. Kratochvil, J., and Dillon, O.W., Jr., "Thermodynamics of Crystalline Elastic-Visco-Plastic Materials," Journal of Applied Physics, Vol. 41, 1970, pp. 1470-1479.

16. Kratochvil, J., and Dillon, O.W., Jr., "Thermodynamics of Elastic-Plastic Materials as a Theory with Internal State Variables," Journal of Applied Physics, Vol. 40, 1969, pp. 3207-3218.

17. Allen, D.H., "A Prediction of Heat Generation in a Thermoviscoplastic Uniaxial Bar," International Journal of Solids and Structures, Vol. 21, 1985, pp. 325-342.

18. Allen, D.H., "Some Comments on Inelastic Strain in Thermoviscoplastic Metals," Texas A&M University Report No. MM NAG 3-31-83-8, June 1983.

19. Allen, D.H., and Beek, J.M., "On the Use of Internal State Variables in Thermoviscoplastic Constitutive Equations," Proc. 2nd Symposium on Nonlinear Constitutive Relations for High Temperature Applications, Cleveland, Ohio, June 1984.

20. Beek, J.M., Allen, D.H., and Milly, T.M., "A Qualitative Comparison of Current Models for Nonlinear Rate-Dependent Material Behaviour of Crystalline Solids," Texas A&M University Report No. MM 4246T-83-14, November 1984.

21. Green, A.E., and Naghdi, P.M., "A General Theory of an Elastic-Plastic Continuum," Archive for Rational Mechanics and Analysis, Vol. 18, 1965, pp. 251-281.

22. Allen, D.H., and Haisler, W.E., Introduction to Aerospace Structural Analysis, John Wiley and Sons, New York, 1984.

23. Tresca, H., "Notes on Yield of Solid Bodies under Strong Pressure," Comptes Rendus de l'Academie des Sciences (Paris), Vol. 59, 1864, p. 754-757.

24. von Mises, R., "Mechanik der Festen Koerper im Plastisch Deformablen Zustand," Goettinger Nachr., Math.-Phys. Kl., 1913, pp. 582-592.

25. Hencky, H., "Zur Theorie Plastischer Deformationen und die Hierdurch im Material Hervorgerufenen Nachspannungen," Zeitschrift fuer Angewandte Mathematik und Mechanik, Vol. 4, 1924, pp. 323-334.

26. Levy, M., "Memoire sur les equations generales des mouvements interieurs des corps solides ductiles au dela des limites ou l'elasticite pourrait les ramener a leur premier etat," Comptes Rendus de l'Academie des Sciences (Paris), Vol. 70, 1870, pp. 1323-1325.

27. Prandtl, L., "Spannungsverteilung in Plastischen Koerpern," Proc. 1st International Congress on Applied Mechanics, Delft, Technische Boekhandel en Druckerij, 1925, pp. 43-45.

28. Reuss, E., "Beruecksichtigung der Elastischen Formaenderung in der Plastizitaetstheorie," Zeitschrift fuer Angewandte Mathematik und Mechanik, Vol. 10, 1930, pp. 266-274.

29. Bingham, E.C., Fluidity and Plasticity, McGraw-Hill, New York, 1922.

30. Hohenemser, K., and Prager, W., "Ueber die Ansaetze der Mechanik Isotroper Kontinua," Zeitschrift fuer Angewandte Mathematik und Mechanik, Vol. 12, 1932, pp. 216-226.

31. Prager, W., "The Theory of Plasticity: A Survey of Recent Achievements," Proc. Institution of Mechanical Engineers, London, Vol. 169, 1955, pp. 41-57.

32. Ziegler, H., "A Modification of Prager's Hardening Rule", Quarterly Of Applied Mathematics, Vol. 17, 1959, pp. 55-65.

33. Drucker, D.C., "A Definition of Stable Inelastic Material," Journal of Applied Mechanics, Vol. 26, 1959, pp.101-106.

34. Freudenthal, A.M., "The Mathematical Theories of the Inelastic Continuum," Handbuch der Physik, Springer-Verlag, Berlin, 1958.

35. Malvern, L.E., "Plastic Wave Propagation in a bar of material exhibiting a strain rate effect," Quarterly of Applied Mathematics, Vol. 8, 1950, pp. 405-411.

36. Malvern, L.E., "The Propagation of longitudinal waves of plastic deformation in a bar of material exhibiting a strain rate effect," Journal of Applied Mechanics, Vol. 18, 1951, pp. 203-208.

37. Lubliner, J., "A generalized theory of strain rate dependent plastic wave propagation in bars," Journal of the Mechanics and Physics of Solids, Vol. 12, 1964, pp. 59-65.

38. Perzyna, P., "Fundamental Problems in Viscoplasticity," Advanced Applied Mechanics, Vol. 9, 1966, pp. 243-377.

39. Perzyna, P., "The Constitutive Equations for Work-Hardening and Rate-Sensitive Plastic Materials," Proc. Vibr. Probl., Vol. 4, 1963, pp. 281-290.

40. Perzyna, P., "On the thermodynamic foundations of viscoplasticity," Symposium on the mechanical behavior of materials under dynamic loads, San Antonio, Texas, 1967.

41. Perzyna, P., and Wojno, W., "Thermodynamics of rate sensitive plastic materials," Arch. Mech. Stos., Vol. 20, 1968, p. 499-509.

42. Argon, A.S., "Physical Basis of Constitutive Equations for Inelastic Deformation," Constitutive Equations in Plasticity, MIT Press, Cambridge, Massachusetts, 1975.

43. Naghdi, P.M., and Murch, S.A., "On the Mechanical Behavior of Viscoelastic/Plastic Solids," Journal of Applied Mechanics, Vol. 30, 1963, pp. 321-328.

44. Snyder, M.D., and Bathe, K.J., "Formulation and Numerical Solution of Thermo-Elastic-Plastic and Creep Problems," National Technical Information Service, Report No. 82448-3, June 1977.

45. Yamada, Y., and Sakurai, T., "Basic Formulation and a Computer Program for Large Deformation Analysis," Pressure Vessel Technology, Part 1, ASME, 1977, pp. 341-352.

46. Allen, D.H., and Haisler, W.E., "A Theory for Analysis of Thermoplastic Materials," Computers and Structures, Vol. 13, 1981, pp. 124-135.

47. Allen, D.H., "Computational Aspects of the Nonisothermal Classical Plasticity Theory," Computers and Structures, Vol. 15, 1982, pp. 589-599.

48. Zienkiewicz, O.C., and Cormeau, I.C., "Visco-Plasticity -- Plasticity and Creep in Elastic Solids -- A Unified Numerical Approach," International Journal for Numerical Methods in Engineering, Vol. 8, 1974, pp.821-845.

49. Robinson, D.N., "A Unified Creep-Plasticity Model for Structural Metals at High Temperature," ORNL Report No. TM-5969, October 1978.

50. Bodner, S.R., and Partom, Y., "Constitutive Equations for Elastic-Viscoplastic Strain-Hardening Materials," Journal of Applied Mechanics, Vol. 42, No. 2, 1975, pp. 385-389.

51. Valanis, K.C., "A Theory of Viscoplasticity Without a Yield Surface , Part I. General Theory," Archives of Mechanics, Vol. 23, 1971, pp. 517-533.

52. Valanis, K.C., "A Theory of Viscoplasticity Without a Yield Surface ; Part II. Application to Mechanical Behavior of Metals," Archives of Mechanics, Vol. 23, 1971, pp. 535-551.

53. Valanis, K.C., "On the Foundations of the Endochronic Theory of Viscoplasticity," Archives of Mechanics, Vol. 27, 1975, pp. 857-868.

54. Allen, D.H., and Milly, T.M., "A Comparison of Constitutive Models for Nonlinear Rate-Dependent Material Behavior of Solids," Virginia Polytechnic Institute and State University Report No. VPI-E-81-16, 1981.

55. Coleman, B.D., and Noll, W., "Foundations of Linear Viscoelasticity," Review of Modern Physics, Vol. 33, 1961, pp. 239-249.

56. Green, A.E., and Rivlin, R.S., "The Mechanics of Non-Linear Materials with Memory -- Part I," Archive for Rational Mechanics and Analysis, Vol. 1, 1957, pp. 1-21.

57. Green, A.E., and Naghdi, P.M., "On Continuum Thermodynamics,"Archive for Rational Mechanics and Analysis, Vol. 48, 1972, pp. 352-378.

58. Walker, K.P., "Representation of Hastelloy-X Behavior at Elevated Temperature with a Functional Theory of Viscoplasticity," ASME Pressure Vessels Conference, San Francisco, California, August 1980.

59. Cernocky, E.P., and Krempl, E., "A Theory of Thermoviscoplasticity Based on Infinitesimal Total Strain," International Journal of Solids and Structures, Vol. 16, 1980, pp. 723-741.

60. Cernocky, E.P., and Krempl, E., "A Theory of Viscoplasticity Based on Infinitesimal Total Strain," Acta Mechanica, Vol. 36, 1980, pp. 263-289.

61. Krempl, E., "On the Interaction of Rate and History Dependence in Structural Metals," Acta Mechanica, Vol. 22, 1975, pp. 53-90.

62. Liu, M.C.M., Krempl, E., and Nairn, D.C., "An Exponential Stress-Strain Law for Cyclic Plasticity," Journal of Engineering Materials and Technology, Vol. 98H, 1976, pp. 322-329.

63. Cernocky, E.P., and Krempl, E., "A Nonlinear Uniaxial Integral Constitutive Equation Incorporating Rate Effects, Creep, and Relaxation," International Journal of Nonlinear Mechanics, Vol. 14, 1979, pp. 183-203.

64. Liu, M.C.M., and Krempl, E., "A Uniaxial Viscoplastic Model Based on Total Strain and Overstress," Journal of the Mechanics and Physics of Solids, Vol. 27, 1979, pp. 377-391.

65. Krempl, E., "An Experimental Study of Room-Temperature Rate-Sensitivity, Creep, and Relaxation of AISI Type 304 Stainless Steel," Journal of the Mechanics and Physics of Solids, Vol. 27, 1979, pp. 363-375.

66. Krempl, E., McMahon, J.J., and Yao, D., "Viscoplasticity Based on Overstress with a Differential Growth Law for the Equilibrium Stress," Proc. 2nd Symposium on Nonlinear Constitutive Relations for High Temperature Applications, Cleveland, Ohio, June 1984.

67. Walker, K.P., "Constitutive Modelling of Engine Materials," AFML Report No. FR-17911, 1983.

68. Walker, K.P., "Research and Development Program for Nonlinear Structural Modelling with Advanced Time-Temperature Dependent Constitutive Relationships," NASA Report No. 165533, 1981.

69. Stouffer, D.C., and Bodner, S.R., "A Relationship Between Theory and Experiment for a State Variable Constitutive Equation," AFML Report No. AFWAL-TR-80-4194, 1981.

70. Cailletaud, G. and Chaboche, J.L., "Macroscopic Description of the Microstructural Changes Induced by Varying Temperature: Example of IN100 Cyclic Behaviour," Proc. 3rd International Conference of Mechanical Behaviour of Materials, Cambridge, England, Vol. 2, 1979, pp. 25-32.

71. Bodner, S.R., "A Procedure for Including Damage in Constitutive Equations for Elastic-Viscoplastic Work-Hardening Materials," Proc. IUTAM Symposium, Springer-Verlag, 1981, pp. 21-28.

72. Coble, R.L., "A Model for Boundary Diffusion Controlled Creep in Polycrystalline Materials," Journal of Applied Physics, Vol. 34, 1963, pp. 1679-1682.

73. Nabarro, F.R.N., "Report on a Conference on the Strength of Solids," Physical Society of London, 1948, pp. 75-79.

74. Herring, C., "Diffusional Viscosity of a Polycrystalline Solid," Journal of Applied Physics, Vol. 21, 1950, pp. 437-445.

75. Orr, R. L.,Sherby, O.D., and Dorn, J.E., "Correlations of Rupture Data for Metals at Elevated Temperatures," Transactions of the ASM, Vol. 46, 1954, pp. 113-128.

76. Sherby, O.D., and Lytton, J.C., "Possible Role of Diffusion in the Creep of Alpha and Gamma Iron," Transactions of the AIME, Vol. 206, 1956, pp. 928-930.

77. Sherby, O.D., and Burke, P.M., "Mechanical Behavior of Crystalline Solids at Elevated Temperature," Progress in Materials Science, Vol. 13, 1968, pp. 325-390.

78. Garofalo, F., Fundamentals of Creep and Creep-Rupture in Metals, Macmillan, New York, 1965.

79. Weertman, J., "Dislocation Climb Theory of Steady-State Creep," Transactions of the ASM, Vol. 61, 1969, pp. 681-694.

80. Alden, T.H., "Strain Hardening and Recovery in Superplastic Pb-5% Cd," Transactions of the ASM, Vol. 61, 1968, pp. 559-567.

81. Kocks, U.F., "Laws for Work-Hardening and Low-Temperature Creep," Journal of Engineering Materials and Technology, Vol. 98H, 1976, pp. 76-85.

82. Hart, E.W., "Constitutive Equations for the Nonelastic Deformation of Metals," Journal of Engineering Materials and Technology, Vol. 98H, 1976, pp. 193-202.

83. Mukherjee, A.K., Bird, J.E., and Dorn, J.E., "Experimental Correlations for High-Temperature Creep," Transactions of the ASM, Vol. 62, 1969, pp. 155-179.

84. Gibbs, G.B., "A General Dislocation Model for High-Temperature Creep," Philosophical Magazine, Vol. 25, 1972, pp. 771-780.

85. Hertzberg, R.W., Deformation and Fracture Mechanics of Engineering Materials, John Wiley and Sons, New York, 1976.

86. Bailey, R.W., "Note on the Softening of Strain-Hardened Metals and its Relation to Creep," Journal of the Institute of Metals, Vol. 35, 1926, pp. 27-43.

87. Orowan, E., Journal of West. Scot. Iron and Steel Institute, Vol. 54, 1946, p. 45-60.

88. Krieg, R.D., Swearengen, J.C., and Rohde, R.W., "A Physically-Based Internal Variable Model for Rate-Dependent Plasticity," Proc. ASME/CSME PVP Conference, 1978, pp. 15-27.

89. Cescotto, S., and Leckie, F., "Determination of Unified Constitutive Equations for Metals at High Temperatures," Proc. International Conference on Constitutive Laws for Engineering Materials, 1983, pp. 105-111.

90. Miller, A.K., "An Inelastic Constitutive Model for Monotonic, Cyclic, and Creep Deformation: Part I -- Equations Development and Analytical Procedures, and Part II -- Application to Type 304 Stainless Steel," Journal of Engineering Materials and Technology, Vol. 98H, 1976, pp. 97-113.

91. Lindholm, U.S., Chan, K.S., Bodner, S.R., Weber, R.M., Walker, K.P., and Cassenti, B.N., "Constitutive Modeling for Isotropic Materials (HOST)," NASA Report No. CR-174718, 1984.

92. Milly, T.M., and Allen, D.H., "A Comparative Study of Nonlinear Rate-Dependent Mechanical Constitutive Theories for Crystalline Solids at Elevated Temperatures," Virginia Polytechnic Institute and State University Report No. VPI-E-82-5, 1982.

93. Cernocky, E.P., "An Examination of Four Viscoplastic Constitutive Theories in Uniaxial Monotonic Loading," International Journal of Solids and Structures, Vol. 18, 1982, pp. 989-1005.

94. Moreno, V., and Jordan, E.H., "Prediction of Thermomechanical Response with a Unified Constitutive Model," Proc. 26th AIAA Structures, Structural Dynamics and Materials Conference, 1985, pp. 113-125.

95. Krieg, R.D., "Numerical Integration of Some New Unified Plasticity-Creep Formulations," Proc. 4th International Conference on Structural Mechanics in Reactor Technology, Vol. M, 1977, pp. 15-19.

96. Jones, W.B., Rohde, R.W., and Swearengen, J.C., "Deformation Modelling and the Strain Transient Dip Test," Mechanical Testing for Deformation Model Development, ASTM STP 765, 1982, pp. 102-118.

97. Jones, W.B., and Rohde, R.W., "An Evaluation of the Kinematic Variable (Back Stress) Response of Metals," Proc. 7th International Conference on Structural Mechanics in Reactor Technology, 1983.

98. Blum, W., and Finkel, A., "New Technique for Evaluating Long Range Internal Back Stresses," Acta Metallurgica, Vol. 30, 1982, pp. 1705-1715.

99. Friedel, J., Dislocations, Addison Wesley, Reading, Massachusetts, 1967.

100. Ahlquist, C.N., and Nix, W.D., "A Technique for Measuring Mean Internal Stress During High Temperature Creep," Scripta Metallurgica, Vol. 3, 1969, pp. 679-682.

101. Ahlquist, C.N., and Nix, W.D., "The Measurement of Internal Stresses During Creep of Al and Al-Mg Alloys," Acta Metallurgica, Vol. 19, 1971, pp. 373-385.

102. Poirier, J.P., "Microscopic Creep Models and the Interpretation of Stress-Drop Tests During Creep," Acta Metallurgica, Vol. 25, 1977, pp. 913-917.

103. Bodner, S.R., and Partom, Y., "A Large Deformation Elastic-Viscoplastic Analysis of a Thick-Walled Spherical Shell," Journal of Applied Mechanics, Vol. 39, 1972, pp. 751-757.

104. Bodner, S.R., Partom, I., and Partom, Y., "Uniaxial Cycle Loading of Elastic-Viscoplastic Materials," Journal of Applied Mechanics, Vol. 46, 1979, pp. 805-810.

105. Stouffer, D.C., and Bodner, S.R., "A Constitutive Model for the Deformation Induced Anisotropic Plastic Flow of Metals," International Journal of Engineering Science, Vol. 17, 1979, pp. 757-764.

106. Bodner, S.R., "Representation of Time Dependent Mechanical Behavior of Rene 95 by Constitutive Equations," Report No. AFML-TR-79-4116, Air Force Materials Laboratory, Dayton, Ohio, 1979.

107. Stouffer, D.C., "A Constitutive Representation for IN100," Report No. AFWAL-TR-81-4039, Air Force Wright Aeronautical Laboratories, Wright-Patterson AFB, Ohio, 1981.

108. Bodner, S.R., and Stouffer, D.C., "Comments on Anisotropic Plastic Flow and Incompressibility," International Journal of Engineering Science, Vol. 21, 1983, pp. 211-215.

109. Bodner, S.R., "Evolution Equations for Anisotropic Hardening and Damage of Elastic-Viscoplastic Materials," Plasticity Today: Modelling, Methods and Applications, Elsevier Applied Science Pub., Barking, England, 1984.

110. Bodner, S.R., "Review of a Unified Elastic-Viscoplastic Theory (the Bodner Equations)," Interim Report No. AFOSR-84-0042, Air Force Office of Scientific Research, October 1984.

111. Chan, K., "Determination of Material Constants in the Bodner-Partom Constitutive Theory," Report on NASA Contract No. NAS 3-23925 (in preparation).

112. Gilman, J.J., Micromechanics of Flow in Solids, McGraw-Hill, New York, 1969.

113. Vreeland, T.J., Techniques of Metals Research, Wiley-Interscience, New York, 1968.

114. Gilman, J.J., "Dislocation Mobility in Crystals," Journal of Applied Physics, Vol. 36, 1965, pp. 3195-3206.

115. Miller, A.K., and Sherby, O.D., "A Simplified Phenomenological Model for Non-Elastic Deformation: Predictions of Pure Aluminum Behavior and Incorporation of Solute Strengthening Effects," Acta Metallurgica, Vol. 26, 1978, pp. 289-304.

116. Miller, A.K., "Modelling of Cyclic Plasticity with Unified Constitutive Equations: Improvements in Simulating Normal and Anomalous Bauschinger Effects," Journal of Engineering Materials and Technology, Vol. 102, 1980, pp. 215-222.

117. Schmidt, C.G., "A Unified Phenomenological Model for Solute Strengthening, Deformation Strengthening, and Their Interactions in Type 316 Stainless Steel," Ph.D. Dissertation, Stanford University, Dept. of Materials Science and Engineering, 1979.

118. Schmidt, C.G., and Miller, A.K., "A Unified Phenomenological Model for Non-Elastic Deformation of Type 316 Stainless Steel -- Part I: Development of the Model and Calculation of the Material Constants, and Part II: Fitting and Predictive Capabilities," Res Mechanica, Vol. 3, 1981, pp. 109-129 and pp. 175-193.

119. Schmidt, C.G., and Miller, A.K., "The Effect of Solutes on the Strength and Strain Hardening Behavior of Alloys," Acta Metallurgica, Vol. 30, 1982, pp. 615-625.

120. Sherby, O.D., and Miller, A.K., "Combining Phenomenology and Physics in Describing the High Temperature Mechanical Behavior of Crystalline Solids," Journal of Engineering Materials and Technology, Vol. 101, 1979, pp. 387-395.

121. Miller, A.K., and Ziaai-Moayyed, A.A., "Some Critical Experimental Tests of the MATMOD Constitutive Equations with Respect to Directional Hardening and Cyclic Deformation,", ASTM STP 765, 1982, pp. 202-222.

122. Oldberg, S., Miller, A.K., and Lucas, G.E., ASTM STP 681, 1979, p. 370-380.

123. Kagawa, H., and Asada, Y., Proc. ASME International Conference on Advances in Life Prediction Methods, 1983, p. 33-43.

124. Imbrie, P.K., "Evaluation of the Numerical Stability and Sensitivity to Material Parameter Variations for Several Unified Constitutive Models," M.S. Thesis, Texas A&M University, May 1985.

VITA

Joachim Michael Erdmann Beek was born on [redacted] in [redacted] the son of Karin Dorothea Beek and Karl Friedo Beek. After graduating from London Central High School, High Wycombe, Bucks., England, in 1978, he enrolled at Texas A&M University, where he completed his B.S. in Aerospace Engineering in 1982. During his undergraduate years he worked two summers at the University of Stuttgart in Stuttgart, West Germany, and one summer for an oil exploration company in East Africa.

His graduate work has centered on constitutive modelling of inelastic deformation in crystalline solids.

Together with his wife Belinda, he may be contacted through Lockheed Engineering and Management Services Company, 2400 Nasa Rd. 1, Houston, Texas, 77258.

APPENDIX 6.5

"Page missing from available version"

APPENDIX 6.5

NO PAGES

INCOMPLETE DOCUMENT